Molecular architecture of Caveolin-3 and the investigation of an interaction with the Ryanodine receptor

A thesis submitted to the University of Manchester for the degree of Doctor of Philosophy in the Faculty of Medical and Human Sciences

2012

Gareth Whiteley

School of Medicine

II Contents

Word Count: 72,120

List of Contents

List of Figures

List of Tables

List of Abbreviations

BCIP-NBT	5-Bromo-4chloro-3-indolyl phosphate-Nitro blue tetrazolium
Ca^{2+}	Calcium ion
CaM	Calmodulin
Cav3	Caveolin-3
CEM	Cryo Electron Microscopy
CHAPS	3-[(3-cholamidopropyl) dimethylammonio]-1-prpanesulphonate
CICR	Calcium Induced Calcium Release
CSQ	Calsequestrin
dd	Double Distilled
DHPR	Dihydropyridine receptor
DMSO	Dimethyl Sulfoxide
EC	Excitation Contraction
EM	Electron Microscopy
FBS	Fetal Bovine Serum
FRT	Fischer Rat Thyroid
GST	Glutathione S-transferase
HEPES	5mM N'-2-hydroxyethylpiperazine-N'-2-ethanesuphonic acid
KO	Knock Out
LB	Lysogeny Broth
LTCC	L-type Voltage Gated Calcium Channel
LUVs	Large Uni-lamellar Vesicles
MDCK	Madin-Darby Canine Kidney cells
MOI	Multiplicity of Infection
Na^{2+}	Sodium ion
NCX	Na+/ Ca2+ exchanger
NEM	Negative-staining Electron Microscopy
NMR	Nuclear Magnetic Resonance
PMCA	Plasma Membrane Calcium ATP-ase
PMSF	Phenylmethylsulphonyl fluoride
RT°C	Room Temperature (°C)
RyR	Ryanodine Receptor
SBL	Soybean Lecithin
SDS-PAGE	Sodium Dodecyl Sulphate Polyacrylamide Gel Electrophoresis
SERCA	Sarcoplasmic Reticulum Calcium ATP-ase

SPA	Single Particle Analysis
SR	Sarcoplasmic Reticulum
TBS	Tris-Buffered Saline
TEM	Transmission Electron Microscopy
TTCC	T-type Voltage Gated Calcium Channel
μM	Micromolar

III Abstract

The University of Manchester.

Gareth Whiteley.

Doctor of Philosophy.

Molecular architecture of Caveolin-3 and the investigation of an interaction with the Ryanodine receptor.

June 2012.

The muscle-specific membrane protein, Caveolin-3, is a building block of caveolae a type of specialised lipid raft. Caveolin-3 is proposed to play a central role in variety of cellular functions both structural and functional, from cell signalling to cholesterol homeostasis. Caveolin-3 has also been implicated in processes involved in targeting membrane proteins to the plasma membrane, as well as mediating a host of cell signalling processes. Initial attempts were made to express full-length Caveolin-3 in *E.coli.* However, more success was achieved in expressing and purifying domains of Caveolin-3. To produce purified full-length Caveolin-3 the baculovirus expression system was employed and we report here that the expression of Caveolin-3 in insect (Sf9) cells leads to the formation of caveolae comparable in size to those observed in native vesicles. We subsequently purified the recombinant Caveolin-3 and determined, using multi-angle laser light scattering, that the isolated protein forms an oligomer with a molecular mass of ~200-220kDa. Using negative-stain transmission electron microscopy in conjunction with single particle analysis we have determined the first three-dimensional structure for Caveolin-3 with data converging to suggest that it forms a nonamer. The 9-fold symmetric three-dimensional Caveolin-3 volume is toroidal, ~16.5nm in diameter and 5.5nm thick, and is characterised by an outer rim of protein connected to a central 'cone-shaped' domain. Labelling studies revealed that the C-terminal domain of each of the contributing Caveolin-3 monomers associate to form the central cone density. There is also evidence to suggest that Caveolin-3 is associated with a range of proteins involved in excitation-contraction coupling. Having identified multiple potential caveolin-binding motifs within the Ryanodine Receptor, one of the key protein components of excitation-contraction coupling, we have purified the skeletal isoform of the Ryanodine Receptor (Ryanodine Receptor-1) from sheep calf muscle and using several biophysical techniques probed whether there is an interaction between Caveolin-3 and Ryanodine Receptor-1. Co-immunoprecipitation experiments indicated that the two proteins do indeed interact, but functional studies for analysis of binding characteristics were inconclusive. In conclusion, this thesis describes both the successfully purification and structural determination of

Caveolin-3, generating the first 3D data for any of the caveolin proteins, as well as work aimed at understanding its functional relationship with Ryanodine Receptor-1.

IV Declaration

I declare that no portion of the work referred to in the thesis has been submitted in support of an application for another degree or qualification of this or any other university or other institute of learning.

V Copyright Statement

The author of this thesis (including any appendices and/or schedules to this thesis) owns certain copyright or related rights in it (the "Copyright") and s/he has given The University of Manchester certain rights to use such Copyright, including for administrative purposes.

Copies of this thesis, either in full or in extracts and whether in hard or electronic copy, may be made **only** in accordance with the Copyright, Designs and Patents Act 1988 (as amended) and regulations issued under it or, where appropriate, in accordance with licensing agreements which the University has from time to time. This page must form part of any such copies made.

The ownership of certain Copyright, patents, designs, trade marks and other intellectual property (the "Intellectual Property") and any reproductions of copyright works in the thesis, for example graphs and tables ("Reproductions"), which may be described in this thesis, may not be owned by the author and may be owned by third parties. Such Intellectual Property and Reproductions cannot and must not be made available for use without the prior written permission of the owner(s) of the relevant Intellectual Property and/or Reproductions.

Further information on the conditions under which disclosure, publication and commercialisation of this thesis, the Copyright and any Intellectual Property and/or Reproductions described in it may take place is available in the University IP Policy (see http://www.campus.manchester.ac.uk/medialibrary/policies/intellectual-property.pdf), in any relevant Thesis restriction declarations deposited in the University Library, The University Library's regulations (see http://www.manchester.ac.uk/library/aboutus/regulations) and in The University's policy on presentation of Theses.

VI Acknowledgements

First and foremost I need to acknowledge my wife, Victoria Whiteley. Without doubt she has been the single most important factor towards me completing this PhD. The PhD is at most times a tumultuous hell of an emotional rollercoaster ride for all those concerned. Anyone who can tolerate their partner during such a time is undoubtedly a strong, tolerant, amazing, and possibly mentally deranged person. I love you more than you could ever imagine, l'll yak. Thanks for keeping me propped up. I owe you the world and much, much more.

I would like to thank my supervisor, Ashraf Kitmitto, a truly great supervisor, who has been infinitely approachable and has been both rapid and detailed in response to my never ending questions. Thank you for bestowing upon me the tomes of your wisdom, and thank you for giving me this opportunity. Top marks.

I would also like to thank the following people for their contributions, both big and small, it all helped: my Family (for accepting that I have not been contactable for over 3 years); Clare Austin as my advisor; Pharaoh Ahmed Handhle (future Egyptian President; I have particular enjoyed our conversations about middle eastern and Africa politics - Shukran jazeelan!); Aini Hamid (first year work-wife/Malaysian cooking tips provider); EM-guru Rich Collins; Pablo Lara Gonzalez, for an infinite supply of healthy insect cells – seriously, thank you very much!; Insect cell master, Eddie McKenzie (and his on-tap advice); Biophysics whizz, Tom Jowitt; all round lab super helper, Monib Iqbal (someone give this guy a PhD already!); Sophie, for going through this whole PhD malarkey at the same time as me; Pastor Simon Forman, for his constant theistic challenging; Saad 'teabag' Shakur, for unrelenting spirit-lifting; Andrew Hamilton, for moral support and lots of advice; Mark, Dave and a selection of the Eisenites, for dragging me from the lab to go for a pint with them. The 'catch-all' lunch group, for constant mad debates and entertainment. The arrival of Hayley Bennett and John-Bernárd Davenport, albeit at a late point in the PhD was excellent. They gave me many ideas, as well as provided a fresh view on what I have achieved and what was still possible. Christian Pinali, for making me aware of the fact that I was becoming obsessed with Fourier space; Willa Yim (aka Wilhelm the philosopher) and the rest of the future Singaporean tyrants with small hand-writing (Amanda, Melicia, Aimen); Lucy Dalton/Claire Reynolds (it was something they said that spurred me on at a low point); Team Ward for printer loan and left field entertainment; Doctors Caroline Dart and Steve Prince for a good viva grilling/discussion; Douglas Adams, for writing spirit lifting books; both *Escherichia coli* and *Spodoptera frugiperda*, for loan of cells; God, in whatever form or manifestation it/he/she/they exists, for their

epically late showing; the BHF, for their funding (FS/08/038/25262), without which I would never have been given this opportunity; anyone, ever, who donated to the BHF – thank you very much! Finally, I would like to thank Dr Steve Prince and Caroline Dart for the painful viva grilling. Err, and anyone else I have forgotten to mention.

This PhD is dedicated to all known (and unknown) transient states of energy transfer; anyone who seeks to help our species; and all those who suffer on a daily basis due to cardiovascular disease, the single biggest killer of my species.

"Great minds discuss ideas; average minds discuss events; small minds discuss people."
~Eleanor Roosevelt

"Give me six hours to chop down a tree, and I will spend the first four sharpening the axe."
~Abraham Lincoln

VII The Author

In 2004, I obtained a BSc Joint Honours Degree in Genetics and Zoology (2:1) from the University of Swansea. In 2006, I then completed a MSc in Bioinformatics (Merit) from the University of Manchester. After this I worked as a technician at UCLAN in the Forensics and Microbiology departments, before moving to Liverpool University, where I worked as a research technician and bioinformatician within the Pharmacology and Therapeutics department until 2009 when I started this PhD.

Chapter 1: Introduction

The plasma membrane is a vital component of the cell for a variety of reasons. It is involved in maintaining cell structure, it controls the ion fluxes essential to many processes, and it is involved in transmitting signals from the extracellular to the intracellular environment, and *vice-versa.* The organisation of its structure is integral to how this is achieved. Traditionally, the structure of the plasma membrane has been viewed as a fluid mosaic model (Singer and Nicolson, 1972). However, the model makes the assumption of a homogenous membrane in which ordered domains do not exist. It is now known that this is not the case, indeed, regions with distinct compositions termed lipid rafts have been shown to exist (Simons and Ikonen, 1997; Simons and Toomre, 2000). Lipid rafts are characterised by their concentration of cholesterol and sphingolipids, their resistance to non-ionic detergents and enrichment in proteins such as glycophosphatidylinositol (GPI)-linked proteins. One type of specialised lipid raft, which is morphologically distinguishable from the typical lipid raft is the caveolae (Palade, 1953; Yamada, 1955). Caveolae are both structurally and functionally distinct to both the general plasma membrane and lipid rafts (Örtegren et al., 2004; Simons and Toomre, 2000). See Figure 1 for summary of the differences between these distinct membrane regions.

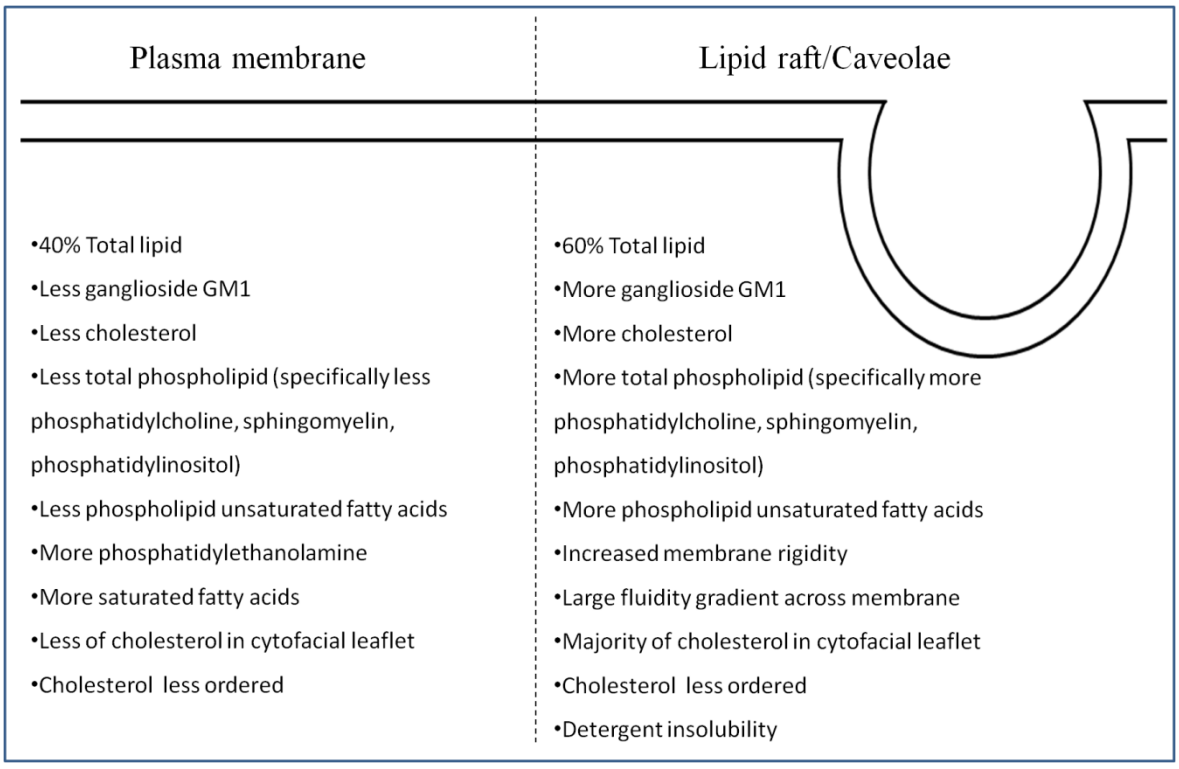

Figure 1: Comparison of plasma membrane to lipid rafts and caveolae.
Lipid rafts and caveolae are distinct regions of the plasma membrane. Further, caveolae differ from lipid rafts by the addition of the protein caveolin, their lack of

glycophosphatidylinositol-anchored proteins and the distinct morphological appearance (Schroeder et al., 2005).

Caveolae

Caveolae form goblet-like invaginations in the cell membrane. It is believed that this conformation is formed by the inclusion of the protein caveolin (Glenney, 1992; Kurzchalia et al., 1992; Rothberg et al., 1992), a protein unique to caveolae that distinguishes them from the lipid rafts and the typical plasma membrane. The central role of caveolin proteins for caveolae formation has been demonstrated by genetic ablation of the protein finding that the formation of caveolae is abolished (Drab et al., 2001; Galbiati et al., 2001c; Park et al., 2002; Woodman et al., 2002). Moreover, the addition of caveolin to cells which ordinarily would not form caveolae can result in *de novo* caveolae formation (Fra et al., 1995). The morphology of caveolae depends upon several factors, such as location within the cell and its designated function. Traditional caveolae are 50-100nm membrane invaginations although several other less well characterised formations exist (discussed in more detail in Chapter 4). For example, plasmalemmal vesicles which reside just beneath the cell membrane on the cytosolic side and fully internalised variants not associated with the membrane, as well as several other distinct forms (Cohen et al., 2004). This dynamism is believed to imbue them with the ability to take on many roles within the cell. Certainly, they increase the surface area of the cell.

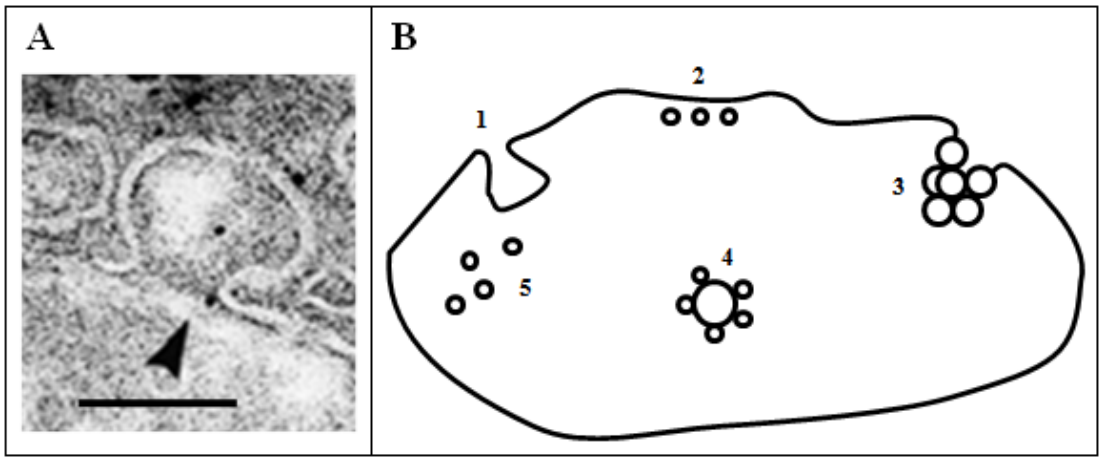

Figure 2: Caveolae morphology.

A: Single membrane caveolae as viewed by EM, Bar=78nm. Taken from Oh, P., McIntosh, D. P. & Schnitzer, J. E. (1998) *J. Cell Biol.*141, 101–114. **B**: A range of different types of caveolae exist: 1) Typical caveolae, 2) Plasmalemmal caveolae, 3) Cluster of caveolae, 4) Caveosome, 5) Internalised caveolae**.**

Caveolae function

Since caveolae were first discovered they have been associated with a myriad of potential roles. Initially thought to be involved in vesicular transport alone, caveolae have since been implicated in countless other cellular functions. There is now substantive evidence to implicate caveolae in 1) vesicular transport, including transcytosis and endocytosis (Kurzchalia et al., 1992; Schnitzer, 2001); 2) cholesterol homeostasis (Murata et al., 1995; Smart et al., 1996); 3) mechanosensing (Parton and Simons, 2007; Radel and Rizzo, 2005; Yagi et al., 1988) and 4) signal transduction (Okamoto et al., 1998). Indeed, a wide-range of functionally varied proteins are localised to caveolae e.g. proteins involved in signalling such as H-Ras (Song et al., 1996a), NOS (Feron et al., 1996; Garcia-Cardena et al., 1996a; Garcia-Cardena et al., 1997), eGFR (Mineo et al., 1999), G-protein coupled receptors (Chun et al., 1994; Sargiacomo et al., 1993a), G-proteins (Lisanti et al., 1994b) and a host of different protein kinases (Razani et al., 1999; Sargiacomo et al., 1993b). In addition, structural proteins have been identified in caveolae e.g. dystroglycan (Song et al., 1996b) and dysferlin (Matsuda et al., 2001) as well as ion channels, such as the L-type voltage-gated calcium channel (Balijepalli et al., 2006; Daniel et al., 2001; Darby et al., 2000), the voltage-gated sodium channel (Vatta et al., 2006; Yarbrough et al., 2002) and the sodium-calcium exchanger (Bossuyt et al., 2002). Specific lipid molecules such as cholesterol (Murata et al., 1995; Smart et al., 1996) and glycosphingolipids (Örtegren et al., 2004) are now recognised as key components of caveolae. Indeed, this is a just a very small selection of a very long list of proteins believed to be localised to caveolae.

Caveolae involvement in signal transduction

It has now been nearly twenty years since Sargiacomo and co-workers (Sargiacomo et al., 1993b) isolated detergent (Triton)-insoluble membrane fractions and determined that they corresponded to caveolae. The group went on to identify several proteins, including G-proteins and Src protein tyrosine kinases as components of caveolae. As new methods of caveolae isolation were developed, other researchers followed suit reporting that a host of proteins resided within caveolae, for example Chang and co-workers (Chang et al., 1994) isolated and analysed caveolae from smooth muscle and found over 30 proteins associated with the caveolae coat. It was noted that many of these caveolae-residing proteins were signalling proteins (Lisanti et al., 1994a; Lisanti et al., 1994b; Ostrom et al., 2001). It was thus not long until the concept of caveolae as signalling compartments was proposed (Lisanti et al., 1994a; Okamoto et al., 1998). Since then,

countless other researchers have added to the collection of growing evidence of caveolae as signalosomes e.g. (Kurzchalia and Parton, 1999; Scherer et al., 1995).

One of the more interesting observations in this early caveolae research was that the caveolin proteins that constitute the caveolae were not only integral to caveolae formation, but that they also played a role as modulators of signalling. For example, caveolin interacts directly with G-proteins and regulates their function (Tang et al., 1996). Indeed, many signalling proteins have now been shown to interact specifically with this protein. There are three distinct isoforms of caveolin (termed Caveolin-1, -2, -3), and these will be discussed in more detail in section Caveolins below.

It should be noted however, that the 'all encompassing' role of caveolae as sites of signal transduction has been met with some scepticism (Gratton et al., 2004). In a review by Parton and Simons (Parton and Simons, 2007) potential issues that need to be addressed were highlighted. They suggest that the theory of caveolae as signalosomes should be treated with caution until functional data can support the involvement of caveolae for the myriad of proteins that they are claimed to interact with. The authors do concede that indeed caveolae appear to be involved in *some* signalling process, but that *all* the claims are not necessary true.

The merit of compartmentalisation

With these compartments containing so many signalling molecules, questions have been asked as to what exactly is the merit of compartmentalising them. It has been proposed that the restricted environment may allow cross-activation of specific pathways, thus providing additional opportunities for pathway interaction and regulation. Moreover, it is suggested that the caveolae volume provides classical pathways alternative/additional functions, as appears to be the case for β-adrenergic receptor cAMP dependent signalling (Rybin et al., 2000), where in cardiac myocytes β_2 receptors are predominantly found within caveolae, whereas β_1 receptors are found in both caveolae and the plasma membrane. Upon stimulation, the β_2 receptor exits the caveolae, but β_1 receptors remain. Another popular belief is that by gathering downstream proteins together the "*system would facilitate and accelerate the response to extracellular stimuli*" (Frank and Lisanti, 2006). Other suggestions include the possibility that caveolae offer protection from negative regulators (Xiang et al., 2002).

It is worth noting here that the lipid environment itself can influence protein activity. When a protein inserts into a lipid bilayer, conformational changes, and hence potential functional changes can occur within the protein. This occurs as the hydrophobic

regions of the membrane protein interact with the hydrophobic core of the bilayer. Such an interaction can disrupt the adjacent bilayer, incurring an energetic cost, which, in turn, contributes to the overall free energy difference between protein conformations. The degree to which the adjacent bilayer is deformed, and hence the subsequent energetic cost incurred, is itself dictated by the properties of the membrane, which are themselves a function of the composition of the lipid bilayer. Thus, bilayers of varying composition can have a varied and direct effect on protein function (Andersen and Koeppe, 2007). Moreover, direct lipid interactions with a range of proteins from receptors to ion channels have been shown to alter receptor activity and channel kinetics (Barrantes, 2002; Epshtein et al., 2009; Fantini and Barrantes, 2009). Therefore, these distinct lipid environments may in themselves alter the activity of residing proteins.

The presence of G-proteins in caveolae is an interesting case, given their signalling pathway association. To date the G-proteins $G_{\alpha s}$ (Lisanti et al., 1994b) $G_{\alpha i1}$ (Lisanti et al., 1994b), $G_{\alpha i2,}$ (Schwencke et al., 1999), $G_{\beta\gamma}$ (Lisanti et al., 1994b) and G_q (Haasemann et al., 1998) have been identified within caveolae and some have been shown to co-fractionate with caveolins. Indeed, many of their associated G Protein-Coupled Receptors (GPCRs) are also present, such as B2 Bradykinin receptor (Murthy and Makhlouf, 2000), Endothelin type A (Chun et al., 1994) and β_2-adrenergic receptors (Balijepalli et al., 2006). One possible explanation for the presence of these 'molecular switches' within caveolae is that binding of G-protein subunits to caveolin, sequesters the unit, preventing it from re-associating with its GPCR, thus causing a desensitised response to further stimulation (Ju et al., 2000). It is also possible that the opposite of this is the case, were movement of G-protein subunits into caveolae allows them to interact with their associated GPCRs (which are also present in the caveolae), allowing it to initiate the signalling cascade. Indeed, the functional significance of proteins coming and going with regards to caveolae location is not entirely understood. It is worth noting, however, that caveolae should not be viewed as some static entity in which signalling molecules are indefinitely confined. It is thought that proteins can both exit or enter the caveolae depending upon their stimulation state. For example, the β_2-adrenergic receptor has been shown in cases to exit the caveolae upon stimulation (Rybin et al., 2000), where as the Bradykinin (BK) receptors are believed to enter the caveolae upon stimulation in a range of cell types (deWeerd and LeebLundberg, 1997; Haasemann et al., 1998; Rybin et al., 2000; Sabourin et al., 2002), though translocation of the BK receptors into caveolae has also been observed upon stimulation (Ju et al., 2000). In contrast, some molecules appear to be permanent residents in caveolae

such as the β_1-adrenergic receptor; although this receptor is also localised in non-caveolar regions of the plasma membrane (Rybin et al., 2000).

Caveolae involvement in endocytosis

Endocytosis is the means by which extracellular material is brought into the cell. Many different mechanisms of endocytosis exist. Perhaps both the most characterised and widely used method is clathrin-mediated endocytosis. However, caveolae have also been shown to be involved in endocytosis, and this process is thought to be the dominant non-clathrin process by which endocytosis occurs. Two main methods of caveolae-based endocytosis are believed to occur. One in which the endocytosed ligand is passed from the caveolae *via* the classical endocytotic mechanism and one in which it is passed *via* a complex termed the caveosome, which is an intracellular membrane-bound structure (Pelkmans et al., 2004; Pelkmans et al., 2001; Pelkmans et al., 2002). The mechanism that dictates which pathway is used is not known. An interesting study by Pelkmans and co-workers (Pelkmans et al., 2004), showed that the two known viral caveolar ligands, Simian Virus 40 (SV40) (Anderson et al., 1996) and the cholera toxin (Orlandi and Fishman, 1998), which both bind the ganglioside, GM1 (Tsai et al., 2003) and are both known to be endocytosed *via* caveolae, end up in different endosomal compartments. SV40 is processed *via* the caveosome and is ultimately passed to the smooth endoplasmic reticulum (Pelkmans et al., 2004), whereas the cholera toxin is passed *via* endosomes and ultimately to the Golgi-complex (Richards et al., 2002). This study highlights that much is still to be understood about the role of caveolae in endocytosis.

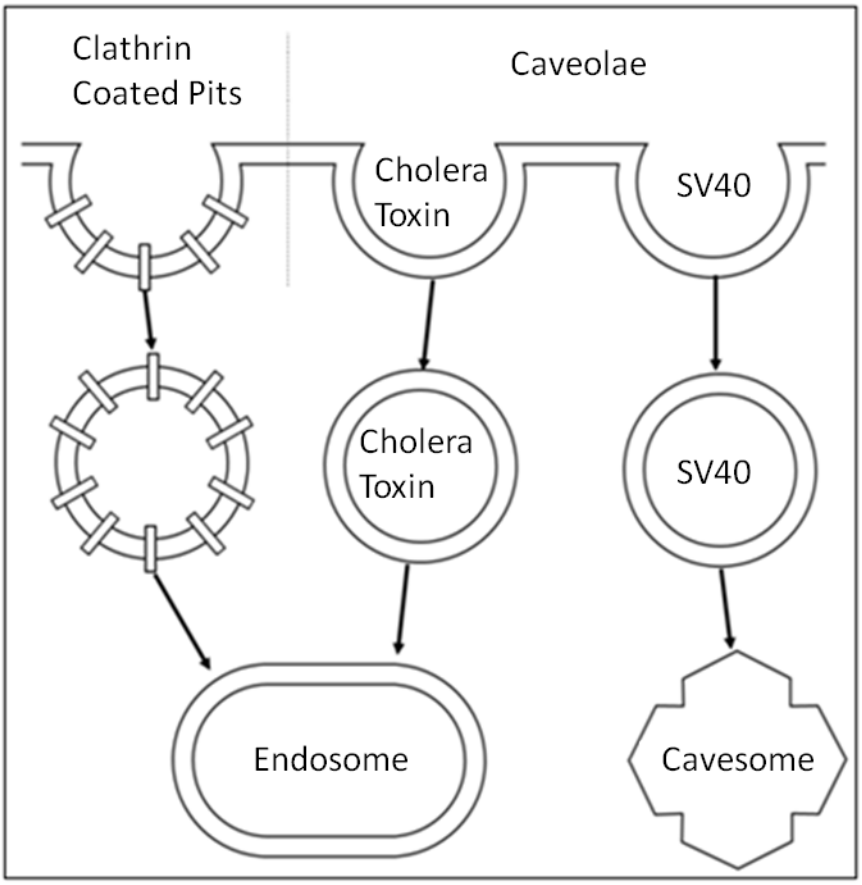

Figure 3: Caveolae role in endocytosis.

Caveolae are thought to play a role in endocytosis. However, they have been shown to process the endocytosed ligand in more than one way. One path involves the endosome, where the ligand is then passed on towards the Golgi complex, and another path in which the caveosome is used, where the ligand is passed to the smooth ER. The actual 'budding off' of the vesicles is thought to involve a protein called dynamin, which forms a collar at the neck of the caveolae that leads to budding off process (Oh et al., 1998).

Caveolae involvement in cholesterol homeostasis

It would appear that both caveolae structure and function are intrinsically linked to cholesterol (Ikonen and Parton, 2000). Cholesterol has been shown to be essential to caveolae formation (Rothberg et al., 1992) and it is a major component of intact caveolae (Smart et al., 1996). Indeed, removal of caveolae cholesterol (*via* the addition of cholesterol oxidase or methyl β-cyclodextrin) results in decreased caveolae formation, the 'flattening' out of caveolae, and the caveolin protein being relocated to the endoplasmic reticulum and Golgi complex (Chang et al., 1992; Rothberg et al., 1992; Smart et al., 1994). The re-addition of cholesterol has been shown to cause caveolin to migrate back to the membrane and caveolae to re-form (Conrad et al., 1995). Moreover, caveolae appear to

be involved in the trafficking of cholesterol both into and out of the cell (Fielding and Fielding, 2001). Caveolae have been shown to be a reversible plasma membrane pool of cholesterol ethers (Graf et al., 1999; Uittenbogaard et al., 2000). Indeed, Graf and co-workers also observed the presence of the class B, type I scavenger receptor in caveolae, which is involved in both the selective uptake of high density lipoprotein and as well as their efflux. In addition to a role in controlling the uptake of cholesterol, caveolae are also involved in the trafficking of newly synthesised cholesterol to the membrane (Smart et al., 1996). Expression of Cav1 in a lymphoid cell line, which does not ordinarily express caveolin or form caveolae, resulted in both the formation of caveolae and the enrichment of membrane cholesterol (Uittenbogaard et al., 1998). The study highlighted the importance of caveolin in the trafficking of newly synthesised cholesterol from the endoplasmic reticulum to the membrane.

Cholesterol binding proteins are not common. However, caveolins have been shown to bind cholesterol both *in vitro* (Murata et al., 1995) and *in-vivo* by using lipid photo-affinity labelling to detect protein-lipid interactions (Thiele et al., 2000). Indeed, the intrinsic relationship between caveolins, caveolae and cholesterol is highlighted further by the fact that cholesterol has been shown to affect the transcription of caveolins, in a manner that results in a decreased gene expression when the levels of cholesterol that are available are low (Bist et al., 1997), thus providing a form of a control system. Indeed, when cholesterol levels increase, more caveolin is found at membrane caveolae (Fielding et al., 1997). As an additional point of interest, a decrease in the cholesterol levels of caveolae has been shown to cause proteins, such as eNOS, to leave caveolae (Blair et al., 1999; Uittenbogaard et al., 2000), highlighting the importance of caveolae cholesterol to caveolae function.

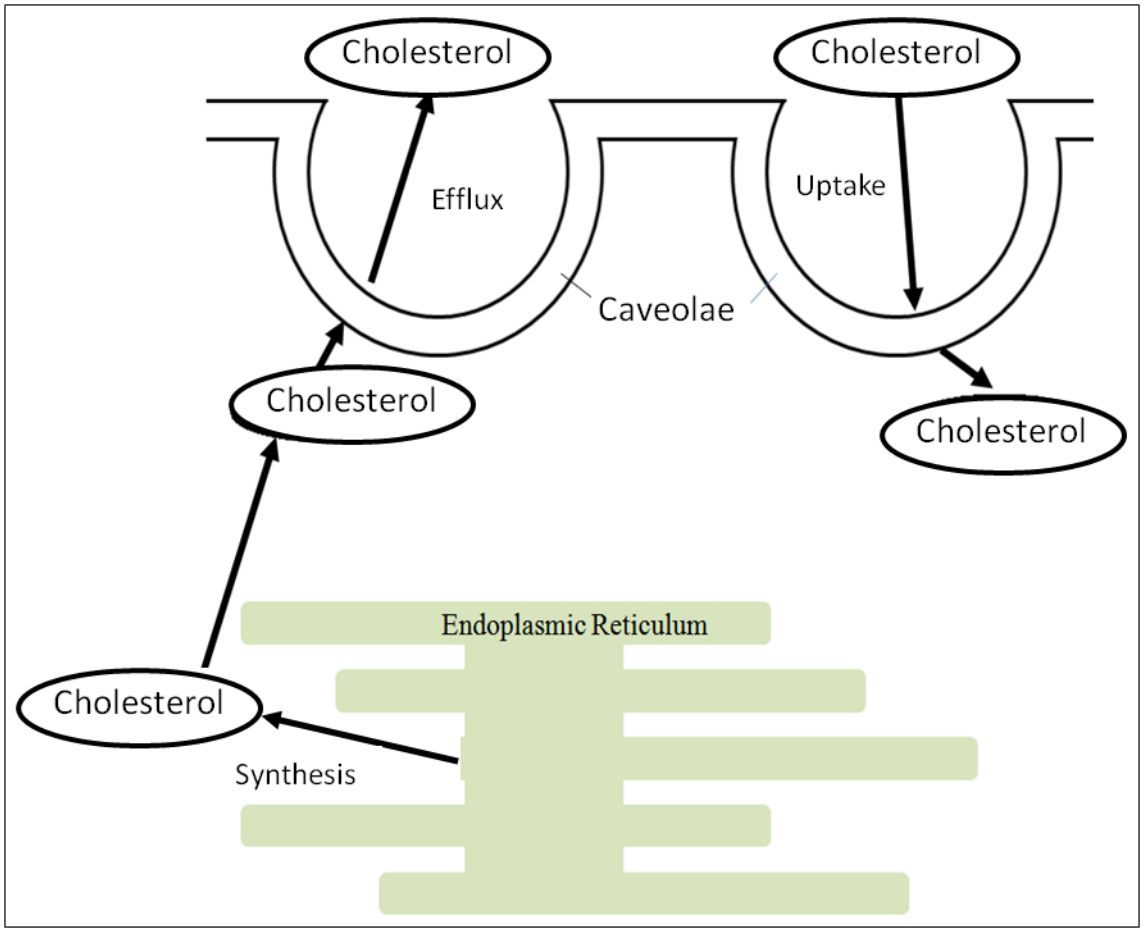

Figure 4: Caveolae role in cholesterol homeostasis.
Caveolae are thought to play a role in cholesterol uptake, efflux and the delivery of newly synthesised cholesterol to the membrane.

Caveolae biogenesis

The point at which caveolae are formed is not fully understood. The individual protein components, caveolins, are co-translationally synthesised at the rough endoplasmic reticulum (Monier et al., 1995), then passed along the secretory system (Luetterforst et al., 1999; Pol et al., 2005), where at some point they form oligomers, are palmitoylated (Parat and Fox, 2001), bind cholesterol (oligomerisation, palmitoylation and cholesterol association are discussed in more detail below), aggregate with glycosphingolipids and sphingomyelin, and convert from the detergent-soluble monomeric form into an oligomeric detergent-insoluble form (Parton et al., 2006). Conformational abnormalities caused by mutations within caveolin can prevent exit from the Golgi complex (Ren et al., 2004). Whether a meshwork of oligomers are incorporated into lipid-raft like domains at this stage before trafficking to the membrane (Tagawa et al., 2005) or whether they migrate as oligomers *to* the plasma membrane where they then form caveolae (Fra et al., 1995) is also not clear. A region termed the scaffolding domain (described in more detail later) is

believed to be the specific region within caveolin that targets the protein to the membrane (Schlegel et al., 1999), and residues within the C-terminus of the protein are believed to direct caveolin to the trans-Golgi complex membrane (Schlegel and Lisanti, 2000). Indeed, although the invagination of the membrane is generally thought to be caused by the presence of the caveolin proteins, even this area is not fully understood. It has even been speculated that these membrane invaginations form independently of the caveolin proteins, but are then stabilised by the presence of caveolin (Nabi and Le, 2003).

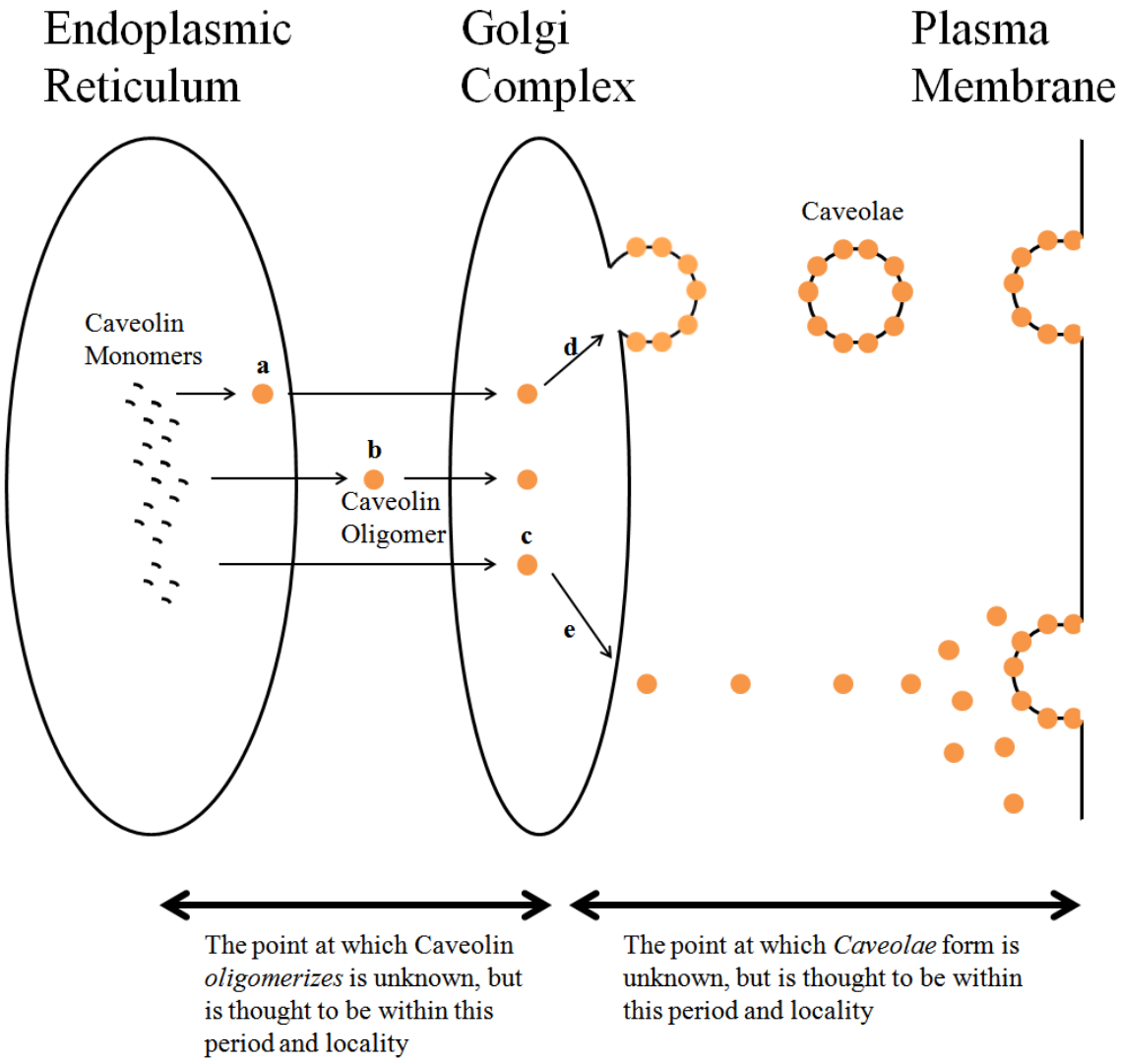

Figure 5: Caveolin oligomerisation and caveolae formation.
Caveolins are believed to be co-translationally inserted into the endoplasmic reticulum *via* the translocation apparatus. The point at which the caveolins oligomerise is not known. However, it is thought to be at some point between leaving the endoplasmic reticulum and leaving the Golgi complex (a, b, c). The point at which the oligomers form caveolae is also not known; two theories prevail: i) Caveolae are formed at the Golgi complex and arrive at the plasma membrane preformed (d), or ii) caveolin oligomers are transported to the membrane where they accumulate and form caveolae at the membrane (e).

With regards to the specific location of caveolae within the cell, there is much debate. Certainly, caveolae are found at the cell membrane, as can be observed by transmission electron microscopy (e.g. (Parton and Simons, 2007)). However, another key cellular structure of myocytes (particularly in skeletal muscle, though they are also present in cardiac muscle as well), with which caveolins have been shown to be associated, is the T-tubule network (Galbiati et al., 2001a; Minetti et al., 2002; Parton et al., 1997; Ueda et al., 2004). T-tubules, which are invaginations of the sarcolemmal membrane, are important regions in excitable cells as they allow deep penetration of the action potential. Although initially believed to be a transient relationship i.e. caveolins are involved in T-tubule biogenesis departing upon their completion (Parton et al., 1997), there is now a growing body of evidence to suggest that caveolins remains present even in the mature T-tubule system of both mature skeletal (Murphy et al., 2009; Ralston and Ploug, 1999) and cardiac cells (Head et al., 2005; Scriven et al., 2005; Woodman et al., 2002). Furthermore, the presence of another key ingredient for caveolae formation, cholesterol, has been shown to be important in the development of the T-tubule system. Indeed, the removal of cholesterol results in a redistribution of the T-tubule associated caveolins to intracellular sites (Carozzi et al., 2000). The specific role of caveolins in the development of the T-tubule system is not fully understood. However, caveolin knockout mice models exhibit an abnormal T-tubule system, but interestingly, not an absence thereof (Galbiati et al., 2001a; Park et al., 2002), suggesting other factors are involved.

With regards to whether caveolins are present predominantly at the sarcolemmal membrane *or* in the T-tubule system of myocytes is also not clear. For example, Ralston et al showed that for mature skeletal myocytes, Cav3 (one of the principal caveolin isoforms described in section Caveolins below) presence was greater *within* the cell as opposed to the surface (Ralston and Ploug, 1999). Murphy et al showed that Cav3 was located predominantly at 'hot spots' at the necks of the T-tubules which are present in the sub-sarcolemmal space (Murphy et al., 2009). Scriven et al showed that Cav3 predominantly forms caveolae at the sarcolemmal membrane (Scriven et al., 2005). Indeed, it would appear that the cellular location of Cav3 is as a result of multiple factors, including the maturation stage of the cell, the species type, the type of cell, size of the cell and likely many other factors. In addition, evidence also suggests that Cav3 is also within the sarcoplasmic reticulum (Li et al., 2006). Thus, the rules governing caveolin/caveolae location are still not clear.

The role of other proteins in caveolae formation

There is growing evidence that the protein, polymerase I and transcript release factor (PTRF), also known as cavin, is required for the formation, organisation and function of caveolae (Hill et al., 2008; Liu et al., 2008; Liu and Pilch, 2008). No caveolae formation in skeletal muscle, intestinal smooth muscle or lung epithelium was observed in KO cavin mice (Liu et al., 2008). Whether cavins are involved in the formation of caveolae or the stabilisation is not clear. Interestingly, there was also a reduced protein (but not mRNA) expression of caveolin observed (Liu et al., 2008). In addition, observations that also lend support to the role of caveolae in both cholesterol homeostasis and forming signalosomes are also found *via* the cavin KO study. Firstly, elevated triglyceride and free fatty acid levels were observed in the serum, suggesting that the ablation of caveolae resulted in aberrant cholesterol homeostasis. Secondly, a reduced membrane association of proteins previously shown to either locate to caveolae or interact directly with caveolins that are involved in insulin signalling, Glut4 (Scherer et al., 1994), and the insulin receptor (Gustavsson et al., 1999; Nystrom et al., 1999; Yamamoto et al., 1998), was observed, as were increased insulin levels in the serum (Liu et al., 2008), suggesting that the disruption of the caveolae based signalling complex had occurred.

Caveolins

Since the first discovery of Caveolin-1 (Glenney, 1992; Rothberg et al., 1992), a total of 3 proteins have now been discovered: Caveolin-1 (Cav1), Caveolin-2 (Cav2), Caveolin-3 (Cav3) (Scherer et al., 1995; Tang et al., 1996), with splice variants raising the total to six different forms (two Cav1 isoforms; three Cav2 isoforms; one Cav3 isoform) of the protein (Fujimoto et al., 2000; Kogo et al., 2002; Scherer et al., 1995). The functional significance of these different splice variant isoforms is not fully understood, but it has been suggested that the different isoforms of Cav1 may be responsible for differently located groups of caveolae (Fujimoto et al., 2000; Scherer et al., 1995), as shown in Figure 2. Cav1 has been the most widely studied and so much of what is inferred about caveolin structure and function in general, wrongly or rightly, is often based upon what is known for Cav1. Indeed, differences exist between the isoforms, for example, Cav1 is 27 amino acids longer than Cav3, and they differ in their molecular masses, albeit slightly; their monomeric mass ranging from 21kDa to 24kDa (Glenney and Zokas, 1989; Rothberg et al., 1992). Further, unlike Cav1 and Cav3, Cav2 does not appear to be required for caveolae formation (Mora et al., 1999), nor does it appear to be involved in vesicular transport (Razani et al., 2002a), although it has been shown to *associate* with both Cav1

and Cav3 (Rybin et al., 2003; Scherer et al., 1997). Thus, although the caveolins share some degree of sequence similarity (see Figure 6, panel A), there is clearly some divergence in function, something that is further highlighted by their different expression locations (see Figure 6, panel B). Cav1 and Cav2 are predominantly expressed in adipocytes, fibroblasts and endothelial cells (Lisanti et al., 1994b; Rothberg et al., 1992; Scherer et al., 1994), but are expressed in most cell types (Smart et al., 1999). Cav3 is muscle specific and is found in both striated muscle (skeletal and cardiac), as well as smooth muscle (Song et al., 1996b; Tang et al., 1996; Way and Parton, 1996) (See Figure 6, panel B).

A

```
Cav1  -MSGGKYVDSEGHLYTVPIREQGNIYKPNNKAMADELSEKQVYDAHTKEIDLVNRDPKHL 59
Cav2  MGLETEKADVQLFMD---------------DDSYSHHSGLEYADPEKFADSDQDRDPHRL 45
Cav3  -MMAEEHTD-------------------------LEAQIVKDIHCKEIDLVNRDPKNI 32
           : .*                          .     * .    .  :***:.:

Cav1  NDDVVKIDFEDVIAEPEGTHSFDGIWKASFTTFTVTKYWFYRLLSALFGIPMALIWGIYF 119
Cav2  NS-HLKLGFEDVIAEPVTTHSFDKVWICSHALFEISKYVMYKFLTVFLAIPLAFIAGILF 104
Cav3  NEDIVKVDFEDVIAEPVGTYSFDGVWKVSYTTFTVSKYWCYRLLSTLLGVPLALLWGFLF 92
      *.  :*:.********  *:*** :*  *.: * ::**  *::*:.::.:*:*:: *: *

Cav1  AILSFLHIWAVVPCIKSFLIEIQCISRVYSIYVHTVCDPLFEAVGKIFSNVRINLQKEI 178
Cav2  ATLSCLHIWILMPFVKTCLMVLPSVQTIWKSVTDVIIAPLCTSVGRCFSSVSLQLSQD- 162
Cav3  ACISFCHIWAVVPCIKSYLIEIQCISHIYSLCIRTFCNPLFAALGQVCSSIKVVLRKEV 151
      * :*  *** ::* :*: *: : .:. ::.    ..  **  ::*:  *.: : * ::
```

B

	Muscle			Non-Muscle		
	Cardiac	Skeletal	Smooth	Endothelial	Fibroblasts	Adipocytes
Cav1	NO	NO	YES	YES	YES	YES
Cav2	NO	NO	YES	YES	YES	YES
Cav3	YES	YES	YES	NO	NO	NO

Figure 6: Expression location of the caveolin isoforms.

A: The primary sequence of Cav1 (NCBI, NP_001744), Cav2 (UniProt, P51636) and Cav3 (NCBI, NP_001225) were automatically aligned using ClustalW. Cav1 and Cav3 share 61% of sequence homology, Cav1 and Cav2 share 30% of sequence homology, and Cav2 and Cav3 share 33% of sequence homology. Indeed, Cav2 is by far the most divergent of the caveolins. One of the more distinct sequence differences between the caveolins is that Cav1 contains an additional 27 residues at its N-terminus (compared to Cav3). Asterisks denote fully conserved residues; colons denote conservation between groups of strongly similar properties; full stops denote conservation between groups of weakly similar properties; gaps denote mismatches. **B:** Cell type expression of the caveolin isoforms.

Caveolin-3

Cav3 is the muscle-specific version of the caveolins. That is not to say that the other caveolins are not found in muscle, but that Cav3 is *only* found in muscle – an

important distinction. Indeed, all the caveolins are found in smooth muscle, whereas *only* Cav3 is found in skeletal and cardiac muscle. Thus, in terms of the cardiac setting, caveolae are abundant throughout the entire organ and Cav3 is found exclusively within the cardiac myocytes, whereas Cav1 and Cav2 are found exclusively in the endothelium and endocardium regions of the heart; though some recent evidence suggests there may be some degree of overlap (Cho et al., 2010; Robenek et al., 2008; Rybin et al., 2003). In mouse heart models Cav3 expression was shown to be detectable at embryonic day 10 (Biederer et al., 2000). In rat heart models Cav3 expression was shown to be at its maximum at day 5 (postnatal) before decreasing to the levels found in adult cardiomyocyte (Ratajczak et al., 2005).

Caveolin-3: Structure and membrane topology

Despite the differences in primary sequence and function mentioned above, a general model for how caveolins oligomerise and integrate with the membrane has been formulated; though, understandably, many of the assumptions should be treated with a certain degree of caution. Indeed, there is currently no three dimensional (3D) structures available for any caveolin protein. Cav1 is the most widely studied protein of the caveolin family with little structural data available for Cav3 in comparison. Cav3 is the focus of this thesis research and so the chapter will focus primarily upon what is known/not known about this isoform.

```
Cav3  ---------------------------MMAEEHTDLEAQIVKDIHCKEIDLVNRDPKNIN
Cav1  MSGGKYVDSEGHLYTVPIREQGNIYKPNNKAMADELSEKQVYDAHTKEIDLVNRDPKHLN
                                          :*. : * * * ***********.:*

Cav3  EDIVKVDFEDVIAEPVGTYSFDGVWKVSYTTFTVSKYWCYRLLSTLLGVPLALLWGFLFA
Cav1  DDVVKIDFEDVIAEPEGTHSFDGIWKASFTTFTVTKYWFYRLLSALFGIPMALIWGIYFA
      :*:**:********* **:****:**.*:*****:*** *****:*:*:*:**:**: **

Cav3  CISFCHIWAVVPCIKSYLIEIQCISHIYSLCIRTFCNPLFAALGQVCSSIKVVLRKEV
Cav1  ILSFLHIWAVVPCIKSFLIEIQCISRVYSIYVHTVCDPLFEAVGKIFSNVRINLQKEI
       :** ***********:********::**: ::*.*:*** *:*:: *.::: *:**:
```

Figure 7: Alignment of Cav1 and Cav3.
The primary sequence of Cav1 (NP_001744) and Cav3 (NP_001225) were automatically aligned using ClustalW. Cav3 and Cav1 share 61% of sequence homology (61% of residues are identical). Asterisks denote fully conserved residue; Colons denote conservation between groups of strongly similar properties; Full stops denote conservation between groups of weakly similar properties; Gaps denote mismatches.

The alignment of the primary sequence of specifically Cav1 and Cav3 above (Figure 7) shows a 61% sequence identity. Based upon a series of different experiments

and observations, it has been found that: 1) Sodium carbonate buffer alone is insufficient to extract Cav1 from the membrane (Sargiacomo et al., 1993a). 2) Antibodies directed against the N- and C- termini do not detect Cav1 of unpermeabilised cells (Aoki et al., 2010; Dupree et al., 1993). 3) Palmitoylation sites are present in the C-terminus (Dietzen et al., 1995). 4) Cell-surface biotinylation does not detect Cav1 (Sargiacomo et al., 1995) and 5) a hydrophobic region of 32 residues is insufficient to completely pass through the membrane, and so the caveolin protein is believed to form a unconventional hairpin like structure with a single partial-membrane region passing through (but not entirely) the plasma membrane, placing both the N- and C-terminals on the cytosolic side. See Figure 8 for the proposed membrane topology of Cav1. Although certainly not a common membrane topology, the incomplete pass of a hairpin-like membrane domain has been described for other proteins (Decaffmeyer et al., 2008; Voeltz et al., 2006).

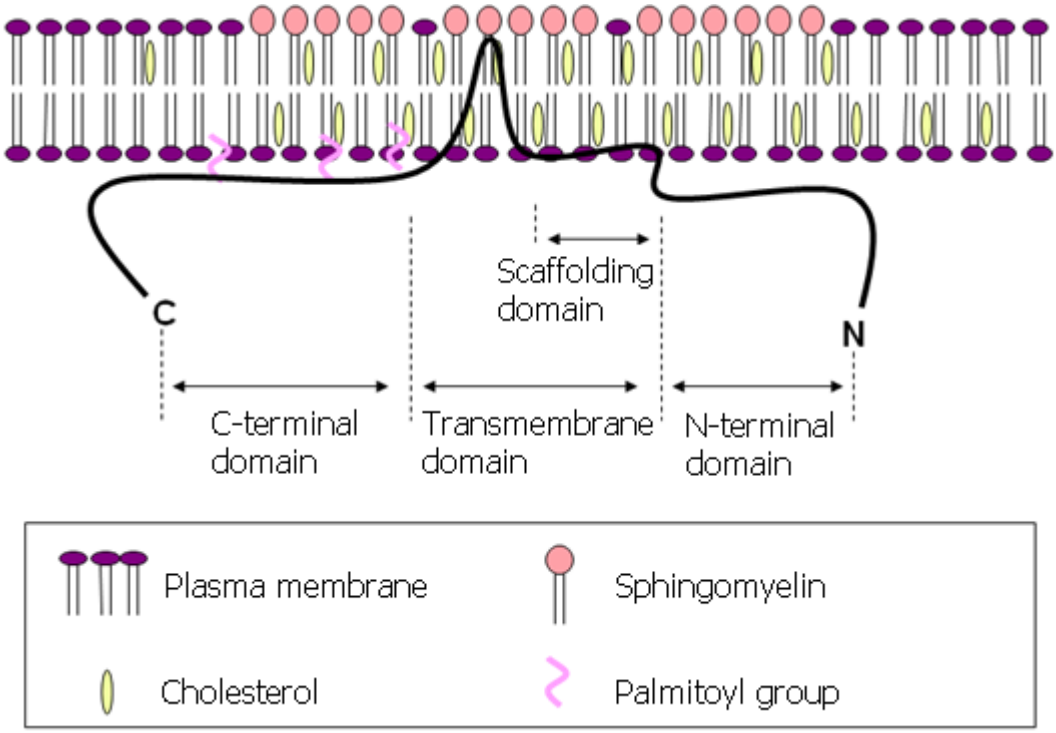

Figure 8: Predicted membrane topology of caveolin (shown as a monomer).
Cartoon of the putative membrane topology of the caveolin monomer. Cav3 is broken into down into three main domains: The N-terminus, the C-terminus and the transmembrane region. These categories are merely used to aid in the understanding of caveolin structure and are not defined domains; indeed, some degree of overlap in delimiting these regions is common is the literature. The caveolin protein is believed to form a hairpin like structures with a single transmembrane region passing through the plasma membrane, leaving both the N- and C- terminals on the cytosolic side (Aoki et al., 2010; Dupree et al., 1993).

Caveolin-3: Transmembrane region

Using secondary structure and hydrophobic region predicting algorithms, the region corresponding to residues 75-107 in Cav3, which consist of a 32 residue stretch of hydrophobic residues has been predicted to be the region that imbeds within the membrane (Monier et al., 1995; Parton et al., 2006). However, this 32 residue region is not thought to be sufficient to pass through the complete membrane, thus it was proposed that caveolins adopt an unconventional partial membrane pass topology. Interestingly, this region is also thought to act as a non-conventional translocation signal peptide that results in the unusual orientation of Cav3 within the membrane (Monier et al., 1995). Very recently, Lee and colleagues successfully produced a recombinant form of a region of Cav1, amino acids 96-136, (equivalent to 65-109 in Cav3), which encompasses the proposed transmembrane region (Lee and Glover, 2012). Circular dichroism revealed that it was composed of 57% α-helix, and nuclear magnetic resonance showed it to be composed of 65% α-helix; both these figures fit well with secondary structure predictions for this region (e.g. PSIPred predictions of this region in Cav3, carried out here, finds it to be 59% α-helix). Monitoring of chemical shifts showed that there are four distinct regions within this transmembrane region: 97-107 is α-helical, 108-110 was a break, 111-129 is a second α-helix, and 130-136 was unstructured (corresponding to Cav3 regions 70-80, 81-83, 84-102, and 103-109 respectively). The prediction of a helix-break-helix conformation, and the flexibility that would be afforded by the break, accommodates the partial-pass membrane topology predicted for Cav1. Interestingly, mutagenesis of residues 109 and 110 (equivalent to residues 82 and 83 in Cav3) dramatically altered the helix-break-helix conformation, suggesting that these residues maybe involved in the stabilising of this complex.

Recent studies, which involved making a range of hybrid, truncated and mutated forms of Cav1 have also predicted that the residues 80-95 (53-68 in Cav3) are also inserted into the membrane (Kirkham et al., 2008). This additional membrane associating region is not thought to penetrate deep into the membrane, but instead only partially enter the membrane due to its amphipathic nature. In addition, residues 67-74 of Cav3 represent a Cholesterol Recognition/Interaction Amino acid sequence and Consensus pattern (CRAC motif), which could be potentially involved in cholesterol binding (Arbuzova et al., 2000; Epand et al., 2005), although the regular expression used to identify this region is rather unspecific and likely predicts many false positives. Peptides of this region have been shown to bind artificial phospholipid vesicles, where the aromatic residues insert into the membrane bilayer (Arbuzova et al., 2000). Interestingly, in the study by Arbuzova and colleagues, further addition of phosphatidylserine (a monovalent acidic lipid present at

elevated levels in caveolae) to the artificial vesicles increased the incorporation of the caveolin peptide into the membrane, thus lending support to the importance of caveolae lipid composition in caveolin membrane association and caveolae formation. See Figure 9 for a summary of key areas within the proposed transmembrane domain.

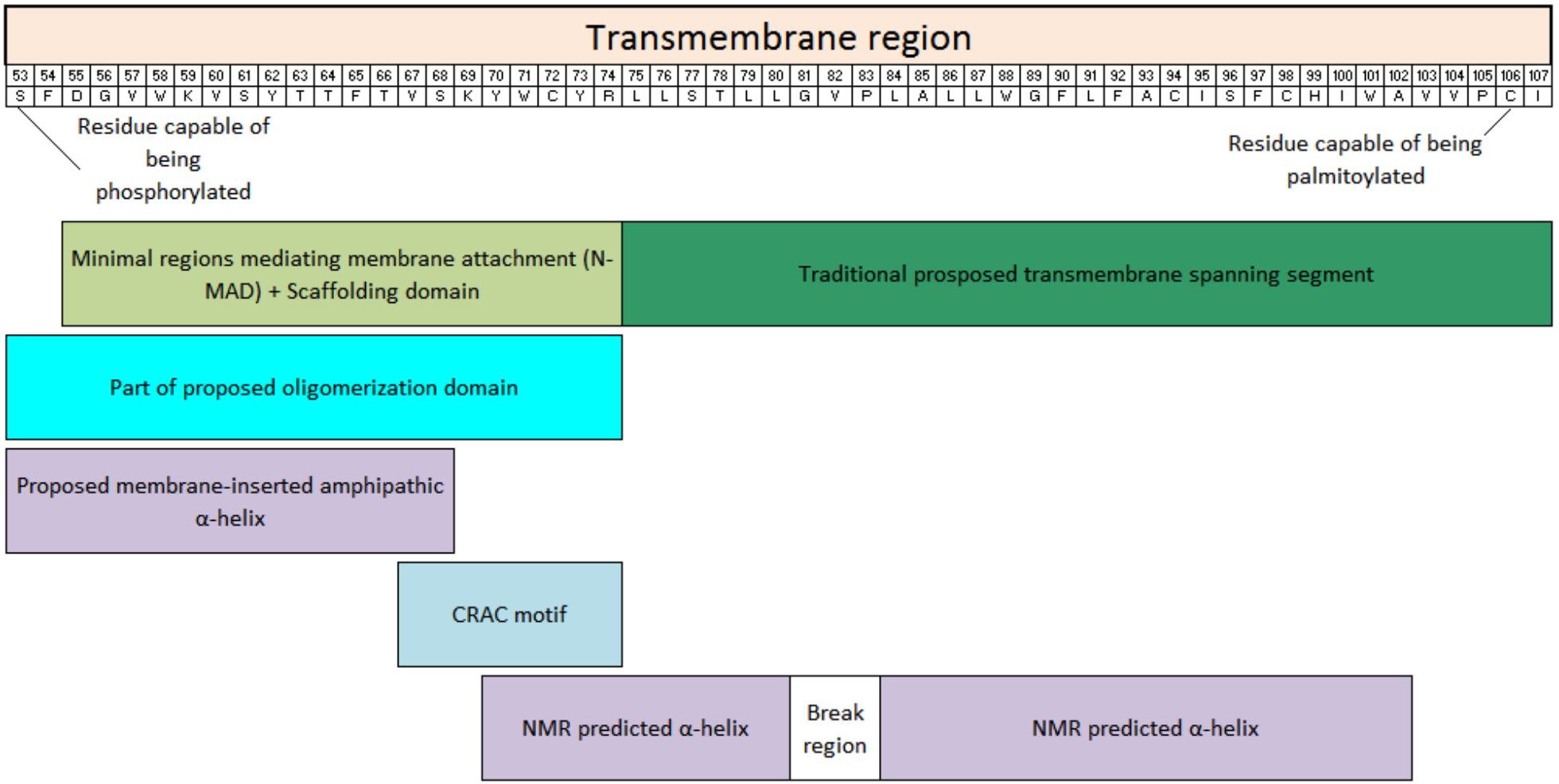
Transmembrane region
53 54 55 56 57 58 59 60 61 62 63 64 65 66 67 68 69 70 71 72 73 74 75 76 77 78 79 80 81 82 83 84 85 86 87 88 89 90 91 92 93 94 95 96 97 98 99 100 101 102 103 104 105 106 107
S F D G V W K V S Y T T F T V S K Y W C Y R L L S T L L G V P L A L L W G F L F A C I S F C H I W A V V P C I
Residue capable of being phosphorylated
Residue capable of being palmitoylated
Minimal regions mediating membrane attachment (N-MAD) + Scaffolding domain
Traditional prosposed transmembrane spanning segment
Part of proposed oligomerization domain
Proposed membrane-inserted amphipathic α-helix
CRAC motif
NMR predicted α-helix
Break region
NMR predicted α-helix

Figure 9: Key features within the proposed transmembrane region of Cav3.
Cartoon representation of the main features of the transmembrane region of Cav3. Many of the assignments are based upon experiments on Cav1. Note the presence of the transmembrane region believed to insert into the membrane, the positioning of the cholesterol recognition motif (CRAC), and the proposed partially membrane inserted alpha helix. This region also contains the N-MAD, the region thought to associate the oligomer with the membrane; and part of the proposed oligomerisation domain. Note the helix-break-helix region predicted by NMR.

Caveolin-3: The N-terminal domain region

The putative cytoplasmic N-terminal domain is believed to contain a number of key features with regards to caveolin membrane association, caveolae formation and protein function. This domain also houses the caveolin signature motif (FEDVIAEP) between residues 41 to 48 of Cav3, a region conserved in all isoforms. The segment termed the N-terminal Membrane Attachment Domain (N-MAD) (at residues 55-74 in Cav3) also known as the Scaffolding Domain has been shown to interact with multiple proteins and has also been shown to be the region of the caveolin responsible for *attaching* the protein to the membrane (Schlegel and Lisanti, 2000; Schlegel et al., 1999). More recent mutagenesis experiments have led to the proposal that it is specifically the residues 53-68 that prise open the membrane in order to allow the transmembrane region to insert, where residues 22-33 are involved in the stabilisation of this process (Kirkham et al., 2008). Cav3 is believed to have one site of phosphorylation at residue 53. Interestingly, studies of Cav1 show that the phosphorylation state of this residue has a direct effect on caveolin/caveolae trafficking to/from the membrane, where the phosphorylated state maintained Cav1 localisation at the Golgi, and the non-phosphorylated state localised Cav1 to the membrane (Kirkham et al., 2008). Residues 1-21 are not believed to be involved in caveolae formation of membrane association (Kirkham et al., 2008). See Figure 10 for a summary of the key areas within what is termed the N-terminal region of Cav3.

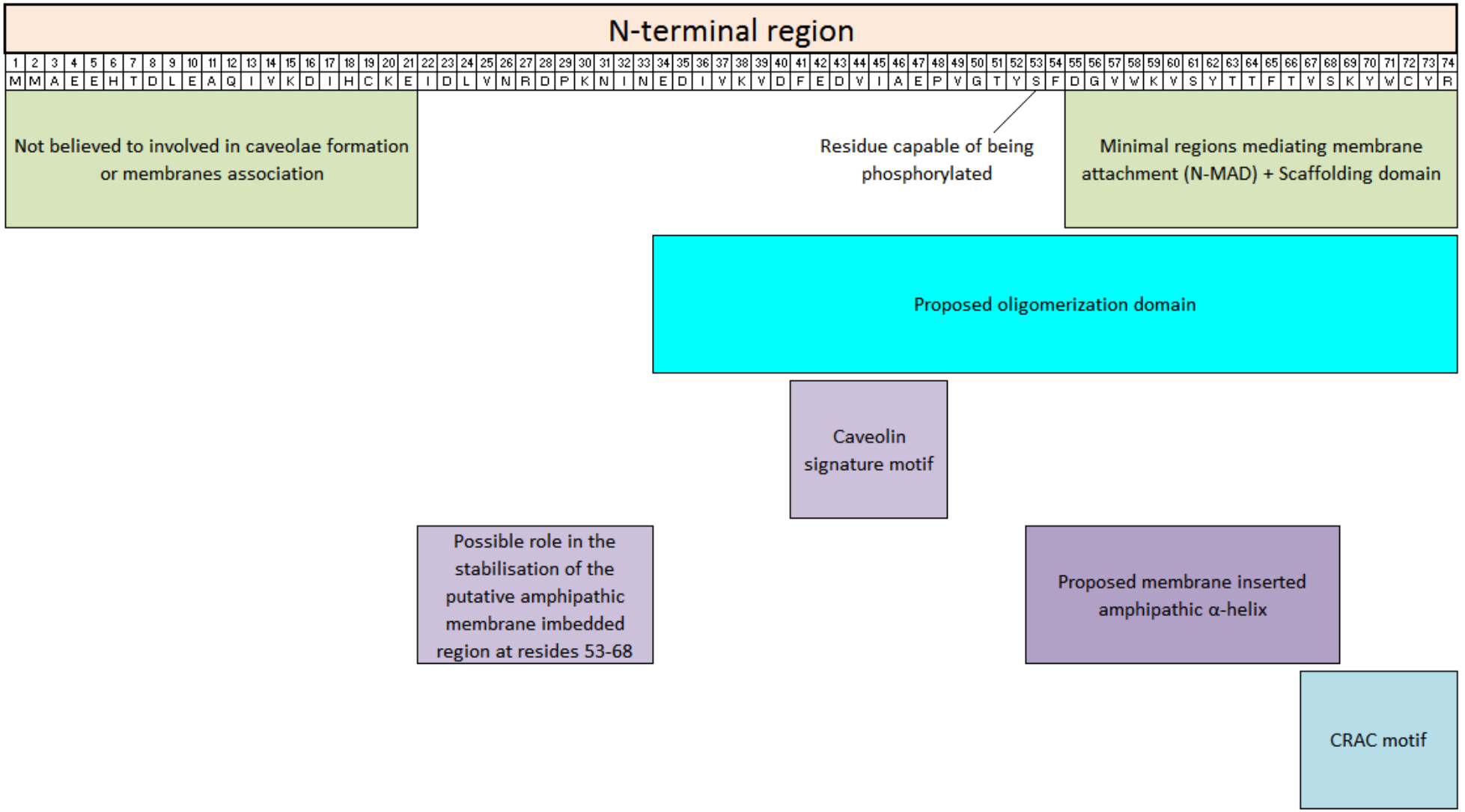
N-terminal region
1 2 3 4 5 6 7 8 9 10 11 12 13 14 15 16 17 18 19 20 21 22 23 24 25 26 27 28 29 30 31 32 33 34 35 36 37 38 39 40 41 42 43 44 45 46 47 48 49 50 51 52 53 54 55 56 57 58 59 60 61 62 63 64 65 66 67 68 69 70 71 72 73 74
M M A E E H T D L E A Q I V K D I H C K E I D L V N R D P K N I N E D I V K V D F E D V I A E P V G T Y S F D G V W K V S Y T T F T V S K Y W C Y R
Not believed to involved in caveolae formation or membranes association
Residue capable of being phosphorylated
Minimal regions mediating membrane attachment (N-MAD) + Scaffolding domain
Proposed oligomerization domain
Caveolin signature motif
Possible role in the stabilisation of the putative amphipathic membrane imbedded region at resides 53-68
Proposed membrane inserted amphipathic α-helix
CRAC motif

Figure 10: Key features within the N-terminal domain of Cav3.
Cartoon representation of the main features of the N-terminal region of Cav3. Many of the observations are based upon experiments on Cav1. Note the presence of the scaffolding domain, the region thought to associate the oligomer with the membrane, and part of the proposed oligomerisation domain. This region also contains the caveolin signature motif, which is conserved throughout the caveolin isoforms.

Caveolin-3: The C-terminal domain region

Like the N-terminal domain region, the C-terminal domain region is believed to be predominantly cytoplasmic and contains a region, at residues 108-123, called the C-terminal Membrane Attachment Domain (C-MAD). This domain is also proposed to mediate the protein association to the membrane, this time the trans-Golgi localisation membrane (Schlegel and Lisanti, 2000). This region contains a series of well-conserved hydrophobic residues potentially involved in the process of insertion of caveolin into the membrane (Kirkham et al., 2008). The C-terminal region is also palmitoylated and, although not essential for caveolae membrane localisation, is thought to stabilise the proteins membrane association (Dietzen et al., 1995; Kirkham et al., 2008). Interestingly, the C-terminal of Cav1 has been shown to interact with both the C-terminal and the N-terminal domain, potentially playing a role in oligomerisation (Song et al., 1997). Oligomerisation is discussed in more detail next. See Figure 11 for a summary of the key areas within what is termed the C-terminal part of Cav3.

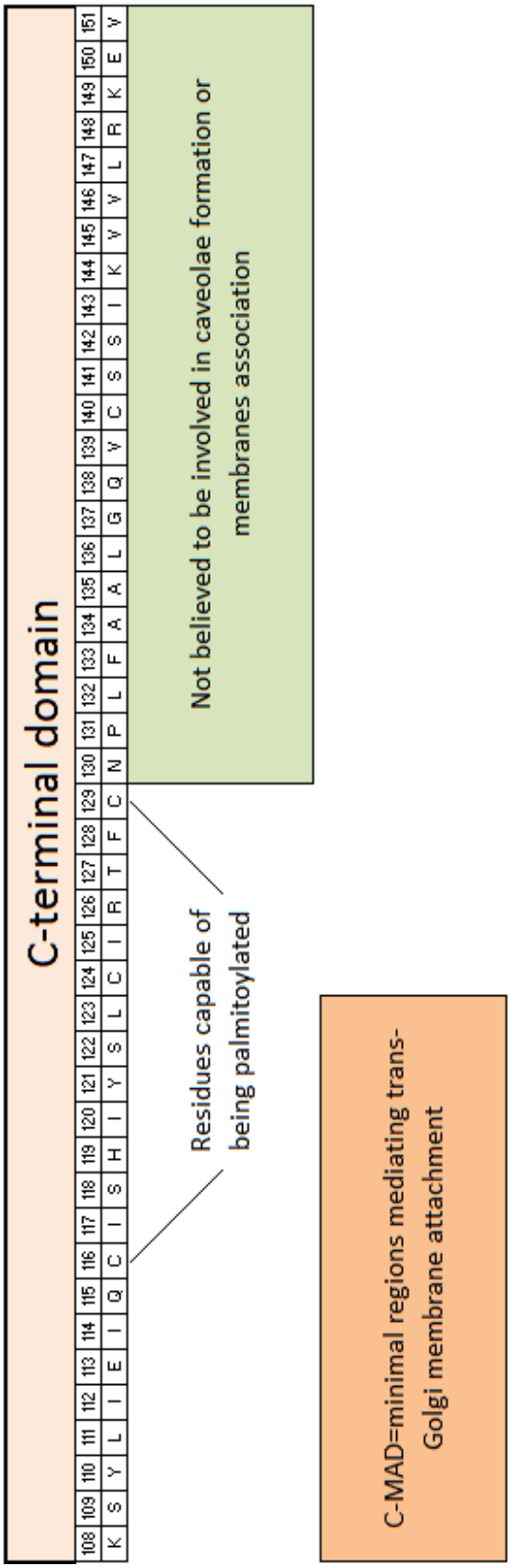

Figure 11: Key features within the C-terminal domain of Cav3.

Cartoon representation of the main features of the C-terminal region of Cav3. Many of the observations are based upon experiments on Cav1. Note the presence of the C-MAD region, the region thought to associate the oligomer with the Golgi membrane. This region also contains two of the cysteine residues believed to be palmitoylated.

Caveolin: Oligomerisation

Conflicting reports exist with regards to the number of caveolin molecules that form oligomers. Historically, the view of caveolin oligomers is that they are 350-400kDa and composed of 14-16 monomers. However, alternative views that depart from this assumption are starting to appear in the literature (Fernandez et al., 2002), including the research here.

Some of the initial experiments that investigated the size of Cav1 oligomers utilised velocity gradient centrifugation to separate Cav1. However, the size predictions varied considerably, finding that the protein migrated as a complex ranging from 200 to 600kDa (Li et al., 1996c; Monier et al., 1995; Sargiacomo et al., 1995; Tang et al., 1996). However, the Monier paper, despite focusing on the 400kDa isoform, shows that the 200kDa isoform is the predominant isoform, though for some reason this is not highlighted. Moreover, the Sargiacomo paper claimed that Cav1 migrates as a complex between 300-325kDa, but inspection of the western blots presented in the report finds that during the purification of Cav1 it migrated as a ~250kDa complex. In later gels, however, they go on to show this same protein migrates at ~360kDa. The Li paper shows that Cav1 predominantly migrates at ~443kDa; however, they extend this predicted size range from 200-443kDa, based upon trace expression detected at the lower molecular mass by immunoblotting. The study by Tang and co-workers specifically looked at Cav3. In this paper, the data clearly show that Cav3 migrated predominantly as an ~200kDa mass, with some trace protein detected at ~400kDa. Despite their clear observation of a predominantly 200kDa form of Cav3, they extend their assumption of size to include previous observances for Cav1 (i.e. the 350-450kDa predictions), thus resulting in their prediction that Cav3 oligomers are 200-450kDa. Thus, it is not clear as to the exact size of Cav1 oligomers, although it would seem likely that they exist as a size somewhere between 200-600kDa. Indeed, it is possible that a mixture of different sized oligomers exist. Based on this range, and on the assumption that Cav1 is ~24kDa, it is possible that Cav1 oligomers are composed of between ~8-25 individual monomers. Clearly, this is an area in need of further investigation.

In more recent research, Fernandez and co-workers utilised transmission electron microscopy (TEM) to examine a fragment of Cav1 (residues 1-101) after negative staining. They concluded that caveolin oligomers were heptamers, (Fernandez et al., 2002). This conclusion was based upon an image of a single raw particle with no image analysis. Furthermore, without immunoblot confirmation it is impossible to confirm what they had

purified/observed was indeed Cav1, as the sample is clearly not homogenous. Although the approach to determine Cav1 size and structure by more modern methods was novel at the time, it is clear that further work needs to be complete before any confidence on Cav1 structure can be taken.

With regards to the specific regions responsible for the oligomerisation, early mutagenesis experiments suggested that residues 61-101 of Cav1, termed the Oligomerisation Domain (OD), were crucial for oligomerisation (Sargiacomo et al., 1995). This region corresponds to residues 34-74 in Cav3. However, in contrast to this N-terminus based oligomerisation, more recent results suggest that when certain residues within the transmembrane region and the C-terminus are mutated, there is a reduction in the observed oligomerisation, suggesting a role for both the transmembrane region and the C-terminus in oligomerisation (Machleidt et al., 2000; Ren et al., 2004). Specifically, the Machleidt study has identified a region of 134-154 (107-127 in Cav3) within the C-terminus as important for oligomerisation, suggesting that the C-terminus is involved in oligomerisation. Further refinement of the specific area involved in oligomerisation eliminated the region corresponding to 130-151, which is not believed to contribute towards membrane localisation or oligomerisation (Kirkham et al., 2008). Thus, it is not clear as to which regions of the protein are responsible for oligomerisation. However, it would appear possible that there are multiple regions throughout all the major caveolin domains that are involved oligomerisation.

Interestingly, caveolins have been shown to form both homo-oligomers (Cav1/Cav1) (Scherer et al., 1997; Song et al., 1997), as well as hetero-oligomers (Cav1/Cav2) (Scheiffele et al., 1998); the functional significance of this oligomerisation is not entirely understood. Recent studies suggest that Cav1 and Cav3 also form hetero-oligomeric complexes in atrial cells (Volonte et al., 2008). Unfortunately, the relationship between Cav2 and Cav3 oligomers is poorly understood.

The C-terminal region of Cav1 (corresponding to residues 108-151 of Cav3) is thought to be involved in facilitating the interaction of oligomers to form higher order oligomer/oligomer structures (Song et al., 1997). This web of interconnected caveolin oligomers, plus the presence of cholesterol is thought to be responsible for the ‘bending’ of the membrane into the goblet formation that is caveolae (Razani et al., 2002b).

Caveolin-3: Scaffolding domain

It is generally believed that the scaffolding domain is the region within caveolin that targets the caveolin to the membrane (Arbuzova et al., 2000; Epand et al., 2005;

Schlegel and Lisanti, 2000), and holds the interacting proteins within the caveolae, thus allowing signalling proteins to concentrate at their locality. The scaffolding domain is a highly conserved region mapped to residues 82-101 of Cav1 (55-74 in Cav3) (Okamoto et al., 1998; Schlegel and Lisanti, 2000) and is believed to be the predominant site of interaction between caveolins and interacting partners. Indeed, a large number of studies attest to the importance of this region in protein-protein interaction (Couet et al., 1997; Davies et al., 2010; Garcia-Cardena et al., 1997; Garg et al., 2009b; Li et al., 1996a; Ohman et al., 2008). Perhaps one of the more characterised examples is that of the interaction of Cav1 with eNOS, where the scaffolding domain acts as a site of interaction, whereby it negatively regulates eNOS (Bucci et al., 2000; Garcia-Cardena et al., 1997). Interestingly, this region is generally shown to have an inhibitory effect on the protein with which it is interacting with e.g. the G-protein GTPase activity is suppressed, Src family tyrosine kinases auto-activation is inhibited, and K_{ATP} open channel probability is reduced (Couet et al., 1997; Davies et al., 2010; Li et al., 1996a; Okamoto et al., 1998). Though there are also instances in which it promotes activation of certain receptors, for example, the insulin receptor (Nystrom et al., 1999; Yamamoto et al., 1998).

Most of the work on the scaffolding domain has involved Cav1, however, alignment of Cav1 and Cav3 show a high degree of sequence similarity (61%; as shown in Figure 7), with the scaffolding region showing 75% identical residues (95% similar), thus it is often assumed to be also the case for Cav3 (Razani et al., 2002b). Indeed, experimental support for the role of specifically the Cav3 scaffolding domain as a key regulatory region has also been shown (Garg et al., 2009b; Kamishima et al., 2007).

As would be expected, mutations in this region have been shown to prevent both the membrane localisation of Cav3 (80-85% reduced cell surface expression), the localisation and activity of certain signalling proteins, and have been associated with a range of different diseases, such as LongQT (LQT9), myopathy, hypertrophic cardiomyopathy and LGMD-1C (de Paula et al., 2001; Fulizio et al., 2005; Hayashi et al., 2004; Matsuda et al., 2001; McNally et al., 1998; Minetti et al., 1998; Smythe et al., 2003; Vatta et al., 2006). The role of Cav3 in these diseases will be discussed in more detail below.

Knowledge of this scaffolding region has been used to scan for other possible interacting proteins. From these interacting proteins two Caveolin Binding Motif (CBM) were identified (Couet et al., 1997): [F/W/Y]X[F/W/Y]XXXX[F/W/Y], [F/W/Y]XXXX[F/W/Y]XX[F/W/Y], where X represents any amino acid. This CBM has

since been used to discover other potentially interacting proteins e.g. the pore forming unit (Slo1) of the MaxiK ion channel (Alioua et al., 2008).

Caveolin-3: Post-translational modifications

Caveolins have been shown to undergo a variety of post-translational modifications (PTMs), including palmitoylation and phosphorylation. Cav1 has been shown to have three palmitoylation sites located to the cysteines 133, 143, 156 in the C-terminal region of Cav1 (equivalent to 106, 116 and 123 in Cav3). Although palmitoylation appears to be involved in targeting proteins to membranes by enhancing their hydrophobicity, it has been shown, *via* triple point mutation, that the palmitoylation of caveolin is not be essential for membrane localisation or caveolae formation (Dietzen et al., 1995; Kirkham et al., 2008). However, this PTM is thought to play a role in the stabilisation of the complex within the membrane. Another potential role for these palmitoylation sites maybe in cholesterol trafficking from the endoplasmic reticulum to the plasma membrane. Indeed, two of the three palmitoylation sites, specifically 143 and 156 in Cav1, have been shown to be required for cholesterol binding and the transport of cholesterol to the membrane as part of a chaperone-complex (Uittenbogaard and Smart, 2000; Uittenbogaard et al., 1998). Interestingly, residue 133 did not appear to be involved in this, suggesting that the palmitoylation of each site may have differing roles to play. As well as a role in cholesterol targeting, the palmitoylation state may have further functional significance. For example, the palmitoylation of 156 has been shown to be required for Cav1 to couple with c-Src tyrosine kinase (Lee et al., 2001).

Cav1 has three known phosphorylation sites within it at Y6, Y14 and S80 (Cao et al., 2002; Fielding et al., 2004; Heibeck et al., 2009; Lee et al., 2000; Li et al., 1996d). Cav3 only has one putative phosphorylation site, S53, which is equivalent to S80 in Cav1. The phosphorylation state of caveolin is thought to play a regulatory role in the trafficking of caveolins/caveolae from the Golgi complex to the plasma membrane. Y14 can be deleted without affecting caveolae formation, indicating that it is not an essential residue for caveolae formation. In contrast the phosphorylation state of residue S80 has a direct effect on caveolin/caveolae trafficking to/from the PM, where its phosphorylated state maintained Cav1 at the Golgi, and its non-phosphorylated state localised Cav1 to the plasma membrane (Kirkham et al., 2008). Interestingly, the phosphorylation of Cav3 was recently shown to be a key event in the caveolae recycling of receptors (Cong et al., 2010).

The phosphorylation state of caveolins would also appear to be linked with cholesterol and the lipid environment. Phosphorylation of S80 in Cav1 resulted in a

decreased association with cholesterol, whereas mutation of this residue showed an increase in sterol binding (Fielding et al., 2004). Further, the elimination of sterol has been shown to dramatically increase the phosphorylation of Y14 (Fielding et al., 2004). An increase in cholesterol influx into the cell results in a reduction of phosphorylation of specifically Cav3 (Cong et al., 2010). Further, the Src phosphorylation of Cav1 has itself been shown to be dependent upon lipid based modifications of the kinase, in that Src needs to be myristoylated to phosphorylate Cav1 (Lee et al., 2001).

Certain protein-protein interactions also appear to be affected by the phosphorylation state of caveolins. For example, only upon the phosphorylation of Cav1 does it bind the proteins, Grb7 (Lee et al., 2000), and the C-terminal Src kinase (Cao et al., 2002). The varied implications of phosphorylation to caveolin function certainly require further elucidation. Indeed, the observance of cholesterol-dependent caveolin phosphorylation, phosphorylation-dependent caveolin interactions, and the caveolae-based recycling of certain receptors point to the possibility of caveolae location being an important site of phosphorylation dependent signalling control.

The role of caveolins in disease: Cancer

A large body of evidence now suggest that caveolins play a role in cancer. Interestingly, the role Cav1 appears to play in these cancers is a dichotomous one, where it acts as a tumour suppressor in some e.g. breast cancer (Mercier et al., 2012), but as a tumour promoter in others e.g. in prostate cancer (Freeman et al., 2012; Williams et al., 2005). Many of the reports of caveolin involvement focus, perhaps not surprisingly, upon Cav1 and Cav2 given that there expression is more ubiquitous than Cav3, which is specific to muscle cells (Song et al., 1996b; Tang et al., 1996; Way and Parton, 1996). Interestingly, Cav1 and Cav2 are located in a tumour suppressor 'hotspot' within chromosome 7 (7q31), a region found to be deleted in a range of different cancers (Engelman et al., 1998b). Further, the Cav1 promoter is observed to be hyper-methylated in multiple cancer cell lines, suggesting that its expression is altered (Cui et al., 2001; Engelman et al., 1999).

With regards to breast cancer, Cav1 expression levels have been found to be lowered in breast cancer cell lines used in cancer studies (Fiucci, 2002). Interestingly, the reintroduction of Cav1 to these cell lines can result in both a decrease in cell proliferation and reduction in epithelial-to-mesenchymal cell transition (EMT; a process characteristic of proliferating cells) (Fiucci, 2002). Cultured cells isolated from Cav1 KO mice models have revealed abnormalities in the growth pattern and shape of cells, as well as an increase

in EMT (Sotgia et al., 2006). Furthermore, in these models mislocation of E-cadherin and β-catenin has been observed (Sotgia et al., 2006), which is indicative of problems with cell-matrix adhesion. *In-vivo* support comes from mice models in which cells over-expressing Cav1 are injected into mice, and then allowing tumours to develop. These tumours have been shown to be markedly smaller and show less signs of proliferation and cell migration (Wu et al., 2008). Further, metastasising cells were shown to revert back to non-motile forms (Zhang et al., 2000). Finally, mammary tumour cell lines expressing mutant forms of Cav1 have been shown to show increased cell migration and invasion, as well as an increase in metastases (Bonuccelli et al., 2009). The mechanistic role of Cav1 in the anti-proliferation of breast cancer is not clear, though it may involve estrogen. Estrogen has a regulatory effect on the gene expression of a range of proteins involved in cell proliferation, and it has also been linked to breast cancer (Sommer and Fuqua, 2001). Moreover, the estrogen receptor is up regulated in cancer cells (Allred and Mohsin, 2000). Cav1 is known to be an important regulator of estrogen receptor levels (Zhang et al., 2005), and has been shown to negatively regulate its proliferative effects (Mercier et al., 2009). Indeed, estrogen receptors have been shown to be hyper-activated in the mammary glands of Cav1 KO mice and expression levels of proteins involved in increasing cell cycle activity have also been observed (Mercier et al., 2009). The mechanism by which Cav1 achieves this regulation of estrogen levels *via* the receptor is not entirely clear.

The role of Cav1 in cancer is by no means limited to just breast cancer, it has been shown to play a role in a multitude of cancer types, including lung (Ho et al., 2002; Williams et al., 2004), prostate (Freeman et al., 2012; Williams et al., 2005), kidney (Joo et al., 2004), and esophageal cancers (Kato et al., 2002), amongst many more. Further, as mentioned above, the role Cav1 plays does not appear to be consistent between cancer types. For example, in contrast to the apparent anti-proliferatory role in breast cancer describe above, Cav1 appears to advance the progress of prostate cancer development. Indeed, over-expression of Cav1 in adenocarcinoma cells and simultaneous decrease in stromal cells are both associated with prostate cancer progression (Freeman et al., 2012), suggesting a different role for caveolin in these two cancer-involved cell types.

Perhaps not surprisingly, given the different cell types in which Cav1 and Cav3 are expressed, Cav1 appears to have a much clearer role in cancer. Carcinomas, cancers which originate from epithelial cells, are by far the most common, and are generally derived from many of the cell types in which Cav1 is expressed, but not Cav3. In contrast, sarcomas, which are cancers derived from the mesenchyme are much rarer and develop in supporting and connective tissue. One such supportive tissue is the muscle. Given that Cav3 is muscle

specific, should it play a role in cancer, it is likely to be confined to this rarer class of cancers, particularly sarcomas of the muscle; for example, leiomyosarcomas and rhabdomyosarcomas. However, no evidence for a role of Cav3 in these types of cancer exists. Despite this, a role for Cav3 in cancer has been suggested, albeit in unexpected cell types. Cav3 KO mice in which breast tumour cells were orthotopically implanted were shown to be protected against tumour formation (Sotgia et al., 2009), suggesting that Cav3, in contrast to Cav1, had a role in tumour promotion. In addition, despite ordinarily not being expressed in the cells of the testis, over-expression of Cav3 was observed in seminomas, which are germ cell tumours of the testis (Kasahara et al., 2002). Clearly, a role for Cav1 is cancer is more established in the more common cancers. However, the role Cav3 may play in less common cancers has not been studied, though a small amount of evidence suggests that it may have a role to play. The differing role of the caveolins in cancer perhaps best highlights that Cav1 and Cav3 are different, and that what is assumed for one cannot always be assumed for the other. Indeed, the tissue specificity of their expression would appear to limit the scope to which disease they are involved in.

The role of caveolins in disease: Muscular dystrophy

Not surprisingly, given the muscle specific expression of Cav3, it has been shown to be associated with several particular forms of muscular disease and dystrophy, namely Limb-girdle Muscular Dystrophy (type 1C) (LGMD-1C), both distal and proximal myopathy, and Rippling Muscle Disease (RMD). Indeed, many Cav3 mutations have been observed in patients with these diseases (see Table 1 below). One of the key complexes involved in maintaining structural integrity in muscle cells is the Dystrophin-Glycoprotein (DG) complex, which is composed of several proteins and acts as a transmembrane link between the cytoskeleton of the cell and the extracellular matrix. Cav3 has been found to co-fractionate with dystrophin and its associated glycoproteins in both skeletal and cardiac muscle (Doyle et al., 2000; Song et al., 1996b; Sotgia et al., 2000). Ablation of Cav3 or alterations in the expression level of Cav3 both affect the ability of this assembly to target to the membrane correctly resulting in defects typical of dystrophic conditions, particularly LGMD-1C (Galbiati et al., 2001b; Galbiati et al., 2000a). Indeed, over-expression of Cav3 shows down-regulation of certain proteins (specifically dystrophin and beta-dystroglycan) of the dystrophin associated protein complex (Galbiati et al., 2000a), with an accompanying Duchenne muscular dystrophy phenotype, suggesting that both increase and decrease in Cav3 levels are associated with forms of dystrophy, and that maintenance of normal Cav3 levels is key towards maintaining normal muscle health (Galbiati et al.,

2001b). Dysferlin is one of the components of this complex, and for that reason the sarcolemmal expression of it is often detected in both dystrophic disease and Cav3 mutant studies. In a clinical study by Matsuda and co-workers, which looked at Cav3 mutations in patients with LGMD-1C, dysferlin sarcolemmal expression was shown to be severely reduced (Matsuda et al., 2001). Although muscular dystrophy is typically associated with skeletal muscle, the association of Cav3 with proteins of the DG-complex in both ventricular and atrial cardiac myocytes has also been observed, but this area has yet to be studied in any detail (Doyle et al., 2000). Indeed, muscular dystrophy has been shown to be associated with cardiomyopathy (Muntoni et al., 1993).

Interestingly, Cav3 null mice have been shown to develop a markedly disorganised T-tubule system in skeletal muscle (Galbiati et al., 2001a; Minetti et al., 2002). Thus, the possibility is plausible that the T-tubule system and hence Cav3 may be linked to dystrophy, due to the fact that T-tubules are important in muscle contraction (Minetti et al., 2002). Indeed, as discussed earlier in the Caveolae biogenesis section, Cav3 is known to localise to T-tubules (Minetti et al., 2002; Parton et al., 1997; Ralston and Ploug, 1999; Ueda et al., 2004).

An alternate possibility for Cav3 involvement in dystrophic conditions has also been suggested where the possibly disrupted Src tyrosine kinase signalling pathway, due to improper localisation caused by Cav3 mutation, may result in apoptosis leading to muscle damage by degeneration (Smythe et al., 2003).

Caveolins and heart disease

Caveolins play an important role in the maintenance of normal signalling events in cardiac physiology. Altered expression levels (both an up-regulation and down-regulation) and caveolin loss have been shown to play a role in a wide range of cardiomyopathies, including arrhythmias, atherosclerosis, cardiac hypertrophy, heart failure and myocardial ischemia (Aravamudan et al., 2003; Cohen et al., 2003; Fujita et al., 2006; Hayashi et al., 2004; Horikawa et al., 2008; Koga et al., 2003; Park et al., 2002; Tsutsumi et al., 2008; Vatta et al., 2006; Woodman et al., 2002). Indeed, the evidence points towards a cardioprotective effect of caveolin in co-ordinating normal signalling pathways.

The heart, although predominantly composed of cardiac myocytes, is also made of endothelial cells, smooth muscle cells and fibroblasts (Banerjee et al., 2007). Thus, all caveolin isoforms are expressed within the heart. Indeed, Cav1, Cav2 and Cav3 KO mice models all show cardiac problems (Drab et al., 2001; Park et al., 2002; Razani et al., 2002a; Woodman et al., 2002; Zhao et al., 2002). Until recently, it was thought that Cav3

was unique to cardiac myocytes, with Cav1 and Cav2 being expressed solely in the other cell types of the heart. However, recently both Cav1 and Cav2 have been shown to be expressed in cardiac myocytes (Cho et al., 2010; Robenek et al., 2008; Rybin et al., 2003), potentially confusing previous assumptions about the role of Cav3 in the cardiac system. However, it should also be noted though these observations are more the exception, rather than the case (Balijepalli and Kamp, 2008), and that other labs have not observed such findings (Woodman et al., 2002).

Some of the cardiovascular disease in which caveolins are believed to play key roles will be discussed next. Although the primary focus of this thesis is Cav3, due to the considerable overlap between all caveolin isoforms within the heart, all will be discussed were relevant.

The role of caveolin in increased blood pressure and atherosclerosis

The maintenance of arterial blood pressure is key to cardiovascular health. One key factor influencing arterial blood pressure is the protein, eNOS. eNOS has been shown to be expressed in both endothelial cells (where it interacts with Cav1) and cardiac myocytes (where it interacts with Cav3) of the heart, and is located at caveolae (Balligand et al., 1995; Feron et al., 1996; Feron et al., 1998; Garcia-Cardena et al., 1997; Shaul et al., 1996). The role of eNOS in endothelial cells of the cardiovascular system is to regulate nitric oxide (NO) levels in order to control the vasodilation/constriction, which directly affects blood pressure (Garcia-Cardena et al., 1996b). The role of NO in the cardiac myocyte is thought to involve the modulation of inotropic and chronotropic activity and thus the contractility of the heart by leading to phosphorylation of both troponin (Layland et al., 2002), L-type voltage-gated calcium channels (LTCCs) (Balligand et al., 1995) and the indirect inactivation of other proteins key in heart contractility, such as the muscarinic receptor (Feron et al., 1998). Both have been shown to interact with caveolins, where the interaction negatively regulates eNOS activity (Feron et al., 1998; Garcia-Cardena et al., 1996a; Ju et al., 1997). Indeed a series of KO mice studies attest to the importance of caveolins in the regulation of eNOS levels, where the reduction or abolition of either Cav1 or Cav3 expression results in the up-regulation or hyper-activation of eNOS respectively (Barouch et al., 2002; Ohsawa et al., 2004; Razani et al., 2001; Sunada et al., 2001), which, in turn, increase the levels of NO leading to a reduction in arterial blood pressure. Furthermore, over-expression of Cav3 has been shown to down-regulate NOS activity (Aravamudan et al., 2003).

Indeed, in the context of eNOS regulation, aberrant vascular tone regulation is often a key step in the development of atherosclerosis (Weiss et al., 2002). Given the importance of the lipid environment to caveolae formation, the role of caveolae in cholesterol homeostasis, and the caveolae location of receptors involved in cholesterol regulation (Babitt et al., 1997; Graf et al., 1999), it is perhaps not surprising that a role for caveolins in atherosclerosis has been suggested. Further, the movement of eNOS from caveolae to intracellular sites has been shown to occur upon elevated levels of oxidised low density lipoprotein (oxLDL), the so called 'bad cholesterol', which acts as a cholesterol acceptor (Blair et al., 1999; Uittenbogaard et al., 2000). The study suggests that the presence of oxidised low density lipoprotein thus impairs the NO-based activity by disruption of the caveolae.

The role of caveolin in arrhythmia

The Excitation-Contraction (EC) coupling process is an important stage in the cardiac cycle (Bers, 2002). It involves the conversion of an electrical stimulus (generated at the sinoatrial node) into a mechanical response, thus linking the cardiac Action Potential (AP) with the contraction of the heart. The efficient working of this process allows for the cells of the heart (cardiac myocytes) to contract systematically and rhythmically, thus causing the heart to beat and transport blood to the other parts of the body. The cardiac AP involves the influx and efflux of charged ions back and forth across the membrane. The whole process is under a great deal of control and the permeability to individual ions changes drastically throughout a single action potential. When this flux is mis-regulated, arrhythmia can generate, and subsequently cardiovascular disorders can manifest.

One particular arrhythmic disease in which Cav3 has been associated is Long QT syndrome, which is characterised by a pronounced QT (waves within the electrical cycle of the heart) propagation resulting in impaired repolarisation (Vatta et al., 2006). This particular form of LongQT is called LQT9 and a variety of mutations in Cav3 have been identified in patients with this disease, many of which locate to the proposed transmembrane region of Cav3 (see Table 1 below). Functional studies have supported a role for the mutation at residue 97 of Cav3 (from F to C), where a gain of function (late I_{Na}) of the $Na_v1.5$ sodium channel was observed (Vatta et al., 2006). Interestingly, the $Na_v1.5$ sodium channel is both located to caveolae and has been shown to co-immunoprecipitate with Cav3 in cardiac myocytes (Yarbrough et al., 2002). Despite the mutation, Cav3 remained associated with the Nav1.5 sodium channel suggesting that a lack of association between the two proteins was not the cause of the observed increase in late

sodium current (Vatta et al., 2006). Another arrhythmic disease in which Cav3 has been associated is Sudden Infant Death Syndrome (SIDS). Cronk and colleagues observed three missense mutations in Cav3 from the tissue of posthumous infants (Cronk et al., 2007). Subsequent voltage-clamp ion channel studies involving the $Na_v1.5$ sodium channel confirmed that all three Cav3 mutations resulted in an increase in late sodium current (I_{Na}) (Cronk et al., 2007). In addition, Cav3 was investigated as a potential candidate gene for Brugada syndrome, an arrhythmic condition characterised by ventricular fibrillation. Mutational analysis of samples from patients was complete. However, although multiple polymorphisms were observed, no mutations were observed, indicating that although Cav3 may still be involved, it is unlikely to be a major causal gene in Brugada syndrome (Koopmann et al., 2007).

The specific involvement of Cav3 in these arrhythmic conditions is not clear. It may be that disruption of the association between Cav3 and ion channel occurs as a result of a breakdown in caveolae formation. It is also possible that the way in which the channel localises or is transported to the membrane is altered. Further, given that caveolae are hubs for signalling, it could be that the ability of Cav3 itself to regulate the channel kinetics, signal transduction or for it to provide scaffolding for other important proteins is disrupted. Indeed, given the large list of supposed functions of caveolins and caveolae, there remain many ways in which it could impact upon ion channel regulation and hence arrhythmia generation. Indeed, many other ion channels are found in caveolae, including those involved in the cardiac action potential and EC-coupling - for example, HCN4 (Ye et al., 2008), $K_v1.5$ (Martens et al., 2001), $K_{ir}6.1$ (Davies et al., 2010; Garg et al., 2009a; Garg et al., 2009b), Na^+/Ca^{2+} exchanger (Bossuyt et al., 2002), and $Ca_v1.2$ (Balijepalli et al., 2006), $Ca_v3.2$ (Markandeya et al., 2011), $K_v11.1$ (Balijepalli et al., 2007). Furthermore, many of these ion channels are also found associated with their accompanying macromolecular signalling complexes, thus implicating many other potential candidates for arrhythmia generation. For example, when a subpopulation of the calcium ion channel, $Ca_v1.2$, were found to co-localise with Cav3 in rat ventricular myocytes, several other key proteins involved in its regulation were also found to be present where they formed a macromolecular signalling complex, namely the proteins β_2-adrenergic receptor, $G_{\alpha s}$, adenylyl cyclase, PKA, and PP2A (Balijepalli et al., 2006). Using siRNA to knock out Cav3 production and disrupt caveolae formation in neonatal mouse cardiomyocytes, they showed that β_2-adrenergic receptor regulation of $I_{Ca,L}$ was eliminated. Further support for large ion-channel associated macromolecular-complexes involvement in arrhythmia comes from one particular interesting observation in the Vatta study (Vatta et al., 2006), in which

a patient who had the F97C mutation in Cav3 remained asymptomatic until they used their albuterol inhaler (a β_2-adrenergic receptor agonist), upon which a pronounced QT was observed, thus linking other proteins to the disease other than just Cav3 or the actual ion channel. Indeed, $Ca_v1.2$ has been also associated with a range of arrhythmic conditions, including those in which Cav3 has been implicated (Long QT) (Splawski et al., 2004). As well as highlighting the importance of a caveolae-based role of β_2-adrenergic receptors in the regulation of the LTCCs, the two studies also show that caveolae localisation of this channel and its associated complex of functionally important regulatory proteins are essential to its regulation, and that this complex may be involved in arrhythmia genesis. These studies thus support the importance of Cav3 caveolae as signalosomes containing macromolecular complexes within them, and the potential importance of caveolae localisation in ion channel regulation and ultimately channelopathy and arrhythmia generation (O'Connell et al., 2004).

Another of the key proteins in regulating EC-coupling is the sarcoplasmic reticulum-bound Ryanodine receptor, which has been associated with a range of arrhythmic conditions (Priori et al., 2001; Tiso et al., 2001), and has been shown to co-immunoprecipitate with Cav3 (Head et al., 2005; Li et al., 2006; Scriven et al., 2005; Vassilopoulos et al., 2010). This will be discussed in detail in Chapter 4.

The role of caveolin in cardiac hypertrophy and heart failure

Hypertrophic cardiomyopathy is characterised by the thickening of the myocardium, and in most cases affects the left ventricular myocardium. Although this cardiac remodelling is often simply a normal result of exercise, it is in many cases pathogenic. The increase in myocardium size can result in the abnormal alignment of cardiac muscle cells, termed myocardial disarray. Thickened, unaligned heart muscle can result in an altered blood flow from the ventricle, which, in turn, can have many deleterious knock on effects. In cases the electrical system of the heart can also be affected resulting in arrhythmia. Unlike when the myocardium thickens as a result of high blood pressure, the cause of the thickening in cases of hypertrophy is not always obvious. A variety of proteins have been associated with cardiac hypertrophy. Cav3 is one such protein which has been shown to be up-regulated in hypertrophic cardiomyocytes (Kikuchi et al., 2005).

A series of KO animal models have helped shed some light on the role of caveolins in cardiac hypertrophy, indicating that caveolins are likely negative regulators of the disease. Mice in which Cav3 has been ablated show severe cardiac hypertrophy and

dilation (Woodman et al., 2002). This increased cardiac mass is thought to be due to hyper-activation of the MAPK cascade pathway, a key pathway involved in cardiac growth. Indeed, the p42/44 MAPK pathway has been shown to be hyper-activated, suggesting that Cav3 has a role as a negative regulator of p42/44 MAPK pathway. Further support for a role of Cav3 as a negative regulator of cardiac hypertrophy by inhibiting the MAPK pathway comes from experiments in which over-expression of Cav3 in rat cardiomyocytes has been shown to inhibit the hypertrophic response, and suppress the MAPK pathway (Koga et al., 2003). An interesting finding given that ERK and MEK are both co-localised to caveolae (Engelman et al., 1998a). Clinical support for a role of Cav3 in cardiomyopathy comes from the finding that some patients with familial hypertrophic cardiomyopathy have been shown to carry Cav3 mutations (threonine to serine at residue 63) (Hayashi et al., 2004). Further, the Hayashi study observed that a reduction in cell surface expression of Cav3 was observed, suggesting that the mutation in Cav3 had resulted in incorrect localisation of Cav3, thus indicating a possible mechanism by which the disease manifests.

The role of Caveolin in Cardiac Ischemia/Reperfusion Injury

Cardiac Ischemia/Reperfusion Injury (CIRI) is the damage to cells/tissue that can occur upon the reintroduction of an oxygen supply after a period of ischemia (reduction in oxygen supply). The reintroduction of oxygen (known as reperfusion) results in oxidative stress, were an imbalance in the normal redox state occurs resulting in an imbalance in reactive oxygen species (ROS) and free radical generation. These molecules then damage the myocardial tissue, cells and proteins of the heart. For example, increased levels of the free radical nitric oxide interact with superoxide (another free radical) to produce peroxynitrite, which is a powerful oxidant that can damage cells. In addition, elevated free radical levels can affect protein activity by modulating their activity, for example, S-nitrosylation of thiol groups can change a proteins function. Interestingly, if cells/tissues are treated to a brief ischemic insult in advance of CIRI, termed Ischemic Pre-Conditioning (IPC), then reperfusion injury is not observed, suggesting an adaptive mechanism can be 'pre-tuned' in readiness for CIRI (Murry et al., 1986). The specifics of this mechanism are not fully understood, though they are thought to involve a potentially cardiac-protective pathway called the Reperfusion Injury Salvage Kinase (RISK) pathway (Hausenloy et al., 2005; Hausenloy and Yellon, 2004), in which ERK1/2 and PI3K-Akt are thought to play a role, both proteins of which have been located to caveolae (Engelman et al., 1998a; Zundel et al., 2000).

Cav3 appears to play a role in both CIRI and IPC. After CIRI, a redistribution of Cav3 is observed (Ballard-Croft et al., 2006), which subsequently results in a decrease in the inhibition of NOS activity, and thus an increase in nitric oxide production (Ballard-Croft et al., 2006; Jasmin et al., 2012), which, although it is a normal biological secondary messenger, at high concentrations can react with superoxide to produce peroxynitrite, which is a damaging oxidant (Pryor and Squadrito, 1995). Furthermore, evidence for a change in Cav3 activity after CIRI is evidenced by an increased activation of the p42/44 MAPK pathway (Ballard-Croft et al., 2006), which Cav3 is believed to be a negative regulator of (Woodman et al., 2002). The role of Cav3 in IPC points towards a positive role in protection from CIRI. A combination of experiments that included the ablation of Cav3 expression or caveolae *via* KO models (Horikawa et al., 2008; Patel et al., 2007) or the use of MBCD (Patel et al., 2006), respectively, fails to exhibit IPC. In contrast, over-expression of Cav3 in mice results in an increased resistance to subsequent CIRI (Horikawa et al., 2008; Tsutsumi et al., 2008).

The evidence points to a dynamic role for Cav3 in both CIRI and IPC, where after CIRI, caveolae are disrupted, with knock-on functional consequences, such as altered NOS and p42/44 MAPK activity, but in IPC, aid in the cardiac tissue protection possibly by providing a role in the RISK pathway.

Clinically observed Cav3 mutations

As discussed above, Cav3 has been associated with many different diseases, many of which, understandably, involve the muscle, both skeletal and cardiac. A number of diseases have been shown *via* clinical studies to have Cav3 mutations associated with them. Furthermore, in some cases, functional assessment of this mutation has been assessed. For example the functional and mis-localisation consequences of mutant Cav3 have been explored using a combination of patch clamp techniques and immunohistochemistry and quantitative immunoblot analysis of patient biopsies. Indeed, aberrant ion channel activity has often been observed and membrane localisation of Cav3 has been shown to be reduced, or in some cases completely eliminated. Many show Golgi-complex accumulation of Cav3 suggesting that mutant forms of Cav3 are unstable and are retained at the Golgi complex where they undergo proteasomal degradation (Galbiati et al., 2000b; Galbiati et al., 1999). A table of all known Cav3 mutations and their associated disease is shown below (Table 1).

Mutation	V14L	R27Q	D28E	P29L	N33K	A46T	A46V	E47K	G56S	S61R	T64S	T64P
Associated Disease	LongQT (LQT9); SIDS	RMD; HyperCKemia; DM; LGMD-1C	RMD; LGMD-1C	HyperCKemia	DM	LGMD-1C; RMD; HyperCKemia	RMD	RMD	LongQT (LQT9); LGMD	Myopathy	Hypertrophic Cardiomyopathy	LGMD-1C
Region of Protein affected	N-terminal Region	N-terminal Region	N-terminal Region	N-terminal Region	N-terminal Region	N-terminal Region; Proposed Oligomerization Domain; Caveolin Signature Motif	N-terminal Region; Proposed Oligomerization Domain; Caveolin Signature Motif	N-terminal Region; Proposed Oligomerization Domain; Caveolin Signature Motif	N-terminal Region; Proposed Oligomerization Domain; Caveolin Signature Motif	N-terminal Region; Proposed Oligomerization Domain; Caveolin Signature Motif	N-terminal Region; Proposed Oligomerization Domain; Caveolin Signature Motif	N-terminal Region; Proposed Oligomerization Domain; Caveolin Signature Motif
Reference	Cronk et al., 2007	Vorgerd et al., 2001; Betz et al., 2001; Fulizio et al., 2005; Carbone et al., 2000; Tateyama et al., 2002	Fischer et al., 2003; Ullrich et al., 2011	Merlini et al., 2002	Fulizio et al., 2005	Herrmann et al., 2000; Vorgerd et al., 1999; Fulizio et al., 2005	Betz et al., 2001	Madrid et al., 2005	Vatta et al., 2006; McNally et al., 1998; de Paula et al., 2001	Fulizio et al., 2005	Hayashi et al., 2004	Matsuda et al., 2001

Mutation	A85T	L87P	A93T	F97C	F97DEL	P105L	R126H	S141R	64-66 ΔTFT	C72W	T78M	L79R
Associated Disease	LongQT (LQT9)	RMD	RMD	LongQT (LQT9)	HyperCKemia; RMD; LGMD-1C	LGMD-1C; RMD	LGMD	LongQT (LQT9)	LGMD-1C	LongQT (LQT9); LGMD	LongQT (LQT9); SIDS; RMD; Proximal Myopathy	LongQT (LQT9); SIDS
Region of Protein affected	Transmembrane domain	Transmembrane domain	Transmembrane domain	Transmembrane domain	Transmembrane domain	Transmembrane domain	C-terminal domain region	C-terminal domain region	N-terminal Region; Proposed Oligomerization Domain; Caveolin Signature Motif	N-terminal Region; Proposed Oligomerization Domain; Caveolin Signature Motif; CRAC motif	Transmembrane domain	Transmembrane domain
Reference	Vatta et al., 2006	Kubisch et al., 2003	Kubisch et al., 2003	Vatta et al., 2006	Cagliani et al., 2003	Minetti et al., 1998; Betz et al., 2001	de Paula et al., 2001	Vatta et al., 2006	Minetti et al., 1998	Vatta et al., 2006; McNally et al., 1998; de Paula et al., 2001	Vatta et al., 2006; Cronk et al., 2007; Ricci etl., 2011	Cronk et al., 2007

Table 1: Clinically observed Cav3 mutations.

Abbreviations: SIDS, sudden infant death syndrome. RMD, rippling muscle disease. DM, distal myopathy. LGMD-1C, limb-girdle muscular dystrophy (type 1C).

It is clear from the table above (Table 1) that despite involvement in a range of clinically different diseases, individual Cav3 mutations are often associated with more than one disease. Further, the symptoms observed for the diseases in which Cav3 mutations are involved often overlap (Fischer et al., 2003). For example, RMD patients exhibit slowly progressive weakness akin to that of LGMD-1C (Kubisch et al., 2003) and both show an abnormal proliferation of the T-tubules (Madrid et al., 2005). Further, immunohistochemistry often shows a reduction in the number of sarcolemmal caveolae concomitant with Cav3 sarcolemmal expression. Indeed, expression and activity of secondary proteins, such as dysferlin, NOS etc are also often affected in the different diseases. Indeed, the suggestion that caveolinopathies present as a clinical continuum is nothing new (Kubisch et al., 2003; Madrid et al., 2005).

Despite the observed molecular similarities between the Cav3 mutant associated diseases, differences are also still apparent. For example, in a study by Cagliani, patients heterozygous for the F97Del mutant showed molecular differences between skeletal and cardiac muscle cells (Cagliani et al., 2003). The skeletal muscle biopsies revealed markedly disorganised caveolae morphology and a severe deficiency in membrane Cav3 expression. In contrast, the cardiac muscle biopsies revealed that surface expression was still high (60% of control) and that caveolae structure and organisation was relatively maintained. This particular study highlighted that even for the same mutation different effects can be observed depending upon cell type. The difference observed is likely due to fundamental molecular network differences between the two cell types.

There are a variety of ways in which mutations in Cav3 could cause the aforementioned diseases. Many of the mutations are in key sites within caveolin believed to be involved in a range of different functions. For example, a mutation within one of the regions shown to be essential for monomer-monomer interactions will likely impair the oligomerisation of Cav3, which could result in large unstable aggregates of Cav3 to form that never get processed correctly and are thus never exported to the membrane from the Golgi complex (Galbiati et al., 1999; Minetti et al., 2002). Indeed, many of the studies found that the protein is not expressed at the cell surface and is, in fact, at the Golgi complex - a key sign of improper oligomerisation (see Caveolae biogenesis section above).

Given caveolin's role in T-tubule development, the observance in many Cav3 related diseases of a disrupted T-tubule system, and the important role of T-tubules in EC-coupling, it is perhaps not surprising that both arrhythmic and myopathic conditions are observed. Indeed, normal muscle calcium control is likely affected by the disrupted T-tubules, which could, in turn, cause improper and abnormal contraction of the muscle cells, both skeletal and cardiac.

Another key feature in the caveolin protein in which disease associated mutations have been observed is the scaffolding domain. This region has a functional role as a regulatory element by influencing the activity of other proteins (as described earlier in the Scaffolding domain section), as well as holding these proteins in the caveolae thus allowing signalling proteins to concentrate at the locality i.e. compartmentalisation. It is thus conceivable why mutations in this region would disrupt function and could easily have a cascade effect leading to impaired signalling.

Overall, it is likely that many factors affect the pathophysiological phenotype observed in the Cav3 associated disease including cell type, residue mutation site, individual mutations, mutations in secondary proteins and genes, and other patient specific factors, such as ethnicity, diet and other predisposing factors.

Protein expression systems for studying Cav3

There are number of ways to obtain a protein for structural and functional analysis, many of which depend upon what analysis is going to be completed with it subsequently. One common approach is to isolate a particularly protein by developing an extraction and purification protocol to get the protein from native tissue, i.e. from its natural environment. Although this has its strengths in that the *actual* protein is being purified, there are multiple downsides: 1) if mutational studies are planned, it is not possible to introduce mutations to the native protein, 2) depending upon the particular protein you are studying the size of the species and the tissue type can be a limiting factor e.g. a protein from the mouse spleen will not provide high yields; in contrast, a protein purified from bovine muscle will potentially provide high yields. 3) Understandably, sourcing a protein of human origin from a human will have its inevitable ethical issues. A common alternative to obtaining the protein of interest from native tissue is to recombinantly express it in a non-native host. For example, a human protein can be inserted into a vector then put into a cell line, such as *E.coli* for large scale expression thus allowing high yields. Furthermore, this approach allows for the introduction of mutations and allows the expression of human proteins without the ethical sourcing issues. There are a range of different expression systems

available that allow for the expression of certain features such as post-translational modifications that may ordinarily be omitted in non-native conditions. For example, prokaryotic cells (e.g. *Escherichia.coli*), yeast (e.g. *Saccharomyces cerevisiae*), insect cells (e.g. Baculovirus/Sf9), mammalian cells (e.g. adenovirus system), *in-vitro* cell-free expression systems (e.g. Rabbit reticulocyte lysate), and others such as Xenopus oocytes and transgenic mice and transgenic plants. However, for the purposes of relevance to this research work only a brief overview of *E.coli* and the Baculovirus/Sf9 system will be given.

E.coli is a well established method for rapid, bulk expression of high levels of heterologous proteins. However, it does not possess certain mechanisms such as those involved in post-translational modifications e.g. glycosylation, phosphorylation and acetylation. In addition, the prokaryote cell wall is quite different to the eukaryote cell wall. This is something to be considered if expression of fully functional membrane proteins is what is desired. Indeed, such proteins are often expressed into the periplasm and more often than not refolding is required.

In contrast to *E.coli*, the baculovirus expression system (that uses the baculovirus to infect the insect cells Sf9) is capable of many more post-translational modifications, including O-linked glycosylation, simple N-linked glycosylation, phosphorylation and acetylation. Moreover, given that they are eukaryotes, insect cells have a membrane more similar (than *E.coli*) to those of mammalian cells and are thus more suited to expression of membrane proteins. However, the downside to insect cells is that they generally take longer to grow. Moreover, given their historically reduced usage compared to well characterised systems such as *E.coli*, techniques are less well established and often much more expensive.

Published literature exists for expression of canine Cav1 in both the *E.coli* and the baculovirus/Sf9 expression systems. These two systems will be discussed in more detail in the relevant chapters (Chapter 2 and Chapter 3).

Structural techniques for protein structure determination

Despite the large amount of genetic information obtained from the many sequencing projects, there remains a distant paucity in the structural information available. This, in part, is due to the number of time-consuming steps required in order to purify a protein to homogeneity. Despite these many obstacles, many proteins have had their structures determined (as of Jun 12, 2012 there are 82347 structures in the Protein Data Bank database; http://www.rcsb.org/pdb). Knowledge of a protein's structure is important

towards understanding not only the individual proteins function, but also for understanding the physico-chemical mechanisms of the molecular machinery that compose the cell; an area of understanding very much still in its infancy. There are multiple examples of how structural biology has advanced our knowledge of the cardiovascular system e.g. (Goll et al., 1998; Minor, 2001; Serysheva et al., 2008; Walsh et al., 2009a; Winther et al., 2010), as well as in other physiological and pathophysiological processes (Wu et al., 2010). Drug design and targeting is greatly aided by knowledge of structure at atomic resolution e.g. (Atwell et al., 2004; Hopkins et al., 2006; Overington et al., 2006). Indeed, it is worthy of note that over 50% of pharmacological targets are membrane proteins (Terstappen and Reggiani, 2001), and that approximately one third of the genome codes for membrane proteins. However, of the number of solved structures in the PDB less than 1% are for membrane proteins (Doerr, 2009).

A variety of different techniques exist for protein structure determination; the principal techniques include X-ray crystallography, Nuclear Magnetic Resonance spectroscopy (NMR), Small-angle X-ray scattering and Transmission Electron Microscopy (TEM) methods. The development of X-ray crystallography for solving protein structure saw a major breakthrough in the 1950's when Perutz and colleagues employed the approach to solve the structure of myoglobin (Kendrew et al., 1958). Since then X-ray crystallography has by far contributed the most of any technique towards determining protein structure. For example, to date, 72242 protein structures have been determined using X-ray crystallography, in comparison NMR has provided 9406 and EM has provide 435 structures (figures acquired from the RCSB PDB Protein Data Bank and correct as of the 12th June 2012). Although, near atomic resolution can be obtained by using X-ray crystallography, the preparation of the protein crystals can be challenging for a number of reasons. Firstly, the technique requires very high concentrations of protein, typically 200µl at 5-25mg/ml. Moreover, membrane proteins often pose a major challenge due to factors such as the presence of detergents, and large extracellular highly flexible loops which can interfere with the crystallisation process. For comprehensive reviews of X-ray crystallography and its applications see (Smyth and Martin, 2000; Wlodawer et al., 2008). NMR is the second most commonly employed method of protein structure determination, having determined 9406 structures (figures acquired from the RCSB PDB Protein Data Bank and correct as of the 12th June 2012), and is also capable of determining structures at near atomic resolution. As with X-ray crystallography, NMR is not without its limitations. For example, high concentrations of protein are generally required, typically 2mg/ml (200µl at 0.1-3mM), and it is more generally suited for solving the structures of smaller

proteins (<70kDa). In addition, NMR-active atomic nuclei are required, and in many cases only naturally occurring isotopes are present, which are not NMR-active, thus making the determination of the protein structure of proteins from native tissue problematic. See (Dyson and Wright, 1996; Wüthrich, 1990) for reviews on NMR. TEM methods include many approaches including cellular tomography, 2D electron crystallisation and single particle analysis. TEM was originally developed in the 1930's by Knoll and Ruska. Since then TEM have now advanced so that the attainable resolution is some 4,000,000x that of the eye with the introduction of high field emission guns, improved optics, stability of the goniometer and software. The main technique employed in this thesis work is negative staining and single particle analysis (SPA). Briefly, the protein under study is imaged in solution, removing the rate-limiting step of crystallisation, requiring only low micrograms of protein, although at the cost of resolution. Typically SPA methods generate 3D structures that are at medium/low resolution i.e. >10Å. This technique has multiple strengths; it is technically simple, does not require high yields of protein sample, high contrast is achieved and radiation damage is minimised. However, preparation using metal stains can physically alter the protein structure, although this is not always the case. This method for protein 3D structure determination, as well as sample preparation methods, will be discussed in greater detail in Chapter 5.

Aims and objectives

As discussed above despite the plethora of claims on putative interactions and functional roles for Cav3, much is still not understood about this complex protein. As has been reviewed in the introduction to this thesis a knowledge of how Cav3 functions is important for not only understanding physiological process but also for the pathogenesis of an array of diseases.

Much is claimed about the structure of Cav3; however, most of this is either based upon observations for Cav1, which although similar in sequence, shows some distinct differences with regards to function. Furthermore, many inferences on structure have been pieced together based upon data from domains. Indeed, to date, no structure exists for any of the caveolins. The primary objective of this thesis was to determine the first 3D structure of this enigmatic protein, Caveolin-3.

Chapter 2 - The initial goal of this thesis work was to express and purify full-length Cav3 in the *E.coli* expression system following a protocol previously reported for Cav1. This was not successful. However, several constructs corresponding to domains of

Cav3 were also attempted, of which one, corresponding to the first 54 residues of Cav3, was successfully expressed in *E.coli*. The methodology development and optimisation of protein expression are described along with the characterisation of the domain that was successfully expressed and then purified.

Chapter 3 - The chapter describes the successful expression and purification of full-length Cav3 using the baculovirus/Sf9 expression system. The extensive optimisation of the expression and purification methods for the development of the protocol is detailed.

Chapter 4 - Caveolins are required for formation of caveolae. Previous research has shown that the recombinant expression of canine Cav1 in Sf9 cells resulted in an accumulation of caveolae-like vesicles. To address whether this could be replicated for human Cav3, we also investigated whether caveolae-like vesicles could be formed by preparing thin sections of infected Sf9 cells and examining the sections by TEM. Using this approach clusters of 'caveolae' were observed, although not in the numbers described for Cav1, the significance of which is discussed in the chapter.

Given that Cav3 is found in the sarcolemmal membrane, mature T-tubules and possibly even in the SR, paired with the fact that each of these regions is involved in EC coupling, it is a logical question to ask of what role Cav3 is playing in these regions? Is it simply structural, in that it helps form and maintain these key cellular structures or, given its known role in the regulation of proteins, including those involved in calcium handling, does it act functionally at these sites by regulating certain proteins involved in EC coupling? One of the proteins underlying EC coupling is the Ryanodine Receptor (RyR2) however, not much is known about the relationship between Cav3 and RyR2. This Chapter investigates, "does Cav3 interact with the RyR"? To probe the putative interaction between Cav3 and RyR, purified RyR was required. Therefore the first step was the purification of RyR1 from sheep skeletal muscle. RyR1 rather than RyR2 was selected as yields of the skeletal muscle isoform are significantly higher as well as there being a more established protocol in the Kitmitto lab. Experiments indicated a direct interaction between the two proteins, with a bioinformatics analysis of both RyR1 and RyR2 primary sequence identifying multiple putative caveolin binding motifs.

Chapter 5 - As mentioned above there are currently no 3D structures available for any full-length caveolin. This chapter describes how the purified full-length Cav3 isolated from infected Sf9 cells was used to determine a 3D structure using transmission electron

microscopy images and single particle analysis. The model is described in relation to its proposed function and compared to the current understanding of Cav3 structure.

Paper submitted for publication: Molecular architecture of human caveolin-3. Gareth Whiteley, Richard F. Collins and Ashraf Kitmitto.

Chapter 2: Expression and purification of full-length Cav3 and several domains in *E.coli*

2.1. Introduction

The main objective of this part of the project was to express pure, homogeneous full-length Cav3, as well as a range of Cav3 domains with yields sufficient for biophysical analysis; including 3D structure determination and characterisation of interactions with putative binding partners. Thus, it is important that the expression system is optimised to ensure maximum yield and homogeneity of the sample. A published protocol (Li et al., 1996c) was used as a starting point, but many subsequent modifications of this expression and purification protocol were also explored.

The earliest attempts to express and purify a member of the caveolin family were by Li and co-workers, and Scherer and co-workers (Li et al., 1995; Scherer et al., 1995). However, in subsequent publications, they concede that this work was only a partial success (Li et al., 1996c). In these earlier attempts, Cav1 fused to a Glutathione S-transferase (GST) protein was expressed in Madin-Darby canine kidney (MDCK) or Fischer rat thyroid (FRT) cells and purification involved two main steps: Firstly, they isolated caveolin rich membrane domains and then isolated the GST-Cav1 fusion protein from this fraction. However, cleavage of the GST-tag from the full-length Cav1 resulted in an unstable non-native Cav1. Given this lack of success, they went on to explore the possibility of expressing Cav1 without the GST-tag (Li et al., 1996c). This system appeared to work, and they successfully expressed and purified Cav1 and therefore it seemed sensible to employ this method here in a first attempt to over-express and purify Cav3; although the protocol was for canine Cav1, and not human Cav3.

More recently, Fernandez and co-workers (Fernandez et al., 2002) expressed peptides of all three human caveolins: Cav1, Cav2 and Cav3. However, these were incomplete proteins, and did not contain large portions of the C-terminus. Moreover, in the published paper there were no details regarding the level of purity of the peptides. In addition, Electron Microscopy (EM) images showed that many other proteins were present, thus indicating a lack of purity. To-date, fully functional, full-length, soluble, recombinant human Cav3 has not been expressed and purified to homogeneity.

2.1.1. *E.coli* expression system

Molecular biology has an array of different protein expression systems (each having its own strengths and weaknesses) that can be used to express heterologous

proteins. For example, prokaryotic cells, yeast, insect cells, mammalian cells, *in-vitro* expression systems, amongst many others such as transgenic animals and plants (for an in-depth review see (Fernandez and Hoeffler, 1999)). A brief overview of the *E.coli* system will be given here as this was the expression system employed in this part of the thesis research work.

E.coli is a well established expression system for rapid, bulk expression of high levels of heterologous proteins, which has the advantage of being relatively affordable. For these reasons, *E.coli* is often the first choice of expression system. However, it is not without downfalls, for example, it does not possess certain mechanisms such as those involved in post-translational modifications e.g. glycosylation (both O-linked and N-linked), phosphorylation and acetylation. In addition, the prokaryote cell wall is quite different to the eukaryote cell wall, which can prove problematic when trying to express fully functional membrane proteins.

Due to *E.coli* lacking many of the mechanisms required to produce the fully folded, functional, recombinant protein it can sometimes lead to the formation of inclusion bodies (Kane and Hartley, 1988). These insoluble aggregates are collections of misfolded or denatured proteins, and are created when the host cell cannot form the correct intermolecular associations required when folding the native protein. Over-expression of recombinant protein can often lead to the formation of insoluble aggregates (inclusion bodies) due to the strain placed on the cells mechanisms and resources. In addition to forming inclusion bodies, another reason why recombinant protein expression can fail, is when the recombinant protein is toxic to its host. Ultimately, when expressing a non-native protein in a foreign host the goal is for it to be in the soluble fraction.

A variety of conditions can affect the expression of soluble recombinant protein; most notably, the growth conditions, the vector and the addition of solubilisation tags. Multiple growth conditions exist, such as the temperature of induction, time of induction, duration of growth, the cell density at induction, the growth media type, IPTG concentrations and antibiotic concentration. These are often the first factors altered when trying to increase expression of soluble recombinant protein.

2.1.2. Growth conditions: Temperature

Lowering the temperature can help reduce the degradation and aggregation of proteins formed from misfolding (Schein and Noteborn, 1988). It can also help in the expression of hydrophobic proteins by reducing the expression rate, and thus preventing the host's translational machinery from becoming saturated. In addition, by reducing the

temperature of induction, and hence slowing the growth of the cells, it can allow the cell to handle the rate of rare codon usage. It has also been shown that lowering the temperature can change the set of proteins expressed by the host (Jones et al., 1987), which may in turn effect the expression of the recombinant protein.

2.1.3. Growth conditions: IPTG

Isopropyl-β-D-thiogalactopyranoside (IPTG) is a compound that induces transcription of the proteins within the *lac* operon i.e. the recombinant protein, by binding to the *lac* repressor, thus preventing repression by the actual repressor. Higher concentration levels of IPTG maximise the likelihood of every vector being expressed, but can come at a cost to the cell. For example, uptake of IPTG by cells require more energy and high concentrations of IPTG can interfere with cell growth. In contrast, low levels of IPTG can sometimes be insufficient to activate every plasmid, thus reducing expression. Getting this level optimum is a common practice for maximising the expression of recombinant proteins and needs to be fine-tuned for each recombinant protein being expressed (Huang et al., 1994).

2.1.4. Growth conditions: Growth media

The growth media provides the nutrients required for the host cells to grow (Bertani, 1951). However, controlling the exact makeup of this media can allow manipulation of certain features and increase cell growth (Schaechter et al., 1958). For example, Super Optimal Broth (SOB), which is usually used during transformation to aid in the transformation efficiency (Hanahan, 1983), can allow greater growth of cells due to increased levels of amino acids, peptides and Mg^{2+}. Another option is to use SOC (Super Optimal Broth with Catabolite repression), which is a growth media that has an increased concentration of glucose. This can be used to help grow cells that carry a potentially toxic protein. Under normal conditions, *E.coli* will utilise glucose as a primary energy source and repress the transcription of genes involved in the utilisation of alternative energy source, such as lactose (Deutscher, 2008). Thus, the *lac* operon is tightly repressed, and leaky transcription is reduced. One way to reduce leaky expression is to suppress the lac operon, in which the potentially toxic protein is inserted, whilst the cells grow (Sun et al., 2009). This can be achieved by increasing the glucose concentration in the media in which the cells are growing. Once cell concentration reaches a high level, expression of the toxic protein can be induced and whatever protein is present collected.

Propriety media, such as Magic media (Invitrogen) are also available, which claim to maximise the yield of fully folded soluble recombinant protein.

2.1.5. Growth conditions: Cell concentration at induction

Certain proteins are expressed more optimally at certain stages of the growth phase. Thus, inducing the expression of the recombinant protein at different cell densities can sometimes alter the express and solubility of recombinant proteins.

2.1.6. Growth conditions: Ampicillin concentration

Although required to ensure only cells that have taken up the plasmid survive, ampicillin can also have the adverse effect of reducing the viability of the cells and in turn affecting the growth curve (Yourassowsky et al., 1985).

2.1.7. Vector and tag choice

Appropriate choice of the vector is important for maximising the yield of purified, soluble, recombinant protein. The vector choice is important for codon usage and the conditions of induction, such as suppression and expression regulation, as well as the fusion protein and affinity/solubility-tags fused to the recombinant protein.

To aid both solubility and purification, recombinant proteins are often expressed with a series of tags fused to them. Two main types of tags are available: Affinity tags and solubilisation tags. The affinity tags, such as the His-tag, do not affect the solubility of the protein, but aid in its purification by allowing the recombinant protein to bind immobilised transition metals, such as Ni^{2+} *via* immobilised metal affinity chromatography (IMAC). Solubilisation tags can help maintain the solubility of the recombinant protein, by helping to prevent degradation of the recombinant protein. The mechanism by which they achieve this is poorly understood, though it is thought that the presence of the solubilisation tag during translation of the fusion protein can increase the efficiency of the translation from mRNA.

Interestingly, the terminus to which the tag is fused is an important factor. For example, the maltose binding protein (MBP) solubilisation-tag only works if expressed at the N-terminus (Sachdev and Chirgwin, 1998). Suggesting that the order by which the fusion proteins emerge from the ribosome strongly influences whether the recombinant protein is folded into a soluble or insoluble state. Examples of solubilisation tags particularly relevant to this chapter include the thioredoxin and SUMO-tags. Both are

thought to assist in the correct folding of the protein, as well as prevent the protein from forming inclusion bodies.

Vector	Size (without insert)	Antibiotic Resistance	Fusion Protein		Terminus of Fusion
			Affinity Tag	Solubility Tag	
pEX-C-His	4.6kb	Ampicillin	6xHis-tag	None	C
pEX-His-Trx	3.2kb	Ampicillin	6xHis-tag	Thioredoxin	N
pET-His-SUMO	5.6kb	Kanamycin	6xHis-tag	SUMO	N

Table 2: Summary of vectors relevant to this chapter.

2.1.8. Lysis

Once the expression system is expressing the recombinant protein, the next important stage is the lysis of the cells in order to extract the recombinant protein into the soluble fraction. A vast myriad of lysis buffer compositions exist, with Tris and PBS being two of the more commonplace ones, as well as the ones used here. The choice of detergent is particularly important when working with membrane proteins since it is unlikely that they will be within the soluble fraction of the cell. Many different categories of detergent are available, each group differing in their hydrophilic head group. The ones relevant to this thesis will be briefly discussed here.

Non-ionic detergents are generally the gentler of the detergents and are suitable for maintaining native conformation and function. Such detergents include n-dodecyl-β-D-maltoside (DDM) and Triton X-100. Anionic detergents, although good for ensuring the membrane is entirely disrupted, are often very strong and can actually denature proteins. Such detergents include N-laurylsarcosine (NLS). Zwitterionic detergents are electrically neutral and, like non-ionic detergents, are often used to maintain the native state of the protein. The choice of detergent is not purely based upon its ability to solubilise the protein away from the membrane, but also should be considered in the context of maintaining protein function as well as the planned purification strategy. For example, detergent with low CMCs would not be optimal for studies involving reconstitution whereby the detergent is removed by dialysis.

Key	Detergent	Category	CMC (mM)
DDM	n-dodecyl beta-D-maltoside	Non-ionic	0.15
TX100	Triton X-100	Non-ionic	0.2-0.9
CHAPS	3-[(3-cholamidopropyl)dimethylammonio]-1-propanesulfonate	Zwitterionic	6
NLS	N-laurylsarcosine	Anionic	14.57

Table 3: A list of detergents used in this thesis.

2.1.9. Dealing with insoluble aggregates

Ideally, the recombinant protein would be found in the soluble fraction. However, if the recombinant protein forms inclusion bodies regardless of the conditions used, this does not necessarily mean that fully functional, correctly folded recombinant protein is not attainable (Carrió and Villaverde, 2001). Indeed, the formation of inclusion bodies can actually facilitate purification as they are usually highly homogeneous. Examples exist of where recombinant proteins that formed inclusion bodes, were treated to strong denaturants, refolded and structural studies were subsequently complete using them (Nagai et al., 1988). Moreover, there are instances where the formation of inclusion bodies has, in fact, protected the recombinant protein from proteolysis (Hellebust et al., 1989). These examples, however, are more the exception rather than the case.

The challenge is to refold the protein into the correct conformation. This involves the initial use of strong denaturants, such as 8M Urea or 6M guanidine, to break down the inclusion bodies and any erroneous protein conformations, by interfering with non-covalent intra-molecular interactions. The proteins are then dialysed into alternative buffers more suited to allow the protein to take on its correct conformation. Establishing the optimum buffer, in which the protein will refold correctly, can be very time-consuming.

2.1.10. Purification

After solubilisation of the membrane protein a purification protocol is required to isolate the protein from the other components. Since the proteins and domains in this chapter were expressed with metal affinity tags the first stage of purification in this chapter involved immobilised metal ion affinity chromatography (IMAC). IMAC is a non-biospecific purification technique that allows proteins to be separated based on the

interaction of proteins with a specific ligand, in this case immobilised charged metal ions. The most commonly used ones are nickel, copper, cobalt and zinc. This interaction is reversible, and the bound proteins can be separated (eluted) from the bound metal ions by increasing the concentration of a competitive ligand, such as imidazole. Certain proteins elute at different imidazole concentrations, so altering the concentration of imidazole is a key factor when trying to purify proteins to homogeneity. See Figure 12 for an outline of the concept.

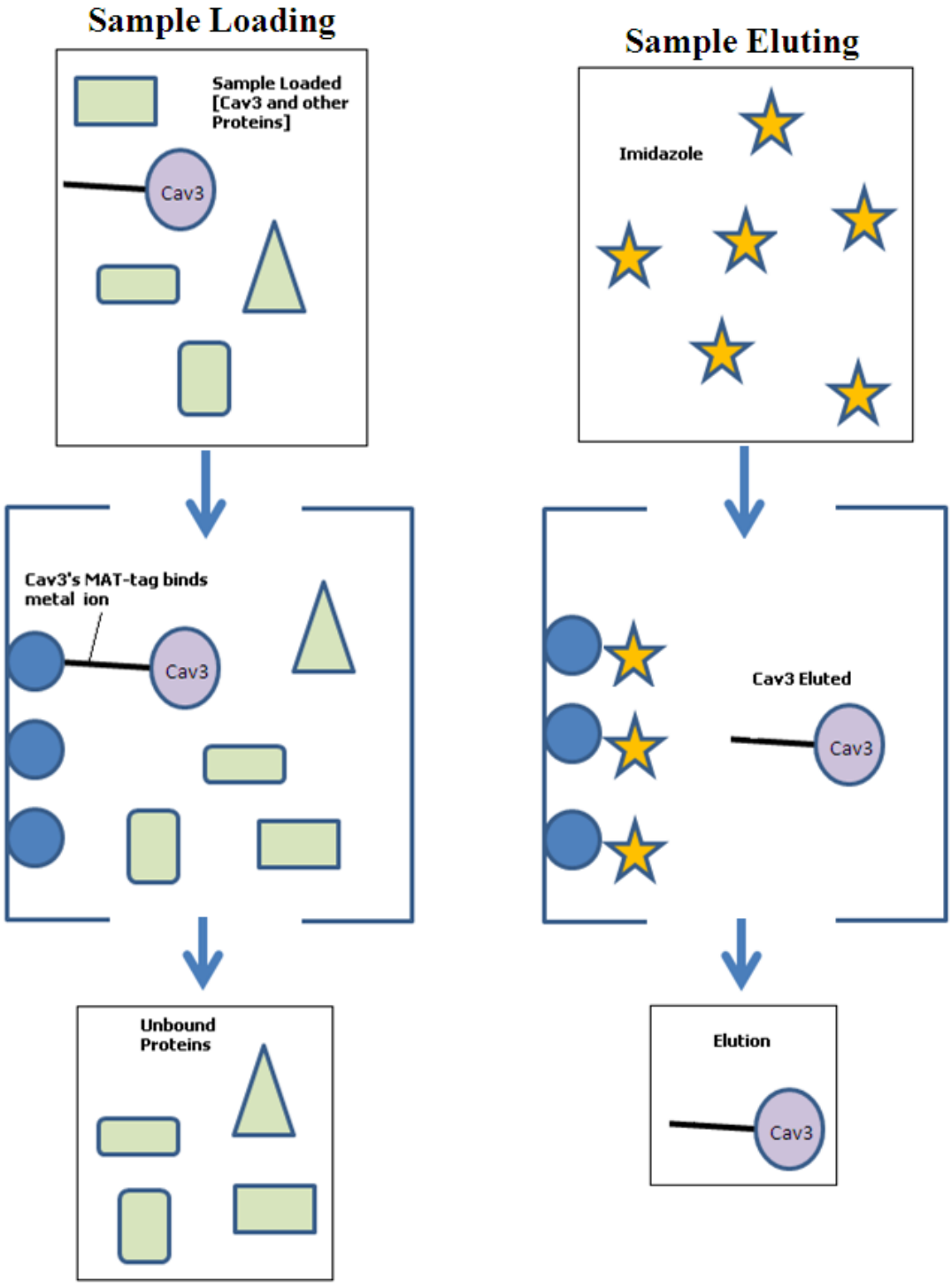

Figure 12: Outline of the IMAC concept.

Left: Proteins that can bind the metal ions are retained, whereas those that cannot bind metal do not. Right: Imidazole can be used to elute the bound proteins.

2.1.11. Expressing protein domains

Expression and purification of full-length proteins can often prove difficult for a myriad of reasons. Certain regions within a protein may prove particularly unsuited to expression. For example, hydrophobic regions can promote aggregation, or certain regions may prove to be toxic, or interfere with the host's housekeeping. To circumvent these potential issues, regions thought to be potentially problematic can be removed from the recombinant protein, and instead chosen domains can be expressed. Generally it is advisable to make a range of different protein domains. The only work previously completed that successfully expressed and purified stable domains of Cav3 was in the aforementioned Fernandez paper (Fernandez et al., 2002). The region they purified correlates to the first 74 residues of Cav3 (termed here N^{1-74}).

Detailed in this chapter is work describing the expression of a range of domains from Cav3. Each domain was designed to incorporate a different subset of the full-length Cav3 features. See Figure 13 for a summary of the domains explored and their key features. Several constructs were designed, including the first 54 residues (termed N^{1-54}), the first 74 residues (termed N^{1-74}), the first 101 residues (termed N^{1-101}), and residues 92-151 (termed here C^{92-151}). Fernandez and co-workers utilised the GST-tag, whereas we have employed both the 6xHis-tag and the SUMO-tag.

Name of the domain used in this thesis	Region of Cav3	Length	Scaffolding Domain	Oligomerization Domain	Transmembrane Region	Additional Features	Associated Mutations	Associated Diseases
N1-54	1-54	54	No	Partial	No	Contains a Phosphorylated Residue	V14L, R27Q, D28E, P29L, N33K, A46T, A46V, E47K	LongQT, SIDS, RMD, DM, LGMD,
N1-74	1-74	74	Yes	Yes	No	N/A	V14L, R27Q, D28E, P29L, N33K, A46T, A46V, E47K, G56S, S61R, T64S, T64P, 64-66ΔTFT, C72W	LongQT, SIDS, RMD, DM, LGMD, Hypertophic cardiomyopathy
N1-101	1-101	101	Yes	Yes	Yes	N/A	V14L, R27Q, D28E, P29L, N33K, A46T, A46V, E47K, G56S, S61R, T64S, T64P, 64-66ΔTFT, C72W, T78M, L79R, A85T, L87P, A93T, F97C, F97Del, P105L, R126H, S141R	LongQT, SIDS, RMD, DM, LGMD, Hypertophic cardiomyopathy, PM
C92-151	92-151	60	No	No	Partial	Contains all three palmitoylation sites	P105L, R126H, S141R	LongQT, LGMD, RMD

Figure 13: Key features of the domains expressed in this thesis.

2.1.12. Secondary structure: Circular dichroism

In order to characterise the secondary structure of expressed and purified Cav3 protein, circular dichroism (CD) was employed in this chapter. In brief, CD is a technique that allows the basic characterisation of a protein or peptide's secondary structure. It works by detecting the difference in the absorption of right-hand *versus* left-hand circularly polarised light by the sample being analysed. Each secondary structure conformation has a distinct CD spectrum. Thus, resultant spectra for the protein being analysed can be compared to this reference set (see Figure 14). There are multiple ways to interpret the data produced from CD: 1) Visual interpretation of the spectra profile, 2) Calculate the α-helix content using specific data from the output, 3) Use the complete data set to calculate the content of multiple structural features.

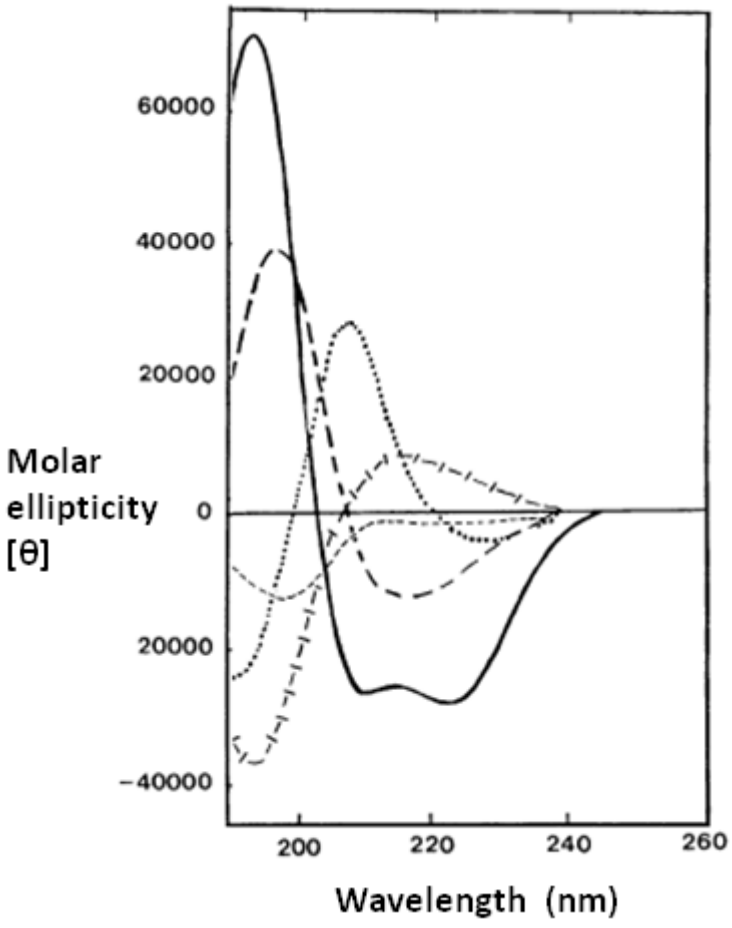

Figure 14: Example CD spectra for various types of secondary structure.
Solid line, α-helix; long-dashed line, anti-parallel β-sheet; dotted line, type I β-turn; cross dashed line, extended 3_{10}-helix; short dashed line, random coil. Adapted from (Kelly et al., 2005).

Unless the CD spectra shares a considerable match with any of those in Figure 14, visual interpretation is often not enough, as individual proteins are often made up of

multiple regions with different secondary structure features, which can skew the CD spectra; in these cases analysis of the raw data is required. Two approaches are available, one which involves using sections of the data, such as data at specific wavelengths that can be used to calculate specific structural features, and one method that utilises the complete data set to examine for multiple different structural features. Examples of the prior include equations that utilise data at 222nm to predict the percentage of α-helical content (Scholtz et al., 1991). However, as with all predictions, interpretations should be made with caution (Kelly et al., 2005). Moreover, this method does not provide any information on β-sheet content. Examples of approaches that utilise the *complete* dataset include DICHROWEB, an online CD interpretation tool (Whitmore and Wallace, 2004, 2008). DICHROWEB employs a number of analysis programmes to help calculate secondary structure, each differing in the exact approach and algorithm. These approaches give more detailed predictions on the secondary structure, and also take into consideration large reference datasets to aid prediction.

2.1.13. Flow of work

An overview of the key sections, the main tasks, the variables considered and the flow of work in this chapter is shown in Figure 15.

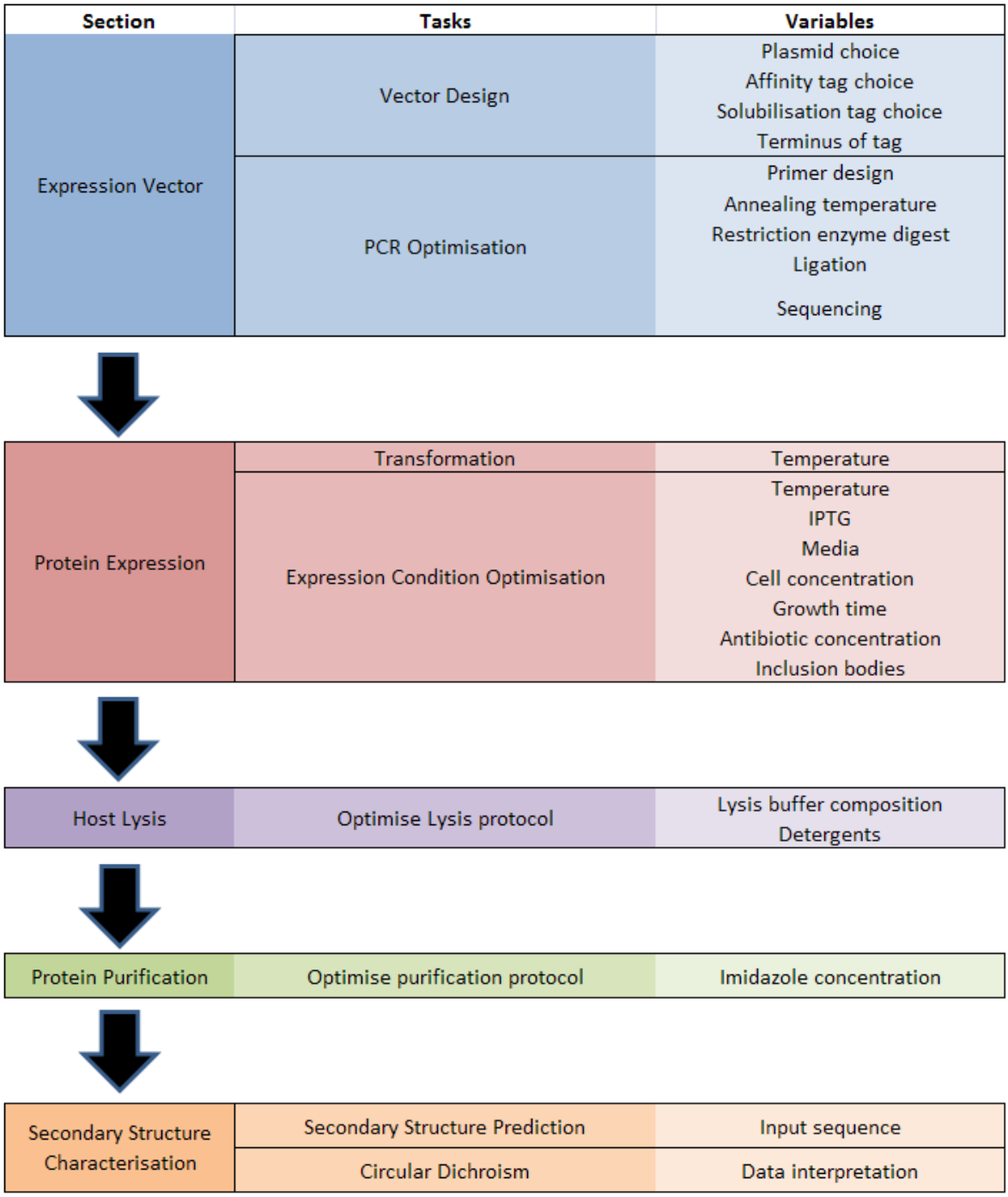

Figure 15: An overview of the research work described in this chapter.

2.2. Materials and Methods

2.2.1. General biochemistry assays

Material suppliers

Unless otherwise stated, all materials were purchased from Sigma.

Gel electrophoresis

Sodium dodecyl sulphate polyacrylamide gel electrophoresis (SDS-PAGE) was performed according to Laemmli (Laemmli, 1970). Protein samples prepared for gel electrophoresis (gel samples) were left at room temperature for 30min before loading. A 5x sample buffer (60mM Tris-HCl, 25% (v/v) glycerol (Fisher Scientific), 2% (v/v) SDS, 14.4mM 2-mercaptoethanol, 0.1% (w/v) bromophenol blue) was added to each sample at a ratio of 4:1 (protein:sample buffer) for visualisation and to aid with gel loading. 15% acrylamide concentration running gels were made (1x0.75mm) using 2.15ml $_{dd}H_20$, 2.5ml 1.5M Tris-HCl pH8.8, 0.4% (w/v) SDS, 5ml 30%acrylamide/0.8%bisacrylamide solution (National Diagnostics, Ultrapure ProtoGel) (v/v), 5µl TEMED (Bio-Rad), 50µl 10% ammonium persulphate. 5% stacking acrylamide concentration gels were made using 2.3ml $_{dd}H_20$, 1ml 0.5M Tris-HCl pH6.8, 0.4% (w/v) SDS, 670 µl 30%acrylamide/0.8%bisacrylamide solution (National Diagnostics, Ultrapure ProtoGel) (v/v), 5µl TEMED (Bio-Rad), 30µl 10% ammonium persulphate. In some experiments 3% and 5% running gels were also employed and made by altering the ratio of acrylamide accordingly. In some cases, precast gels were purchased (Mini-Protean TGX any kD, 165-8005, Bio-Rad).

Depending upon the concentration of the protein, either Coomassie or silver staining was used to visualise the proteins in a gel. Coomassie staining was generally used when protein was at least 50ng per band. If less than this, silver staining was used which can detect protein concentrations as low as 2ng per band. For Coomassie staining, gels were stained in Coomassie staining solution (45% (v/v) methanol (Fisher Scientific), 10% (v/v) glacial acetic acid (Fisher Scientific), 0.1% (w/v) Coomassie blue R-250 for 10min then drained. Gels were then washed twice in destaining solution (10% (v/v) methanol (Fisher Scientific), 10% (v/v) glacial acetic acid (Fisher Scientific) for 20mins, before storage in $_{dd}H_20$. Gels for silver staining were immersed in destaining solution for 30mins, followed by three 20min washes in 50% (v/v) ethanol (Fisher Scientific) then drained. The gel was then washed twice for 30secs in 0.02% (w/v) sodium thiosulphate, followed by two 1 min washes in $_{dd}H_20$. The gel was then incubated in 0.2% (w/v) silver nitrate for

20mins and covered in foil (silver nitrate is light sensitive), followed by two 1min washes in $_{dd}H_20$. The gel was developed by adding developing solution (5% (w/v) sodium carbonate, 0.005% (w/v) sodium thiosulphate, 0.05% (v/v) formaldehyde Fisher Scientific)) until bands could be visualised, before staining was terminated by immersing the gel in 5% acetic acid (Fisher Scientific). Note that developing times for silver staining were not standardized and instead developed simply for detection purposes.

Western blotting

Protein bands separated by gel electrophoresis were transferred to Whatman Protran nitrocellulose transfer membrane for 90mins at 100V, 400mA and 4°C. The transfer buffer composition was 25mM Tris-HCl pH 8.3, 192mM Glycine, 20% (v/v) methanol (Fisher Scientific). After protein transfer the membrane was washed in 10mM Tris-HCl pH8, 150mM NaCl for 10min followed by incubation in 10mM Tris-HCl pH8, 150mM NaCl, 1% (w/v) milk powder (Sainsburys), 0.5% (v/v) Tween for 1hr to minimise non-specific antibody binding. The membrane was next incubated for 1hr with the primary antibody (see Table 4 below), diluted 1:500 times in 10mM Tris-HCl pH8, 150mM NaCl, 1% (w/v) milk powder (Sainsburys), 0.5% (v/v) Tween. To remove any unbound primary antibody the membrane was then washed three times with 10mM Tris-HCl pH8, 150mM NaCl, 1% (w/v) milk powder (Sainsburys), 0.5% (v/v) Tween for 5mins and then incubated with the secondary antibody diluted 1:500 in 10mM Tris-HCl pH8, 150mM NaCl, 1% (w/v) milk powder (Sainsburys), 0.5% (v/v) Tween. The excess secondary antibody was removed by washing in 10mM Tris-HCl pH8, 150mM NaCl, 0.5% (v/v) Tween three times for 5min. The membrane was then washed in alkaline phosphate buffer (100mM Tris-HCl pH9.5, 100mM NaCl, 5mM $MgCl_2$) for approximately 5min and then developed using SIGMA FAST BCIP/NBT tablets dissolved in alkaline phosphate buffer. Note that developing times were not standardized and instead developed simply for detection purposes, not quantitative analysis.

Antibodies used

Type		Raised against	Sequence	Detection	Company	Product ID
Primary	Rabbit Polyclonal	Residues 1-18 of the N-terminus of Cav3	MMTEEHTDLEARIIKDIH (Rat)	N/A	Abcam	ab2912
Primary	Rabbit Polyclonal	His-Tag	HHHHHH	N/A	Santa Cruz	G-18:sc-804
Primary	Mouse Monoclonal	His-TagG	HHHHHHG	N/A	Invitrogen	R94025
Secondary	Goat Monoclonal	Anti-Rabbit IgG (whole molecule)	N/A	Alkaline Phosphatase	Sigma	A3687
Secondary	Goat Monoclonal	Anti-Mouse IgG (Fab specific)	N/A	Alkaline Phosphatase	Sigma	SigmaA1682

Table 4: A table of the various antibodies used in this project

Note that although the polyclonal antibody was raised against rat Cav3, Abcam have shown its cross reactivity with human Cav3.

2.2.2. Mass spectrometry confirmation of protein/domain

Protein samples separated by SDS-PAGE were sent for analysis to the Protein Mass Spectrometry Core Facility (Manchester University). Proteins were sent as either a band within a gel, or in solution (20µl at 50ng/ml) with glycerol and detergents removed. Protein bands were digested using trypsin and the peptide fragments analysed by tandem mass spectrometry (MS/MS) on electrospray mass spectrophotometers (Ultimate 3000 (LC-Packings, Dionex) coupled to a HCT Ultra ion trap mass spectrometer (Bruker Daltonics)). Protein identifications was made using the Mascot software (version 2.2.06; produced by Matrix Science), and searched for in the Swiss-Prot (version 57.15) database. The results from this are fed into the statistical validation software, Scaffold (version 3.0.04; produced by Proteome Software).

2.2.3. Molecular biology techniques

Agarose gels – for separation of DNA

Agarose gels (1, 5, 2.5 and 5% (w/v) agarose) were utilised to aid separation of different sized DNA fragments. For a typical 1% agarose gel, 1g of agarose was added to 100ml of 89mM Tris pH8, 89mM Boric Acid, 2mM EDTA, and microwaved on medium power for 8minutes until the agarose was fully dissolved. Once cooled (but not set),

ethidium bromide (1µg/ml) was added. The liquid agar was then poured into gels, and the appropriate well comb applied. 6X loading buffer (40% (w/v) sucrose, 0.25% (w/v) bromophenol blue made up in TBE buffer) was added to the samples at ratio of 1:4 (loading buffer:DNA product). Gels were completed at 90V, 200mA for a range of times (50min to 3hrs, depending upon sample size) in 89mM Tris pH8, 89mM Boric Acid, 2mM EDTA. Two different ranged markers were used: 1.5kb-0.1kb and 10kb-0.5kb (New England Biolabs). To retrieve the sample from the gel, a QIAquick Gel Extraction Kit (28706) was used.

Vector design

A total of three different vectors were used, each differing in the solubilisation tags and terminus to which they are fused. Vectors with a hexahistidine (His)-tag had a T7 promoter, used IPTG for the induction of the protein and conferred resistance to either Ampicillin or Kanamycin. See Vector maps in Figure 16.

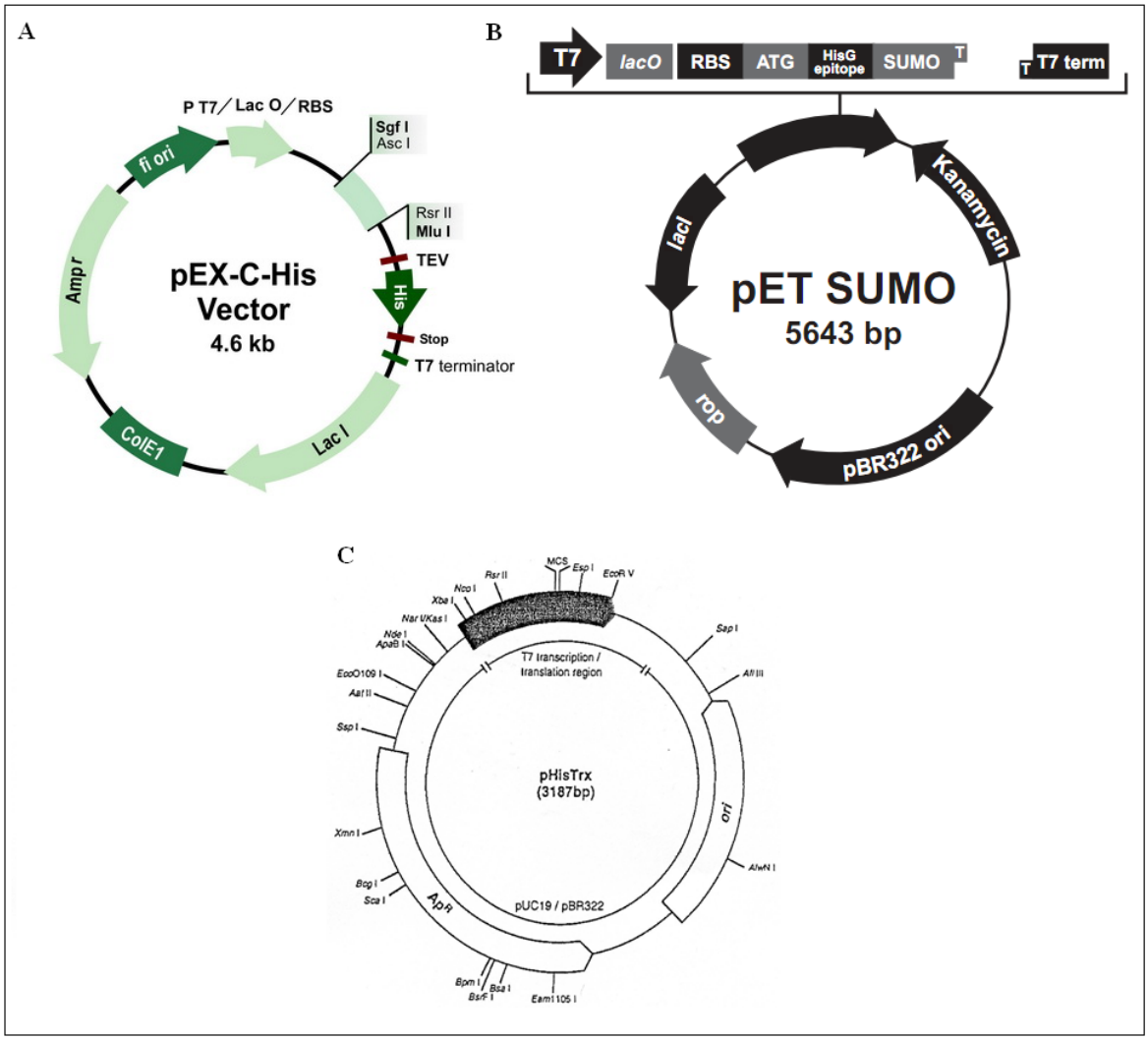

Figure 16: Vector maps for the vectors used in this thesis chapter.

A: OriGene pEX-C-His. **B:** pET-His-SUMO. **C:** pEX-His-Trx. See Table 5 for source of vectors.

Cav3 was inserted into each vector, except the OriGene vector, which was bought from OriGene with the full-length human Cav3 ORF clone transcript variant 2 (NCBI entry NP_001225.1) already inserted. See Table 5 below for individual vector details.

Vector	Company	Product ID	Size (without insert)	Antibiotic Resistance	Fusion Protein	Terminus of fusion	Domain inserted				
							FL	N1	N2	N3	C1
pEX-C-His	Origene	PS100031	4.6kb	Ampicillin	6xHisTag	C	yes				
pEX-His-Trx	Custom Build	N/A	3.2kb	Ampicillin	6xHisTag + Thioredoxin	N		yes	yes		
pET-His-SUMO	Invitrogen	K300-01	5.6kb	Kanamycin	6xHisTag + SUMO	N	yes	yes		yes	yes

Table 5: Vectors used and protein/domains inserted

pEX-His-Trx vector

Using the *OriGene pEX-C-His* as a template, forward and reverse primers were designed upstream and downstream of the desired domains. The forward primers were designed to incorporate a start codon and the relevant cut site, and the reverse primers designed to incorporate a stop codon and the relevant cut site. All primers were purchased from Sigma-Aldrich with no 5' or 3' modification and made up to 200µM by adding 10mM Tris pH7.5, 1mM EDTA.

To create the inserts for the pEX-His-Trx vector, a total of 100µl reaction mixture was prepared: 20µl 10X Polymerase Buffer, 10mM dNTP mix, 200-400ng forward primer, 200-400ng reverse primer, 20-55ng template plasmid DNA (OriGene pEX-C-His vector, containing full length cav3 ORF), 50mM $MgCl_2$, 2units polymerase (Finnzymes Phusion High-Fidelity DNA Polymerase F-530L), and made up to 100µl with $_{dd}H_20$. The PCR mixture was loaded into a Veriti Thermal cycler (Applied Biosystems). DNA amplification was carried out by one cycle of initial denaturation for 0.5-2min at 98°C and was followed by 35 cycles of annealing for 30 sec at a temp gradient (55°C to 85°C), extension for 15-30 sec at 72°C and denaturing for 6-20secs at 95-98°C. This was followed by a one 8-19min cycle of extension at 72°C. Samples were held at 4°C after amplification was complete. The PCR product was loaded onto a gel and the annealing temperature with the strongest band was then extracted using a QIAquick Gel Extraction Kit (28706). A NanoDrop ND-1000 Spectrophotometer was used to quantify the product.

For insertion into the pEX-His-Trx vector, both the isolated PCR product and the pEX-His-Trx vector were treated to restriction enzyme digestion to create sticky ends. For the PCR product, 40µl (7.5ng/µl) of the PCR product, 10µl 10xNEB4 buffer, 1µl BamHI-HF (New England Biolabs, R3136S), 1µl EcoRI-HF (New England Biolabs, R3101S) and 48µl ddH_2O was added together. For the pHisTrx vector (kind gift form Eddie McKenzie, University of Manchester) 75µl (18ng/µl) of the vector, 10µl 10XNEB4 buffer, 1µl BamHI-HF, 1µl EcoRI-HF and 13µl ddH_2O were added together. Both the vectors and the PCR product were incubated with the restriction enzymes for 3hrs at 37°C. Post digestion, the samples were loaded onto a gel and extracted using a QIAquick Gel Extraction Kit (28706).

The inserts were ligated into the restriction digested vectors. In a 10µl reaction mix, 50ng of the restriction digested vector was added with the restriction digested Cav3-domains (at a 1:3 [vector: insert] molar ratio) in ligation buffer (6mM Tris-HCl, 6mM MgCl2, 5mM NaCl, 0.1mg/ml bovine serum albumin, 7mM β-mercaptoethanol, 0.1mM ATP, 2mM dithiothreitol, 1mM spermidine). The mixture was incubated at 45°C for 5min, and then chilled at 0°C for 5min. 4 Weiss Units of T4 DNA ligase (New England Biolabs) was then added and the mixture was incubated at 16°C for 16hrs.

pET-His-SUMO vector

A similar protocol as that described in the section above (pEX-His-Trx vector) was employed with the following modifications: 1) the BIOTAQ Taq polymerase (Bioline) was used. This polymerase lacks extensive 3'to5' exonuclease activity, thus the 3' A-overhangs are not removed, which allows subsequent TA cloning. The corresponding polymerase buffer (NH4 buffer) for this polymerase was also used. 2) Primer design did not need to incorporate a start codon. 3) Due to the nature of TA cloning, restriction digest of the pET SUMO vector and the domains to be inserted was not required.

Vector sequencing

In-house sequencing (Stopford Building sequencing service, Manchester University) was employed to confirm that inserts were correctly inserted and orientated. The plasmid sequences were aligned with the NCBI entry (NM_001234) using ClustalW2 (v 2.0.10) (Larkin et al., 2007).

2.2.4. Transformation

100µl of competent BL21 cells (*E. coli* B F^- *dcm ompT hsdS*(r_B^- m_B^-) *gal* λ(DE3)) were treated with 1.7µl β-mercaptoethanol and incubated on ice for 10mins. 5µl of the

plasmid DNA was added and the cells incubated on ice for a further 30min. Cells were heat-shocked at 42°C for 45 seconds then transferred to ice for 2min. 0.9ml of SOC (at 37°C) was added, and the mixture incubated at 37°C for 20mins and shaken horizontally (200rpm) in an incubator at 37°C for 40-60mins.

2.2.5. Plasmid amplification and purification

200µl was taken from this transformation mixture once transformation was complete and plated (selecting successful transformants for antibiotic resistance), and grown at 37°C for 15hrs. Single colonies were picked from these plates and grown at 37°C in 5ml lysogeny broth (LB**)** (containing 0.5mM ampicillin or Kanamycin at 50µg/ml of LB) in an orbital shaker until stationary phase was reached (0.6 at OD_{600}). A QIAprep spin Miniprep kit (QIAGEN 27104) was used to purify the plasmid from 1.5ml of the crude cell solution sample. The plasmid concentration was subsequently quantified using a NanoDrop ND-1000 UV-Vis Spectrophotometer. Plasmid concentrations ranged between 33 to 77ng/µl. Plasmid DNA was stored at -20°C.

2.2.6. Glycerol stock production

1ml of the transformed cell culture was used to create glycerol stocks of transformed BL21 (DE3) cells for future use, by adding 80% (v/v) glycerol (Fisher Scientific) (at 266µl/1ml culture). Samples were frozen in liquid nitrogen and stored at -80°C.

2.2.7. Expression

To optimise expression, transformed *E.coli* were grown in a variety of different medium (LB, MagicMedia (Invitrogen), SOB (Super Optimal Broth - 2% (w/v) bacto-tryptone, 0.5% (w/v) bacto-yeast extract, 8.56mM NaCl, 2.5mM KCl, pH7) and SOC (Super Optimal Broth with Catabolite repression - SOB, plus 10mM MgCl2 and 20mM glucose)), at a range of temps (18°C, 22°C, 26°C, 28°C, 30°C, 37°C), induced at range of IPTG concentrations (0.1mM, 0.5mM, 1mM, 1.5mM, 2.5mM, 3.5mM), treated to different antibiotic concentrations (0.5mM and 0.25mM ampicillin), and grown for different lengths of time (1, 2, 3, 4, 5, 6, 16, 21 and 30hours). A summary of the various conditions is shown in Table 6 below.

In general, 1ml of vector transformed *E.coli* were added to 50ml liquid broth (1L=10g tryptone, 5g yeast extract, 10g NaCl, pH7, plus 0.5mM ampicillin or kanamycin

at 50μg/ml of LB) and added to a shaking incubator at a chosen temperature (see Table 6). Cells were grown until absorbance at 600nm reached 0.8 (unless otherwise stated – see Table 6). Once this level of growth was attained, IPTG at a range of molarities (see Table 6) was used to induce the expression of the vector. Cells were then grown over a range of incubation periods (see Table 6), after which they were moved to 4°C for 10mins to cease growth. Aliquots were taken at all time points to check for protein expression. The bulk cell solution was centrifuged at 5465xg for 10mins at 4°C (Sorvall Evolution RC, Rotor SLA-1500). The supernatant was discarded and the cell pellet frozen in liquid nitrogen and stored at -80°C for future use.

Magic media

This proprietary media (Invitrogen) uses two different protocols depending upon the temperature of expression selected, and does not require manual induction; instead opting for auto-induction. Inoculation protocol: For expression at 30°C and 37°C the media was inoculated with a single colony and grown with vigorous shaking (300rpm) for 21hours. Dual-temperature protocol: For expression at 18°C, 5ml LB was inoculated and incubated at 30°C for 16hours with shaking (300rpm). Magic media was inoculated with the overnight culture at a 1:40 dilution and incubated at 30°C (300rpm) for 6hours until $O.D._{600}$ was >0.6, then transferred to a 18°C incubator and grown for 30hours. Cells were harvested as described above in the Expression section above.

Protein/Domain	Vector	Temperature	Media	Induction OD (@600nm)	Growth Time (hours)	IPTG Concentration (mM)
Cav3	pEX-C-His	37°C	LB	0.8	1	0.5
					2	0.5
					3	0.5
					4	0.5
					5	0.5
						1
						1.5
						2.5
						3.5
					6	0.5
				0.4	3	0.1
			Magic	N/A	21	N/A
		30°C	LB	0.8	5	0.5
						1
						1.5
						2.5
						3.5
				0.4	3	0.1
			SOC	0.8	3	0.1
			Magic	N/A	21	N/A
		22°C	LB	0.8	1	0.1
					2	0.1
					3	0.1
					4	0.1
					5	0.5
						1
						1.5
						2.5
						3.5
					6	0.1
				0.4	3	0.1
			SOB	0.8	5	0.1
			Magic	N/A	30	N/A
	pET-His-SUMO	37°C	LB	0.8	1	1
					2	1
					3	1
					4	1
					5	1
		26°C	LB	0.8	1	1
					2	1
					3	1
					4	1
					5	1
		18°C	LB	0.8	16	1
N_{1-54}	pEx-His-Trx	37°C	LB	0.8	4	1
	pET-His-SUMO	37°C	LB	0.8	4	1
N_{1-74}	pEx-His-Trx	28°C	LB	0.8	5	1
$N_{1-101} + C_{92-151}$	pET-His-SUMO	37°C	LB	0.8	1	1
					2	1
					3	1
					4	1
					5	1
	pET-His-SUMO	18°C	LB	0.8	16	1

Table 6: Summary table of expression conditions

2.2.8. Isolation of Cav3 recombinant proteins: Lysis/solubilisation

Li and co-workers lysis/solubilisation protocol (Li et al., 1996c).

Cell pellets were defrosted and re-suspended on ice in STE buffer (Tris pH8.0, 150mM NaCl, 10mM 2mM EDTA, lysozyme (100mg/ml), protease inhibitor (1mini tablet per 10ml - cOmplete, Mini, EDTA-free protease inhibitor cocktail tablets (Roche)) (300µl buffer per ml culture) for 15min. The sample was then adjusted to 1.5% (w/v) N-lauroylsarcosine (Sigma) before two 30second rounds of homogenisation (Microson Ultrasonic cell Disrupter). The solution was centrifuged at 12,000xg (Sorvall Evolution RC, SLA-1500) for 15min at 4°C and adjusted to 2% (v/v) Triton X-100. The resultant supernatant was termed the soluble fraction.

Alternative protocols – for SUMO expression system

Cell pellets were defrosted and re-suspended on ice in 50mM Tris pH7.8, 400mM NaCl, 100mM KCl, 10% (v/v) glycerol (Fisher Scientific), 0.5% (v/v) Triton X-100 (Sigma), 10mM imidazole, protease inhibitor (1mini tablet per 10ml - cOmplete, Mini, EDTA-free protease inhibitor cocktail tablets (Roche)) (1:1 buffer:original cell solution ratio). Cells were sonicated (two 30 second rounds), and centrifuged at 12,000xg (Sorvall Evolution RC, SLA-1500) 4°C for 15 minute to pellet the insoluble proteins. The supernatant was deemed the soluble fraction (Alternative Protocol #1). In one experiment, Tris was replaced with 50mM potassium phosphate pH7.8 to investigate the effect of the lysis/solubilisation buffer on the lysis/solubilisation process (Alternative Protocol #2).

Lysis protocol	Key features	Cav3	N1-54	N1-74	N1-101	C92-151
Li and co-workers Lysis protocol	Published protocol	yes		yes		
Alternative Protocol #1	Tris buffer	yes	yes		yes	yes
Alternative Protocol #2	PBS buffer		yes			

Table 7: Summary table for lysis/solubilisation conditions used for each protein/domain

Treatment of the insoluble fraction (pellet)

In some expression trials the expressed protein formed inclusion bodies. The following section describes the methods employed to isolate the protein aggregates.

Increased lysozyme, DNase, Triton X-100, 8M Urea

The post-lysis pellet (non-soluble fraction) was treated to several further stages of lysis/solubilisation. Pellets were resuspended in 10mM Tris pH8.0, 150mM NaCl, 2mM EDTA, protease inhibitor (1mini tablet per 10ml - cOmplete, Mini, EDTA-free protease inhibitor cocktail tablets (Roche)) with the addition of DNase (10µl/ml), the lysozyme concentrations increased from (100mg/ml to 300mg/ml), and the percentage of Triton X-100 increased from 0.5% to 1% (v/v). The mixture was sonicated (three 30second bursts, Microson Ultrasonic cell disrupter) then incubated on ice for 20mins. The sample was then adjusted to 8M Urea and incubated for a further 30mins at room temperature. Samples were centrifuged at each stage (12,000xg for 15min at 4°C), the supernatant removed and the pellet responded in the next step. The supernatants obtained were deemed the secondary soluble fractions.

Strong denaturants and detergent exchange

In another approach the post-lysis pellet (non-soluble fraction) was resuspended in the chaotropic agent 8M Urea or 6M Guanidine (3:10 buffer:original cell solution ratio. The mixture was sonicated (three 30second bursts) Microson Ultrasonic cell disrupter) then incubated at room temperature for 20min. To remove the urea, and to solubilise the protein into a buffer (10mM Tris pH8.0, 150mM NaCl, 2mM EDTA, lysozyme (100 mg/ml), protease inhibitor (1mini tablet per 10ml - cOmplete, Mini, EDTA-free protease inhibitor cocktail tablets (Roche))) containing an alternative detergent (1.5% (w/v) CHAPS, 1.5% (w/v) n-Dodecyl-ß-maltoside (Thermo Scientific), 1.5% (v/v) Triton X-100 or 1.5% (w/v) n-octyl-β-D-glucoside), stepwise dialysis (increments 3M, 1.5M, 0.8M, 0.4M, 0.2M, 0M) was complete using a Slide-A-Lyzer 7K dialysis cassette (7000 MWCO) over 2 days. Samples were centrifuged (12,000xg for 15min at 4°C). The supernatant was referred to as the secondary soluble fraction.

Lysis protocol	Key features	Cav3	N1-54	N1-74	N1-101	C92-151
Increased lysozyme, DNAse, 8M Urea	Used on pellets. DNAse, Increased Lysozyme, 8M Urea,	yes				
Strong denaturants and detergent exchange	Used on pellets. Strong denaturants: 8M Urea, 6M Guanidine. Detergents exchanged to: 1.5% CHAPS, 1.5%DDM, 1.5%TX100, 1.5% OG			yes		

Table 8: Summary table for treatment of the insoluble fraction used for each protein/domain

Abbreviations: DDM, n-Dodecyl-ß-maltoside. TX100, Triton X-100. OG, n-octyl-β-D-glucoside.

2.2.9. Storage

All transformed E.coli samples and glycerol stocks were frozen in liquid nitrogen and subsequently stored at -80°C. Vectors, plasmids, PCR products and peptides were stored at -20°C.

2.2.10. Purification

Nickel affinity gel (Sigma HIS-Select® HF Nickel Affinity Gel H0537) was equilibrated at 4°C by mixing with the same buffer as the post-lysis supernatant fraction, at 1ml/50µl resin, followed by centrifugation to remove the liquid fraction. This was repeated 4 times to ensure the ethanol had been removed from the nickel affinity gel. The post-lysis soluble fraction was added to the equilibrated nickel affinity gel and mixed for 5min at 4°C. The solution was then centrifuged at 5000xg (eppendorf Minispin plus) for 5min. The supernatant fraction was termed 'unbound'. The nickel affinity gel was then washed three times with wash buffer (the samples buffer with 20mM imidazole) and then centrifuged at 3000xg (eppendorf Minispin plus) for 5min; the supernatant from each was discarded. The bound protein was eluted from the matrix with 300mM imidazole (including 60mM octyl glucoside for the Li and co-workers protocol) after incubation for 15min at 4°C, followed by centrifugation at 5000xg (eppendorf Minispin plus) for 5min.

2.2.11. Cleavage of the 6xHis-SUMO-tag

To remove the 6xHis-SUMO tag, fusion protein eluted from the nickel affinity resin was incubated with 2.5 Units of SUMO protease (Ulp) in 55mM Tris pH8, 150mM NaCl, 7% (v/v) glycerol (Fisher Scientific), 0.03% (v/v) Triton X-100, 16mM imidazole, 1mM DTT, 0.3% (v/v) NP-40 at 4°C for 3 hours. The sample was then dialysed into the following buffer: 10mM Tris pH8, 150mM NaCl, 10mM imidazole, 0.03% (v/v) Triton X-100, and applied to a fresh nickel affinity gel matrix (pre-washed in the same buffer). However, the unbound fraction was retained as this contained the cleaved recombinant protein with the SUMO tag bound the affinity gel.

2.2.12. Circular dichroism

Far-UV circular dichroism (CD) was used to aid in the detection of any potential secondary structure within the purified N^{1-54} domain. Samples at 10µM were loaded into

0.2mm cuvettes and a Jasco J810 CD spectrometer was used to acquire a spectrum. The spectrometer settings were as follows start: 260nm, end: 190nm, data pitch: 0.5, scanning mode: step, response: 0.5seconds, bandwidth: 1nm, accumulations: 8. Experiments were complete in triplicates and averaged. Consistent CD spectra were observed for each run.

2.2.13. Dichroweb

The CD output (delta epsilon) was uploaded to the DICHROWEB server (Whitmore and Wallace, 2004, 2008). To predict secondary structure content, the SELCON3 analysis programme (Sreerama et al., 1999; Sreerama and Woody, 1993) was used with a reference set optimised for 190-240nm, the region where peptide contributions dominate.

2.2.14. Bioinformatics

Secondary structure prediction was made using both PSIPRED (version 2.6 http://bioinf.cs.ucl.ac.uk/psipred/), which utilises position specific iterated blast searches and neural networks to predict secondary structure.

2.3. Results and Discussion

2.3.1. Expression of full-length Cav3 in *E.coli* using the pEX-C-His vector

The cardiac Cav3 gene was purchased from OriGene supplied in a vector suitable for expression in *E.coli. E.coli* was chosen as the expression system to express Cav3 as previous published work had shown that canine Cav1 expression and purification had already been achieved using this system (Li et al., 1996c). As can be seen from the vector map (See Figure 17), Cav3 has a C-terminal polyhistidine tag which allows purification by nickel affinity gel chromatography.

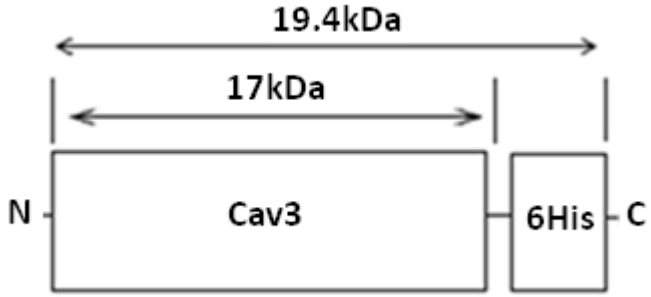

Figure 17: Schematic of the Cav3-His-tag fusion protein.
The figure illustrates that he recombinant Cav3 has a C-terminal 6xHis-tag. The total fusion protein is approximately 19.4kDa.

Li and co-workers expression protocol

Following the methods reported by Li and co-workers (Li et al., 1996c), cells were grown at 37°C and induced with 0.5mM IPTG when the OD at 600nm was 0.8. Cell samples were then taken at 1, 2, 3, 4, 5 and 6hrs post-induction and lysed and the soluble fraction examined by SDS-PAGE.

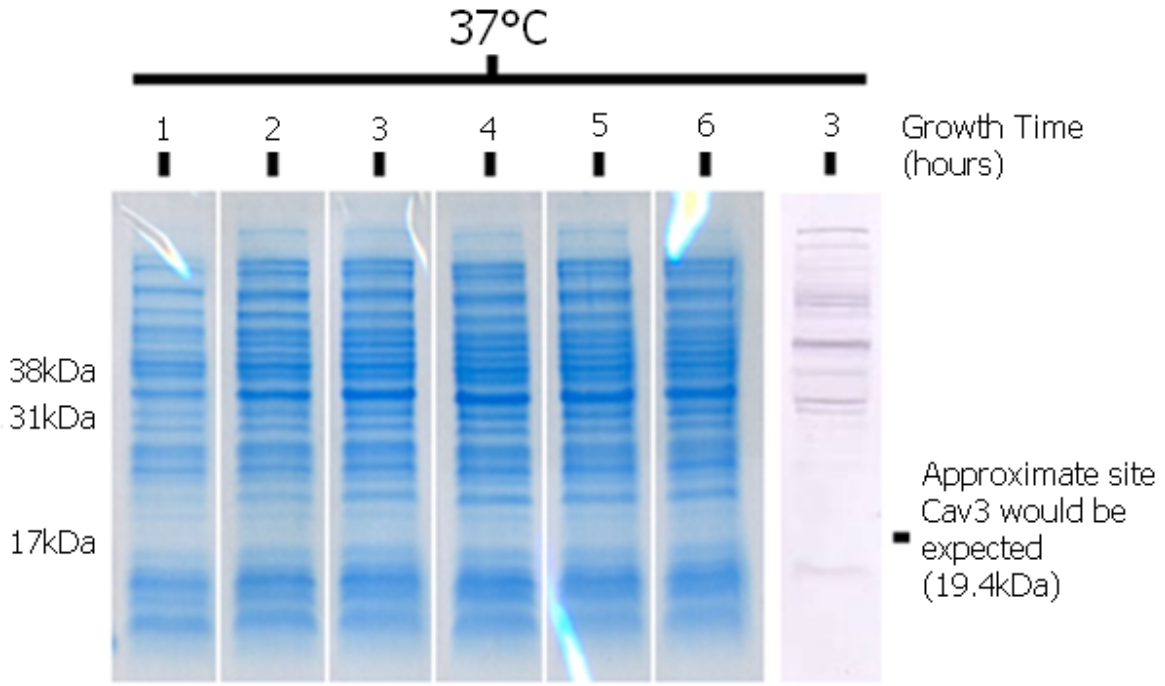

Figure 18: Protein expression profile of Cav3 transformed *E.coli* at different stages of the growth period post-induction. Induced at 37°C with 0.5mM IPTG.

Cells grown at 37°C and induced with 0.5mM IPTG (at a cell density of 0.8 OD^{600}) were solubilised following the published protocol (Li et al., 1996c). The soluble fraction from different time-points post-induction were examined by SDS-PAGE gel and stained in Coomassie staining solution. Western-blotting was carried out for the 3hrs post-induction sample using an antibody raised against residues 1-18 of the N-terminus of Cav3. Over-expression of Cav3 was not achieved, as shown by the lack of a prominent band on the Coomassie stained gel. Western blotting did not detect the presence of Cav3. The approximate position that the Cav3 fusion protein (19.4kDa) would be expected is shown on the right.

As can be seen in Figure 18, soluble Cav3 was not obtained at any of the time points post-induction. Moreover, western blotting did not confirm the presence of Cav3 in any of the fractions. As an example the blot for 3hour post-induction is shown.

Alternate expression conditions

Due to the lack of success from following the published expression protocol (Li et al., 1996e), and with no prior knowledge as to what expression conditions would be optimum for the expression of full-length human Cav3 in *E.coli*, a broad range of conditions were devised (see Table 6 for a summary of the conditions explored). Expression variables explored included testing a range of different IPTG concentrations, growth media, growth time, cell concentration and temperature. The various combinations

and trials conducted for full-length Cav3 are summarised in Table 6. Examples of some of the expression trials are described below. The first two expression conditions that were modified were IPTG concentration and temperature. Cells were grown at the reduced temperature of 22°C and induced with a reduced concentration of IPTG (0.1mM). The lysis protocol was kept as described by Li and co-workers (Li et al., 1996c).

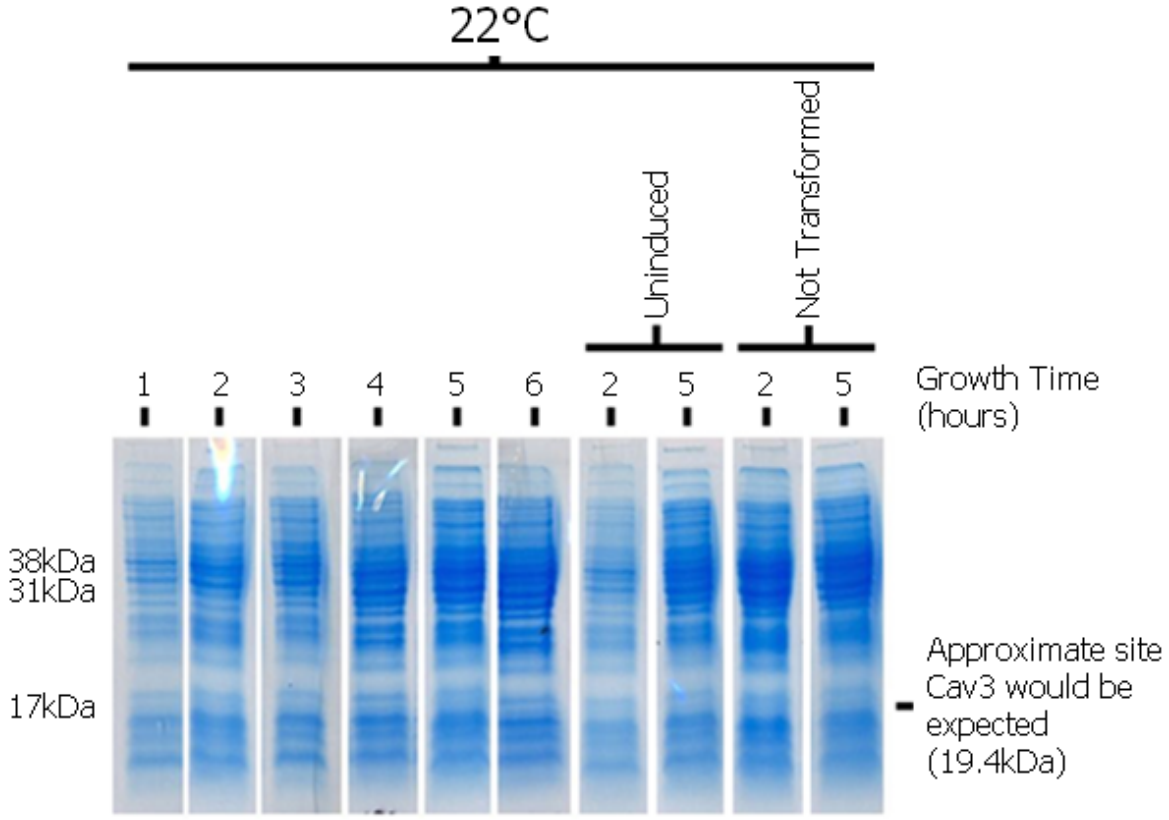

Figure 19: Protein expression profile of Cav3 transformed *E.coli* at different stages of the growth period post-induction. Induced at 22°C with 0.1mM IPTG.
Cells grown at 22°C and induced with 0.1mM IPTG (at a cell density of 0.8 OD^{600}) were solubilised following the published protocol (Li et al., 1996c). The samples of the soluble fraction from different time-points post-induction were examined by SDS-PAGE and stained in Coomassie blue solution. Controls included both un-induced (no IPTG) and non-transformed (no Cav3 containing vector) cells after 2 and 5 hours growth. Over-expression of Cav3 was not achieved, as shown by the lack of a prominent band on the Coomassie stained gel. Note that there is no obvious difference between the protein profiles in the controls and those that have been induced to express Cav3. The approximate position that the Cav3 fusion protein (19.4kDa) would be expected is shown on the right.

As can be seen in Figure 19, there did not appear to be any detectable Cav3 expression detected in the soluble fraction. Moreover, the cell expression profile did not differ greatly from that of the cell profile for the cells induced at 37°C with 0.5mM IPTG

(see Figure 18). In addition, a comparison of the protein expression profiles for the un-induced and untransformed cells found no obvious significant differences from those of the induced cells.

Although no prominent Cav3 band was observed in either condition (37°C + 0.5mM or 22°C + 0.1mM), some proteins were detected by western blotting (37°C, 0.5mM, 3hr; see Figure 18). However, these bands were not at a molecular mass expected for Cav3. The fact that multiple bands were observed suggested that either the antibody was non-specific, or there were multiple forms of Cav3 being expressed. Even if some form of Cav3 was being expressed, the yields desired for further structural analysis were clearly not being achieved.

Induction of expression at varied IPTG concentrations

The first condition explored in detail was the IPTG concentration. As mentioned in the introduction, the concentration of IPTG is a factor to consider when inducing expression. Generally speaking, 0.1mM to 1.5mM is used, but this was extended to include 2.5mM and 3.5mM here.

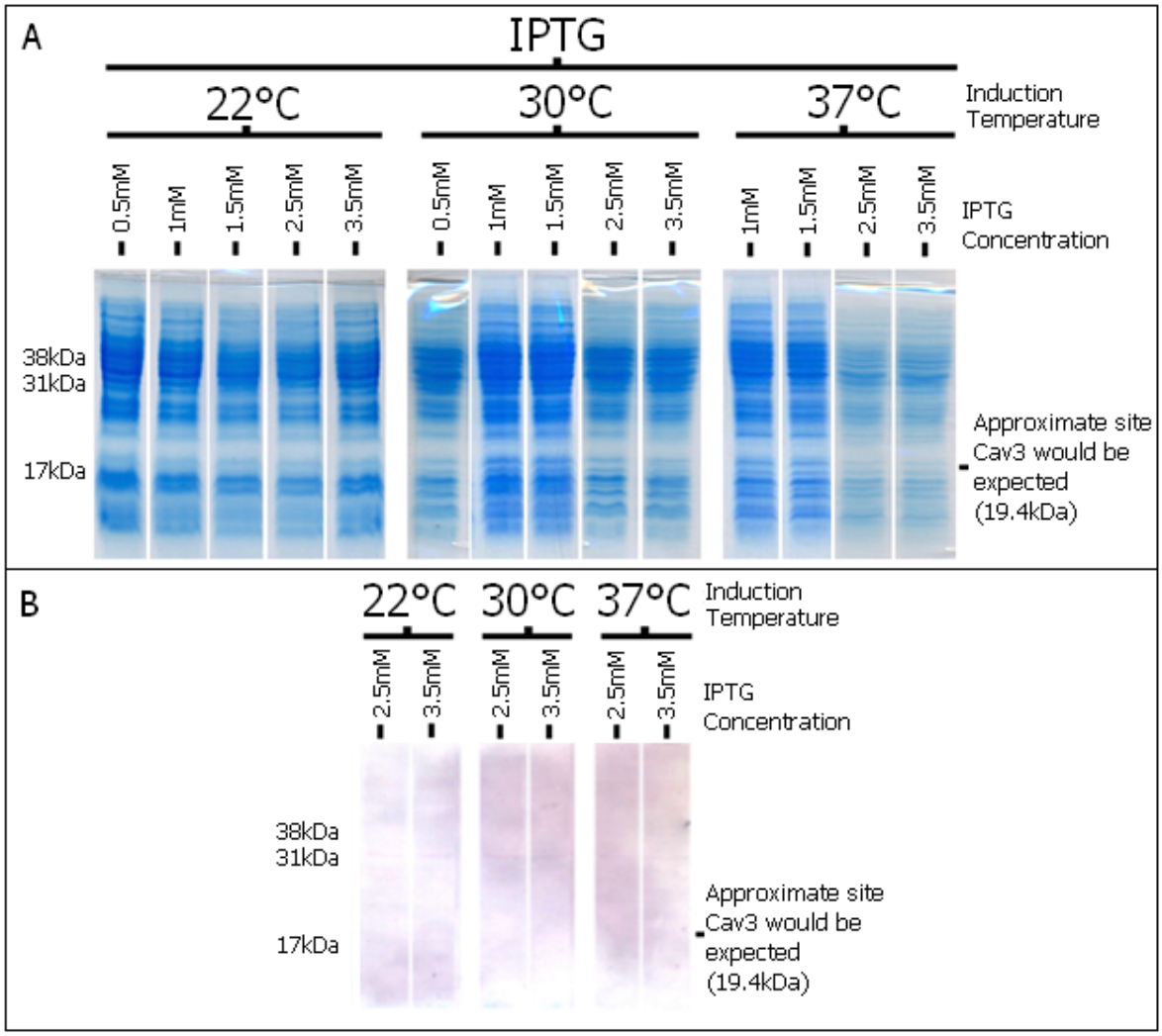

Figure 20: Protein expression profile of Cav3 transformed in *E.coli* grown at 22°C, 30°C and 37°C and induced with a range of IPTG concentrations: 0.5, 1, 1.5, 2.5 and 3.5mM IPTG.

Cells were grown for 5hours at 22°C, 30°C and 37°C and induced with 0.5, 1, 1.5, 2.5 and 3.5mM IPTG (at a cell density of 0.8 OD^{600}) then solubilised following the published protocol (Li et al., 1996c). **A:** The soluble fractions were examined by SDS-PAGE and stained in Coomassie. **B:** Western-blotting was completed for a selection of the samples, 22°C (2.5 and 3.5mM IPTG), 30°C (2.5 and 3.5mM IPTG) and 37°C (2.5 and 3.5mM IPTG), using an antibody raised against the His-tag fused to the C-terminus of Cav3. The approximate position that the Cav3 fusion protein (19.4kDa) would be expected is indicated. Over-expression of Cav3 was not achieved, as shown by the lack of a prominent band on the Coomassie stained gel. Western blotting using an anti-His-tag antibody showed that Cav3 was not expressed.

As can be seen in Figure 20, altering the IPTG concentration did not result in soluble Cav3 being expressed at a detectable level. Given the possible non-specific binding of the anti-Cav3 antibody an anti-His antibody was employed. However, as can be seen in Panel B of the figure no protein bands were identified.

Induction of expression in varied growth media

Up to this point, all cells had been grown in Lysogeny Broth (10g tryptone, 5g yeast extract, 10g NaCl, 1L dH_2O). There are numerous reports of successful protein expression from altering, for example, the composition of the media. Both Super Optimal Broth (SOB) and Super Optimal Broth with Catabolite repression (SOC) were employed here (see Materials and Methods Expression section for buffer compositions). SOB is usually used during transformation as it can aid in the transformation efficiency. However, given its increased levels of amino acids and peptides, it can also allow greater growth of cells.

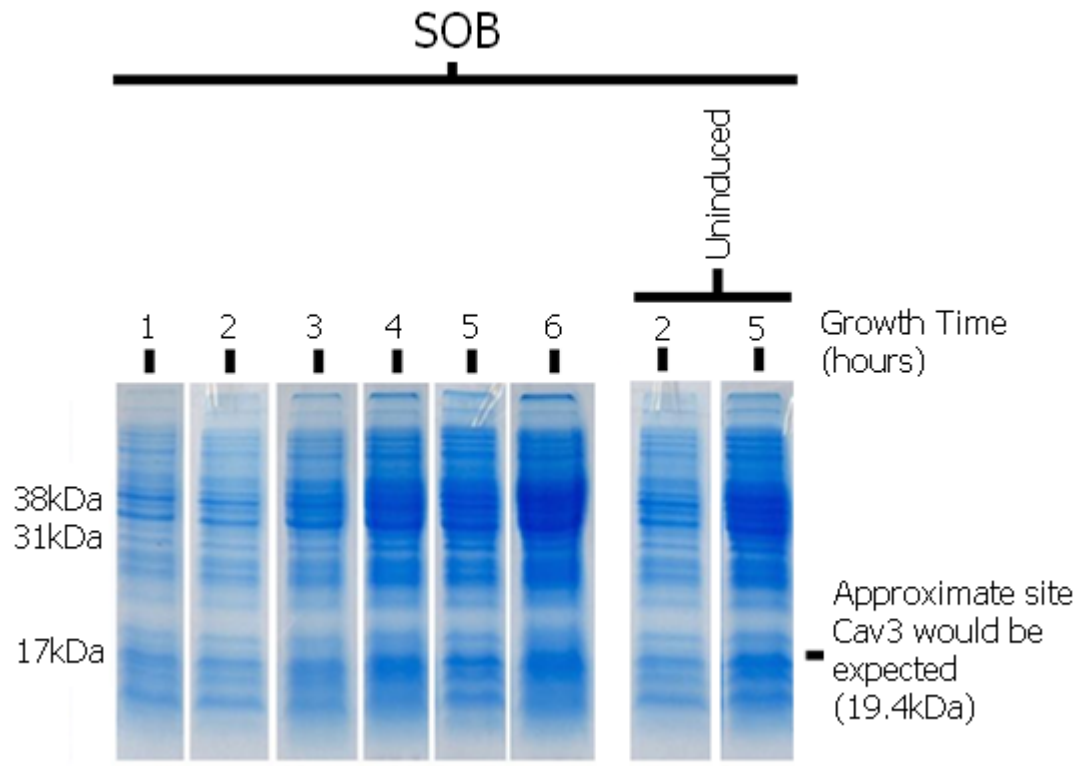

Figure 21: Protein expression profile of Cav3 transformed *E.coli* grown in Super Optimal Broth at 22°C and induced with a 0.1mM IPTG.

Cells grown in SOB at 22°C and induced with 0.1mM IPTG (at 0.8 OD^{600}) were solubilised following the published protocol (Li et al., 1996c). The soluble fractions from several time points (1, 2, 3, 4, 5, and 6hours) were examined by SDS-PAGE and stained in Coomassie blue staining solution. The soluble fractions from an un-induced control (2 and 5hours) are also shown. The approximate position that the Cav3 fusion protein (19.4kDa) would be expected is shown on the right. Over-expression of Cav3 was not achieved, as shown by the lack of a prominent band on the Coomassie stained gel.

As can be seen in Figure 21, growing the cells in SOB media did not result in the obvious expression of soluble Cav3. A band at the approximate site of Cav3 can be seen; however, this band was also present in the un-induced control. This raised the possibility that Cav3 was being expressed even in the un-induced control; so called, 'leaky transcription'. If Cav3 was toxic to *E.coli*, and it was being expressed during the growth stage of the cells, then this might provide an explanation as to why Cav3 was not being *over-expressed*, as the host's proteolytic machinery would break the non-native Cav3 down. One way to reduce leaky expression is to suppress the *lac* operon, in which the gene for the potentially toxic protein is inserted, whilst the cells grow. This can be achieved by increasing the glucose concentration in the media in which the cells are growing. By default, *E.coli* will utilise glucose as a primary energy source, and repress transcriptions of

genes involved in the utilisation of alternative energy sources, such as lactose (as described in the chapter introduction). Thus, the *lac* operon is tightly repressed, leaky transcription is reduced and the leaky expression of a potentially toxic protein is reduced. However, this repression is not absolute and once the cells have managed to achieve a good level of growth, the addition of IPTG can override the repression of the *lac* operon and express the potentially toxic protein. In theory, the increased cell concentration achieved allows a greater yield of toxic proteins. To test this hypothesis SOC media was employed. Again a range of induction temperatures were employed with the results for 30°C shown below.

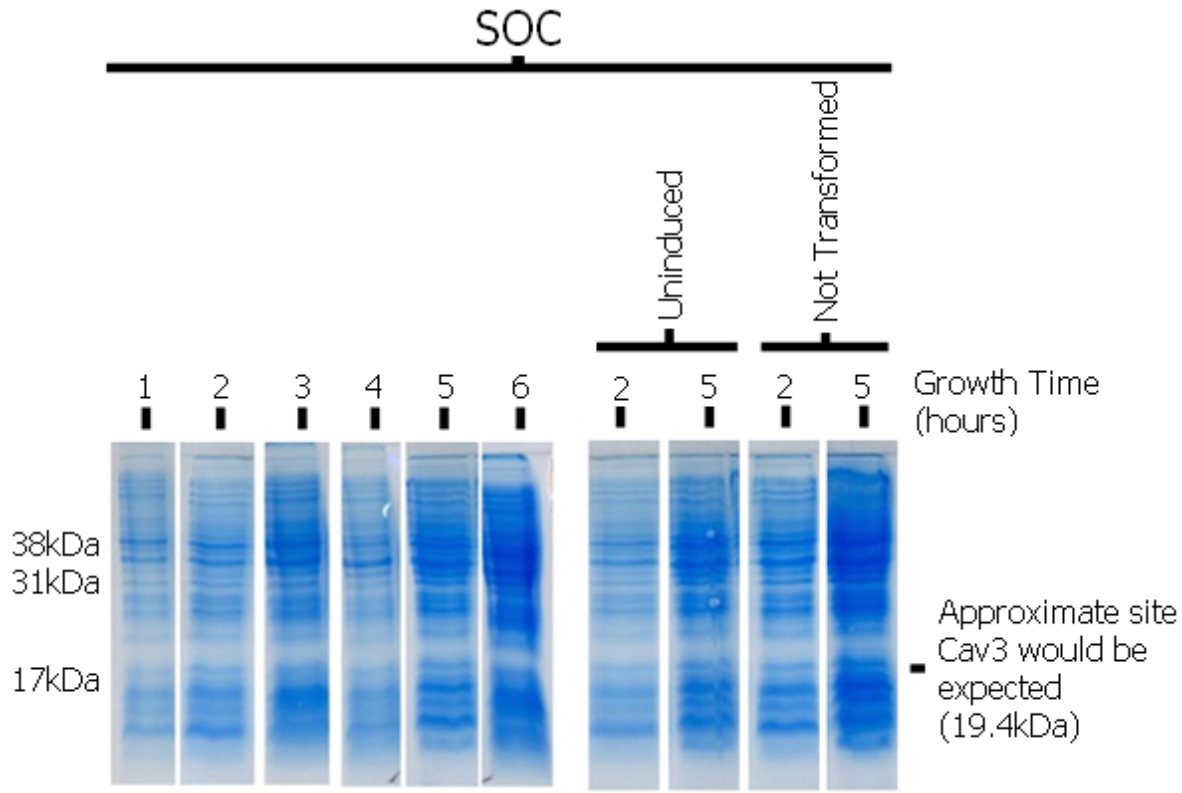

Figure 22: Protein expression profile of Cav3 transformed in *E.coli* grown in super optimal broth with catabolite repression (SOC) at 30°C and induced with a 0.1mM IPTG.

Cells grown in SOC at 30°C and induced with 0.1mM IPTG (at 0.8 OD^{600}) were solubilised following the published protocol (Li et al., 1996c). The soluble fractions from several time points (1, 2, 3, 4, 5, and 6hours) were examined by SDS-PAGE and stained in Coomassie. The soluble fractions from an un-induced control and a non-transformed control (2 and 5hours) are also shown. The approximate migration position that the Cav3 fusion protein (19.4kDa) would be expected at is shown on the right. Over-expression of Cav3 was not achieved, as shown by the lack of a prominent band on the Coomassie stained gel.

Despite the potential repression of leaky transcription, there was no noticeable effect on the expression of Cav3 by using the SOC media. Moreover, the band that was thought to potentially be leaky expression of Cav3 was again observed in both the un-induced control and the non-transformed control. Furthermore, comparison of the control polypeptide profile with that of the induced fractions did not identify any other bands that could correspond to oligomers of Cav3.

Induction of expression at varied cell concentrations

Certain proteins are expressed more optimally at certain stages of the growth phase. In the experiments described above, induction had been when the cell density reached 0.8 OD (at 600nm), which is during the exponential growth phase. Therefore, induction in the early log phase was explored.

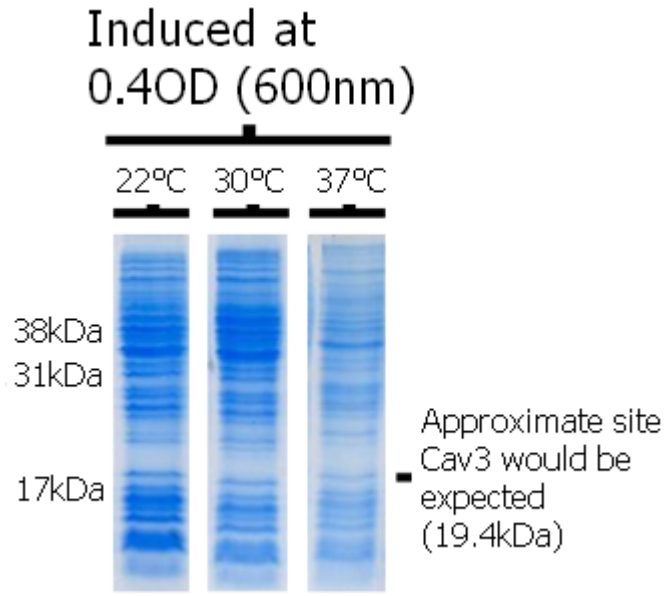

Figure 23: Protein expression profile of Cav3 transformed in *E.coli* and grown at 22, 30 and 37°C and induced with a 0.1mM IPTG at a reduced cell density (0.4 at OD^{600nm}).

Cells were grown for 3hours in LB at a range of temperatures (22, 30, 37 °C) and induced with 0.1mM IPTG at a reduced cell density of 0.4 (OD^{600}) were solubilised following the published protocol (Li et al., 1996c). The soluble fractions were examined by SDS-PAGE and stained in Coomassie blue solution. The approximate position that the Cav3 fusion protein (19.4kDa) would be expected to migrate is indicated. Over-expression of Cav3 was not achieved, as shown by the lack of a prominent band on the Coomassie stained gel.

As can be seen in Figure 23, inducing the cells to express Cav3 at an early stage of the growth phase did not result in any obvious band that would correspond to soluble Cav3, regardless of temperature.

Magic media

Magic media is a propriety media developed by Invitrogen that claims to be able promote high yielding protein expression in *E.coli*. The protocol provides different protocols for different temperatures. For cells induced at 22°C the 'dual temperature' protocol was followed, and for cells induced at 30°C and 37°C the 'inoculation' protocol is suggested (see Magic media section in Material and Methods for individual protocol details).

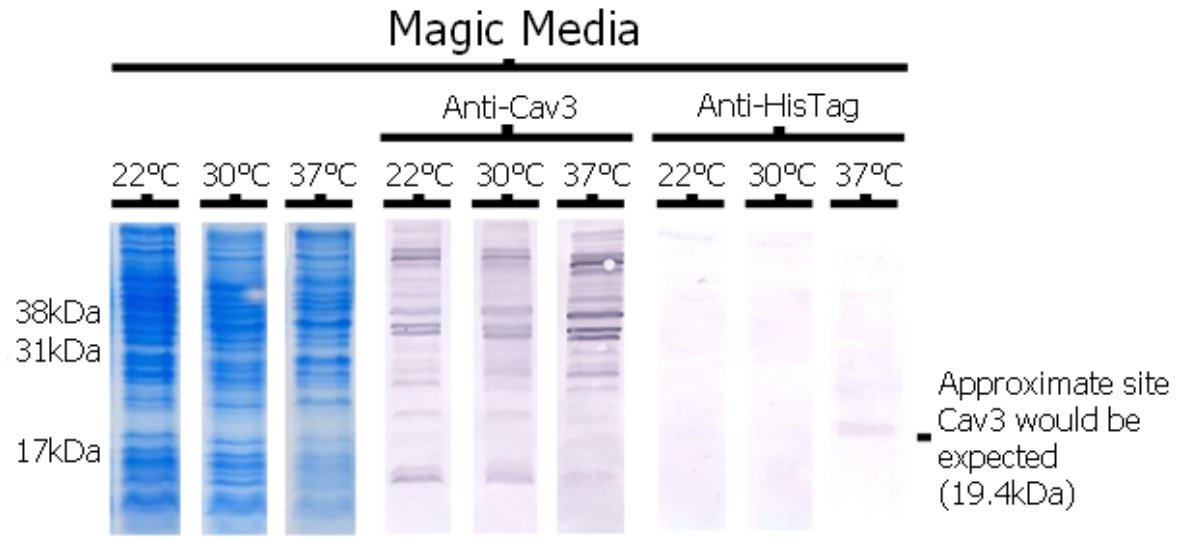

Figure 24: Protein expression profile of Cav3 transformed *E.coli* grown in Magic media at 22, 30, 37°C.

Cells grown in Magic media (Invitrogen) at a range of temperatures (22, 30, 37°C) and induced as per the products protocol were solubilised following the published protocol (Li et al., 1996c). The soluble fractions were examined by SDS-PAGE and Coomassie stained. Western-blotting was completed using two different antibodies (anti-Cav3, ab2912; anti-His-tag, sc-804). Over-expression of Cav3 was not achieved, as shown by the lack of a prominent band on the Coomassie stained gel although western blotting with the anti-His-tag antibody, but not the anti-Cav3 antibody, detected a faint band at 37°C, which is at the approximate position a Cav3 monomer would be expected.

As can be seen in Figure 24, there is no large Cav3 band between the 17 and 31kDa markers, which is the approximate position a monomer of Cav3 would be expected to migrate to. Intriguingly, hybridisation with the anti-His-tag antibody did find a weak

protein band at around 22kDa. However, this was at a different position from the any of the bands detected using the anti-Cav3 antibody, which again can be seen to produce multiple higher molecular mass bands.

Ampicillin

Knowing that the ampicillin can sometimes have an adverse effect on cell growth (Yourassowsky et al., 1985), the concentration of ampicillin was reduced in order to test whether this had any effect on the expression of soluble Cav3. All previous experiments employed an ampicillin concentration of 0.5mM. Cells were grown in LB containing half the usual concentration of ampicillin (0.25mM).

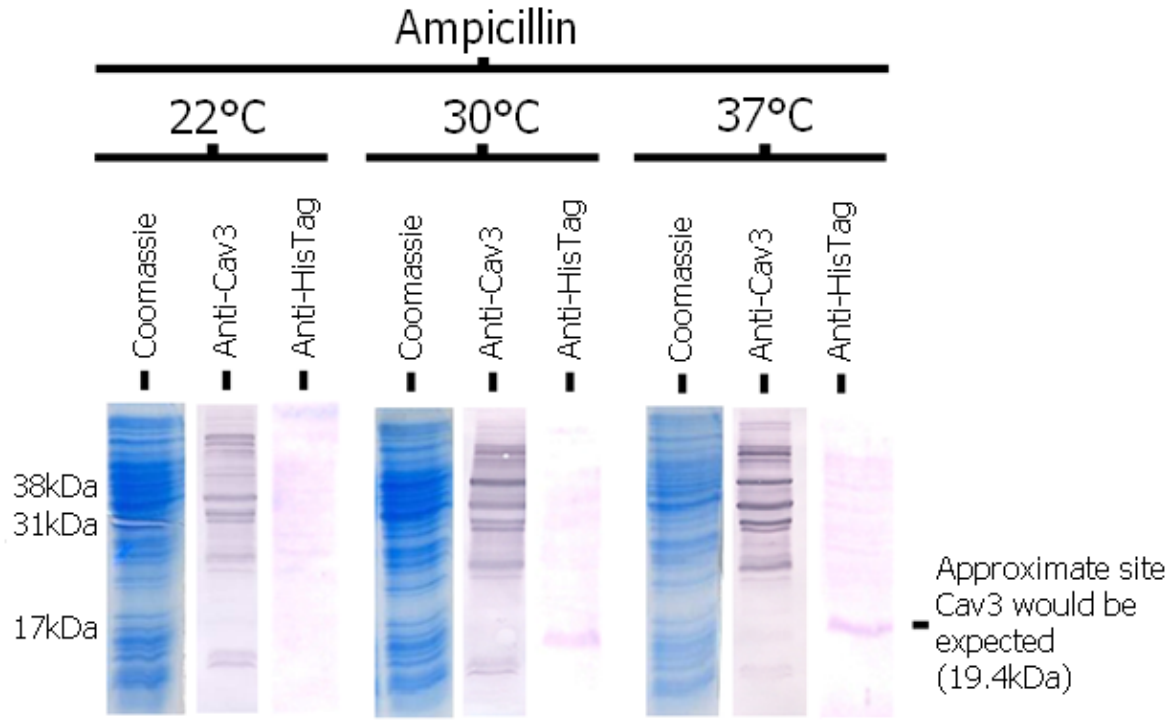

Figure 25: Protein expression profile of Cav3 transformed in *E.coli* grown in LB at 22, 30 and 37°C and induced with a 1.5mM IPTG at a reduced ampicillin concentration.

Cells grown in LB containing a reduced concentration of ampicillin (0.25mM) for 5hours at a range of temperatures (22, 30, 37°C) and induced with 1.5mM IPTG (at 0.8 OD^{600}) were solubilised following the published protocol (Li et al., 1996c). The soluble fractions were examined by SDS-PAGE and stained in Coomassie solution. Western-blotting was undertaken using two different antibodies (anti-Cav3, ab2912; anti-His-tag, sc-804). The approximate position that the Cav3 fusion protein (19.4kDa) would be expected is shown on the right. Over-expression of Cav3 was not achieved, as shown by the lack of a prominent band on the Coomassie stained gel. As can be seen, the anti-Cav3 antibody resulted in multiple bands, although none of them at the expected position of a monomer.

Blotting using an anti-His-tag antibody detected a faint band in fractions from cells induced at 30 and 37°C, at the approximate position Cav3 would be expected.

A faint band was detected using the anti-His-tag antibody in both the 30°C and 37°C conditions. However, this band was not matched by the anti-Cav3 antibody. In addition, no obvious band was observed in the Coomassie blue stained gels, suggesting that if Cav3 were being expressed it was only very weakly.

Nickel affinity gel purification

Although not one condition was shown to express soluble Cav3 at a yield observable by Coomassie staining, the anti-His-tag antibody hinted at some trace expression, although it was not particularly encouraging that this was not identified by the anti-Cav3 antibody. In order to investigate whether low levels of Cav3 were being expressed as suggested by the western blots using the anti-His antibody, nickel affinity gel purification was undertaken on the soluble fraction from the cells grown in Magic media at 37°C. If Cav3 was being expressed, then it should have had a 6xHis-tag attached to it at the C-terminus. This tag can be used to purify the recombinant protein by binding it to Ni^{2+}.

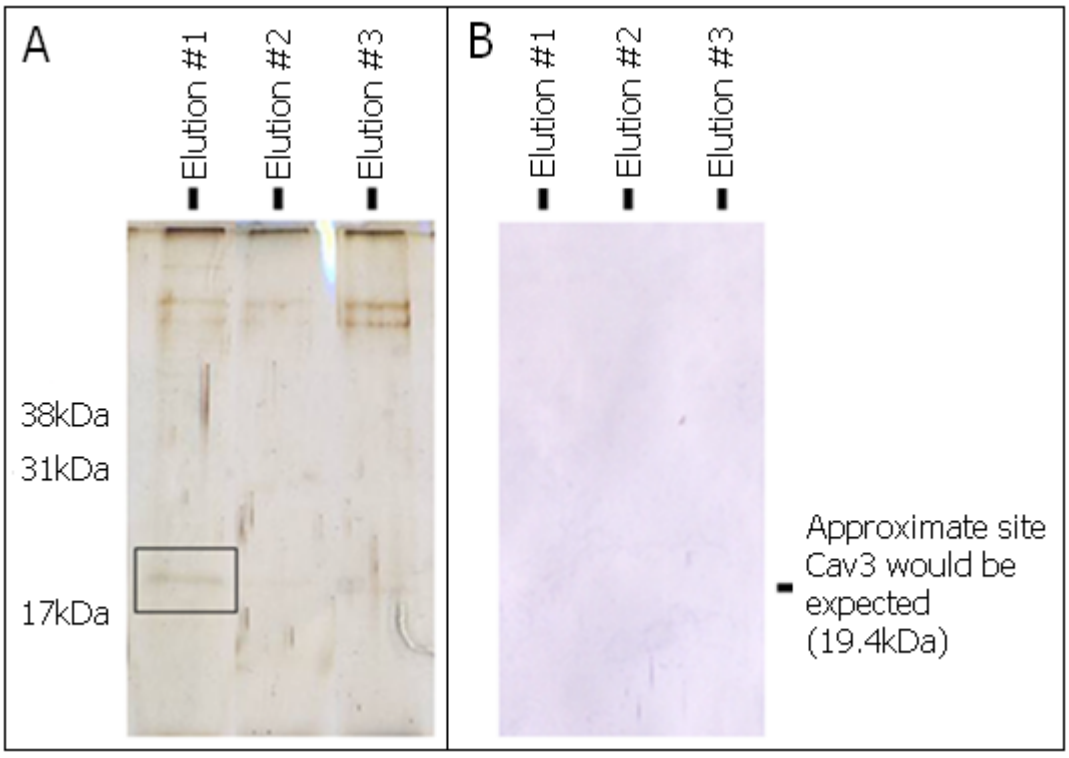

Figure 26: Nickel affinity gel purification of the soluble fraction.

The soluble fraction (from 37°C, Magic media) was applied to nickel affinity gel. The column was washed several times and the bound proteins were eluted with 300mM imidazole. The eluted fractions were examined by SDS-PAGE and the gel silver stained (**A**). A very faint band at ~21kDa was found in the elution fraction (boxed) at the

approximate position Cav3 would be expected. However, western blotting (using the anti-His-tag antibody) revealed no bands (**B**).

As can be seen in Figure 10 a very faint band was detected in the first elution fraction (Elution#01), which was located at the approximate position where Cav3 would be expected. However, western blotting using an anti-His-tag antibody did not hybridise against this protein band; in fact, there was an absence of any detectable bands. The band from the SDS-gel was excised and sent for mass spectrometry/trypsin digest sequencing identification, but this was not successful, likely due to the very low concentration. Thus, there was no evidence that the protein eluted from the nickel affinity matrix was Cav3.

Alternative lysis/Solubilisation conditions

The goal of expressing full-length human Cav3 was to develop conditions so that it was expressed in the soluble fraction. However, it became clear that obtaining a high yield of Cav3 in the soluble fraction using the Li and co-workers lysis/solubilisation protocol was not working. There did remain the possibility that Cav3 was being expressed, but that it was remaining in the insoluble fraction, i.e. the pellet. Cav3 is a membrane protein, therefore, it was possible that if Cav3 had formed part of the membrane fraction, or inclusion bodies, the lysis/solubilisation stage would be insufficient to break down these Cav3-containing membranes (Georgiou et al., 1999; Rinas and Bailey, 1992).

Given the successful protocol for Cav1 expression reported by (Li et al., 1996c) all the above experiments employed the same lysis/solubilisation buffer. To explore the possibility that this protocol had been insufficient to isolate Cav3 from the soluble fraction (by not fully breaking down the membrane), and to examine whether Cav3 was in the post-lysis *pellet* fraction, the protocol was modified to incorporate a range of more stringent solubilising conditions (intended to break down any potential membrane fraction that contained Cav3). These included the stepwise re-suspension of the pellet fraction in an increased concentration of lysozyme (to help break down any remaining cell wall), the addition of DNase, increased Triton X-100 (to help solubilise any remaining membrane) and the addition of the strong denaturant 8M Urea. At each stage, the samples were centrifuged, and the supernatant was analysed for Cav3.

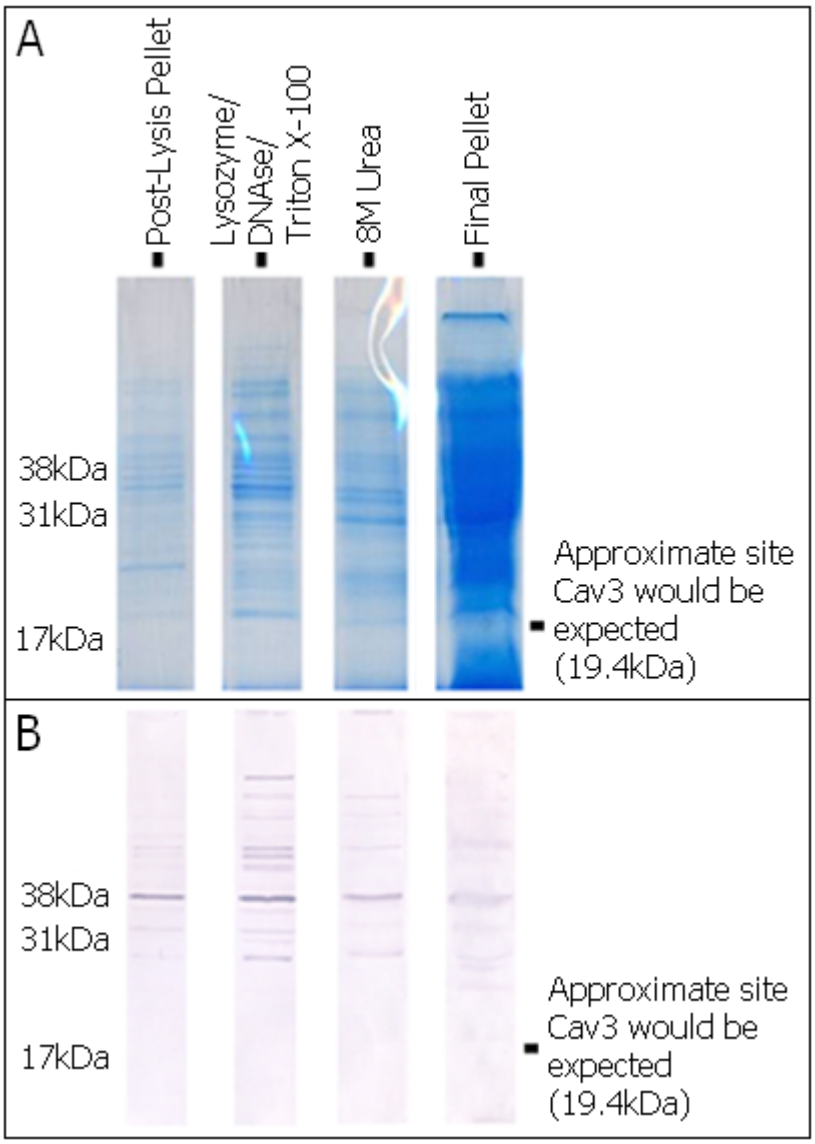

Figure 27: Solubilisation of the pellet fraction from cells grown for 5 hours in LB at 37°C and induced with 1.5mM IPTG at 0.8 OD^{600nm}.

Following the protocol outlined in the Materials and Methods (Treatment of the insoluble fraction, section Increased lysozyme, DNase, 8M Urea) the pellet fraction (from cells grown for 5 hours in LB at 37°C and induced with 1.5mM IPTG at 0.8 OD^{600nm}) was treated to several further stages of stepwise lysis/solubilisation: the addition of DNase (10µl/ml), an increase in lysozyme concentration (from 100mg/ml to 300mg/ml) and an increase in Triton X-100 concentration (from 0.5% to 1% (v/v)), then the addition of 8M Urea. **A:** Samples of the original pellet, the lysozyme/DNase treated, the Urea treated and the final pellet were boiled at 100°C then analysed by SDS-PAGE and stained in Coomassie solution. No obvious Cav3 band at the position predicted to correspond to a monomer is observed in any of lanes. **B:** Western blotting (anti-Cav3) shows multiple bands, but none corresponding to Cav3 at ~ 20 kDa.

As can be seen in Figure 27 none of the additional solubilisation conditions resulted in detectable Cav3. Further, no detectable Cav3 was found in the final pellet. Therefore it is possibly that Cav3 was never even expressed, or, if it was expressed, then it was possibly degraded rapidly by the host cell's proteolytic machinery. Thus, in the interest of time, attempts to express and purify full-length Cav3 using the pEX-C-His vector were discontinued.

2.3.2. Expressing full-length Cav3 in *E.coli* using the pET-His-SUMO vector

It would appear that the pEX-C-His vector may not be suitable for producing the full-length Cav3. One potential reason for the lack of success in expressing soluble Cav3 is due to the fact that Cav3 is a membrane protein. This means that it has an increased likelihood of possessing hydrophobic regions, which can be problematic for expressing recombinant proteins in hosts that lack the appropriate membrane composition/formation to accommodate the recombinant protein. Another possibility was that it was being rapidly degraded soon after production, or possibly never even expressed. In order to increase expression by enhancing the solubility of Cav3 the solubility-enhancing fusion protein, SUMO, was attached.

Primers were designed (not shown) to extract the Cav3 ORF from the OriGene vector that contained the full-length gene for Cav3, and it was then inserted into the pET-His-SUMO vector. This vector incorporates a SUMO-tag at the N-terminus. This vector also fuses a 6xHistag to the N-terminus of the SUMO fusion protein, resulting in the following: 6His-SUMO-Cav3 (see Figure 28). This 6xHis-SUMO fusion protein can be cleaved by the SUMO protease Ulp.

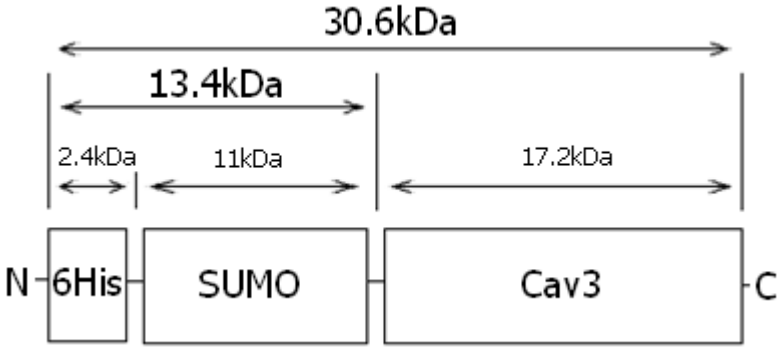

Figure 28: Schematic of the 6xHis-SUMO-Cav3 fusion protein

The Cav3 ORF has a N-terminal 6xHis-tag and SUMO-tag. The SUMO-tag is intended to enhance the solubility of the recombinant protein and lead to high protein yields. The

6xHis-tag will aid in the purification of the protein using nickel affinity gel. The total fusion protein is approximately 30.6kDa.

PCR optimisation

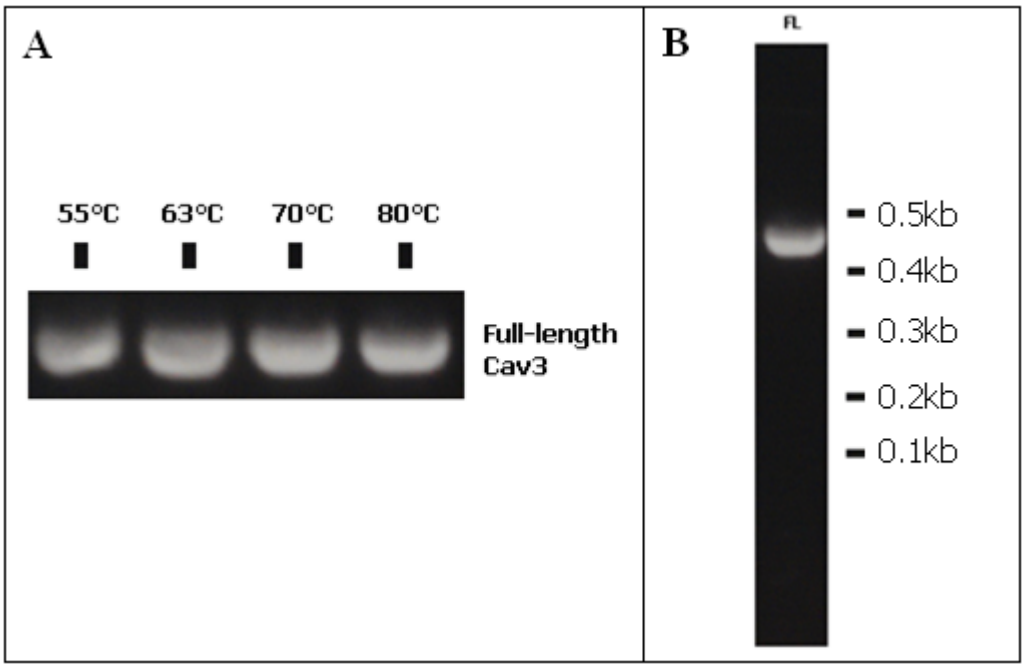

Figure 29: PCR optimisation for the full-length Cav3 gene.
A: Four different annealing temperatures were tested to optimise amplification: 55, 63, 70, 80°C. All temperatures produced comparable quantities of the PCR product. **B:** The post-PCR gel shows migration of a single 0.45kb PCR product, indicating a single PCR product had been produced.

To optimise PCR amplification a range of primer annealing temperatures were tested. 70°C proved negligibly optimum, although all temperatures appeared to work well (Figure 29, panel A). Only one band was produced (Figure 29, panel B), indicating that PCR amplification had successfully produced a homogenous PCR product. This PCR product was cloned into the pET-SUMO vector. To test if this ligation had been successful, *E.coli* was transformed with the newly created vector, pET-SUMO-Cav3, and cells were grown selecting for antibiotic resistance conferred by the vector. Colonies were selected for purification of the plasmid, and this was sent for DNA sequencing, where it was subsequently confirmed to have the correctly orientated Cav3 insert.

Expression of pET-SUMO-Cav3 at 26°C

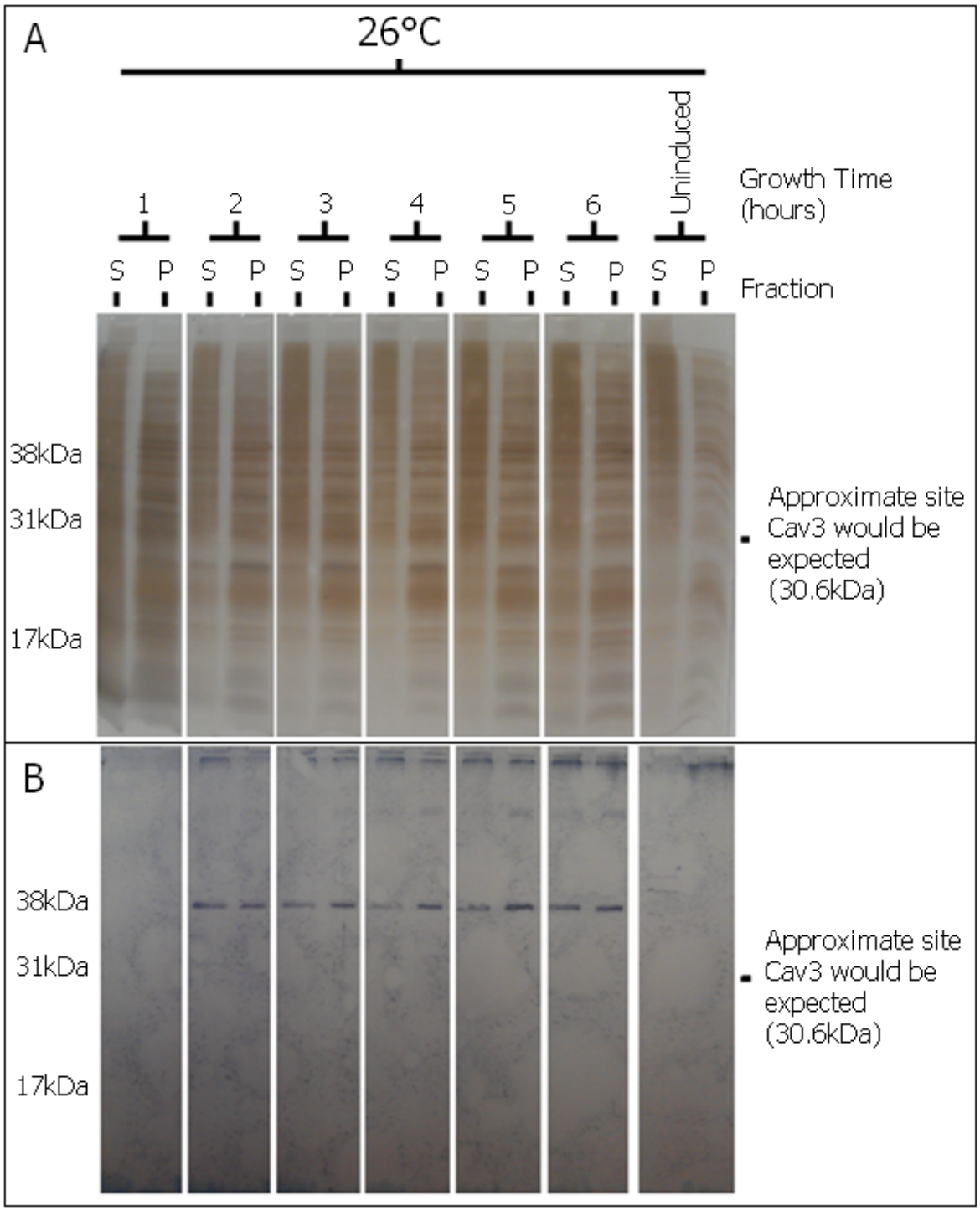

Figure 30: Protein expression profile of Cav3 transformed *E.coli* grown in LB at 26°C and induced with a 1mM IPTG (0.8 OD at 600nm).

Cells grown in LB for 1, 2, 3, 4 and 5hours at 26°C and induced with 1mM IPTG (at 0.8 OD^{600}) were solubilised following the protocol outlined in the Materials and Methods (Alternative protocols – for SUMO expression system). **A:** The soluble fraction, the SDS-resuspended pellet, and an un-induced (after 5hours) control were examined by SDS-PAGE and silver stained. Over-expression of Cav3 was not achieved, as shown by the lack of a prominent band at the expected position of Cav3 (~31kDa) **B:** Western-blotting was

carried out using an anti-Cav3 antibody. Note that western blotting detected a band of ~38kDa that was not present in the control or at the start point of induction (t=0). There are also bands at the top of the wells that might suggest that Cav3 has aggregated. However, the presence of similar band in the un-induced pellet fraction would make this conclusion less likely.

As can be seen from the SDS-PAGE gel in Figure 30 (panel A), no prominent Cav3 band was observed in the soluble or the pellet fractions. Interestingly, there appeared to be a band detected by immunostaining (Figure 30). However, it was at a position corresponding to ~38kDa, instead of the expected ~30.6kDa. This band was not observed in the un-induced control, nor the time point before induction (t=0), which would support the fact that the band did represent Cav3, albeit at the unexpected size. Gel migration abnormalities can occur for a variety of reasons, so it was possible that this was still Cav3. Regardless, the lack of a discernible soluble Cav3 band on the SDS-PAGE gel indicated that the expression system was not producing the high levels of soluble Cav3 desired. Western blotting has also identified bands at the top of the gel lanes that would usually indicate that the protein has aggregated and is unable to enter the gel. However, a similar band is also observed in the un-induced pellet fraction meaning either the well band does not correspond to Cav3, or that some degree of leaky expression has occurred in the control.

Expression of pET-SUMO-Cav3 at 37°C

Due to the lack of success in expressing high-levels of soluble Cav3 by inducing the cells to express at 26°C, as judged by SDS-PAGE, the expression temperature was adjusted to 37°C in order to test whether this would increase the expression of Cav3.

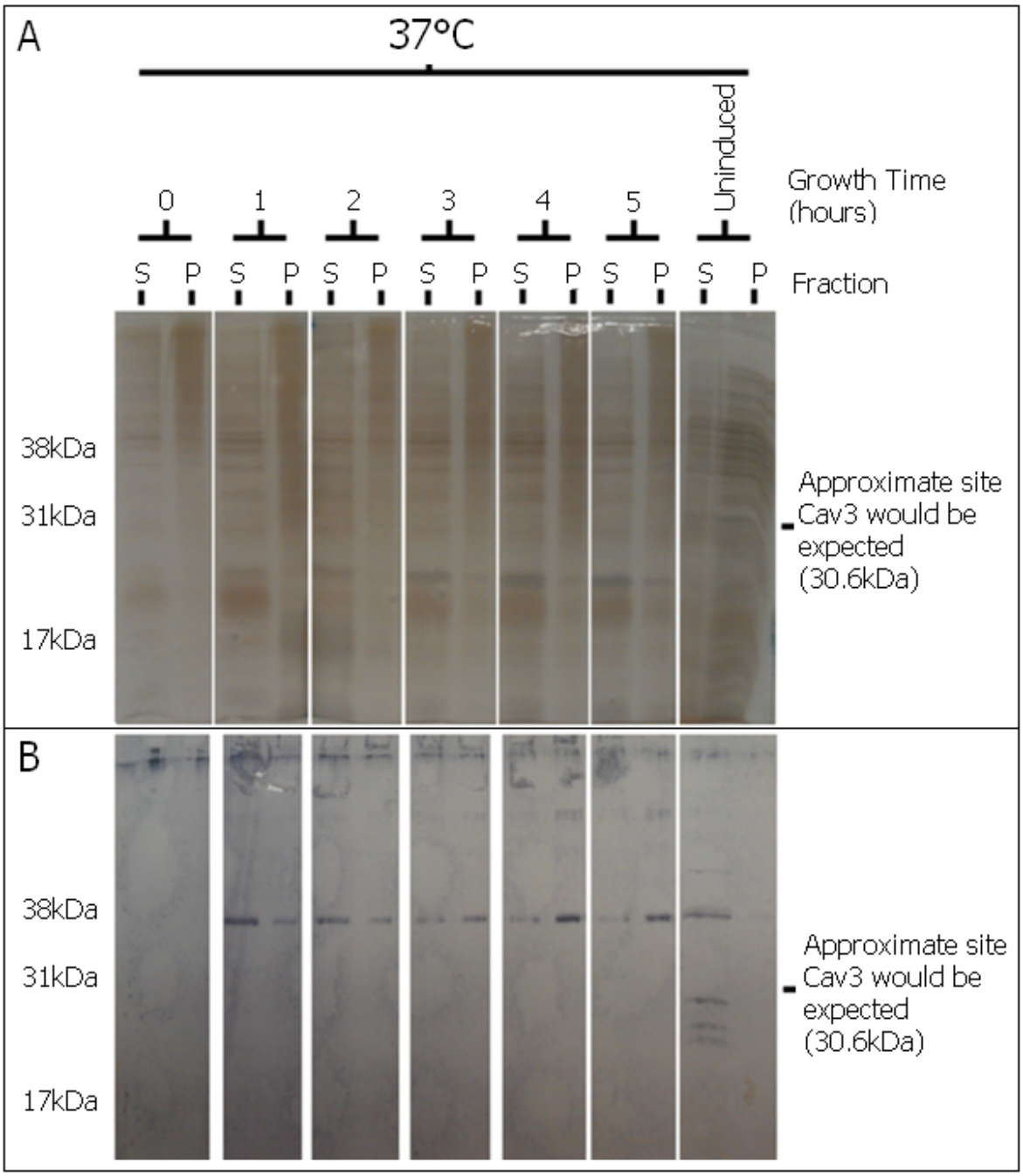

Figure 31: Protein expression profile of Cav3 transformed in *E.coli* grown in LB at 37°C and induced with a 1mM IPTG (0.8 OD at 600nm).

Cells grown in LB for 1, 2, 3, 4 and 5hours at 37°C and induced with 1mM IPTG (at 0.8 OD^{600}) were solubilised following the protocol outlined in the Materials and Methods (Alternative protocols – for SUMO expression system). **A:** The soluble fraction, the SDS-resuspended pellet, and an un-induced (after 5hours) control were examined by SDS-PAGE and silver stained. Over-expression of Cav3 was not achieved, as shown by the lack of a prominent band **B:** Western-blotting was carried out using an anti-Cav3 antibody. Note that western blotting detected a band of ~38kDa, but that this was also present in the un-induced control.

Shown in Figure 31 (panel A) are the polypeptide profiles for both the supernatant and cell pellets after induction and growth at 37°C. Comparison with the protein components of un-induced cells indicates that temperature has not had any notable effect on the expression levels, except that immunostaining revealed a band at ~38kDa in the uninduced control in these experiments (Figure 31, panel B). This finding can be interpreted as either1) the incorrectly sized band detected by immunostaining was not Cav3, 2) the antibody was unspecific, or 3) leaky expression of the protein was occurring. However, since there are no obvious 'additional' bands in either the pellet or supernatant fractions compared to the control un-induced samples then it would suggest that Cav3 is not being over-expressed.

Expression of pET-SUMO-Cav3 at 18°C

It was noted that there was generally a large amount of protein that remained in the pellet (see Figure 30 and Figure 31, panel A). It was also noted that the signal from immunostaining was stronger in the supernatant at the earlier time points post-induction, but stronger in the pellet fraction in the later time points (see Figure 31, panel B). These two observations could be due to Cav3 aggregation and subsequent separation into the pellet fraction post-lysis. Thus, it was decided to lower the temperature for induction to 18°C, in order to help reduce the potential degradation and aggregation of Cav3. In addition to the temperature change, efforts were made to address whether the antibody was non-specifically binding to *E.coli* proteins. *E.coli* cells were transformed with a control pET-SUMO vector with a chloramphenicol acetyl transferase (CAT) fusion protein instead of the Cav3 insert. In addition, this control would be a positive control for growth and induction. Cells were grown under the exact same conditions as the non-control cells.

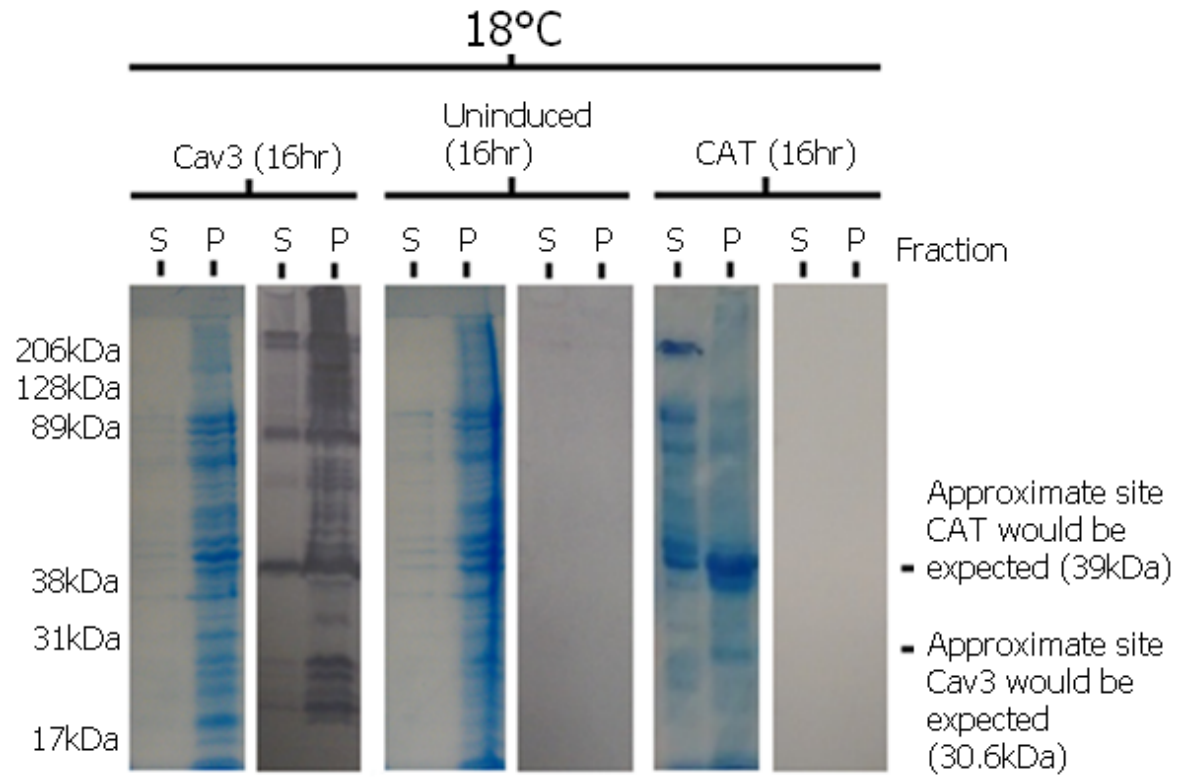

Figure 32: Protein expression profile of Cav3 and CAT transformed in *E.coli* grown for 16hours in LB at 18°C and induced with a 1mM IPTG (0.8 OD at 600nm).
Cells grown in LB for 16hours at 18°C and induced with 1mM IPTG (at 0.8 OD^{600}) were solubilised following the protocol outlined in the Materials and Methods (Alternative protocols – for SUMO expression system). The soluble fraction (S) and the SDS-resuspended pellet (P) for the pET-SUMO-Cav3 induced cells, the un-induced (after 16hours) control, and the pET-SUMO-CAT induced control were examined by SDS-PAGE and Coomassie stained. Over-expression of Cav3 was not achieved, as shown by the lack of a prominent band. Over-expression of CAT was achieved, although unexpectedly it remained predominantly in the pellet fraction**.** Western-blotting was carried out using an anti-Cav3 antibody. Note that many different bands were observed in the Cav3 induced cells that were not detected in the un-induced control. No non-specific bands were observed in the CAT expressing control. The approximate positions that the Cav3 fusion protein (30.6kDa) and the CAT fusion protein would be expected are shown on the right.

As can be seen in Figure 32 reducing the induction temperature did not result in any increase in Cav3 yields. Moreover, and somewhat confusingly, western blotting identified a range of bands of varying molecular mass, which might indicate either a non-specific binding of the antibody, or that the Cav3 being expressed was not homogenous in size. Interestingly, in contrast to induction at 37°C, there did not appear to be any bands

detected by immunostaining in the un-induced fraction, indicating that an increased induction temperature may have been responsible for the leaky expression observed at 37°C (see Figure 31). Another interesting observation was that there was generally more total protein expression at lower temperatures, which may be in some way attributed to Cav3 being toxic to the host.

As can be seen there is a large band (~39kDa) corresponding to the CAT protein found in the pellet fraction. This ensures that the growth and induction conditions were sufficient for expression of the pET-His-SUMO vector. However, it would appear that the cell lysis, in this particular example, was not sufficient, as the CAT fusion protein appears to have remained in the pellet fraction, possibly as a result of an inappropriate choice of lysis buffer or lysis conditions. Interestingly, immunostaining revealed that the anti-Cav3 antibody did not detect any proteins, which may suggest that the antibody is not non-specific and that the multiple bands being detected by immunostaining in the Cav3 containing induced cells may represent multimers of Cav3. However, although the cell lines for the control and Cav3 were genetically the same, the presence of two different vectors, and thus the expression of different fusion proteins would have an effect on the other proteins being expressed within the cell.

Nickel affinity gel purification

Since the protein bands detected by western blotting may have corresponded to Cav3 oligomers the soluble fraction was applied to a Ni^{2+} affinity resin.

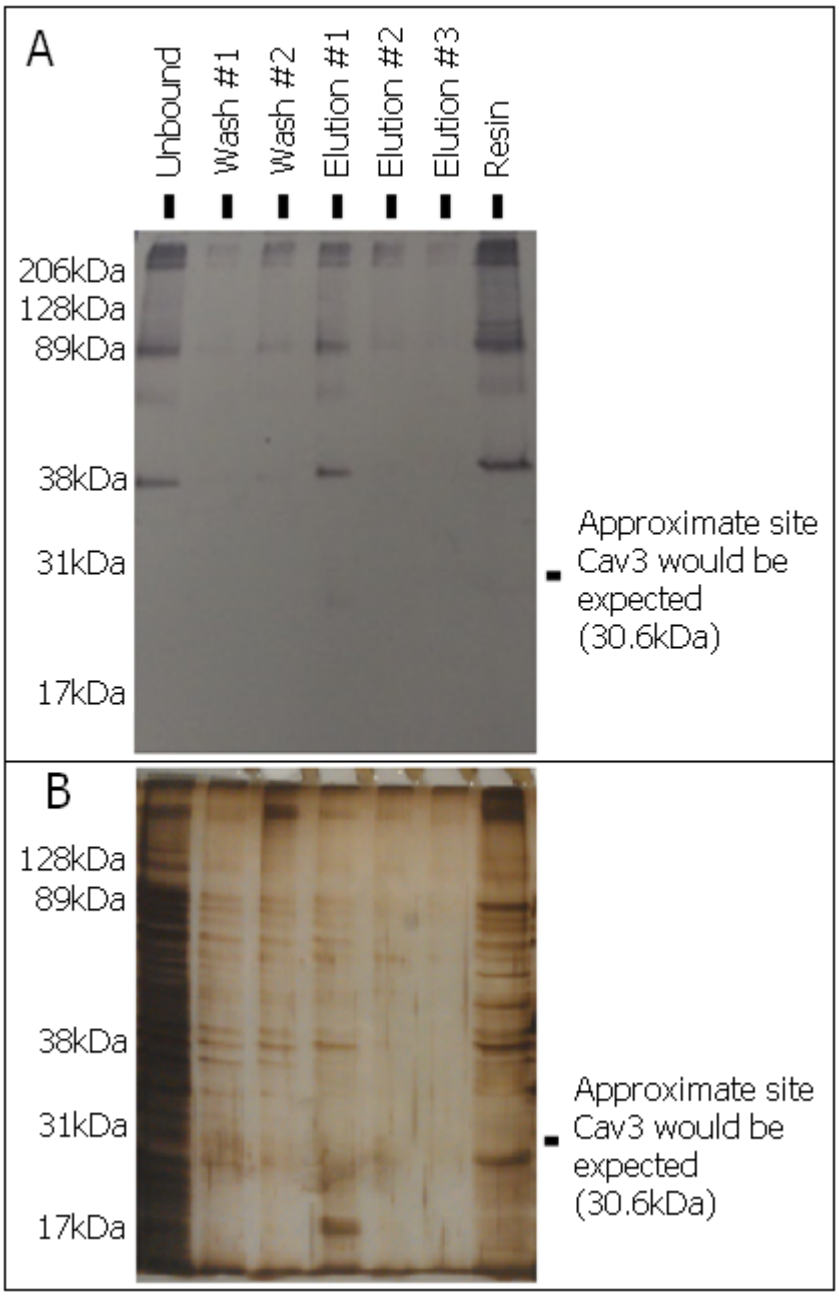

Figure 33: Nickel affinity gel purification of the soluble fraction.

The soluble fraction (from 18°C, 16hr, LB, 1mM IPTG) was applied to nickel affinity gel. The column was washed several times and the bound proteins were eluted with 300mM imidazole. **A:** Western blotting (using the anti-His-tag antibody) revealed that a ~38kDa protein was found in both the elution and the final resin fraction, indicating that whatever it was, it had bound to the nickel affinity gel. Several other large bands were also present. **B:** The eluted fractions were examined by SDS-PAGE and the gel silver stained. The elution fraction contained the ~38kDa protein, as well as a 17kDa protein. This ~17kDa protein was not detected on the western blot, thus it is unlikely to be Cav3. The final resin showed multiple protein bands, including the 38kDa band and another band at ~28kDa. This

~28kDa, although approximately at a size corresponding to the Cav3 fusion protein was not detected on the western blot, thus it is unlikely to be Cav3.

The results of attempts to separate out proteins expressed with a His-tag from the other *E.coli* proteins are shown in Figure 33. Although the ~38kDa band, which was suspected to be a potentially variant of Cav3, was found in the elution, it was also found in the final resin. Moreover, the elution fraction also contained another rather large band, which, although of a similar size to that expected for the Cav3 fusion protein was not Cav3 (according to the western blot in panel A). Thus, not only was the purification method not fully purifying what was only *potentially* a form of Cav3, it was also purifying another protein that was not Cav3. At this point a decision was made to discontinue any attempts to express and purify full-length soluble Cav3 in *E.coli*.

2.3.3. Expressing the N^{1-74} domain in *E.coli* using the pEX-His-Trx vector

The experiments above suggest that *E.coli* may not be suitable for producing the *full-length* Cav3 and thus a *domain* expression approach was taken. Four domains were selected N^{1-54}, N^{1-74}, N^{1-101} and C^{92-151}. Note that 'N' here refers to a domain that incorporates the N-terminus, and 'C' refers to domains that incorporate the C-terminus of Cav3. The numbers correspond to the residues.

This section reports studies of the N^{1-74} domain. Primers were designed to extract the region corresponding to the first 74 residues (hereby referred to as N^{1-74}) from the OriGene vector that contained the full-length gene for Cav3 to be inserted into the pEX-His-Trx vector. This vector incorporates a N-terminal thioredoxin fusion protein. This vector also fuses a 6xHis-tag to the N-terminus of the thioredoxin fusion protein, resulting in the following: 6xHis-Thioredoxin-N^{1-74} (see Figure 34). The 6xHis-Thioredoxin fusion protein can be cleaved from the N^{1-74} domain by the thrombin protease.

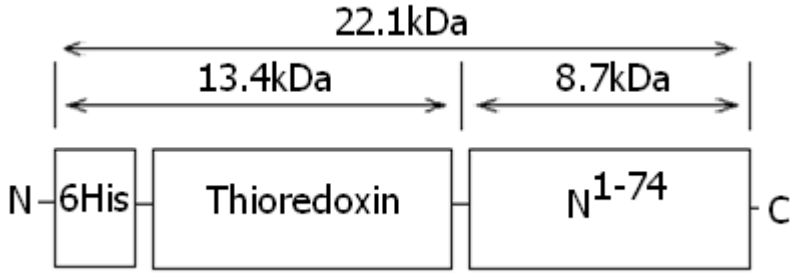

Figure 34: Schematic of the 6xHis-Thioredoxin-N^{1-74} fusion protein.
The N^{1-74} ORF has a N-terminal 6xHis-tag and Thioredoxin-tag. The thioredoxin-tag is intended to enhance the solubility of the recombinant protein and to optimise protein

yields. The 6xHis-tag will aid in the purification of the protein using nickel affinity gel. The total fusion protein is approximately 22.1kDa.

PCR optimisation

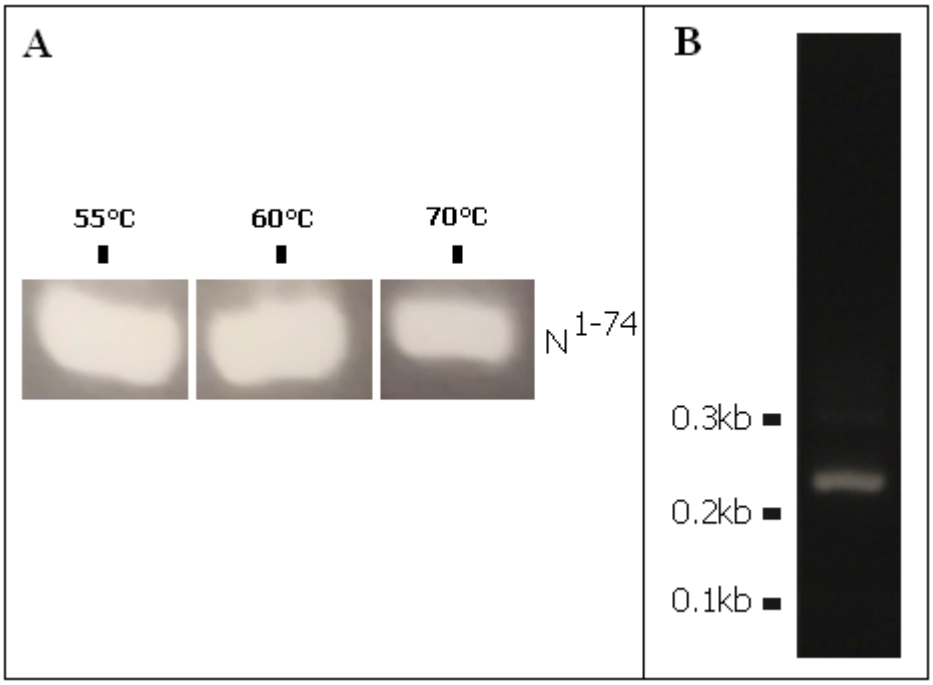

Figure 35: PCR optimisation for the DNA coding for the N^{1-74} domain.
A: Three different annealing temperatures were tested to optimise amplification: 55, 60, 70°C. 55 and 60 °C produced comparable quantities of the PCR product. **B:** A post-PCR gel shows migration of a single ~0.22kb PCR product, indicating a single PCR product had been produced.

To optimise PCR amplification, a range of primer annealing temperatures was tested; 55°C and 60°C appear to be optimum as shown in Figure 19A. In addition, only one band was produced (Figure 35, panel B), indicating that amplification had successfully produced a homogenous PCR product. This PCR product was cloned into the pEX-His-Trx vector. To test if this ligation had been successful, *E.coli* was transformed with the newly created vector, pEX-His-Trx-N^{1-74}, and cells were grown selecting for antibiotic resistance conferred by the vector. Successful colonies were used for purification of the plasmid, and sent for DNA sequencing, where it was subsequently confirmed to have the correctly orientated N^{1-74} insert within it.

Expression of N^{1-74} at 28°C

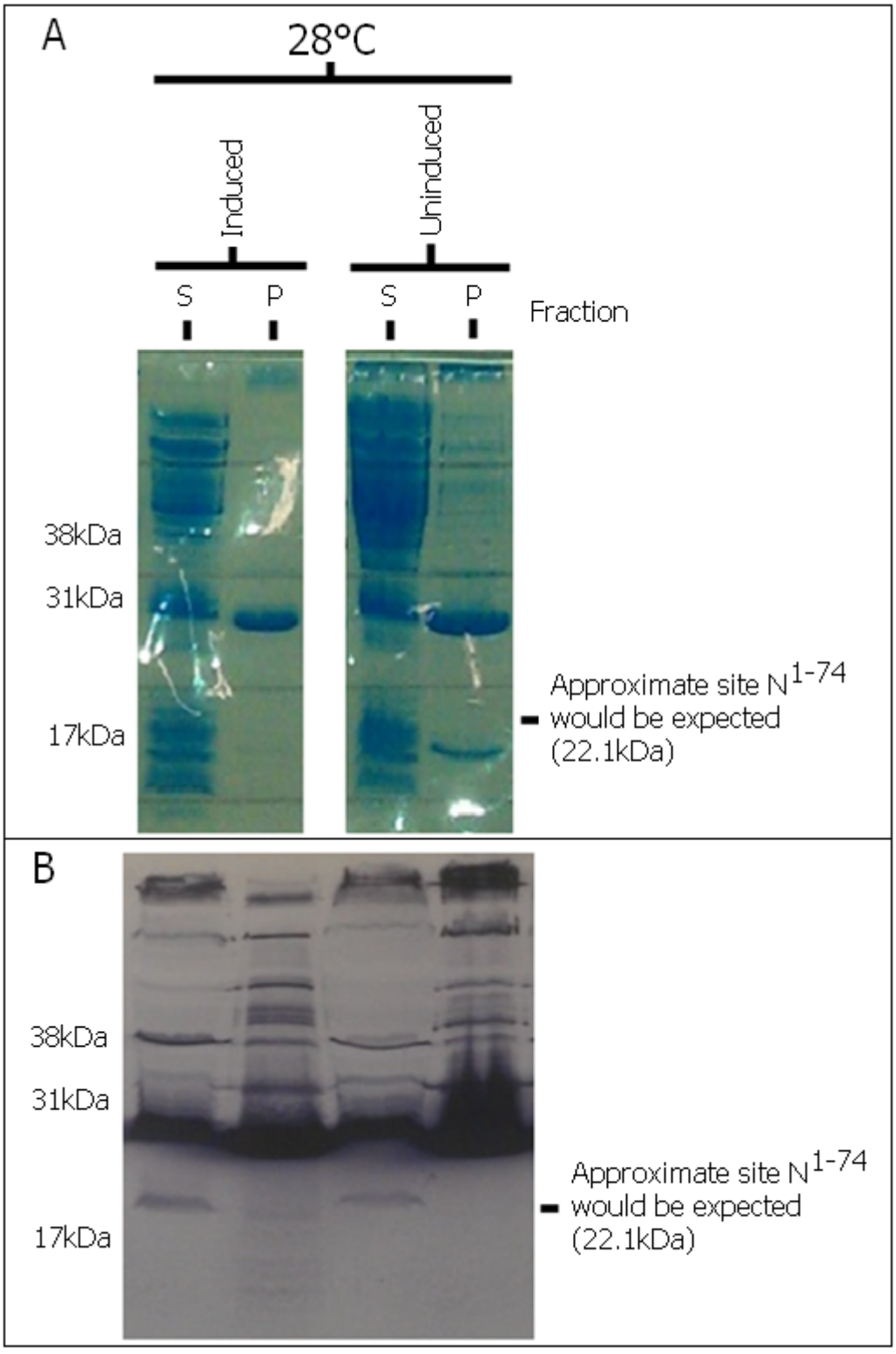

Figure 36: Protein expression profile of N^{1-74} transformed *E.coli* grown for 5 hours at 28°C and induced with a 1mM IPTG (cell density 0.8 at OD^{600nm}).

Cells were grown for 5hours in LB at 28°C and induced with 1mM IPTG (at 0.8 OD^{600}) and lysed. **A:** The soluble fraction (S) and the SDS-resuspended pellet (P) for both the induced cells and the un-induced (after 5hours) control cells were examined by SDS-PAGE stained in Coomassie blue solution. Examination of the SDS-PAGE gel did not find

a protein band at the position expected for the N^{1-74} fusion protein (~22.1kDa). However, a large band corresponding to a protein of approximately 27kDa in mass was observed. This band is predominantly found in the pellet fraction, and is also observed in the un-induced control. **B:** Western-blotting was completed using an anti-His-tag antibody. Note that the 27kDa band is detected by the antibody, indicating that this protein likely houses a His-tag. In addition a fainter band at approximately the correct positions is observed. However, this band is observed in both the induced and the uninduced samples.

As can be seen in both the Coomassie stained gel (Figure 36, panel A) and the Western blot (Figure 36, panel B), a large band was observed. However, this same band was also found in the uninduced control. Moreover, the bands are not quite at the correct size location expected for the N^{1-74} fusion protein. The N^{1-74} fusion protein has a calculated molecular mass of 22.1kDa, whereas the large band observed on the Coomassie gel corresponds to approximately 27kDa. However, the 27kDa band was also detected by immunostaining. Since this band was also detected in un-induced cells it would seem unlikely that it corresponds to the N^{1-74} fusion protein although it is also possible that the vector is expressing the N^{1-74} fusion domain regardless of induction, possibly due to an insertion error and/or very leaky-expression. However, even if this band did correspond to the N^{1-74} fusion protein, it predominantly remained in the pellet fraction. In addition, a faint band at approximately the expected position for the N^{1-74} fusion protein (~22kDa) is observed. However, this band is also observed in the uninduced control, and it does not have a corresponding over-expressed band on the Coomassie stained gels.

Detergent trial

In the event that the cells were expressing the N^{1-74} fusion protein without the need for induction, the peak fraction (pellet, 28°C, Induced) was treated to the strong denaturant 8M Urea, then dialysed into STE buffer containing one of the following detergents: 1.5% (w/v) CHAPS, 1.5% (w/v) n-Dodecyl-ß-maltoside, 1.5% (v/v) Triton X-100, 1.5% (w/v) n-octyl-β-D-glucoside in order to investigate whether this protein could be solubilised, a step essential for any further analysis.

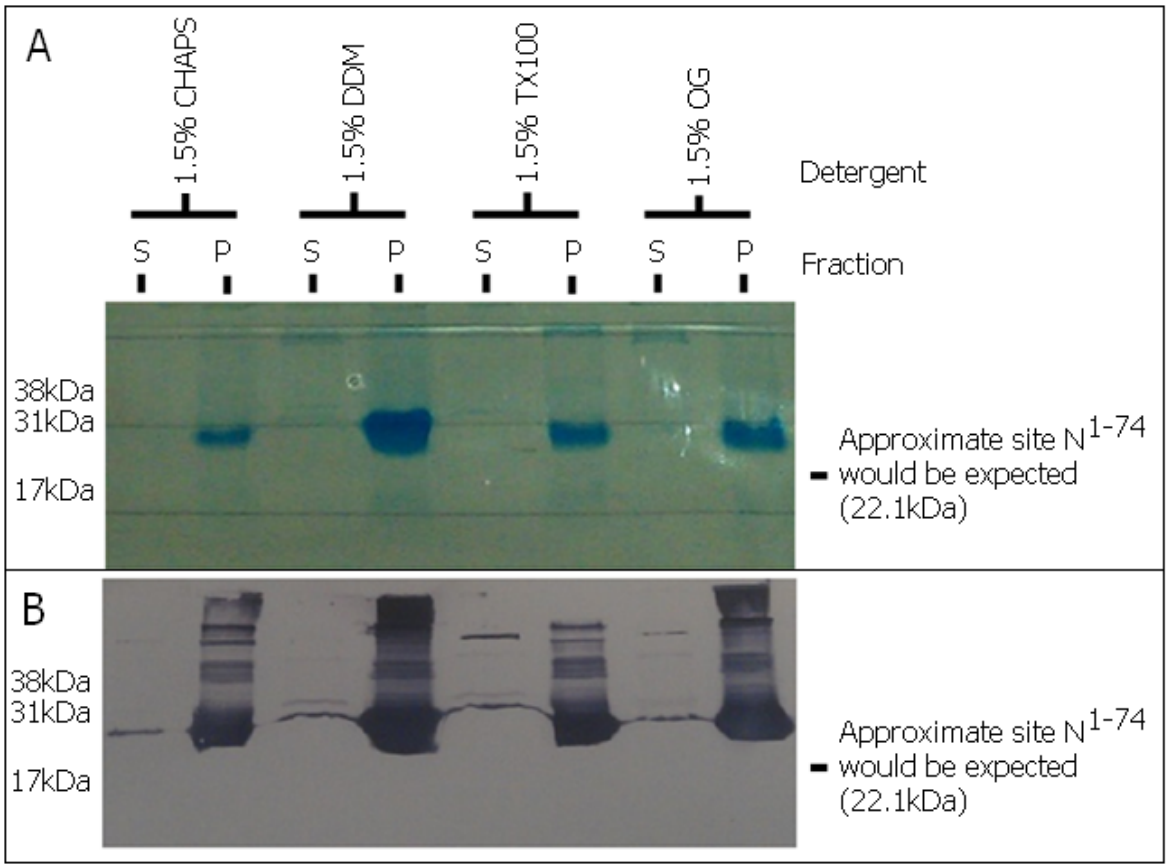

Figure 37: Detergent trial.

Pellets from Induced cells (28°C, 1mM IPTG, time point 5hours) were treated with 8M urea, then dialysed into STE buffer containing one of the following detergents: 1.5% CHAPS, 1.5% (w/v) n-Dodecyl-ß-maltoside, 1.5% (v/v) Triton X-100, 1.5% (w/v) n-octyl-β-D-glucoside, as described in the Materials and Methods section Strong denaturants and detergent exchange. **A:** Samples of the supernatant and SDS-resuspended pellet fractions were examined by SDS-PAGE and Coomassie stained. **B:** Western blotting employed an anti-His antibody. Examination of the gel and western blot reveal that the ~27kDa protein band was not solubilised by any of the conditions employed.

As can be seen in Figure 37, the treatment of the cell pellet with the strong denaturant 8M urea and subsequent dialysis into alternate detergent containing buffers did not lead to solubilisation of the ~27kDa protein. Therefore, even if this band corresponded to the N^{1-74} fusion protein, with an anomalous migration on the SDS-gel, then solubility was clearly an issue that would hinder further study. Moreover, attempting to break down inclusion bodies (inactive aggregates of protein) using strong denaturants such as urea or guanidine, and then refolding the protein, is in itself fraught with further potential pitfalls. Thus, in the interest of time, no further expression conditions were explored and attention was turned to another construct.

2.3.4. Expressing the N^{1-54} domain in *E.coli* using the pEX-His-Trx vector

Primers were designed to extract the region corresponding to the first 54 residues (hereby referred to as N^{1-54}) from the OriGene vector that contained the full-length ORF for Cav3. This region was inserted into the pEX-His-Trx vector. As described above, this vector fuses a 6xHis-tag and thioredoxin protein to the N-terminus of the N^{1-54} domain. The total fusion protein is approximately 19.6kDa (see Figure 38).

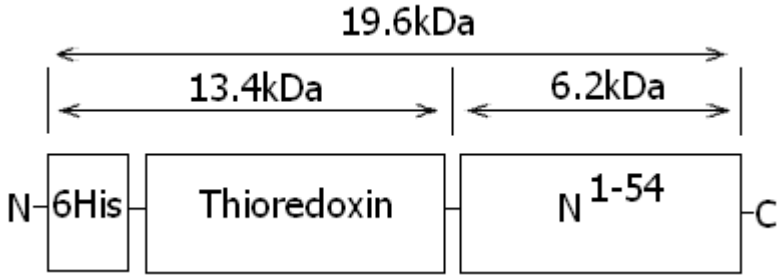

Figure 38: Schematic of the 6xHis-Thioredoxin-N^{1-54} fusion protein.
The N^{1-54} ORF has a N-terminal 6xHis-tag and thioredoxin tag. The thioredoxin-tag is intended to enhance the solubility of the recombinant protein and increase the observable yield. The 6xHis-tag will aid in the purification of the protein using nickel affinity gel. The total fusion protein is approximately 19.6kDa.

PCR optimisation

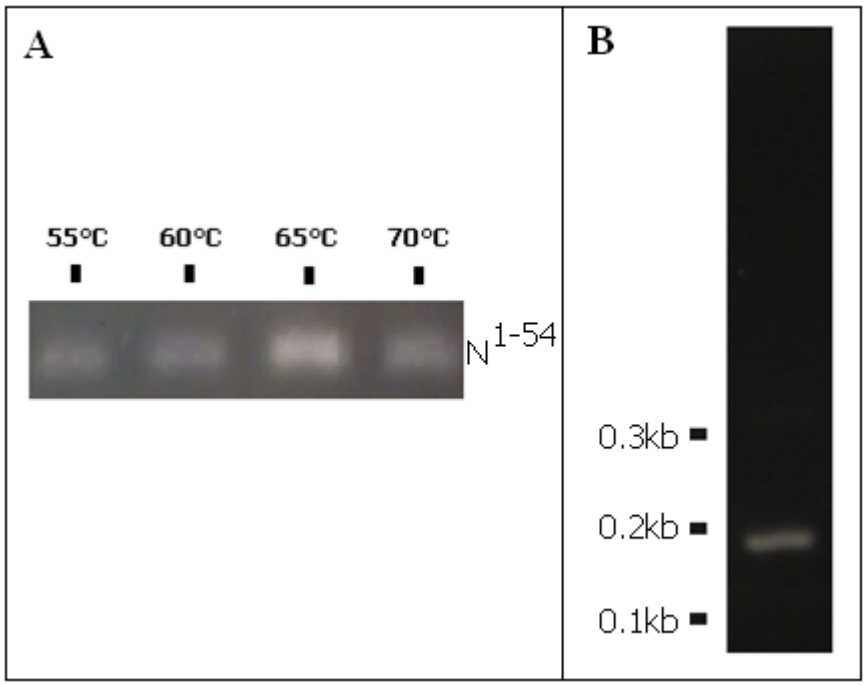

Figure 39: PCR optimisation for the DNA coding for the N^{1-54} domain.

A: Four different annealing temperatures were tested for amplification: 55, 60, 65 and 70°C. 65°C produced the most PCR product. **B:** A post-PCR gel shows migration of a single ~0.16kb PCR product, indicating a single PCR product had been produced.

To optimise PCR amplification a range of primer annealing temperatures were tested; 65°C proved optimum, as shown in Figure 23 above. In addition, only one band was visualised, indicating that amplification had successfully produced a homogenous PCR product. This PCR product was cloned into the pEX-His-Trx vector. To test if this ligation had been successful, *E.coli* was transformed with the newly created vector, pEX-His-Trx-N^{1-54}, and cells were grown selecting for antibiotic resistance conferred by the vector. Successful colonies were used for purification of the plasmid and sent for DNA sequencing, where it was subsequently confirmed to house the correctly orientated N^{1-54} insert.

Expression of N^{1-54} at 37°C

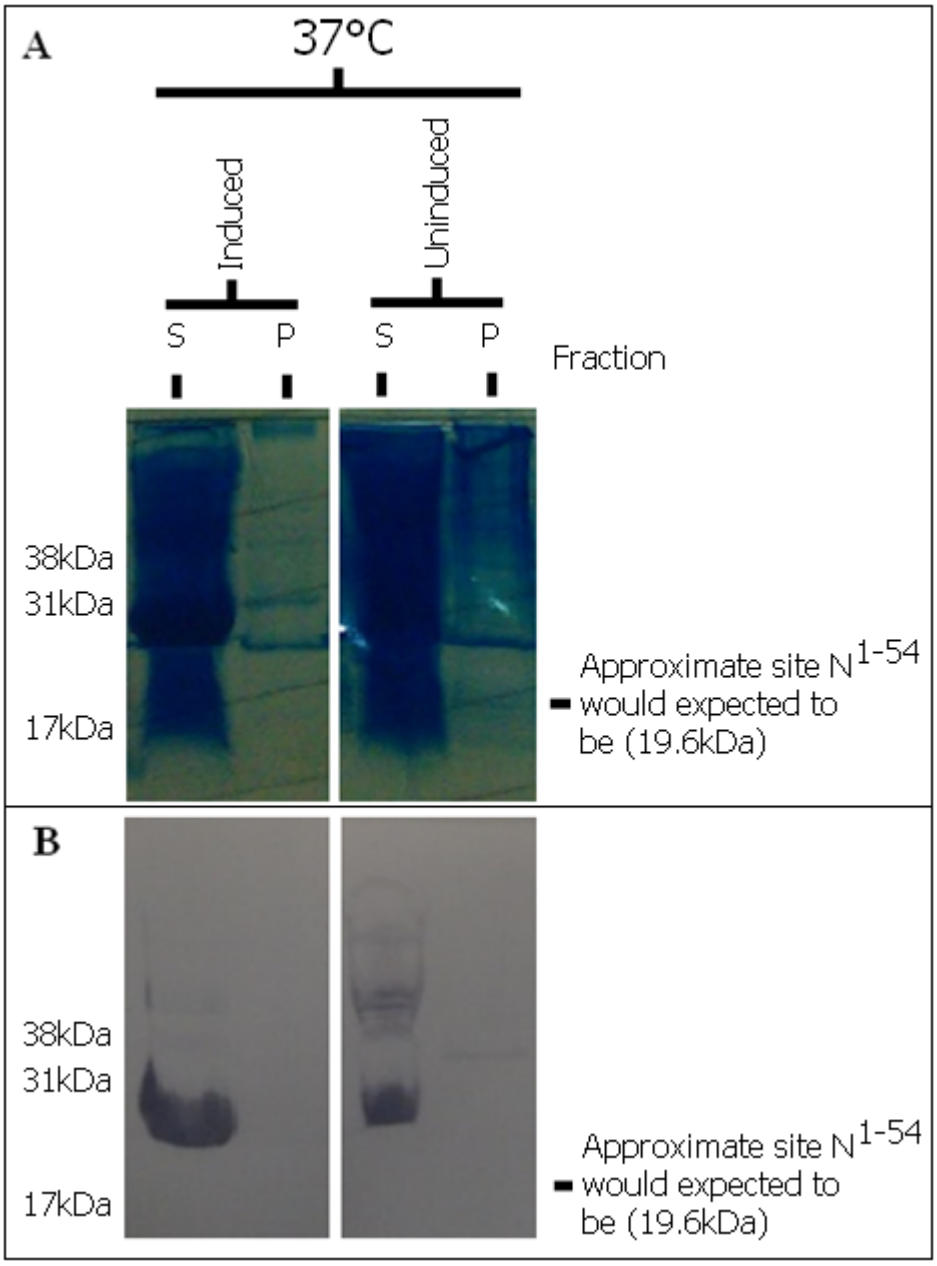

Figure 40: Protein expression profile of N^{1-54} transformed *E.coli* grown for 4 hours at 37°C and induced with a 1mM IPTG (cell density 0.8 at OD^{600nm}).

Cells grown for 4hours in LB at 37°C and induced with 1mM IPTG (at 0.8 OD^{600}) lysed. Both the pellet and supernatant were analysed by SDS-PAGE and western blotting **A:** The soluble fraction (S) and the SDS-resuspended pellet (P) for both the induced cells and the un-induced (after 5hours) control cells were examined by SDS-PAGE stained in Coomassie staining solution. No over-expressed protein was located at the position expected for the N^{1-54} fusion protein. However, a large band corresponding to a protein of approximately 29kDa in mass was observed. This band was found in both the induced cells and the un-induced control cells. **B:** Western-blotting was completed using an antibody

raised against the His-tag fused to the N-terminus of the fusion protein. Note that the 29kDa band is detected by the antibody, indicating that this protein possesses a His-tag.

As was the case for the N^{1-74} domain above, both the Coomassie stained gel and the immunostaining detected over-expression of a fusion protein in both the un-induced control at ~29 kDa. Given the lack of success with the expression of the N^{1-74} domain using the pEX-His-Trx vector expressing trials using the pEX-His-Trx vector were discontinued.

2.3.5. Expressing the N^{1-54} domain in *E.coli* using the pET-His-SUMO vector

The N^{1-54} domain was inserted into the pET-His-SUMO vector. This vector incorporates a N-terminal SUMO-tag. This vector also fuses a 6xHis-tag to the N-terminus of the SUMO fusion protein, resulting in the following: 6xHis-SUMO-N^{1-54}. This 6xHis-SUMO fusion protein can be cleaved by the SUMO protease Ulp.

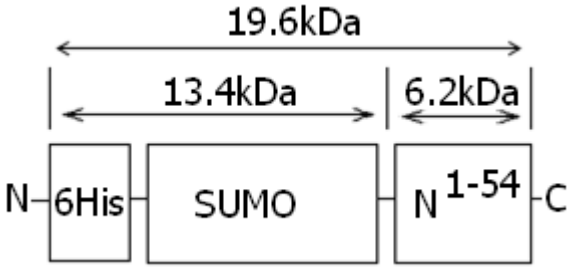

Figure 41: Schematic of the 6xHis-SUMO-N^{1-54} fusion protein.
The N^{1-54} ORF has a N-terminal 6xHis-tag and SUMO-tag. The SUMO-tag is intended to enhance the solubility of the recombinant protein and increase the observable yield. The 6xHis-tag will aid in the purification of the protein using nickel affinity gel. The total fusion protein is approximately 19.6kDa.

PCR optimisation

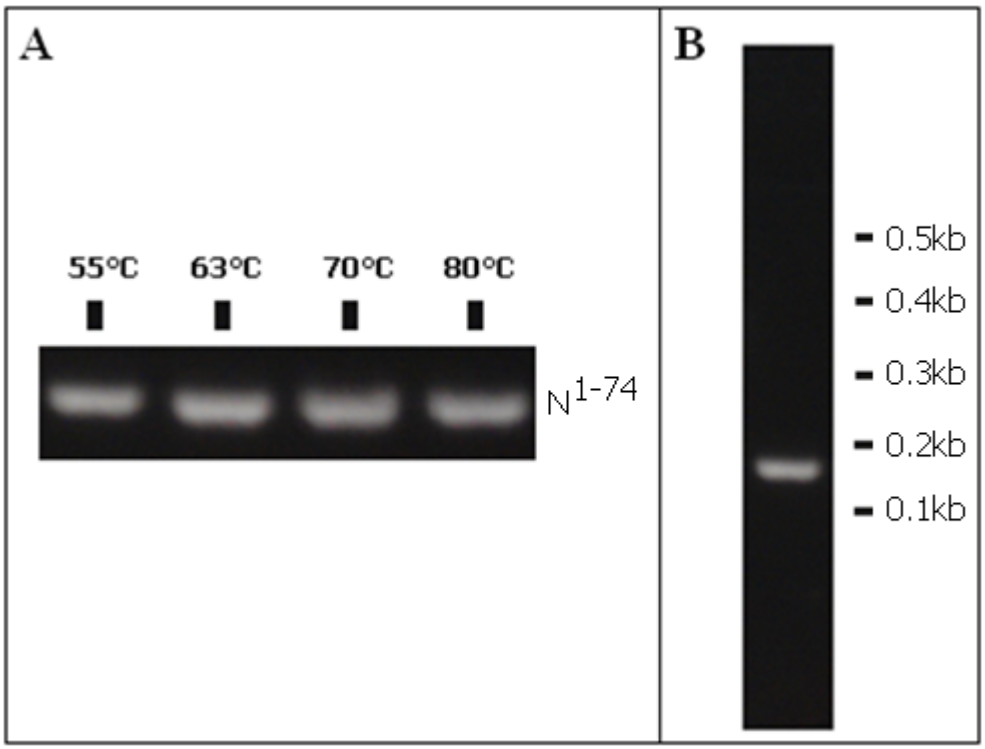

Figure 42: PCR optimisation for the DNA coding for the N^{1-54} domain.
A: Four different annealing temperatures were examined for optimisation of amplification: 55, 63, 70 and 80°C. 63°C produced the most PCR product. **B:** A post-PCR gel shows the migration of a single ~0.16kb PCR product, indicating a single PCR product had been produced.

To optimise PCR amplification a range of primer annealing temperatures were tested; 63°C proved optimum (see Figure 42, panel A). In addition, only one band was produced, indicating that amplification had successfully produced a homogenous PCR product (see Figure 42, panel B). This PCR product was cloned into the pET-His-SUMO vector. To test if this ligation had been successful, *E.coli* was transformed with the newly created vector, pET-His-SUMO-N^{1-54}, and cells were grown selecting for antibiotic resistance conferred by the vector. Successful colonies were used for purification of the plasmid, and this was sent for DNA sequencing confirming the presence of the correctly orientated N^{1-54} insert.

Expression at of N^{1-54} at 37°C

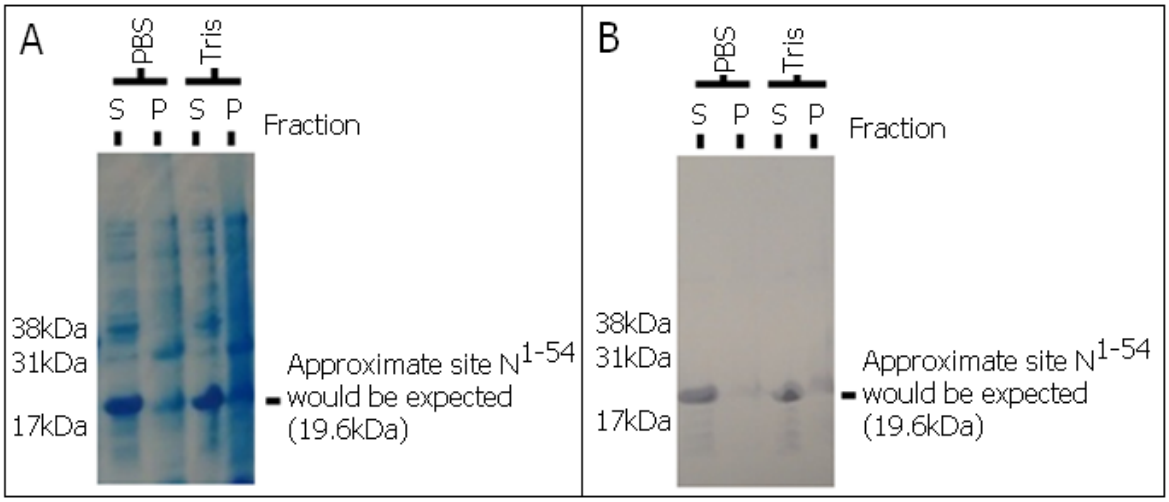

Figure 43: Protein expression profile of N^{1-54} transformed in *E.coli* cells grown for 4 hours at 37°C and induced with a 1mM IPTG (cell density 0.8 at OD^{600nm}) and solubilised using two different buffer systems.

Cells grown for 4 hours in LB at 37°C and induced with 1mM IPTG (at 0.8 OD^{600}) were solubilised following the protocol outlined in the Materials and Methods (Alternative protocols – for SUMO expression system). **A:** The soluble fraction (S) and the SDS-resuspended pellet (P) obtained *via* either a Tris-based solubilisation buffer or PBS-based solubilisation buffers were examined by SDS-PAGE stained in Coomassie blue solution. An over-expressed band was located at the position expected for the N^{1-54} fusion protein. This band was predominantly found in the soluble fraction. Both buffer systems resulted in soluble N^{1-54} fusion protein. **B:** Western-blotting using an anti-Cav3 antibody revealed a band with a molecular mass that corresponded to that predicted for the N^{1-54} fusion protein.

The SDS-PAGE and western blot presented in Figure 43 shows that the N^{1-54} fusion domain is expressed and that both solubilisation buffers (Tris and PBS-based buffers) employed lead to soluble protein. Moreover, the large band indicated that the fusion domain was being expressed at a high concentration. Given this successful expression, the next stage was to purify the fusion protein.

Nickel affinity gel purification of N^{1-54}

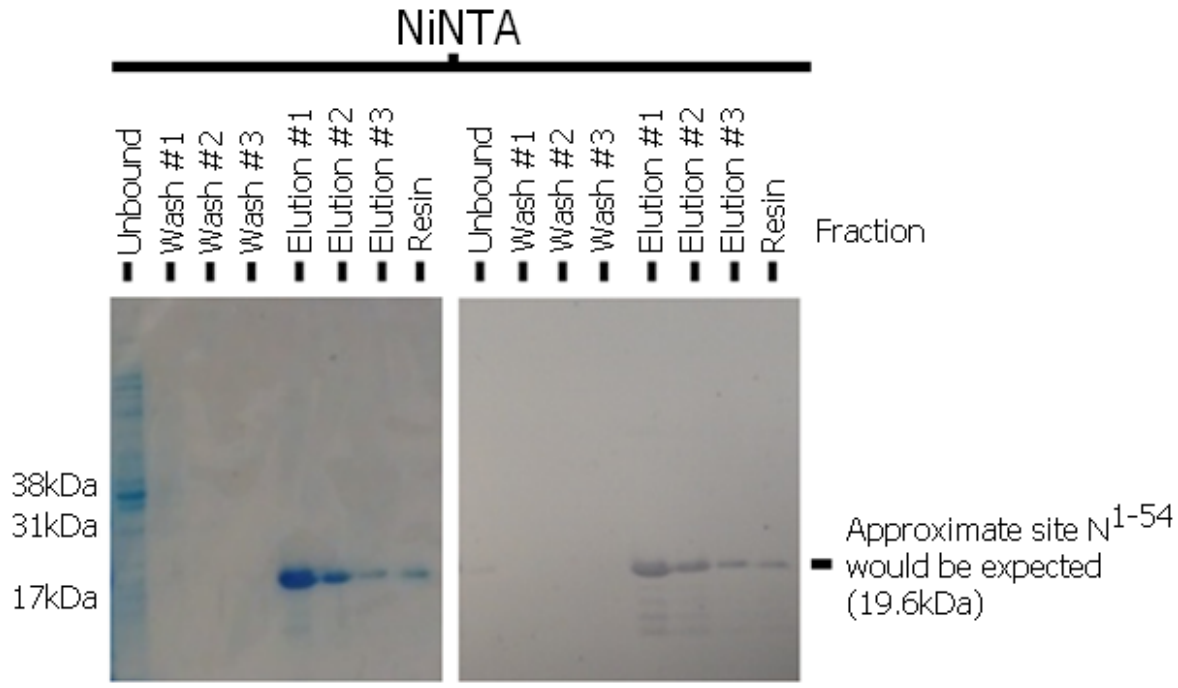

Figure 44: Nickel affinity gel purification of the N^{1-54} domain.
The soluble fraction from lysed cells grown at 37°C (4hr, LB, 1mM IPTG) was applied to nickel affinity gel. The column was washed several times and the bound proteins were eluted with 300mM imidazole. **A:** Fractions were examined by SDS-PAGE and Coomassie stained. There is a band at ~20kDa which would correspond to the predicted molecular mass of the N^{1-54} fusion protein with the majority of the protein in the first elution. **B:** Western blotting using an anti-Cav3 antibody confirmed the identity of the ~20kDa band as the N^{1-54} fusion protein.

The soluble fraction of the cell lysate was applied to a nickel affinity column. The SDS-PAGE and western blot in Figure 44 show that the N^{1-54} fusion domain has been purified to near homogeneity. Western blotting confirmed the identity of the ~20kDa band as the N^{1-54} fusion domain although several lower molecular mass bands were observed in the first elution. These likely correspond to truncates of the construct. However, it is clear by their absence from the Coomassie stained gel that these are minor components and the majority of the isolated protein is the full-length N^{1-54} fusion domain. In order to remove the SUMO tag for a pure N^{1-54} domain a range of different cleavage conditions were explored.

SUMO cleavage

The fusion protein is designed in such a way that the 6xHis-tag-SUMO fusion protein can be cleaved by the SUMO protease, Ulp. In order to determine the optimum cleavage conditions, a range of factors known to affect cleavage efficiency were tested. They included the protease concentration, NaCl concentration and the presence/absence of protease inhibitors (cOmplete, Mini, EDTA-free protease inhibitor cocktail tablets (Roche)).

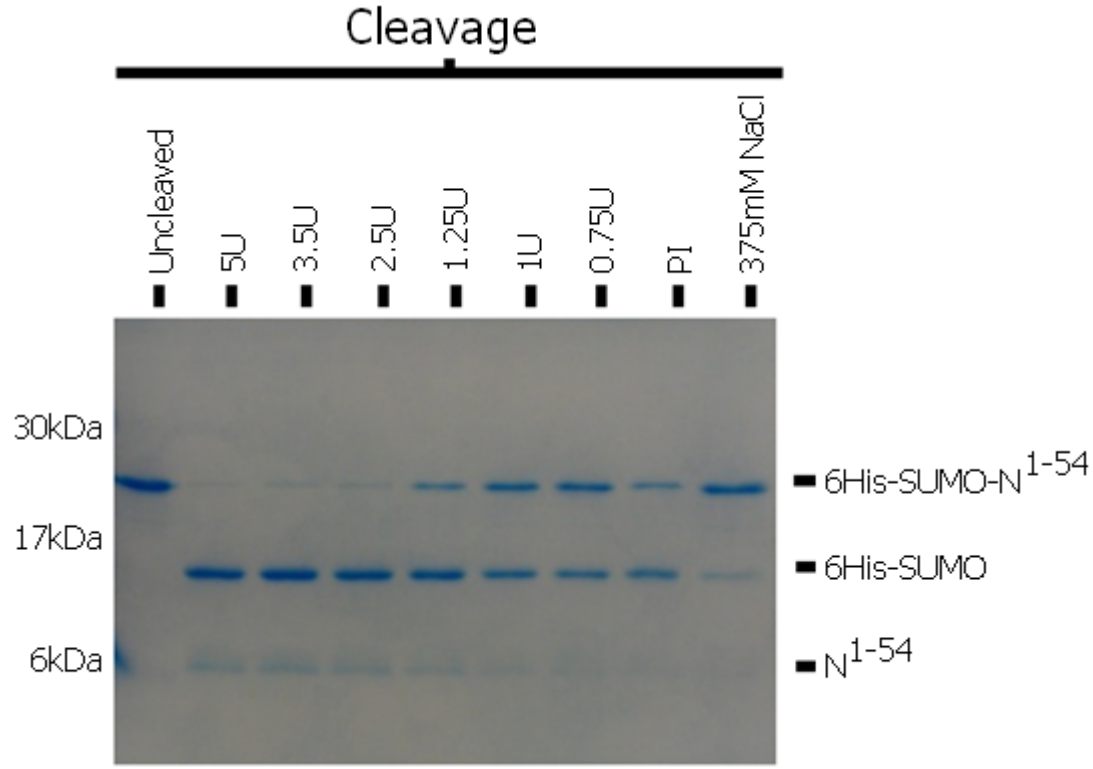

Figure 45: SUMO cleavage trials – protease concentration, NaCl concentration and protease inhibitors effect.

A range of different protease concentrations were employed to remove the SUMO-tag from the N^{1-54} domain (5, 3.5, 2.5, 1.25, 1, 0.75 Units). All samples were without protease inhibitors, unless otherwise stated. The NaCl concentration for all samples was at 150mM, unless otherwise stated. Samples were incubated with protease at 4°C for 3 hours. Aliquots from each reaction mix were examined by SDS-PAGE/Coomassie staining. The approximate position of the N^{1-54} domain (6.2kDa), the 6xHis-SUMO fusion protein (13.4kDa) and the uncleaved N^{1-54} fusion protein (19.6kDa) are indicated. These experiments indicated that optimum cleavage conditions was when using 2.5-5U protease. ≤1.25U protease, an increased NaCl concentration and the presence of protease inhibitor (cOmplete, Mini, EDTA-free protease inhibitor cocktail tablets (Roche)) all seem to have reduced the amount of successful cleavage.

As can be seen in Figure 45, all conditions explored resulted in a cleaved N^{1-54} product; albeit, to varying degrees of success. It can be seen that 5Units of protease cleaved 100% of the product in the 3hours incubation time at 4 °C. Fortunately, given the cost of the enzyme, 2.5Units seemed to be almost as efficient. It can be seen that 1.25U protease and less did not cleave as efficiently in the 3hour window at 4°C as judged by the presence of the band at ~20kDa corresponding to 6xHis-SUMO- N^{1-54}. This might suggest that for complete cleavage a longer incubation might be required. However, an increased cleavage incubation period was undesirable as this may result in protein aggregation. As expected, protease inhibitors clearly affected the efficacy of the protease, thus future purifications included a subsequent dialysis step, in which the protease inhibitors (used during the lysis stage) were removed. A high NaCl concentration also appeared to have an effect on protease activity, thus future purifications involved an adjustment of the NaCl concentration accordingly.

Nickel affinity gel purification of Cav3 N^{1-54} domain

Having successfully cleaved N^{1-54} from the 6xHis-tag fusion protein, a final stage of purification was now possible, in which the cleaved N^{1-54} product could be purified from the 6xHis-tag-SUMO cleavage product, any un-cleaved 6xHis-tag-SUMO-N^{1-54} and the protease (which has a 6xHis-tag). Since the N^{1-54} domain does not have a His-tag then this should not bind to the column and instead be collected in the flow-through.

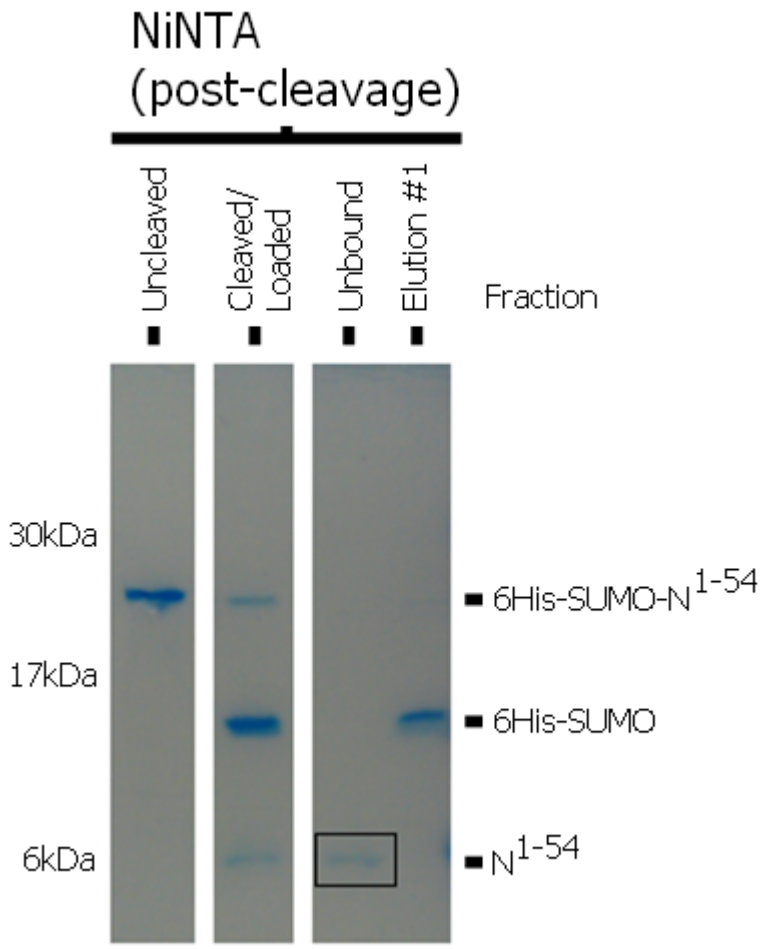

Figure 46: Nickel affinity gel purification of Cav3 N^{1-54}.

The post cleavage N^{1-54} mix was applied to nickel affinity gel purification. As can be seen from the gel above the N^{1-54} domain did not bind to the column and was collected in the unbound fraction (boxed). The 6xHis-tag-SUMO and any uncleaved 6His-tag-SUMO-N^{1-54} were eluted with 300mM imidazole. The approximate position the N^{1-54} domain (6.2kDa), the 6xHis-SUMO fusion protein (13.4kDa) and the uncleaved N^{1-54} fusion protein (19.6kDa) are indicated.

As can be seen in Figure 46, N^{1-54} was successfully purified from the other post-cleavage products. This fraction was sent for mass spectrometry identification (Protein Mass Spectrometry Core Facility, Manchester University), where 37% coverage of the N^{1-54} domain was identified.

Secondary structure characterisation

In order to characterise the secondary structure of the purified N^{1-54} domain a combination of in-silico prediction and circular dichroism was undertaken.

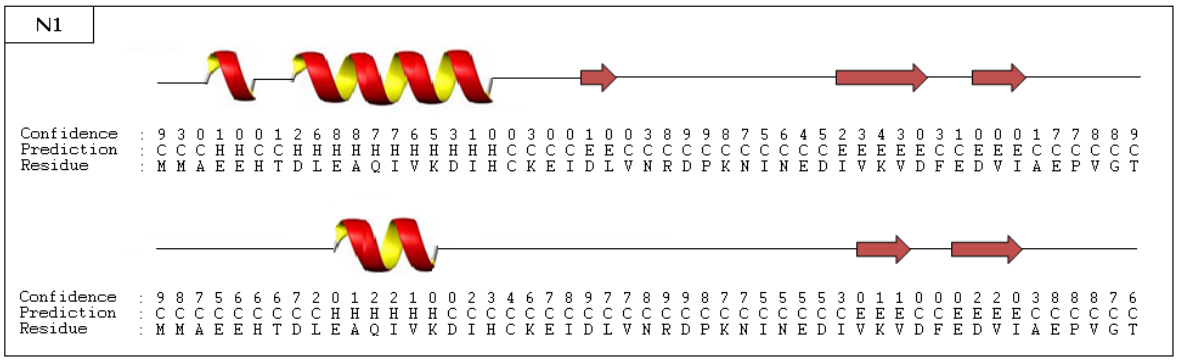

Figure 47: Secondary structure prediction for the N^{1-54} domain.

The N^{1-54} domain's secondary structure was predicted based upon the domain primary sequence alone (**A**), and based upon the complete protein primary sequence (**B**), using PSIPRED. Note that although the same approximate regions are predicted to contain α-helix and β-sheet regardless of whether the full sequence or the domain sequence is used as the primary input for structure prediction, both the extent of the secondary structure regions and the prediction confidence differ, with the structural regions being less likely when the full protein is considered. KEY: H=α-helix, E=β-strand, C=Random coil.

As can be seen in Figure 47, predictions differ slightly depending upon whether the peptide/domain sequence alone or the complete protein sequence is used as the input for *in-silico* secondary structure prediction. Despite these differences, it can still be seen that the N^{1-54} domain is predicted to be predominantly random coil, with a small amount of β-strand and α-helix. *In-silico* secondary structure prediction is not an exact art. Indeed, prediction of structure based upon primary sequence alone ignores any conformation changes afforded by the tertiary or quaternary structure. In addition, different prediction methods often vary in their structure prediction. Thus, it is always advisable to support the findings by experimental methods. Therefore to investigate further the secondary structure of this domain of Cav3, circular dichroism (CD) was employed. As described in the Introduction (section Secondary prediction: Circular dichroism), CD is a useful technique to examine the secondary structure properties of proteins and peptides. This has been applied here to the N1 domain.

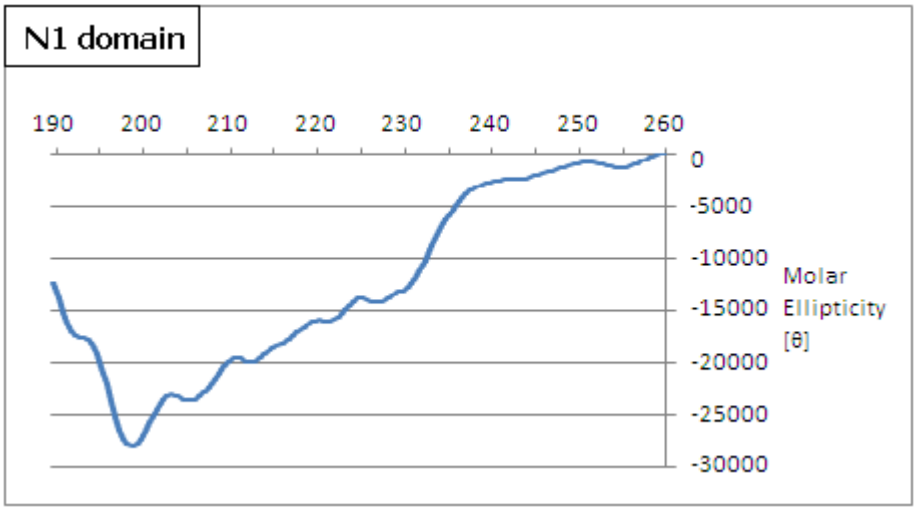

Figure 48: Circular dichroism spectra for the N^{1-54} domain.
Secondary structure was examined in the N^{1-54} domain using CD. Samples at 10μM were loaded into 0.2mm cuvettes and a Jasco J810 CD spectrometer was used to calculate the mdeg, which was adaptively-smoothened and was then used to calculate the molar ellipticity [θ], which takes into consideration the molarity of the sample, the residue length of the sample and the cuvette path length (Sreerama et al., 2004). Experiments were done in triplicates and averaged. The CD spectra does not show similarity with any of the secondary structure spectra observed in Figure 14 in the chapter introduction, indicating that secondary structure in this region is unlikely. X-axis is wavelength (nm).

As can been seen in Figure 48, the CD spectra for the N^{1-54} domain does not clearly represent any of the typical secondary structures outlined in Figure 14 in the chapter introduction. It is more characteristic, although not typical, of an unstructured type of signal. However, it should be noted that the mdeg ellipticity (before conversion into molar ellipticity) for this dataset was in the range of 3mdeg (data not shown), whereas typically data should look to be in the range of 10mdeg (Kelly et al., 2005). Thus, this implies that the signal obtained here is rather weak, which is likely as a result of the low sample concentration used (10mM). Unfortunately, due to the cost of the sumo protease required to cleave the SUMO-tag from the final N^{1-54} domain, insufficient quantity of the cleaved domain could be made. To investigate further the predictions made by visual interpretation of the CD spectra, DICHROWEB was used.

DICHROWEB

Caution must be understandably taken when visually interpreting CD spectra to calculate α-helices content. Therefore, to check for the presence of secondary structure, the complete raw CD dataset was analysed using the online tool, DICHROWEB.

Region of Cav3	α-helix content	β-strand content
N^{1-54}	None	2.1 strands of 3.6 residues length

Table 9: Summary of the DICHROWEB secondary structure prediction.

As can be seen in Table 9, the DICHROWEB predictions show no α-helical content for the N^{1-54} domain. This fits with the CD spectra for the N^{1-54} domain. The domain was predicted to have the presence of two β-strands of 3.6 residues in length, which in isolation would be insufficient to form β-sheet, but together may form a small amount of β-sheet (Penel et al., 2003). It is perhaps understandable why such little β-sheet would have been detected by CD. Although the weak signal afforded by the low concentration of the sample must be factored in, the secondary structure prediction, the CD spectra and DICHROWEB would all appear to support the likelihood that this 54 residue region of Cav3 does not contain any well defined secondary structure.

Summary: Expressing the N^{1-54} domain in E.coli using the pET-His-SUMO vector

Here, we have shown the successful expression and purification of the first 54 residues of Cav3, termed here N^{1-54}. A range of expression systems were tried, but the SUMO expression system was the one that proved successful. Optimum expression was at 37°C, 1mM IPTG, and 4hours, and a simple Tris lysis/solubilisation buffer containing 0.5% (v/v) Triton X-100 was sufficient to obtain the domain to be in the soluble fraction. Purification using the nickel affinity gel worked well. A range of cleavage conditions were explored and an optimised protocol was established. Nickel affinity gel was also used as a final stage of purification (post-cleavage), and this also proved very successful in separating N^{1-54} from the other unwanted cleavage products.

2.3.6. Expressing the N^{1-101} and C^{92-151} domains in *E.coli* using the pET-His-SUMO vector

Given the success expressing and purifying the N^{1-54} domain into the soluble fraction using the pET-His-SUMO vector, attempts were made to use this vector system to express two further domains; N^{1-101} and C^{92-151}. Primers were designed to extract the regions corresponding to the first 101 residues (hereby referred to as N^{1-101}) and the residues 92-151 (hereby referred to as C^{92-151}) from the OriGene vector that contained the

full-length ORF for Cav3. These regions were independently inserted into the pET-His-SUMO vector. See Figure 49 below for a schematic of the domains.

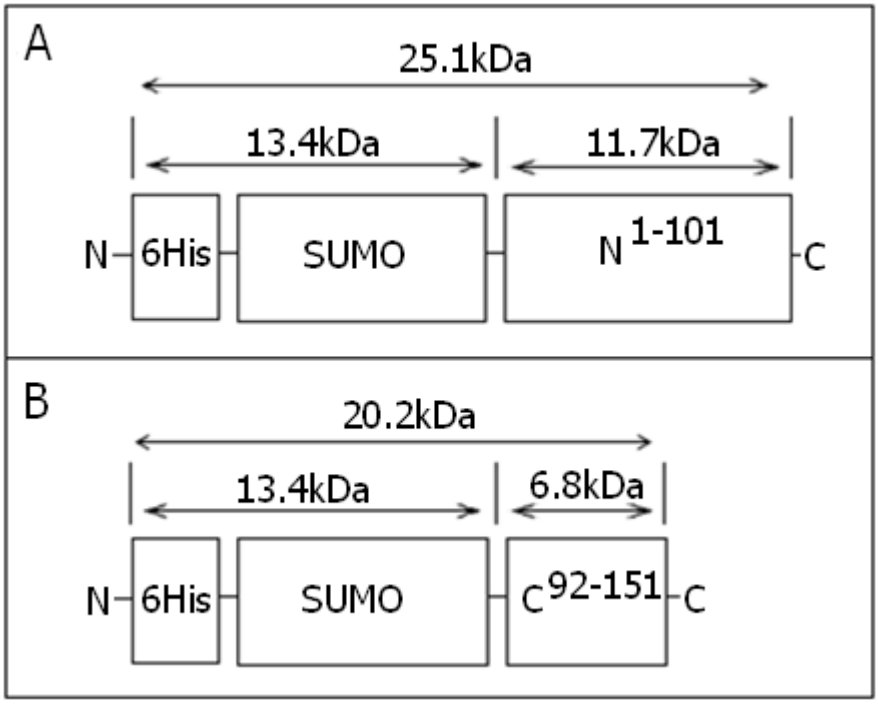

Figure 49: Schematic of the 6xHis-SUMO-N^{1-101} and 6xHis-SUMO-C^{92-151} fusion protein.

Both the N^{1-101} and C^{92-151} domains have a N-terminal 6xHis-tag (to aid purification) and SUMO-tag (to enhance the solubility). The total fusion proteins are approximately 25.1kDa and 20.2kDa respectively.

PCR optimisation

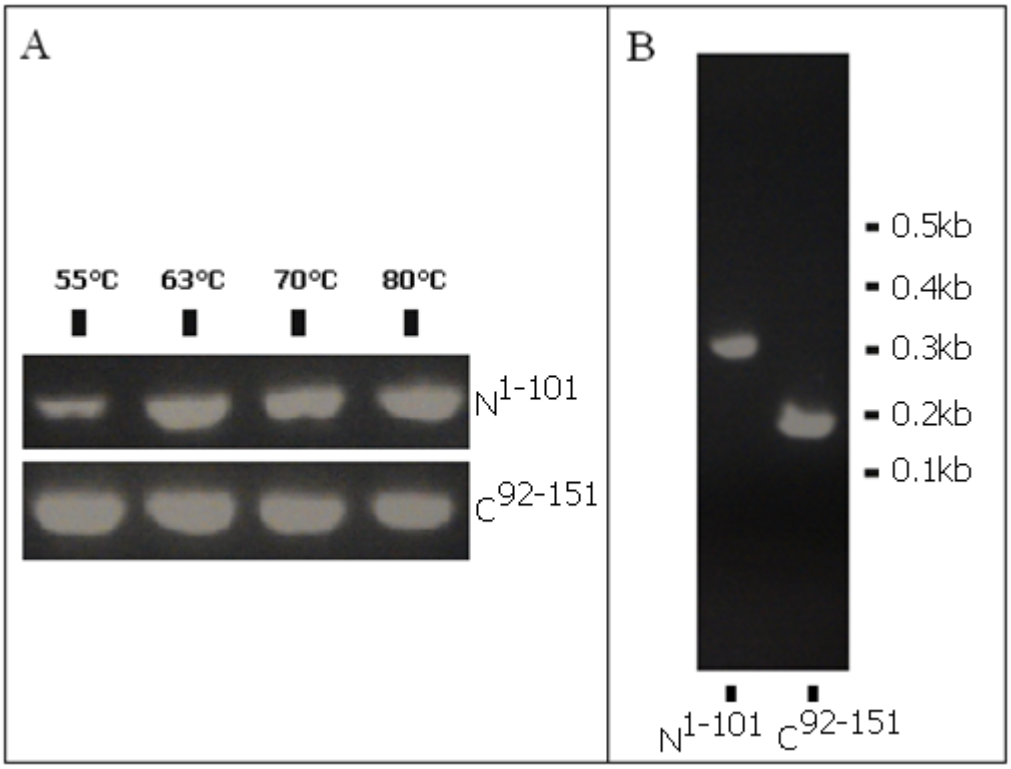

Figure 50: PCR optimisation for the N^{1-101} (0.3kb) and C^{92-151}(0.18kb).
A: Four different annealing temperatures were tested for amplification: 55, 63, 70 and 80°C. 63°C produced the most PCR product for N^{1-101}, whereas 55°C produced the most PCR product for C^{92-151}. **B:** A post-PCR gel shows migration of single PCR products, indicating that a single PCR product had been produced.

63°C proved to be the optimum primer annealing temperatures for the N^{1-101} construct, whereas 55°C was optimum for C^{92-151} (Figure 50, panel A). PCR amplification successfully produced a homogenous PCR product, as evidenced by the presence of only one PCR product (Figure 50, panel B). The PCR products were independently cloned into the pET-His-SUMO vector. To test if the ligations had been successful, *E.coli* cells were independently transformed with the newly created vectors, and cells were grown selecting for antibiotic resistance conferred by the vector. Successful colonies were used for purification of the plasmid, which were sent for DNA sequencing, where each vector was subsequently confirmed to house the correctly orientated insert.

Expression of N^{1-101} and C^{92-151} at 37°C

Given the success expressing the N^{1-54} domain at 37°C, the same induction conditions (37°C, 1mM IPTG) were tested first for the N^{1-101} and C^{92-151}domains.

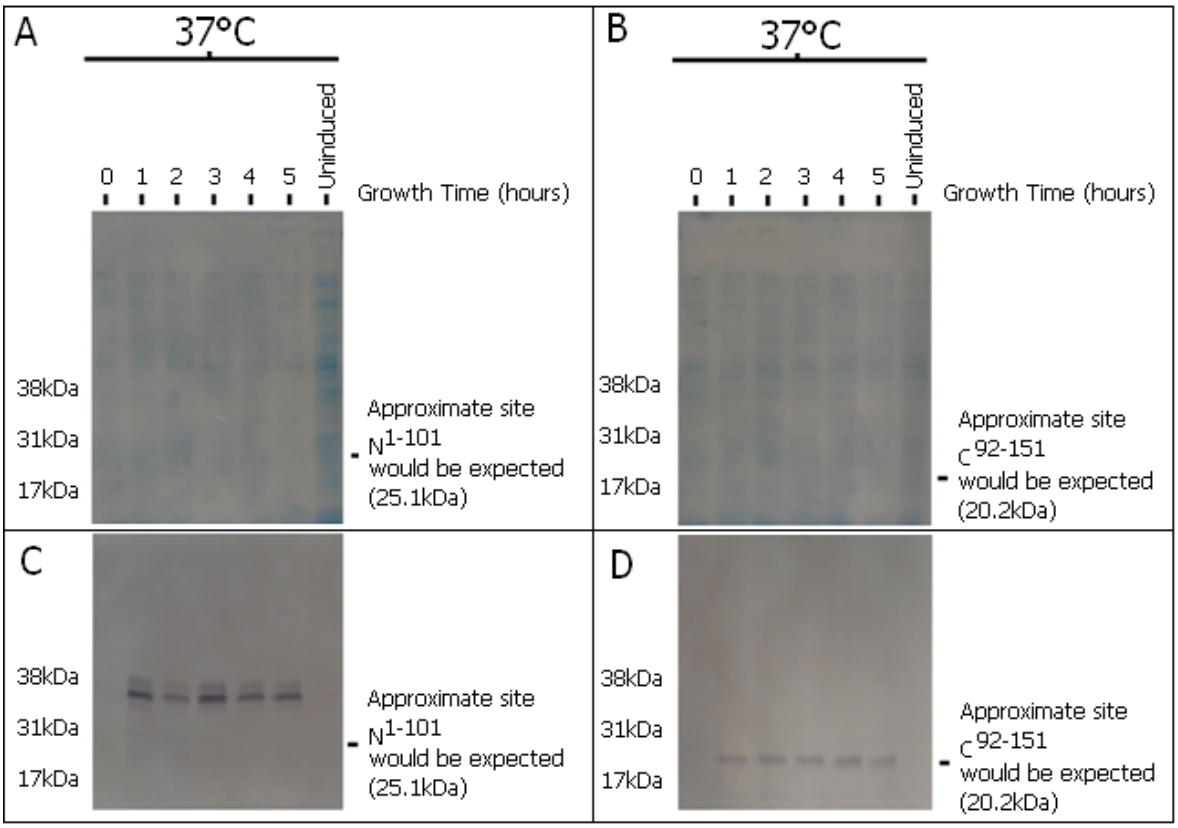

Figure 51: Protein expression profile of N^{1-101} and C^{92-151} transformed *E.coli* cells grown for 1, 2, 3, 4 and 5 hours at 37°C and induced with a 1mM IPTG (cell density 0.8 at OD^{600nm}).

Cells grown for 1, 2, 3, 4 and 5 hours in LB at 37°C and induced with 1mM IPTG (at 0.8 OD^{600}) were solubilised following the protocol in the Materials and Methods (Alternative protocols – for SUMO expression system). The soluble fraction for the induced cells expressing the N^{1-101} domain (**A**) and the C^{92-151} domain (**B)** and those cells un-induced after 5hours (control) were examined by SDS-PAGE and stained in Coomassie staining solution. No over-expressed proteins were observed in the soluble fraction. Moreover, the total protein present in the soluble fraction was barely detectable *via* Coomassie staining. Western-blotting for the N^{1-101} domain (**C**) and the C^{92-151} domain (**D**) was completed using an antibody raised against the HisG-tag as the primary antibody. Note that western blotting shows that a protein of ~37kDa was observed in the cells induced to express the N^{1-101} domain. However, no protein is detected at the size the N^{1-101} domain would be expected. However, it can be seen in panel D that western blotting detects a protein with the size expected for the C^{92-151} domain. These bands detected by western blotting are not present in the un-induced controls or at the start of the induction (t=0).

As shown in Figure 51 (Panels A and B), there are no clear bands detected by Coomassie staining that would correspond to over-expression of either N^{1-101} or C^{92-151}.

Interestingly, immunostaining reveals that a correctly sized band for C^{92-151} is present at approximately 20kDa (Figure 51, panel D). However, the band for N^{1-101}, which would be expected to be found at approximately 26kDa is found at approximately 37kDa (Figure 51, panel C). Neither domain is present in the un-induced control or the pre-induction (t=0), which would indicate that the bands observed on the western blots are likely as a result of the Cav3 domain expression. However, if either domain was being expressed, they were not in high yields.

Expression of N^{1-101} and C^{92-151} at 18°C

Both the N^{1-101} and C^{92-151} domains include regions that are believed to be part of the transmembrane region. This may partly explain why the domains were not being over-expressed. Lowering the temperature of expression can help in the expression of hydrophobic proteins by reducing the expression rate, and by reducing the activity of any of the host's proteolytic machinery that may degrade the non-native protein. Thus, the induction temperature was lowered to 18°C.

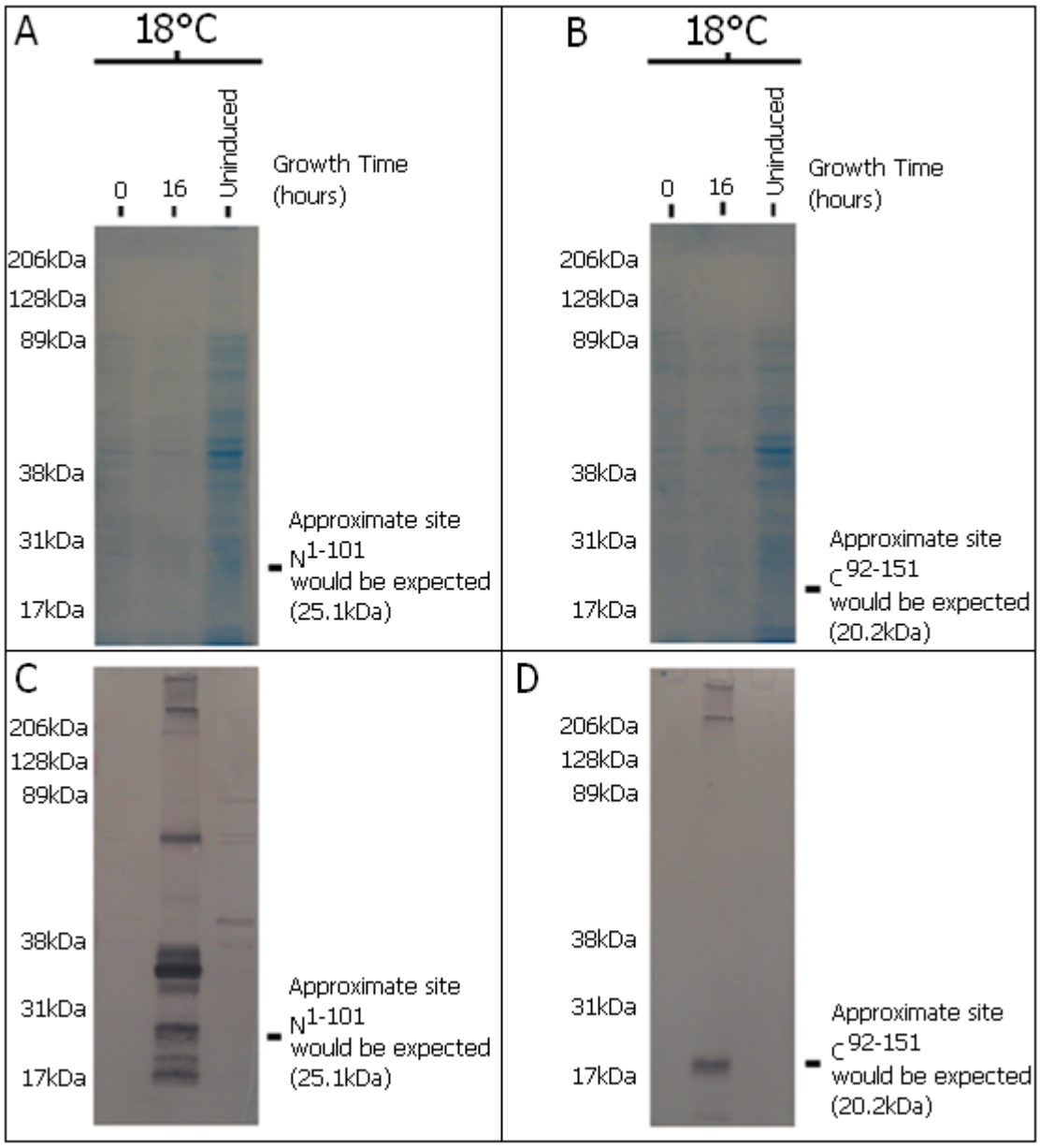

Figure 52: Protein expression profile of N^{1-101} and C^{92-151} transformed *E.coli* cells grown for 16 hours at 18°C and induced with a 1mM IPTG (cell density 0.8 at OD^{600nm}).

Cells grown for 16 hours in LB at 18°C and induced with 1mM IPTG (at 0.8 OD^{600}) were solubilised following the protocol outlined in the materials and methods (Alternative protocols – for SUMO expression system). The soluble fraction for the induced cells expressing the N^{1-101} domain (**A**) and the C^{92-151} domain (**B)** and those cells un-induced after 16hours (control) were examined by SDS-PAGE and stained in Coomassie blue solution. No clear bands with a molecular mass that could be attributed to the over-expressed Cav3 protein domains were observed in the soluble fraction. Moreover, it can be seen that the total protein present in the soluble fraction detected by Coomassie staining was very low. Western-blotting for the N^{1-101} domain (**C**) (anti-HisG) shows the presence of multiple different sized proteins, including the ~37kDa protein (observed at 37°C , see

Figure 52, panel C) in the cells induced to express the N^{1-101} domain. Some bands are detected at the size the N^{1-101} domain would be expected; however, given that multiple bands are present, it is unclear which may correspond to N^{1-101}. (**D**) Western blot of soluble fraction from cell over-expressing the C^{92-151} domain. A protein band with the size expected for the C^{92-151} domain is detected as highlighted on the figure; although there are also a few higher molecular weight bands. The bands detected by western blotting for both constructs are not present in the un-induced controls or at the start of the induction (t=0).

Although it was encouraging that western blotting detected protein that would be consistent with over-expression of each of the Cav3 domains it can be seen from Figure 52 (panels A and B), that there are no corresponding discernible bands upon Coomassie staining, suggesting poor expression. Interestingly, the reduction in expression temperature is associated with more proteins being detected *via* western blotting in the N^{1-101} containing cells (Figure 52, panel C). Whether these bands represent unspecific binding or multiple forms of N^{1-101} is not clear. A band at the correct position expected for the C^{92-151} is observed in Figure 52 (panel D), as had been observed for expression at 37°C (Figure 51, panel D), indicating that the protein expressed is likely the C^{92-151} domains.

Nickel affinity gel purification

Although induction of recombinant N^{1-101} or C^{92-151} at both 18°C and 37°C did not appear to lead to over-expression of soluble forms of the domains (as judged by Coomassie staining of SDS-gels), the western blotting did indicated that the C^{92-151} domain was present in the soluble fraction and at the mass location expected, albeit at a low concentration, and that the N^{1-101} was possibly being expressed. Therefore, the soluble fraction from each expression trial was applied to nickel affinity gel in order to purify any potential soluble N^{1-101} or C^{92-151} domains *via* the N-terminal 6xHis-tag.

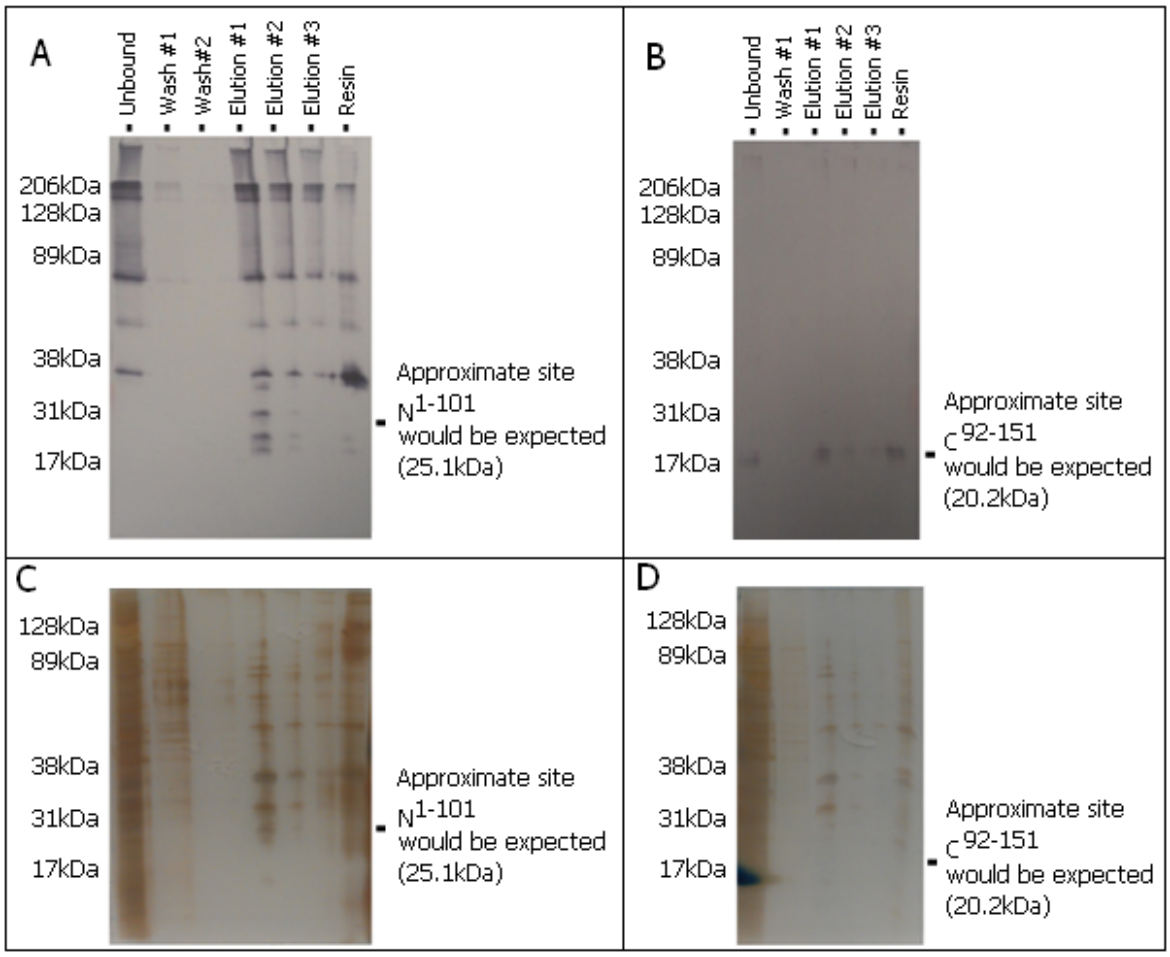

Figure 53: Nickel affinity gel purification of the N^{1-101} and C^{92-151} domains.

The soluble fraction (from 18°C, 16hr, LB, 1mM IPTG) was applied to nickel affinity gel. The column was washed several times and the bound proteins were eluted with 300mM imidazole. **A:** The elution fractions were separated by SDS-PAGE and western blotted (anti-HisG-tag) for N^{1-101}(**A**) and C^{92-151}(**B**). Note that the band corresponding to ~37kDa is found in both the elution fraction as well as the final resin. The suspected band for C^{92-151} was also found in both the elution and final resin fractions. SDS-PAGE gels were also silver stained. No prominent bands were detected for either the purified N^{1-101}(**C**) or C^{92-151}(**D**) domains. Further, multiple bands of different sizes were observed in the eluted fractions. The approximate positions the N^{1-101} and C^{92-151} fusion proteins (25.1kDa and 20.2kDa respectively) would be expected are shown on the right.

As can be seen in the western blotting in Figure 53, although the putative N^{1-101} and C^{92-151} bands were found in the elution fraction (Figure 53, panels A and B), much also remained in the final resin. The fact that in both experiments protein was still associated with the resin may suggest that a higher concentration of imidazole is required. In addition, the polypeptide profiles of both the eluted domains (Figure 37 C, D) show that the purification step was not successful since multiple bands are eluted. Moreover, there was

no distinct band corresponding to either domain, even when silver stained (Figure 53, panels C and D). It is possible that the multiple bands observed in Figure 53 (panel A) correspond to oligomeric forms of the N^{1-101} domain. However, these bands do not necessarily correspond to those on the silver stained gel (Figure 53, panel C), thus they are likely very low in concentration.

Summary: Expressing the N^{1-101} and C^{92-151} domains in E.coli using the pET-His-SUMO vector

Attempts to express and purify the N^{1-101} and C^{92-151} domains using the SUMO system proved problematic. Multiple issues were highlighted during this purification protocol, including poor expression, poor purification, the presence of multiple impurities, and ultimately, and arguably most importantly, a very poor yield. At this stage of the project attention was refocused upon the goal of expressing the full-length Cav3.

2.4. Conclusion

The primary objective of this section of the project was to express full-length, soluble, fully-folded, native Cav3 in *E.coli*. The secondary objective was to express a range of different Cav3 domains (N^{1-54}, N^{1-74}, N^{1-101} and C^{92-151}), each representing different sections of the full length protein. The N^{1-54} domain was successfully expressed and purified to homogeneity. However, the remaining domains, and full-length Cav3 were not successfully purified. The possible reasons for the lack of success are discussed here.

Expressing a non-native protein in a foreign host in order to over-express it can cause many problems. Firstly, the vector many never actually express the inserted gene. Secondly, even if the gene is transcribed, this does not necessarily lead to successful mRNA translation. Indeed, ribosomes will stall translation if the protein they are producing is detrimental to the host; hence, the use of solubility tags to improve translation. Thirdly, even if the protein is successfully translated its presence may lead to toxicity. If the protein proves to be toxic to the cell it may interfere with cellular proliferation and differentiation, and it will likely be degraded rapidly by the host's proteolytic machinery within the cell. If not degraded it may kill the cell, thus potentially dramatically reducing the protein yield. Moreover, if the protein is produced but is unstable within the cell it may form, or be forced into inclusion bodies. For example, a membrane protein will have hydrophobic regions within it. If the host cell cannot accommodate these regions the protein is likely to degrade and form inclusion bodies. In addition, if the host lacks the machinery to correctly post-translationally modify the protein the protein can become unstable and be degraded.

There are many potential reasons why this system failed to express full-length Cav3 or the N^{1-74}, N^{1-101} and C^{92-151} domains. One reason is that each of these proteins/domains that failed to be expressed possessed regions thought to interact with the membrane (Monier et al., 1995; Parton et al., 2006; Sargiacomo et al., 1995; Schlegel and Lisanti, 2000). These regions likely contain hydrophobic regions that cannot be accommodated by the *E.coli* membrane. This lack of accommodation may have caused the protein to degrade. In contrast, the only successfully expressed and purified domain (N^{1-54}) does not contain any region thought to insert into the membrane. This may be, in part, the reason for the successful expression and purification of the N^{1-54} domain. However, although this explanation would appear to make sense, it should be noted that the regions thought to represent the minimal regions required to associate with the membrane have been inferred for Cav3 from initial studies on Cav1.

Another reason for why full-length Cav3 failed to express could have been due to the fact that *E.coli* does not contain cholesterol. Cholesterol is important for the membrane

association of caveolins with the membrane (Rothberg et al., 1992; Smart et al., 1996) and it may be that the lack of the ability to form caveolae (due to the lack of cholesterol) resulted in the proteolysis of Cav3 i.e. without the option of forming caveolae the protein degraded.

In theory, the addition of thioredoxin and SUMO proteins to the recombinant Cav3 proteins/domains should have helped reduce the chance of internal digestion by the foreign host, by enhancing its solubility *via* stabilisation and localisation changes. However, for the full-length Cav3, and the N^{1-74}, N^{1-101} and C^{92-151} domains, this was not the case. Indeed, it has been noted that sometimes solubilisation tags "*simply don't work*" (Waugh, 2005).

The full-length Cav3 could not be expressed here using the *E.coli* expression system following the published protocol described by Li and co-workers (Li et al., 1996c), despite exhaustive attempts. Many different expression conditions were also tested but without success. There are a number of possible reasons why the protocol that Li and co-workers used did not work here. Firstly, and likely most importantly, the protocol used by Li and co-workers reported the expression of Cav-1 and not Cav3. Despite many similarities, many differences also exist between the two proteins (as discussed in the thesis introduction). In addition, Li and co-workers expressed a *canine* variant of Cav1, not the human form of Cav3 in these studies (60% similarity). The only other variable between the protocol described by Li and co-workers and the method employed in this thesis research was the presence of a myc-tag in their recombinant protein. However, the sole purpose for this tag was to aid identification when immunostaining using an anti-myc antibody to detect expression of the caveolin fusion protein. Indeed, the myc-tag is not used to increase solubility, so it is unlikely that this is the reason for the observed difference.

Importantly it should be noted that Li and co-workers did not characterise the purified Cav1, nor did they illustrate the level of purity since the main method of detection they employed was western blotting, which only shows presence, not purity. They did also use biotinylation to detect the presence of Cav1 after elution using Ni^{2+}agarose resin, however, biotinylation is used to detect very small levels of protein, which might hint that yields of Cav1 were very low. The rationale for using biotinylation as a means of detection was based on a previous study from the same group describing that caveolin does not stain by conventional means such as Coomassie staining (Scherer et al., 1995), although within that same paper a Coomassie stained gel showing caveolin was presented. However, this may, in part, be explained by the presence of a fusion protein, which has aided in the

Coomassie detection. Indeed, in the subsequent chapters we also show that a Cav3 fusion protein is detectable by Coomassie staining.

The N^{1-54} domain was successfully purified here and some preliminary analysis of the protein secondary structure was undertaken. Both experimental and in-silico secondary structure prediction algorithms suggested that this region is mainly composed of random coil. The software, PSIPRED, uses primary sequences alone and visual interpretation of the CD spectra can be biased; it is likely that the predictions made by DICHROWEB are the most accurate. However, it should be noted, that even the predictions made by DICHROWEB, although based on experimentally derived data are, ultimately, made using prediction software. Despite this, all approaches indicated that this region was likely random coil. The quality of CD spectra can vary depending upon the concentration of the protein. Future work might consider testing a range N^{1-54} domain concentrations. In addition, the propensity of the N^{1-54} domain to adopt a secondary structure could be probed by the addition of TFE, an organic compound that favours local interactions by strengthening intra-molecular H-bonds, and thus can be used to help study secondary structure.

Perhaps the existence of random coil instead of any defined secondary structure affords some degree of flexibility to this region, possibly pertaining to its function. This region composes part of what is termed the oligomerisation domain (Sargiacomo et al., 1995), and as will be discussed in Chapter 5, some degree of disorder in this region could possibly be beneficial in allowing oligomerisation. In addition, this region also contains what is known as the caveolin-signature motif, which is the most conserved region throughout all caveolin isoforms. Given the conserved nature of this region it may be that it has a function, as of yet unknown, that demands a random coil conformation. Indeed, mutations in this region have been associated with a range of different diseases including longQT syndrome, sudden infant death syndrome, rippling muscle disease, limb-girdle muscular dystrophy, distal myopathy (Betz et al., 2001; Carbone et al., 2000; Cronk et al., 2007; Fischer et al., 2003; Fulizio et al., 2005; Herrmann et al., 2000; Madrid et al., 2005; Merlini et al., 2002; Tateyama et al., 2002; Vorgerd et al., 2001), thus suggesting this region is physiologically important.

Another important consideration when interpreting secondary structure is that it may be that in isolation, the domain has an altered propensity to form specific secondary structure conformations, compared to when it is part of the complete protein. This point highlights the potential importance of working with full-length proteins when possible, as studying fragments of the proteins alone neglects to consider the vast myriad of potential

interactions afforded by the complete structure. Indeed, the isolation of high yields of full-length protein can only be beneficial to this line of study.

Although there was a lack of success working with other constructs of Cav3, many other options still exist for development of the *E.coli* expression system to optimise expression should this be pursued in the future. For example, using N2CYM, M9 or induction media, altering the pH of the media, using more extreme temperatures e.g. <18°C or IPTG concentrations e.g. 8mM, and even different speciality cell types e.g. RIL or RP in case the problem is not stability but expression. In addition, other tags and fusion protein systems exist that could be further employed to improve yield as well as express domains previously unsuccessfully expressed. The choice of expression system is also an important factor to consider. Trying alternative *E.coli* strains designed with certain issues in mind, for example, strains that supplement rare codons (Kane, 1995), is also something worth considering. However, since the primary goal of this thesis research project was to express the full-length Cav3 the use of the Baculovirus expression system and the insect cell line Sf9 was next explored, as described in Chapter 3.

Chapter 3: Expression and purification of full-length Cav3 in Sf9 cells

3.1. Introduction

Chapter 2 has described attempts to over-express and purify full-length Cav3 using the *E.coli* expression system. Although examples of soluble fragments of Cav3 were successfully isolated using this approach it was clear that it was not suitable for the full-length protein. The Kitmitto laboratory has previously employed the baculovirus expression system (Sf9) to produce the T-type voltage-gated calcium channel (Walsh et al., 2009a) and thus this system was explored for full-length Cav3.

The main objective of this part of the project was to use the baculovirus expression system to express pure, homogeneous full-length Cav3 at a yield sufficient for subsequent biophysical analysis.

3.1.1. Baculovirus expression system

The baculovirus expression system (BES) utilises two main living components: the insect cell, most often Sf9 or Sf21 cells, and the baculovirus. The insect cell line is derived from the pupal ovarian tissue of the fall army worm *spodoptera frugiperda*, and the baculovirus is a nucleopolyhedrovirus that naturally infects this insect cell type. This relationship between cell/virus can be manipulated in order to introduce non-native genetic material into the insect cell. This system can then be used to produce large amounts of recombinant protein.

One of the advantages of this system over the *E.coli* expression system is that it is capable of many more post-translational modifications, including O-linked glycosylation, simple N-linked glycosylation, phosphorylation, palmitoylation and acetylation (Fernandez and Hoeffler, 1999). In addition, the baculovirus expression is known for yielding high levels of correctly folded recombinant proteins, including correct disulphide bond formation and oligomerisation. Moreover, being eukaryotic, insect cells have a membrane much more similar (than *E.coli*) to those of, for example, human cardiac myocytes, and are thus much more suited to the expression of membrane proteins. Indeed, the baculovirus system has proven very successful for producing functional membrane proteins, including the T-type calcium channel, in this laboratory (Walsh et al., 2009a).

The downside to using insect cells is that, compared to *E.coli* they generally take longer to grow. In addition, getting the system started can take a great deal more time, as there are a lot more preparatory steps such as the amplification of the baculovirus, and the

bulking up of cell concentration can take weeks, as opposed to hours. Moreover, given their historically reduced usage compared to well characterised systems such as *E.coli*, techniques are less well established and often much more expensive. For the above outlined advantages, the baculovirus expression system is now a routinely used expression system (Kato et al., 2008; Kodan et al., 2009; Pattanaik et al., 2009).

Alternative eukaryotic expression systems do exist; however, the baculovirus expression system was opted for here over the alternatives, as this system has been shown to express canine Cav1 (Li et al., 1996b). Moreover, although recombinant expression of canine Cav1 has been shown to occur in the COS-7, 293-T, MDCK and FRT cell lines, caveolae formation was not observed (Scherer et al., 1996; Scherer et al., 1995; Song et al., 1996b; Tang et al., 1996). Although caveolae formation was not key to this project, the fact that over-expression in insect cells had allowed native-like conformations to form indicated that it was possibly more suited to maintaining protein function.

Three particular types of insect cell are commonly used in conjunction with the baculovirus expression system, namely Sf9, Sf21and High-five cells, each having slight differences (Gerbal et al., 2000). Sf9 cells are generally smaller and slightly less fragile to shear stress. In addition they usually give higher titre. Sf21 cells are thought to yield slightly higher protein expression than Sf9. Both Sf21 and Sf9 cells can be grown in suspension, whereas High-five cells cannot be. Generally, Sf9 and Sf21 cells are interchangeable. For this project, Sf9 cells were selected.

3.1.2. Expression

A variety of factors influence the expression levels that can be achieved using the baculovirus expression system, the most common being the incubation time, the multiplicity of infection (MOI) and the cell density upon infection, all of which can be addressed by completing a small scale expression trial. Ultimately, it is optimum to infect the cells whilst they are in the log phase ($2x10^6$ cells/ml), as well as to infect them all at the same time.

The MOI is the ratio of infectious virus particles to cells. Getting the optimum MOI is important for a number of reasons. Although a high MOI often results in a higher degree of infection, an MOI that is too high can end up killing the cells, whereas a low MOI can result in not all the cells being infected, which means the uninfected cells continue to grow, thus redirecting the nutrient in the media away from protein expression.

Optimising the length of growth time is another important factor to consider when optimising the expression of the protein. Growing the cells for the maximum amount of

time does not necessarily mean that protein expression will be at its maximum, as the protein being expressed, for example, may be toxic. If the protein being expressed is toxic, then shorter expression times may be required, whereas, if not, it may be worth growing for up to 72hours to maximise the possible yield. However, growing for too long can use up the available nutrients, so finding the optimum growth time is an important stage to optimise.

3.1.3. Purification

After solubilisation of the membrane protein a purification protocol is required to isolate the protein from the other components. The level of purity required completely depends upon what techniques are to be used next. For the techniques employed here a homogenous sample of Cav3 was required. A brief summary of some of the key purification techniques employed in this project are outlined here.

Affinity chromatography is a typical starting point in a purification protocol. Multiple different types of affinity chromatography exist, such as immobilised metal ion affinity chromatography, dye affinity and antibody affinity. Each utilises a different feature of the protein in order to purify it. Since the Cav3 was expressed with a C-terminal MAT-tag (metal affinity tag) the first stage of purification in this chapter involved immobilised metal ion affinity chromatography (IMAC). Note that immobilised metal ion affinity chromatography (IMAC) has been discussed in detail in the introduction to Chapter 2.

Ion exchange chromatography

Ion exchange chromatography (IEX) separates proteins based upon their net surface charge, which is determined by the presence of ionisable groups on the proteins surface. This charge is dependent upon the pH of the buffer. For example, a protein with an isoelectric point (pI) of 7.14 may have a charge of +3 in a buffer at pH6.5, whereas it may have a charge of -3.6 in a buffer at pH8. Certain ion exchange columns have been developed that allow you to take advantage of the charge differences between proteins in order to purify specific proteins. In the above example, a cation (negative charge) exchanger, such as quaternary ammonium or diethylaminoethyl, would be used for the prior, and an anion (positive charge) exchanger, such as sulfopropyl or carboxymethyl, for the later. In brief, negatively charged proteins will bind the positively charged columns, and vice-versa.

There are several challenges with IEX: 1) pI calculation, and 2) elution resolution (see Figure 54). Determining the correct pI is paramount to success. Indeed, the entire

concept of IEX is dependent upon this value, as it dictates both the buffer and column choice. Fortunately, if the charge is not known, it can be predicted. However, factors such as oligomeric state and protein folding can mean the pI predicted on primary sequence alone can be very different from the actual net surface charge once the protein takes on its tertiary and quaternary conformation.

Given that purification involves the separation of one protein from many others, there is a considerable chance that other proteins have similar net surface charges. Ensuring that these similarly charged proteins are separated during the purification process can be quite problematic. Despite these concerns, IEX is a commonly used purification technique.

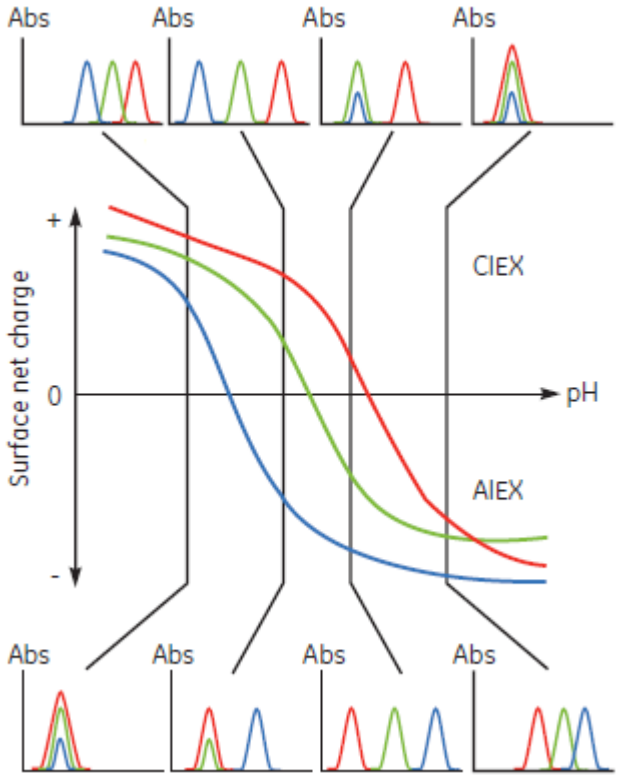

Figure 54: Effect of pH on pI and elution resolution.
The central diagram shows the net surface charge of three example proteins (red, blue, green). The chromatograms show how the elution profiles (with NaCl) can be expected to look when a cation (above) or anion (below) ion exchanger is used. Note the resolution differences. Figure adapted from GE Healthcare Strategies for protein purifications handbook.

Molecular mass (size): Gel filtration

Gel filtration is a method of size exclusion chromatography that aims to separate proteins based upon their size. By loading the sample containing the protein to be purified (with other impurities) onto a column made up of a series of different sized pores and

pathways, separation of large proteins, which cannot enter the extensive pore system and are thus eluted rapidly, from the smaller proteins that enter the porous network, and take considerably longer to reach the end of the column and elute, is possible. Strictly speaking, it is not *size* that proteins are separated by, but instead the hydrodynamic volume of the protein i.e. the space a particular protein takes up when it is in solution.

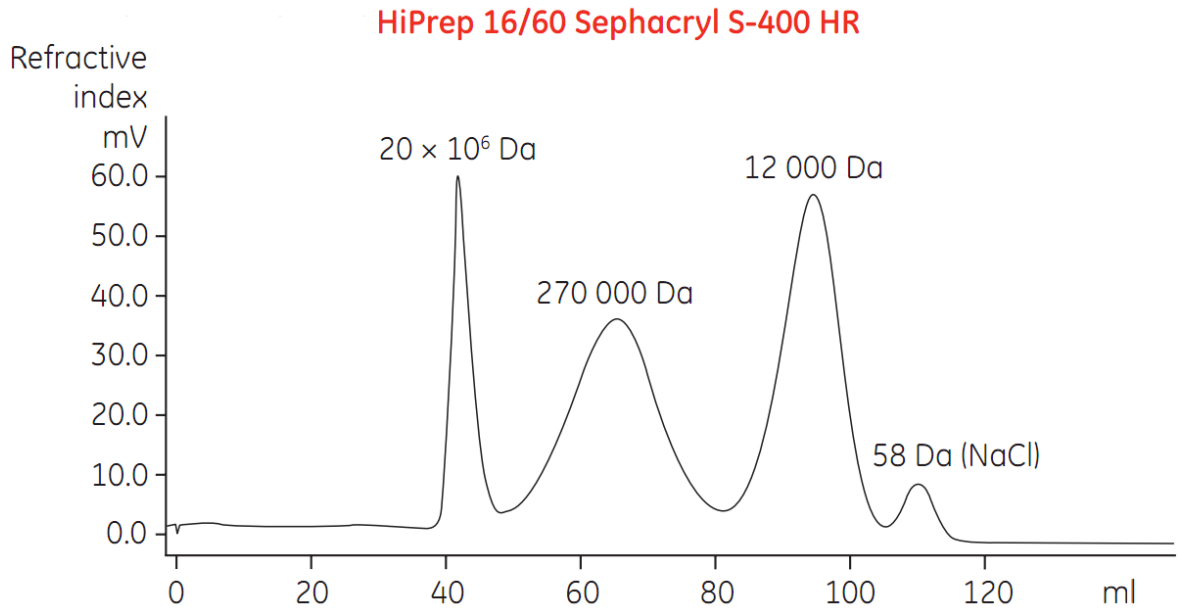

Figure 55: Typical elution profile for size exclusion chromatography.
Larger proteins are eluted first, whereas smaller proteins are eluted later. Adapted from GE Healthcare Instructions (28-4026-53 AD).

Density: Sucrose gradient fractionation

Sucrose gradient fractionation (SGF) is a method of purification that separates proteins based upon their densities. Layers of decreasingly concentrated sucrose buffers are layered upon one another and the sample is loaded on top of this sucrose fractionation. The sample is then centrifuged at high speed which causes the proteins to migrate to the bottom of the gradient. However, the distance the proteins can travel is limited by the individual proteins density (they travel until their density matches the surrounding), thus proteins are separated into sub-fractions based upon their density. See Figure 56 for an outline of the concept.

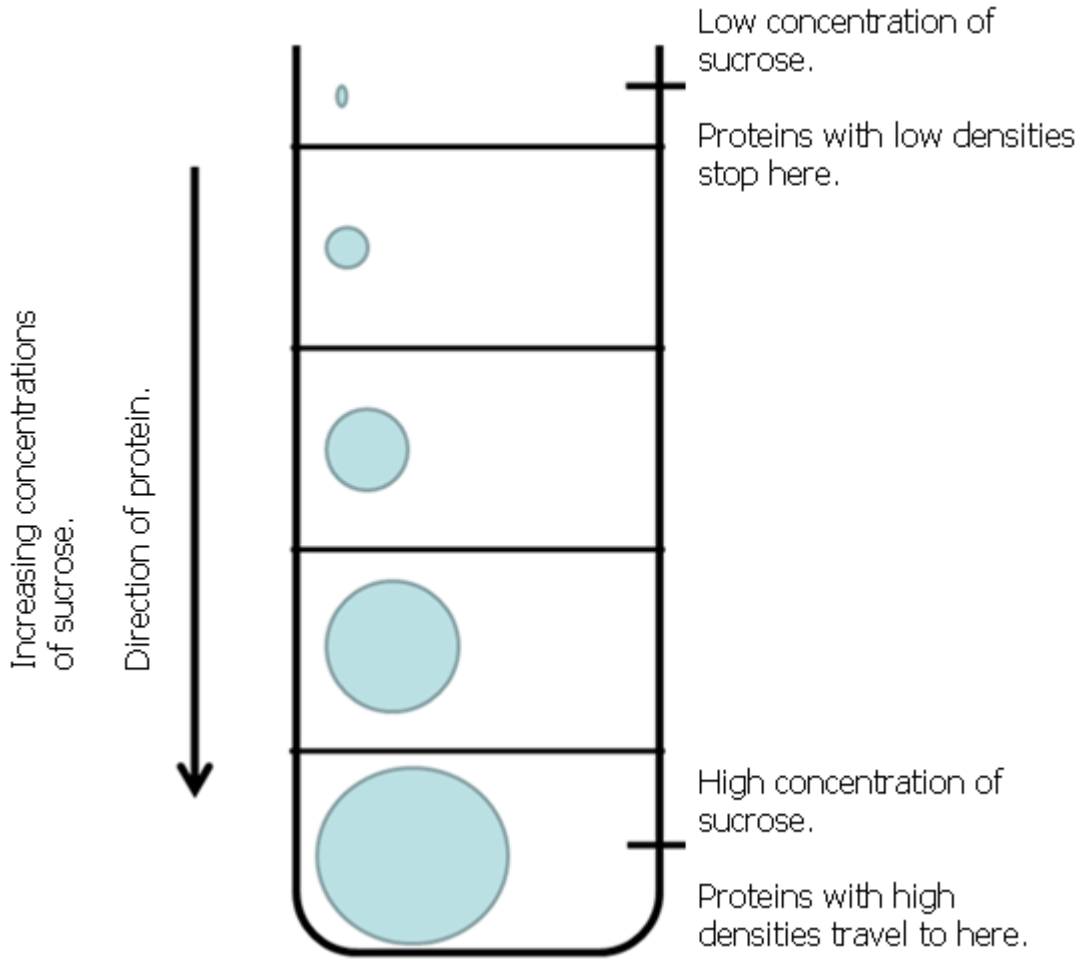

Figure 56: Sucrose gradient centrifugation concept.

3.1.4. Flow of work

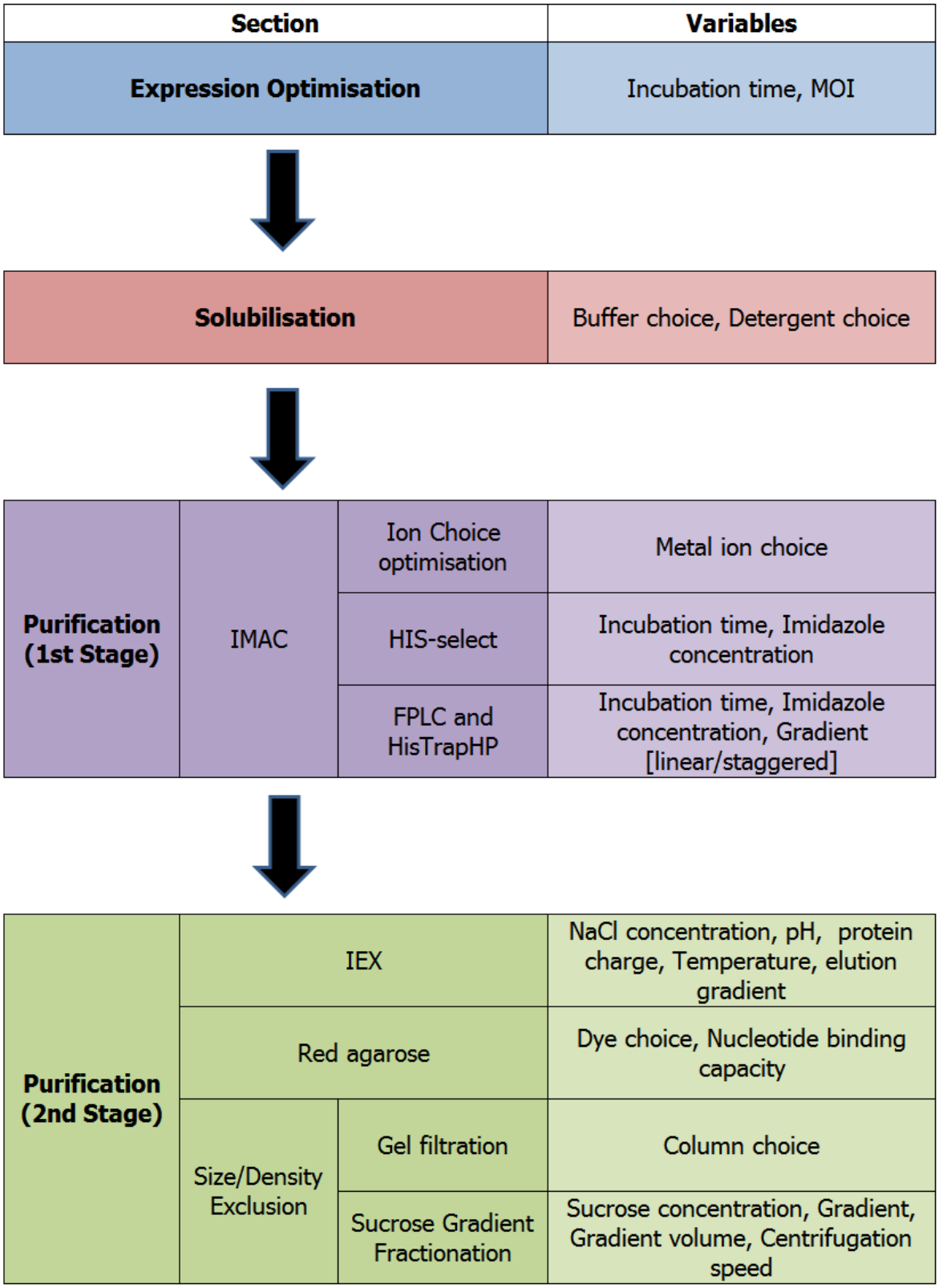

Figure 57: An overview of the research work described in this chapter.

3.2. Materials and Methods

3.2.1. General biochemistry assays

General biochemistry assays, such as gel electrophoresis, running/making SDS-PAGE gels, Coomassie staining, silver staining, western blotting and mass spectrometry protein identification were as described in Chapter 2 - Materials and Methods - section General Biochemistry Assays.

Antibodies used

Type		Raised against	Sequence	Detection	Company	Product ID
Primary	Rabbit Polyclonal	Residues 1-18 of the N-terminus of Cav3	MMTEEHTDLEARIIKDIH (Rat)	N/A	Abcam	ab2912
Primary	Mouse Monoclonal	MAT peptide	HNHRHKHGGGC (Synthetic)	N/A	Sigma	M6693
Secondary	Goat Monoclonal	Anti-Rabbit IgG (whole molecule)	N/A	Alkaline Phosphatase	Sigma	A3687
Secondary	Goat Monoclonal	Anti-Mouse IgG (Fab specific)	N/A	Alkaline Phosphatase	Sigma	A1682

Table 10: A table of the various antibodies used in this project.

3.2.2. Cloning

Cloning and insect cell expression of human Cav3

A sequence verified plasmid containing Cav3 was sent to the Protein expression facility (Manchester University). Primers were designed to PCR amplify the full length human Cav3 for insertion into pPolh-MAT-Tag-2 (Sigma T6574) baculovirus transfer plasmid. A consensus Kozak sequence was included in the forward primer to ensure optimal baculovirus expression. The sequence verified (in-house, Stopford Building sequencing service, Manchester University) pPolh-MAT-Tag-2:cav3 clone was co-transfected with linearised baculovirus into Sf9 insect cells to produce circular recombinant baculovirus DNA. This circular recombinant baculovirus DNA was then amplified and subsequently purified. This virus was termed P1, and is what was used for any subsequent infection.

Vector features

The pPolh-MAT-2 vector is a baculovirus transfer vector that adds a MAT-tag (metal affinity tag) to the C-terminus of the fusion protein, which allows purification in the same way as a His-tag i.e. by binding to transition metals. The vector also contains the

polyhedrin (polh) promoter, which can help achieve high level expression during the very late phase of infection.

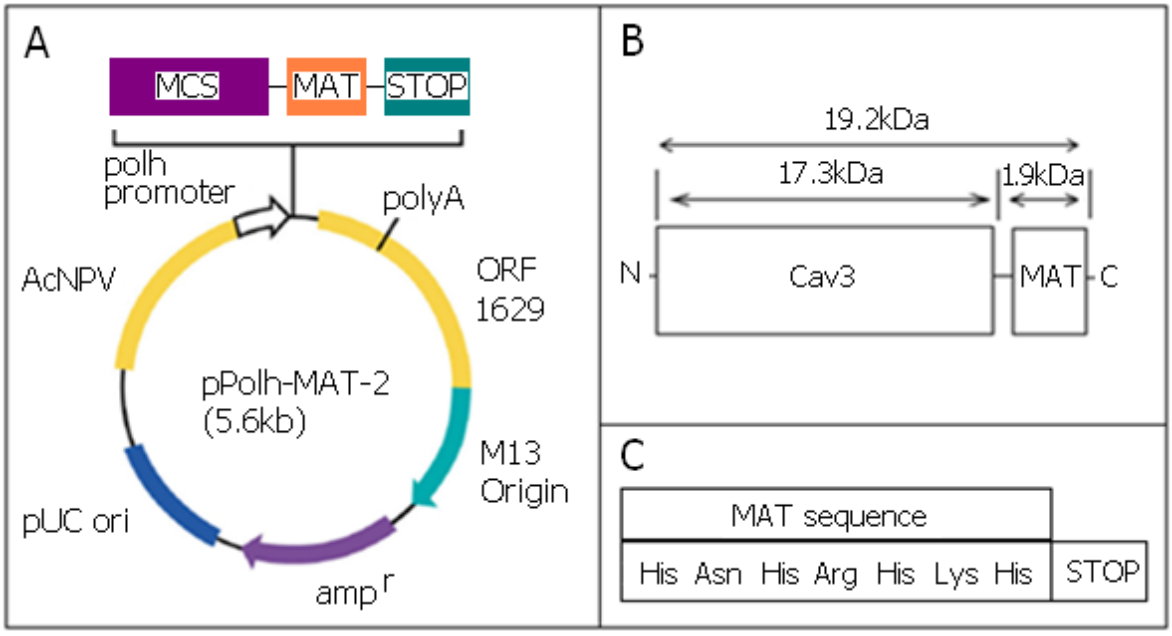

Table 11: Vector map of pPolh-MAT-2 and a schematic of the Cav3/MAT-tag fusion protein

A: pPolh-MAT-2 (5.6kb) transfer plasmid. **B**: Schematic of the Cav3/MAT-tag fusion protein. Cav3 has a C-terminal MAT-tag. The total fusion protein is approximately 19.2kDa. **C**: the MAT-tag sequence. Note the MAT sequence that will be used to purify the recombinant Cav3 protein after expression.

3.2.3. Cell culture

Growth of Sf9 cells in suspension

Cells were grown at 28°C in a shaking incubator (120rpm) in Erlenmeyer flasks. Cell density was kept between $0.5x10^6$ and $4x10^6$cells/ml. The exponential growth phase of the cells is at $2x10^6$cells/ml. Cell density was maintained at the desired concentration by monitoring using a haemocytometer to count the cells and passaging the cells at the desired concentration into fresh media. When growing in optimal conditions, cells double every 24hrs. The maximum culture volume was maintained at ⅕ of the total flask volume; for example, 400ml in a 2L flask.

Storage and recovery of the Sf9 cells

To freeze Sf9 cells, the cell density was adjusted to $4x10^6$ cells/ml. An equal volume of insect cell media (containing 20% (v/v) Dimethyl sulfoxide (DMSO) and 5%

(v/v) Fetal Bovine Serum (FBS) was added drop wise and mixed gently. 1ml aliquots in cryogenic vials were then stored at -20°C for 2hr then transferred to -80ºC for 12-16hrs. Samples were then moved to liquid nitrogen for long term storage. To defrost the cells, the vials were rapidly thawed in a 37ºC water bath. Cells were transferred to a 50ml falcon tube containing 5ml of fresh media, then centrifuged at 200xg (Sigma 3-13k; Sigma 11180) for 5 min. The supernatant was aspirated off and the cells were gently resuspended in 5ml of media. Cells were transferred to T25 flasks and incubated at 28ºC until confluent. Once confluent, they were transferred to a T75 flask and grown until confluent again. Once confluent they were transferred to a 50 ml flask and grown as a shaking culture.

3.2.4. Storage and amplification of the virus

$25x10^6$ cells were added to T75 flasks and then left in the incubator for 30min to allow the cells to attach. The baculovirus was added to each T75 flask at a MOI of 1. This was incubated at 28ºC for 7days. The media was removed and centrifuged at 10,000xg (Sorvall Evolution RC; SLA-1500) for 5 min to removed debris. The liquid fraction was then adjusted to 5% FBS (v/v). This baculovirus stock was stored in the dark at 4ºC.

3.2.5. Infection, expression and solubilisation

Small-scale expression

Before bulk expression of Cav3 was complete, a small-scale expression trial was undertaken in order to establish the optimum expression conditions. The assay helped identify the optimum viral titre and incubation time. $1x10^6$ cells were added to each well of a 6-well plate and then incubated at 28°C for 30min to allow the cells to adhere to the surface. Cells were infected with different concentrations of the baculovirus: 0, 0.5, 2. 5, 5, 12.5, 25 MOI, and then incubated for 24, 48 or 72 hrs. The media was removed and 500µl of solubilisation buffer #1 (see Table 12: Solubilisation buffers) was added to each well. The plates were incubated at 4°C for 30min with gentle agitation. This solution was termed Total lysate.

Large-scale expression

Cells were grown to $4x10^6$ cells/ml and then passaged to $1x10^6$ cells/ml in fresh media containing the baculovirus at a final MOI of 5. Cells where shaken (120rpm) at 28°C in an incubator for 72 hours. After the 72 hour incubation, cells were collected by centrifuging at 200xg (Sigma 3-13k centrifuge; Sigma 11180 rotor) for 5 min.

Optimisation of solubilisation buffer

The cell pellets were resuspended in solubilisation buffer (see Table 12: Solubilisation buffers), at a ratio of 20ml buffer to 400ml original cell solution. The resupended cell pellet solution was sonicated three times at 20amplitude microns for 30secs, resting 30secs in between to allow probe to cool. Cells were rotated for 1hour at 4°C. The cell solution was centrifuged at 45,000xg (Sorvall Evolution RC; SS-34) for 30 min at 4ºC. The supernatant was termed the soluble fraction.

Bulk solubilisation

As in the section above (Optimisation of solubilisation buffer), but with the following modifications: Solubilisation buffer #4 (see Table 12: Solubilisation buffers) was used.

	Buffer System		pH	NaCl	Protease Inhibitors	Detergent				Used for:
	Sodium Phosphate	Tris				TX100	NLS	CHAPS	DDM	
#1	50mM		8	150mM	yes	1%		1%		Small-scale expression
#2	50mM		8	150mM	yes	2%	1.5%	1%		Optimisation of Solubilisation buffer
#3		20mM	7.7	150mM	yes	1%	1.5%	1%		Optimisation of Solubilisation buffer
#4		20mM	7.7	150mM	yes	1%			1.2%	Optimisation of Solubilisation buffer; Bulk expression
#5		20mM	7.7	150mM	yes	1%	1.5%		1.2%	Optimisation of Solubilisation buffer
#6		20mM	7.7	150mM	yes	1%		1%	1.2%	Optimisation of Solubilisation buffer

Table 12: Solubilisation buffers

A range of different buffers were used during the optimisation of the solubilisation protocol. Ultimately, buffer #4 was used for bulk solubilisation. cOmplete, Mini, EDTA-free protease inhibitor cocktail tablets (Roche) were used. Abbreviations: DDM, n-Dodecyl-ß-maltoside (w/v); TX100, Triton X-100 (v/v); CHAPS, 3-[(3-cholamidopropyl)dimethylammonio]-1-propanesulfonate (w/v); NLS, N-laurylsarcosine (w/v).

3.2.6. Primary purification: Affinity chromatography

Metal ion choice optimisation

The post-lysis supernatant fraction was clarified by spinning it in a clarification mini spin column for 5min at 200xg. Various metal salt solutions (0.5M Nickel sulphate, 0.5M Cobalt chloride, 0.5M Copper sulphate, 0.5M Zinc chloride) were added to a pre-wet Vivapure metal chelate spin column and centrifuged for 1min at 1500xg (eppendorf Minispin plus). The metal ion loaded membrane was equilibrated with the sample buffer, and then the sample was loaded. The sample was then centrifuged for 3min at 1500xg (eppendorf Minispin plus). The membrane was then washed twice with the sample buffer and centrifuged for 3min at 1500xg (eppendorf Minispin plus). Finally, the bound proteins were eluted by adding the sample buffer (with 250mM imidazole) and centrifuging for 3min at 1500xg (eppendorf Minispin plus).

HIS-Select

HIS-Select agarose (Sigma HIS-Select® HF Nickel Affinity Gel H0537) was equilibrated at 4°C by mixing with the relevant buffer corresponding to the post-lysis supernatant fraction (see Table 12: Solubilisation buffers) at 1ml/50µl resin, followed by centrifugation to remove the liquid fraction. This was repeated 4 times to ensure the ethanol had been removed from the HIS-Select agarose. The post-lysis soluble fraction was added to the equilibrated HIS-Select agarose and mixed for 5min at 4°C. The solution was then centrifuged at 5000xg (eppendorf Minispin plus) for 5min. The supernatant fraction was termed unbound. The HIS-Select agarose was resuspended and washed three times with wash buffer (the samples buffer, plus 20mM imidazole) then centrifuged at 5000xg (eppendorf Minispin plus) for 5min. To elute what was bound to the HIS-Select agarose, the agarose was resuspended in elution buffer (the samples buffer with 250mM imidazole), and rotated for 15min at 4°C and then centrifuged at 5000xg (eppendorf Minispin plus) for 5min. This fraction was termed the Elution.

HisTrap HP

As a first stage of purification, a HisTrap HP Column (5ml column volume 17-5247-01 GE Healthcare) was connected to an AKTAprime plus fast protein liquid chromatography (FPLC) purification system, in order to purify Cav3 *via* the C-terminal MAT-tag with an affinity for charged metal ions. The column and the system were washed out with $_{dd}H_20$, then equilibration buffer (20mM Tris pH7.7, 150mM NaCl, 0.25% (v/v) Triton X-100, 0.3% (w/v) n-Dodecyl-ß-maltoside (Thermo Scientific), plus cOmplete,

Mini, EDTA-free protease inhibitor cocktail tablets (Roche)). The post-lysis supernatant was then diluted (to reduce the detergent concentration), filtered, degassed and loaded onto the system at a flow rate of 1ml/min. To elute the bound protein, the imidazole concentration was increased over a range of concentrations (see individual purifications in Results and Discussion, section Primary purification, for specific concentrations). Elution was at a flow rate of 0.5ml/min. All buffers and columns were kept on ice.

3.2.7. Secondary purification

Reactive red agarose

Reactive Red 120 agarose (Sigma R0503) was equilibrated at 4°C with the sample buffer (elution buffer from post-HisTrap HP FPLC) at 1ml/10µl agarose, followed by centrifugation to remove the liquid fraction. This was repeated 4 times to ensure the agarose was equilibrated. The peak Cav3 elution fraction from post-HisTrap HP FPLC was added to the equilibrated agarose and mixed for 20min at 4°C. The solution was then centrifuged at 5000xg (eppendorf Minispin plus) for 5min, and the supernatant (termed unbound) was removed. The agarose was resuspended and washed three times with wash buffer (the buffer in which the sample was in) then centrifuged at 5000xg (eppendorf Minispin plus) for 5min. To elute protein bound to the agarose, the agarose was resuspended in elution buffer (the samples buffer with 1.5M NaCl), and rotated for 15min at 4°C and then centrifuged at 5000xg (eppendorf Minispin plus) for 5min. This fraction was termed the Elution.

Ion exchange chromatography

A HiTrap Q Sepharose (17-5053-01 GE Healthcare) was connected to an AKTAprime plus Fast Protein Liquid Chromatography (FPLC) purification system in order to purify Cav3 based upon its charge. The column and the system were washed out with $_{dd}H_20$ and then equilibrated with the sample's buffer. The sample was then filtered, degassed and loaded onto the system at 1ml/min. To elute, the NaCl concentration was increased over a range of concentrations (see individual IEX purifications in Results and Discussion, section Secondary purification, for specific concentrations for specific concentrations) designed to elute the bound proteins into various fractions. Elution was at a flow rate of 0.5ml/min. All buffers and columns were kept on ice.

Charge prediction: Bioinformatics

The PROTEIN CALCULATOR v3.3 tool (found at http://www.scripps.edu/~cdputnam/protcalc.html) was used to calculate predicted charge.

Gel filtration

A HiPrep 16/60 Sephacryl S-400 HR column (28-9356-04 GE Healthcare) was connected to an AKTAprime plus FPLC purification system in order to purify Cav3 based upon its size. The column and the system were washed out with $_{dd}H_20$, and then equilibrated with the sample's buffer. The sample was then filtered, degassed and loaded onto the system *via* the injection valve. 1.5column volumes of equilibration buffer were passed through at 0.5ml/min until all proteins were eluted. All buffers and columns were kept on ice.

Sucrose gradient fractionation

Decreasing concentrations of sucrose (in 20mM Tris pH7.5, 115mM NaCl, 0.075% (w/v) n-Dodecyl-ß-maltoside (Thermo Scientific)) were carefully overlaid over each other in a ultracentrifuge tube resulting in the following sucrose concentration fractionation: [top] 10% (5ml), 12.5% (5ml), 15% (3ml), 20% (3ml), 22.5% (3ml), 30% (6ml) and 40% (7ml) [bottom]. The partially purified, post-HisTrap HP purification peak Cav3 sample was loaded onto the top of the gradient. The gradient was ultracentrifuged for 16hours at 132,000xg (Beckman Optima L-90K ultracentrifuge; SW28 rotor) at 4°C.

3.2.8. Thrombin cleavage of MAT-tag

0, 10, 20 or 50U thrombin (per mg protein) was added to the partially purified, post-HisTrap HP purification peak Cav3 sample and incubated at 4°C or 28°C for 5, 8, 13, 16, 22 or 24hours, with/without the presence of imidazole (400mM) or protease inhibitors (cOmplete, Mini, EDTA-free Protease Inhibitor Cocktail Tablets - Roche). Specific conditions are described in the Results and Discussion.

3.2.9. Dialysis

Many of the solubilisation and purification techniques employed result in the sample being in buffers that are not suited for other purification techniques or subsequent biophysics techniques. In these cases, dialysis cassettes (Slide-A-Lyzer Dialysis Cassettes 10k MWCO) were used to exchange certain constituents of the samples buffer.

3.3. Results and Discussion

3.3.1. Optimising full-length Cav3 expression in Sf9 cells using the baculovirus system

In order to establish the optimum expression conditions for bulk expression, a small scale expression assay was completed to identify both the optimum viral MOI and the incubation time.

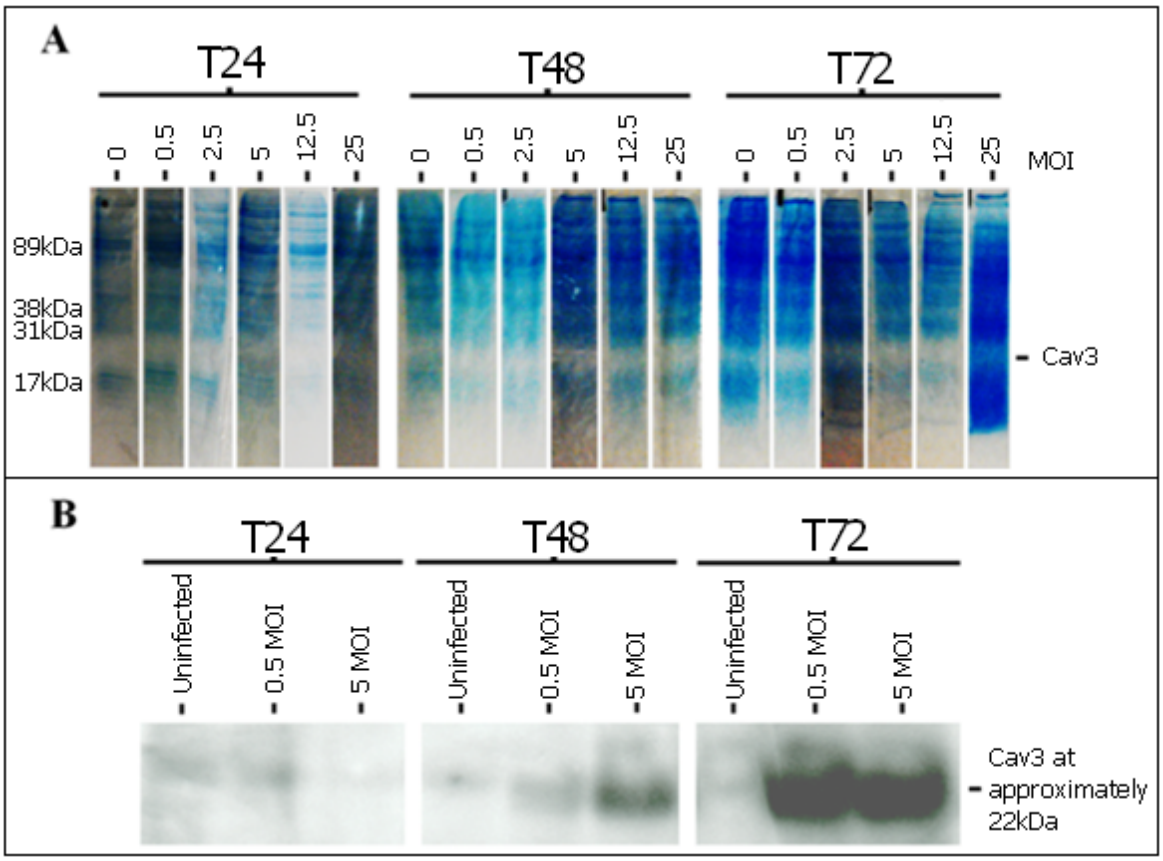

Figure 58: Protein expression profile of Cav3-transformed Sf9 cells at different stages of the growth period post-infection with different concentrations of the baculovirus. Samples of the total lysate fraction from different time-points post-infection at a range of MOIs (0.5, 2. 5, 5, 12.5, 25) were examined by SDS-PAGE and stained with Coomassie solution (**A**). The approximate position Cav3 would be expected is shown on the right. Western blotting for the expressed MAT-tagged Cav3 was complete for a selection of expression conditions (**B**). Over-expression of Cav3 was not achieved, as shown by the lack of a prominent band on the Coomassie stained gel. However, Cav3 expression was clearly present as indicated by the western blotting. Control: uninfected Sf9 cells (0 MOI). A mouse monoclonal antibody raised against the MAT-peptide was used as the primary antibody.

As can be seen in Figure 58, no prominent Cav3 bands were observed by staining with Coomassie. However, western blotting revealed that Cav3 was being expressed. As can be seen, Cav3 is being expressed after 48hrs, but is even more abundant after 72hours. For this reason, 72hours incubation was selected as optimum for bulk expression of Cav3. Expression appeared to be equivalent for both 0.5 and 5 virus MOI, so the upper figure of 5MOI was chosen for bulk expression. The protein migrated at approximately 22kDa, slightly larger than expected. However, this small increase in size is likely due to the presence of the tag. In addition, given the Sf9 expression, post-translational modification may have also affected the migration of the protein. Control experiments showed that the band detected by immunostaining was not present in the uninfected cells (Figure 58, panel B), thus indicating that it was likely to be Cav3.

3.3.2. Lysis

Since Cav3 is an integral membrane protein a series of cell lysis conditions employing detergents were tested for optimum solubilisation of Cav3.

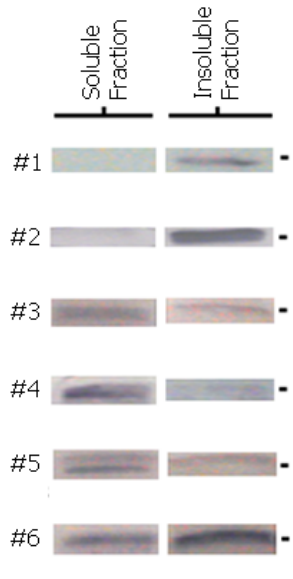

	Buffer System		pH	Detergent				Used for:
	Sodium Phosphate	Tris		TX100 (v/v)	NLS (w/v)	CHAPS (w/v)	DDM (w/v)	
#1	50mM		8	1%		1%		Cav3 completely in insoluble fraction
#2	50mM		8	2%	1.5%	1%		Cav3 completely in insoluble fraction
#3		20mM	7.7	1%	1.5%	1%		Cav3 predominantly in soluble fraction, but some remains in insoluble fraction
#4		20mM	7.7	1%			1.2%	Cav3 predominantly in soluble fraction
#5		20mM	7.7	1%	1.5%		1.2%	Cav3 predominantly in soluble fraction, but an unspecific band is also present
#6		20mM	7.7	1%		1%	1.2%	Cav3 predominantly in insoluble fraction

Figure 59: Optimisation of the Solubilisation buffer.

Sf9 cells were grown for 72 hours having been infected with the Cav3 containing baculovirus at a MOI of 5. These cells were collected and lysed using one of a range of solubilisation buffers. Samples were centrifuged and the pellets (insoluble fraction) and supernatants (soluble fraction) were analysed by SDS-PAGE/western blotting. Note that for each of the sodium phosphate buffers Cav3 remains in the pellet fraction, though this is possibly due to the lack of the detergent DDM. All the Tris buffers resulted in soluble Cav3, particularly the one containing 1% (v/v) TX100 and 1.2% (w/v) DDM (Buffer #4). A mouse monoclonal antibody raised against the MAT-peptide was used as the primary

antibody. Abbreviations: Triton X-100, TX100; N-laurylsarcosine, NLS; 3-[(3-Cholamidopropyl)dimethylammonio]-1-propanesulfonate, CHAPS; n-Dodecyl-ß-maltoside, DDM.

As can be seen in Figure 59, neither of the sodium phosphate based solubilisation buffers used (#1, #2) appeared to result in the solubilisation of Cav3. Indeed, Cav3 was found entirely in the pellet fraction. However, this is likely due to the lack of DDM detergent, not the sodium phosphate buffer. Indeed, even the combination of 2% (v/v) Triton X-100, 1.5% (w/v) N-laurylsarcosine and 1% CHAPS (w/v) did not appear to work when in the sodium phosphate buffer. Detergents in a Tris buffer can be seen to be more effective for solubilising Cav3; however, certain combinations of detergents appear to have varied in success. The most effective was solubilisation buffer #4, which contained the detergents 1% (v/v) Triton X-100 and 1.2% (w/v) n-Dodecyl-ß-maltoside (DDM). DDM is thought to maintain protein activity better than detergents such as CHAPS. Indeed, there are extensive reports in the literature for the use of DDM in maintaining protein activity (Bujarski et al., 1982; Olivari et al., 1998; Xu et al., 2008; Yagi et al., 1988).

3.3.3. Primary purification

Immobilised metal ion affinity chromatography

Charged metal ion optimisation

Once the optimum cell lysis protocol had been established, work on the optimisation of the purification protocol was undertaken. One of the advantages of expressing a protein is the ability to engineer a tag to aid in purification, in this case a MAT-tag. A series of charged metal ions were tested (nickel, copper, cobalt and zinc) to determine which ion was optimum for isolation of the Cav3-MAT-tag fusion protein.

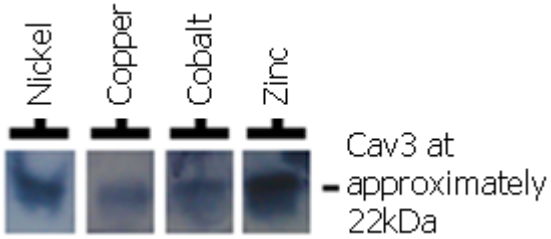

Figure 60: Comparison of metal ions for binding Cav3.
Cav3 was purified *via* the VivaPure metal chelate spin column kit using a range of different charged metal ions (nickel, copper, cobalt and zinc). Since these experiments were carried out on a small scale, western blotting (anti-MAT) was employed to detect

binding of the Cav3-MAT fusion protein to the individual metal columns. A mouse monoclonal antibody raised against the MAT-peptide was used as the primary antibody. Note that each of the four metal ions successfully bound Cav3.

As can be seen in Figure 60, all four ions worked suitably well to purify Cav3, with nickel and zinc performing best, which meant that the recombinantly attached MAT-tag was functional and had not been occluded during folding.

NiNTA purification

Before embarking on a bulk isolation of Cav3, a small scale purification of Cav3 was tested using HIS-select resin.

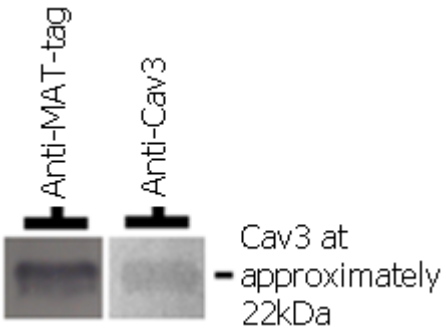

Figure 61: Small scale purification of Cav3 with HIS-select resin
The soluble fraction containing Cav3 was applied to HIS-Select Resin. The column was washed several times and the bound proteins were eluted with 300mM imidazole. Western blotting using two different primary antibodies (anti-Cav3, abcam ab2912; anti-MAT, Sigma M6693) demonstrated that Cav3 had bound and was present in the elution fraction. The identification by western blotting of both the MAT-tag as well as Cav3 indicated that the complete fusion protein had been purified.

As can be seen in Figure 61, the HIS-select resin successfully bound the solubilised Cav3. Immunostaining with two different antibodies raised against different parts of the recombinant protein confirmed that the large band purified in the elution fraction was indeed Cav3.

HisTrap HP

To scale up the isolation of Cav3, several batches of cells were lysed (and solubilised) and the supernatants pooled. The combined supernatant was then applied to a HisTrap HP column and the chromatography conducted using an AKTA Prime FPLC system.

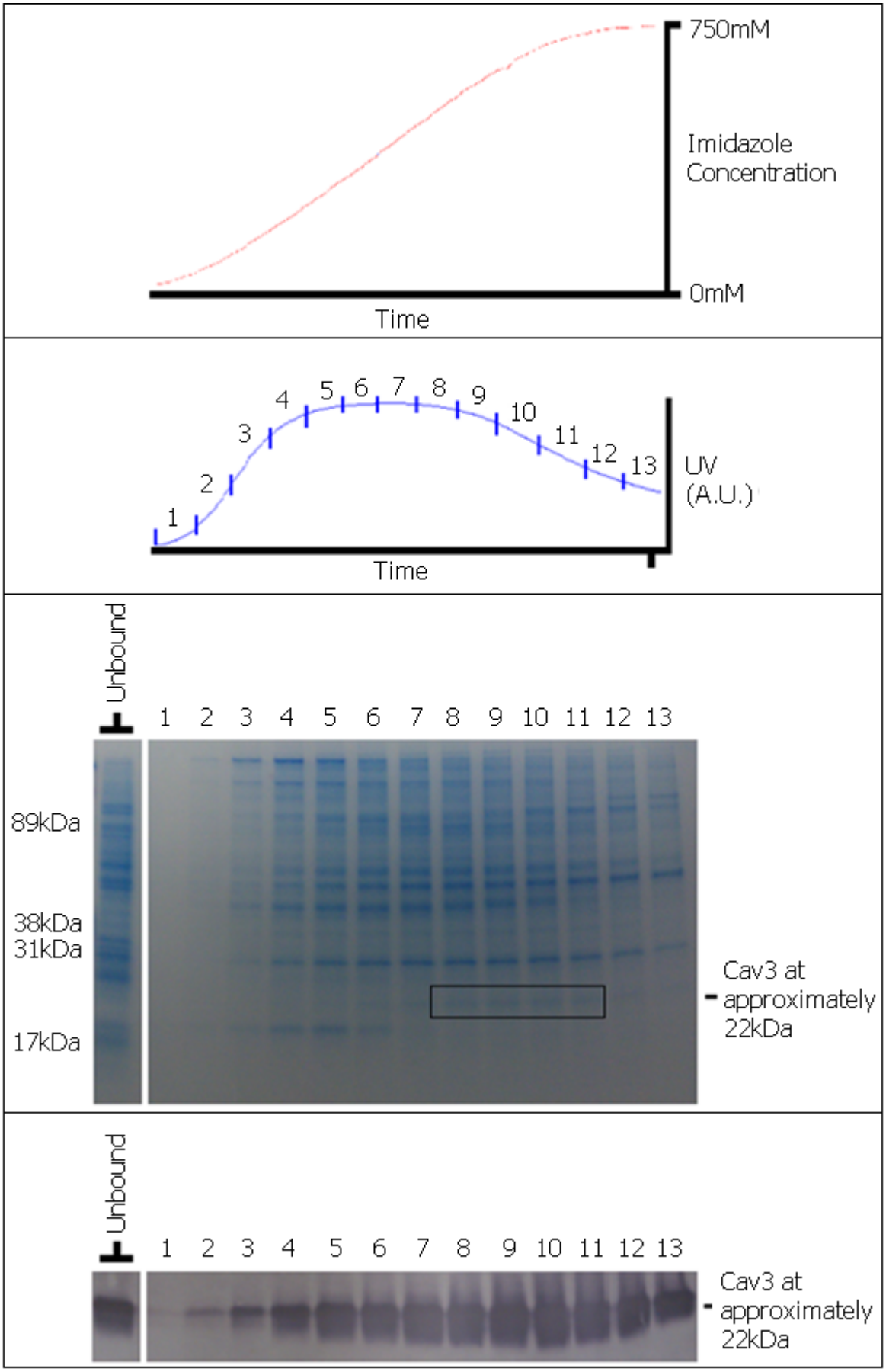

Figure 62: Purification of Cav3 using the HisTrap HP column coupled to the FPLC system.

The soluble Cav3 containing fraction was applied to the HisTrap HP column. **A**: a linear elution gradient (0-750mM over 15ml) using imidazole was employed. **B**: the UV trace shows one elution peak, with the peak being at fraction #7. **C**: samples of the elution fractions were ran on an SDS-PAGE gel and stained in Coomassie. Cav3 expression was achieved (boxed) in fractions #9-11. **D**: Western blotting (anti-MAT-tag) confirmed the presence of Cav3 in all fractions. Numbers denote the fractions collected.

As can be seen in Figure 62, Cav3 was in the purified elution fraction. However, many impurities also remained. From looking at the Coomassie it was noticed that certain impurities were eluted at different imidazole concentrations. Altering the imidazole concentration from a linear gradient (0-750mM) to a step-wise gradient (200mM imidazole, hold, 750mM imidazole) was next employed as a means of separating the proteins based on the concentration of imidazole required to elute them.

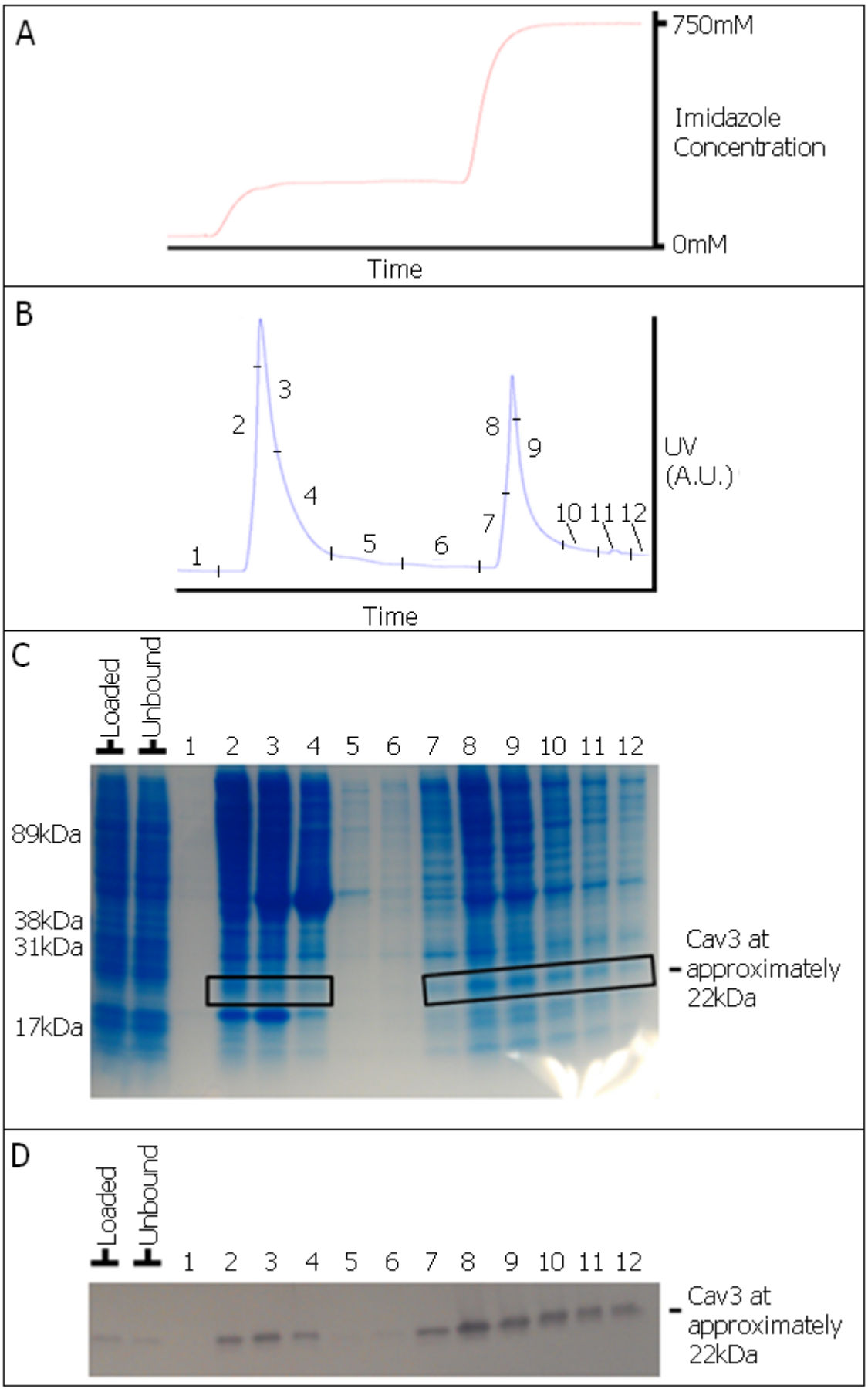

Figure 63: Optimisation of Cav3 purification using the HisTrap HP column coupled to the FPLC system.

The solubilised Cav3 fraction was applied to a HisTrap HP column. **A:** a stepwise (200mM imidazole held over 100ml, 750mM imidazole held indefinitely) elution gradient was employed. **B:** the UV trace during the elution shows the presence of two separate UV (protein) peaks. As can be seen, the two UV peaks correlate with the two separate increases in imidazole (200mM and 750mM) indicating that the increase in imidazole is responsible for the observed protein elution. **C:** the polypeptide profiles of the eluted fractions after separation by SDS-PAGE. As can be seen Cav3 (boxed) elutes at both imidazole concentrations, although there is clearly more in the 2nd elution peak (corresponding to 750mM imidazole). **D:** Western blotting using an antibody raised against the MAT-peptide confirms the presence of Cav3 in both elution peaks. Numbers denote the fractions collected.

As can be seen in Figure 63, by employing a step-wise gradient of imidazole, it resulted in two distinct elution peaks. Although, this approach did not fully purify Cav3 from the rest of the impurities, it removed many of them, as can be seen by looking at the different protein profiles for each peak (Figure 63, panel C). In addition, by solubilising more cell pellets, Cav3 was now readily detectable by Coomassie staining. The samples corresponding to the second peak were used in any subsequent secondary purification.

3.3.4. Secondary purification

Ion exchange purification of Cav3

IMAC alone was not sufficient to purify Cav3 to completion; therefore, a second stage of purification was required. Ion exchange chromatography (IEX) is a commonly employed method of purification that separates proteins based upon the differences in their net surface charge. However, the process is greatly aided by knowledge of the net surface charge of your protein of interest; unfortunately, such data has not been determined experimentally for Cav3. Thus, determination of charge had to be predicted by primary sequence alone. However, it should be noted that this approach is fraught with potential error, as it does not take into consideration any secondary structure, nor the consequence of higher order oligomeric formation on charge, both of which can result in the charged residues being imbedded, and both likely to be of significance to Cav3.

Assumptions had to be made that a) the charge predicted on primary sequence alone was the same as when the protein was fully folded, b) that the charge predicted based on primary sequence of the monomer represented the net charge of Cav3 oligomers – both

assumptions being particularly large, and likely erroneous. Since it is predicted (PROTEIN CALCULATOR v3.3 tool found at http://www.scripps.edu/~cdputnam/protcalc.html) that a Cav3 monomer at pH7.5 is expected to be slightly negatively charged (-1.4), it seemed reasonable to use an anion exchanger column. The partially purified Cav3 from the HisTrap HP column was diluted to reduce the concentration of the NaCl and the imidazole (to 38mM and 150mM respectively). Having previously established that a steep linear NaCl gradient (38mM-1M over 6ml) was insufficient to separate Cav3 from the impurities (data not shown), a less steep NaCl gradient (38mM-1M over 12ml) was employed. The diluted elutant (from the HisTrap HP column elution) was applied to a HiTrap Q FF anion exchanger column which lead to a much better resolution of the UV peaks, see Figure 64.

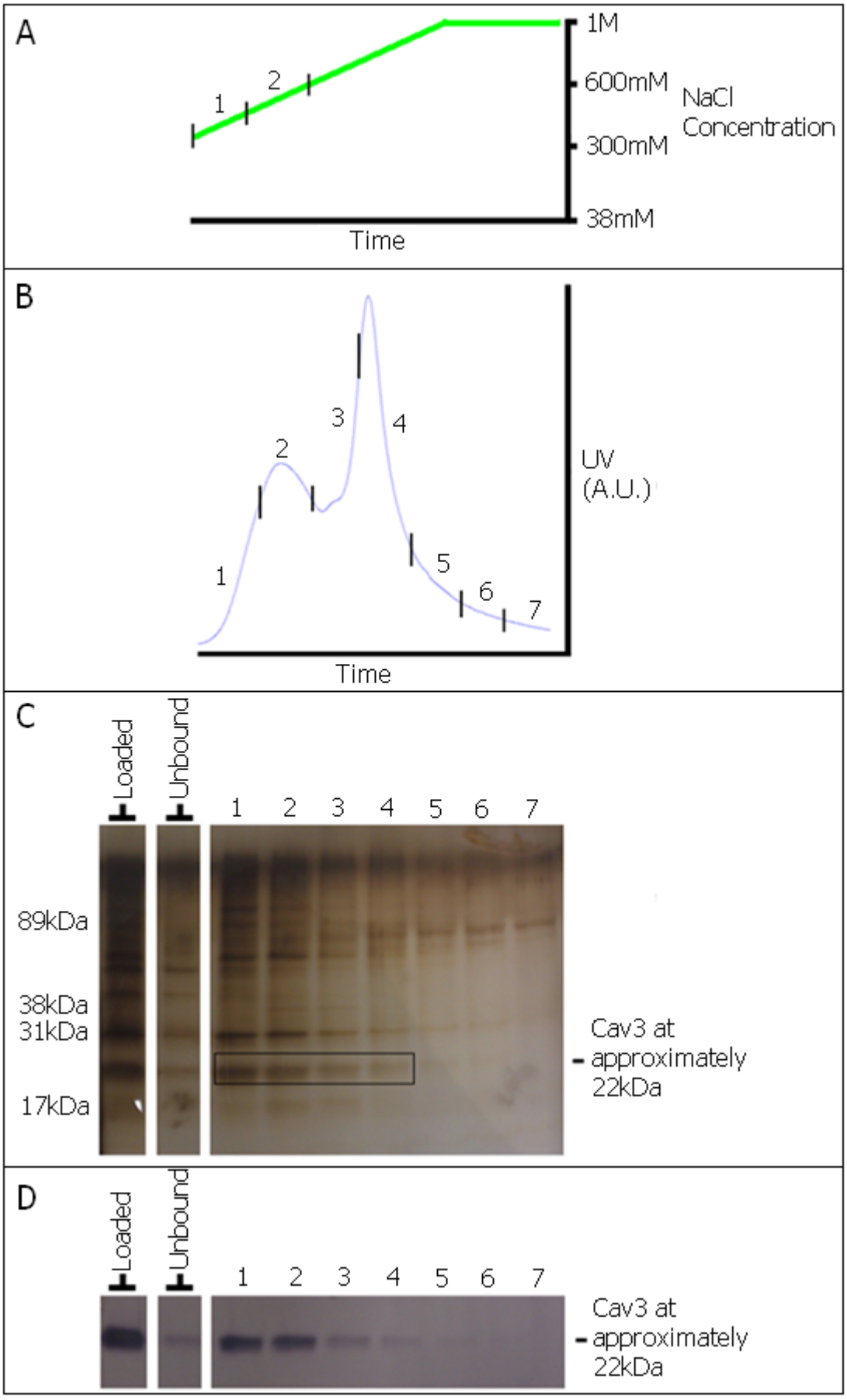

Figure 64: Ion exchange purification of Cav3.

The partially purified Cav3 from the HisTrap HP column elution fraction was applied to a HiTrap Q FF column. **A:** a linear (38mM-1M NaCl over 12ml) elution gradient was employed. **B:** the UV trace during the elution shows the presence of two separate UV (protein) peaks with incomplete separation. **C:** the polypeptide profiles of the eluted fractions after separation by SDS-PAGE (shown here as a silver stain). As can be seen Cav3 (boxed) eluted at 300-600mM NaCl concentrations. **D:** Western blotting using an antibody raised against the MAT-peptide confirmed the presence of Cav3 in the first elution peak. Numbers denote the fractions collected.

As can be seen in Figure 64, two distinct UV (protein) peaks are separated out (~fractions #2 and #3+4), with the peak Cav3 fraction (#1 and #2) eluting at ~300-600mM NaCl. The polypeptide compositions of each of the fractions corresponding to the two peaks show that Cav3 is predominantly in the first peak; however, so are many of the impurities. Moreover, there remained incomplete resolution of the two peaks. In order to improve upon this separation a step-gradient was employed.

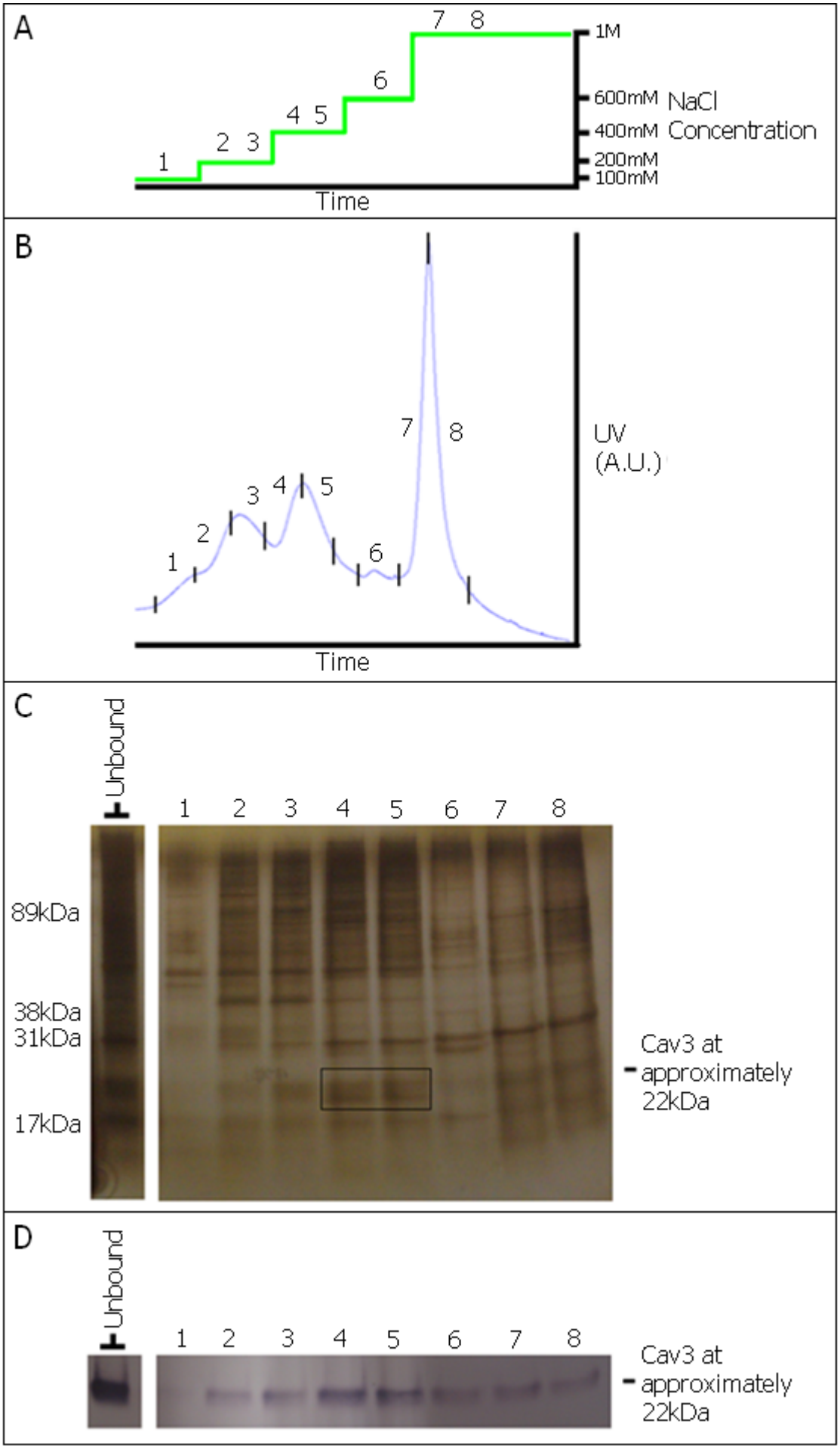
A
1
2 3
4 5
6
7 8
1M
600mM
400mM
200mM
100mM
NaCl
Concentration
Time
B
1
2
3
4
5
6
7
8
UV
(A.U.)
Time
C
Unbound
1 2 3 4 5 6 7 8
89kDa
38kDa
31kDa
17kDa
Cav3 at
approximately
22kDa
D
Unbound
1 2 3 4 5 6 7 8
Cav3 at
approximately
22kDa

Figure 65: Ion exchange purification of Cav3: Step-gradient.
The partially purified Cav3 from the HisTrap HP column elution fraction was applied to a HiTrap Q FF column. **A:** a step-gradient (100mM, 200mM, 400mM, 600mM all held for 4ml, then held at 1M indefinitely) elution gradient was employed. **B:** the UV trace during the elution shows the presence of multiple UV (protein) peaks, with incomplete separation. **C:** the polypeptide profiles of the eluted fractions after separation by SDS-PAGE (shown here as a silver stain). As can be seen Cav3 (boxed) eluted at 400mM NaCl concentrations. **D:** Western blotting using an antibody raised against the MAT-peptide confirmed the presence of Cav3 in multiple elution peaks. Numbers denote the fractions collected.

Employing a step-gradient can be seen to lead to a greater separation of the protein components, with four distinct UV peaks resolved. However, it can still be seen that the fractions containing Cav3 are far from pure and a comparison of the polypeptide profiles in Figure 63 with Figure 65 illustrates that there has been little increase in the purity of Cav3. Moreover, even with further optimisation of the elution conditions by increasing the number and duration of the NaCl steps had little impact upon Cav3 purity. In order to further improve upon the resolution of the first few elution peaks, the hold time of each elution step was increased (from 4ml/step to 12ml/step).

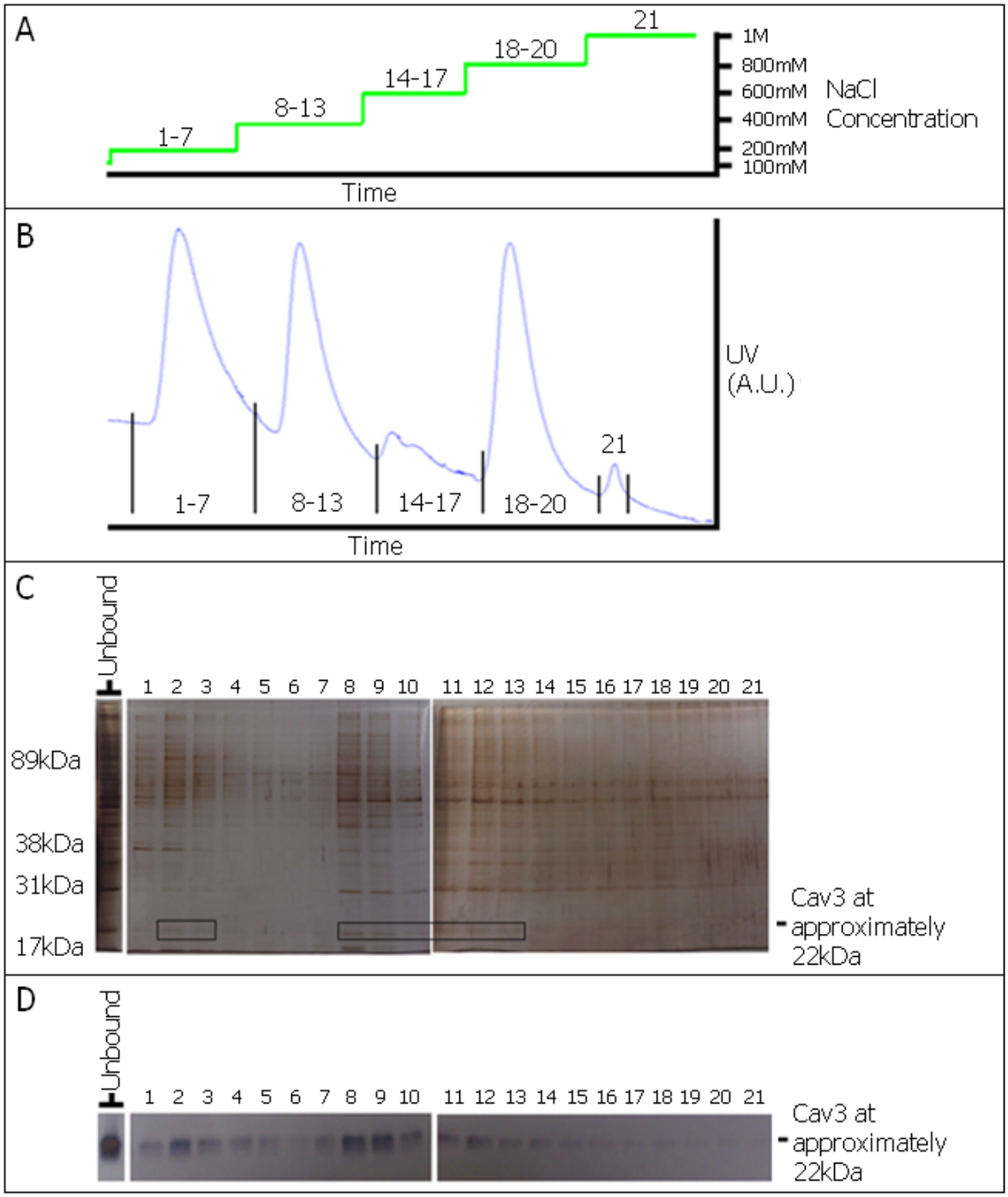

Figure 66: Ion exchange purification of Cav3: Step-gradient, plus extended hold times.

The partially purified Cav3 from the HisTrap HP column elution fraction was applied to a HiTrap Q FF column. **A:** a step-gradient with extended hold times (100mM, 200mM, 400mM, 600mM all held for 12ml, then held at 1M indefinitely) was employed. **B:** the UV trace during the elution shows the presence of multiple UV (protein) peaks with incomplete separation. **C:** the polypeptide profiles of the eluted fractions after separation by SDS-PAGE (shown here as a silver stain). As can be seen Cav3 (boxed) eluted at 400mM NaCl concentrations. **D:** Western blotting using an antibody raised against the MAT-peptide confirmed the presence of Cav3. Numbers denote the fractions collected.

Although five separate peaks were achieved, with Cav3 found predominantly in the 2nd peak (eluted with 400mM NaCl), and although many of the impurities were lost in the first peak, many still remained in the Cav3 fraction. Moreover, some Cav3 was still present in the first peak (eluted at 200mM). It was clear that to purify Cav3 further by employing the IEX purification approach was not going to yield the homogenous, high levels of Cav3 that were required. It was at this point that the use of IEX as part of the purification process was discontinued.

Reactive Red 120-Agarose

One persistent impurity was consistently observed to co-elute with Cav3 was a protein of approximately 30kDa in size. This protein was excised from a Coomassie gel and sent for identification by tandem mass spectrophotometry (Protein Mass Spectrometry Core Facility, Manchester University), where it was confirmed to be ATP/ADP translocase, also known as adenine nucleotide translocase. ATP/ADP translocase is a protein that is 33kDa in size, forms dimers and is involved in nucleotide transportation. Knowing that the impurity was ADP/ATP translocase, experiments were devised to eliminate it based upon its unique biophysical property.

An important consideration for developing a strategy to eliminate the impurity was to question whether the translocase impurity had been co-purified with Cav3 because it possessed similar properties, such as nickel binding ability or a similar charge, or whether it been co purified with Cav3 because it had been physically associated with Cav3 or one of the other impurities that remained, and had therefore been eluted *with* Cav3.

No reports exist for translocase being able to bind nickel or charged metals. Moreover, the known nickel binding motifs [MLA]-[RK]-H-A-F-D-[AS]-D-H-I-[AV]-[AC]-I-D-N-T and/or G-A-M-E-R-V-R-P-V-L-M-T (Fulkerson, Garner et al. 1998), were also not found in its primary sequence (SwissProt entry Q86PG2). In addition, using PROSITE (http://prosite.expasy.org/ Release 20.81) to search for domains and functional sites associated with metal binding also yielded no matches. Furthermore, assuming that all charged residues were fully exposed, and that monomeric charge was the same as dimeric charge, the pI was calculated as 9.87, with a strong positive charge of 17.6 at pH7.5, which would have meant it would not have been purified using the anion exchangers used in the above IEX. However, given that the impurity *was* in the eluted fraction, either this charge prediction is incorrect, or the protein was being co-purified with another protein that had bound the anion exchanger. To address the possibility that there may be a physical association of Cav3 with ATP/ADP translocase, the translocase sequence was searched for

the caveolin binding motifs [FWY]-x-[FWY]-x-x-x-x-[FWY], [FWY]-X-X-X-X-[FWY]-X-X-[FWY] (Couet et al., 1997), but none were found.

One interesting finding discovered when researching the ATP/ADP translocase protein was that of it being a nucleotide binding protein. Reactive Red 120-Agarose is a reactive textile dye that has been shown to have an affinity for nucleotide binding sites of certain proteins (Billington et al., 2004; Denizli and Pişkin, 2001), which would allow the ATP/ADP translocase to be removed from the sample. Therefore, a new purification step to remove the translocase using Reactive Red 120-Agarose was devised.

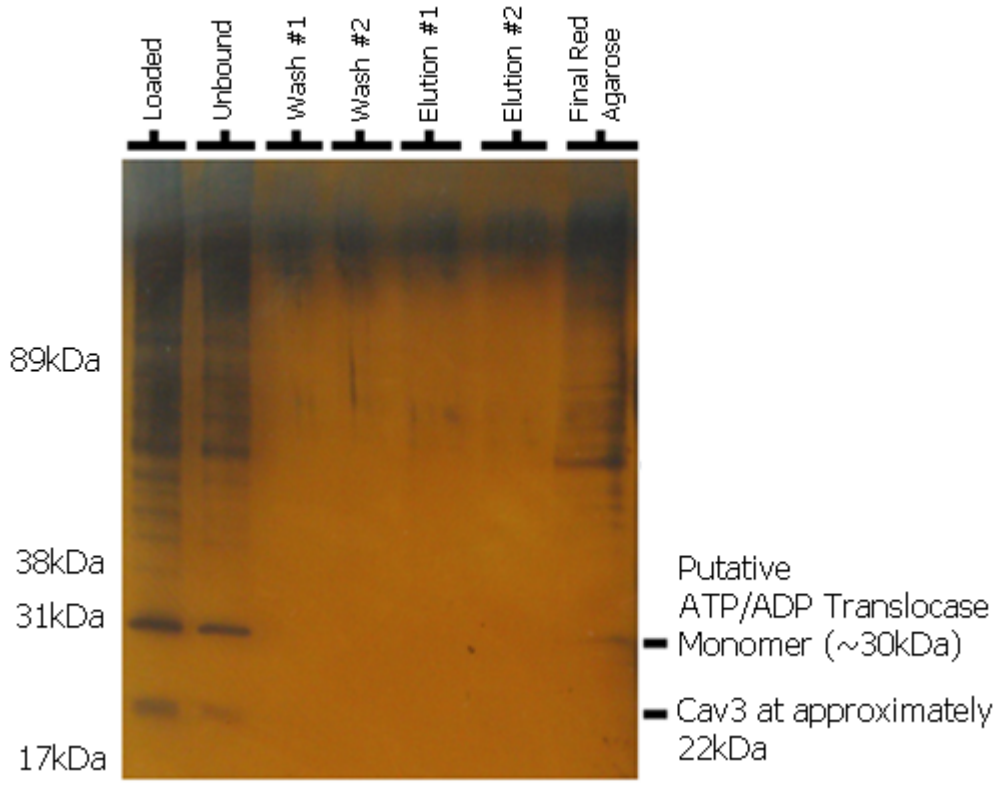

Figure 67: Reactive Red 120 agarose purification of Cav3.
The partially purified Cav3 from the HisTrap HP column elution fraction was applied to the reactive red-agarose. Unbound proteins were collected *via* centrifugation and the bound proteins were eluted with a 1.5M NaCl concentration (Elution #01 and #02). Samples of the loaded, unbound, wash and elution fractions were ran on an SDS-PAGE gel and silver stained. Most proteins remained unbound, including Cav3; however, some proteins, including the suspected ATP/ADP Translocase, remained bound to the resin, even after treatment with 1.5M NaCl.

As can be seen in Figure 67, as expected, the majority of the proteins loaded onto the agarose did not bind. However, although some of the suspected ATP/ADP translocase was observed in the final agarose, much of it remained in the unbound fraction.

Interestingly, the attempts to elute using 1.5M NaCl did not seem to elute what proteins had bound the agarose, and only by boiling the agarose in SDS did the proteins observed dissociate from the resin. Interestingly, as well as the suspected ATP/ADP translocase band at ~30kDa, a ~60kDa band was observed associated with the final resin. It is possible that this is the dimerised form of the ATP/ADP translocase.

One possible reason for the failure of this approach is due to the presence of non-ionic detergent (in this case n-Dodecyl-ß-maltoside), which encapsulates immobilised dye in micelles and can prevent proteins from binding. Unfortunately, it was not possible to eliminate the detergent at this stage, because Cav3 is a membrane protein and requires its presence for stability. Regardless, this approach was clearly not sufficient to remove the major impurity.

Size exclusion: Gel filtration

Knowing that the ATP/ADP translocase impurity was predicted to be only small (33kDa; 66kDa as dimer), and some of the other identified impurities (namely Ribosomal protein S2, 60S ribosomal protein L13, Cathepsin L-like cysteine proteinase, Tricarboxylate transport protein) were also only small proteins, we decided to try and purify Cav3, which has been predicted by several groups to form large oligomers between 200-600kDa (Li et al., 1996c; Monier et al., 1995; Sargiacomo et al., 1995; Tang et al., 1996), based on differences in their sizes. From previous work, our lab had a HiPrep 16/60 Sephacryl S-400 HR column available. This particular column was not the most suitable size exclusion column for the size separation we had in mind; indeed, it is more suitable for the separation of much larger proteins (up to 8MDa). Despite this, we decided to see if it would allow us to separate the remaining impurities from the Cav3.

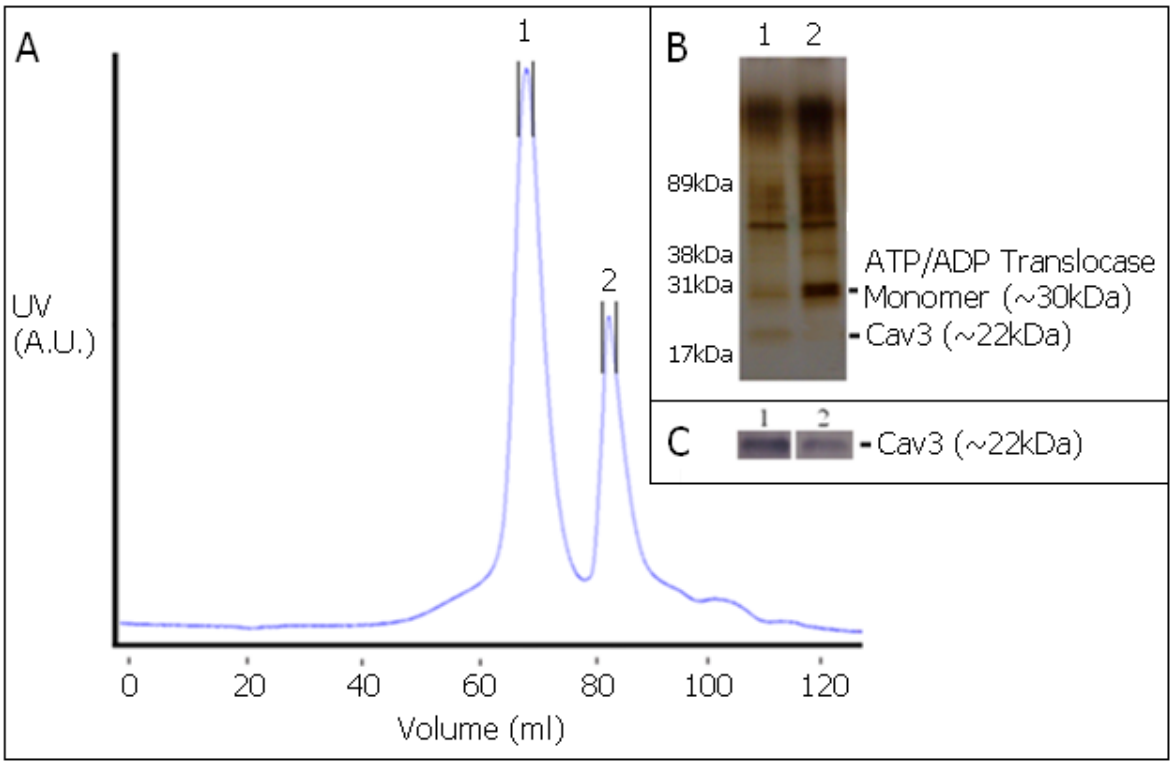

Figure 68: Secondary purification *via* HiPrep 16/60 Sephacryl S-400 HR.
The partially purified Cav3 from the HisTrap HP column elution fraction was applied to a HiPrep 16/60 Sephacryl S-400HR gel filtration column. **A:** the UV trace during the elution shows the presence of two UV (protein) peaks. Proteins eluted based upon size, with the larger proteins eluting first (peak #1), and the smaller proteins last (peak #2). **B:** Samples of the elution fractions from each peak were analysed on an SDS-PAGE gel and silver stained. Cav3 is predominantly in peak #1, whereas the putative ATP/ADP translocase impurity was in peak #2. **C:** Western blotting using an antibody raised against the MAT-peptide confirmed the presence of Cav3 in both peaks, especially the first elution peak. Numbers denote the fractions collected.

As can be seen in Figure 68, as predicted, the column choice was not suitable for the separation of the impurities and Cav3. Although, some degree of purification had been achieved, full separation of the impurities from Cav3 had not been achieved. Encouragingly, much of the main impurity thought to be the ATP/ADP translocase was indeed in the fraction associated with the smaller proteins and Cav3 was in the fraction associated with the larger eluted proteins. It was noted that one impurity, the putative ATP/ADP Translocase dimer, was equally present in both fractions, indicating that this may not actually be a dimer of ATP/ADP Translocase as had been suspected. In summary, a column designed for the separation of proteins up to 8MDa did not provide the resolution required for the separation of 200kDa and 66/33kDa proteins.

Sucrose gradient fractionation purification of Cav3

Although size exclusion using the above column had only been partially successful, this was likely due to the inappropriate column choice. Gel filtration columns are very expensive, so buying a new and more suitable column was not desirable. Fortunately, another, considerably cheaper method of size/density exclusion was available: Sucrose gradient fractionation (SGF).

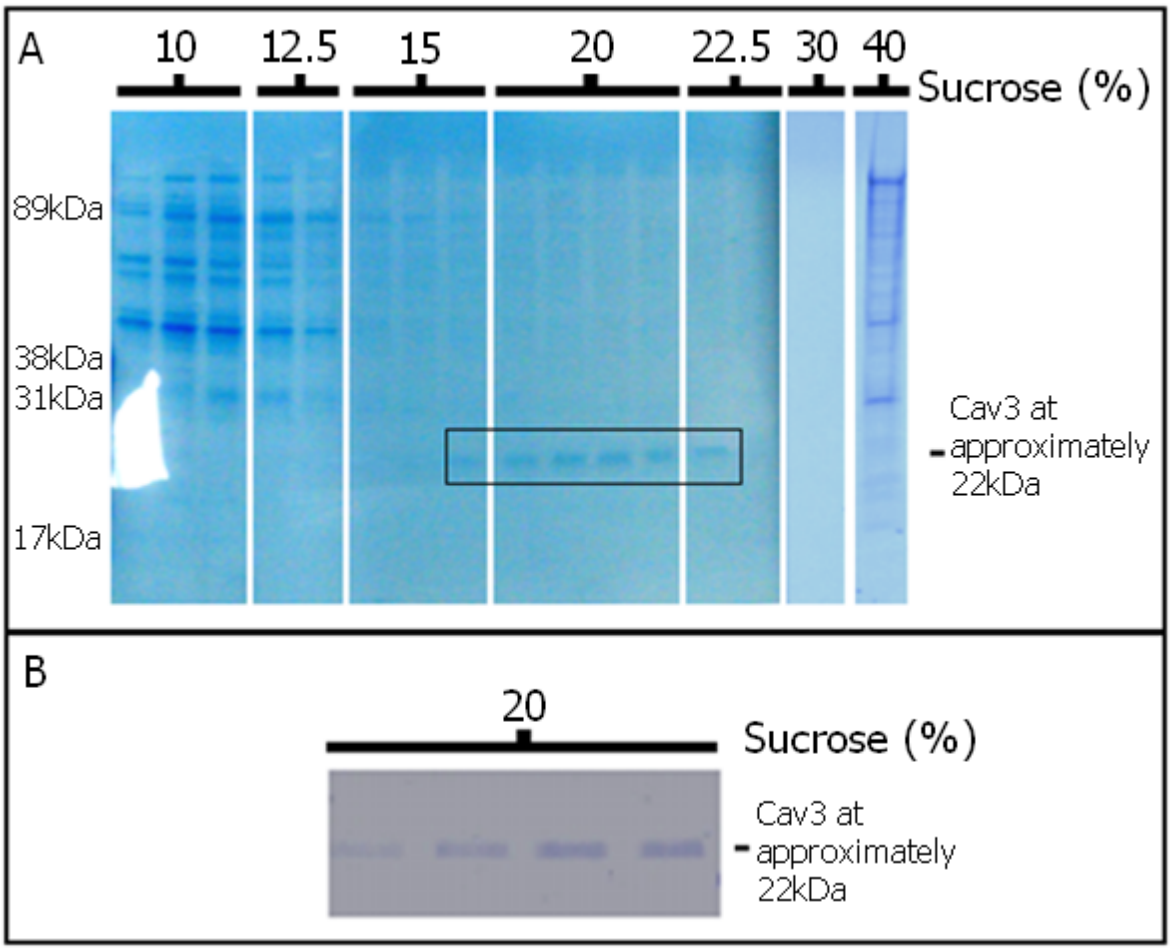

Figure 69: Secondary purification *via* sucrose gradient fractionation.
The partially purified Cav3 from the HisTrap HP column elution fraction was loaded onto a sucrose gradient. Proteins migrated varying distances based upon their density, with the denser proteins migrating further through the sucrose gradient, and the less dense proteins migrating less distance. **A:** Samples from the sucrose fractions 10, 12.5, 15, 20 and 22.5, 30, 40% were analysed on an SDS-PAGE gel. Purified Cav3 migrates to the 20% sucrose fraction and can be seen here as a single monomeric band at ~22kDa. Some proteins migrated into the final fraction (40%) and pelleted at the bottom of the gradient; these proteins were likely aggregated. **B:** Western blotting using an antibody raised against the MAT-peptide confirmed the presence of Cav3.

As can be seen in Figure 69, separation of Cav3 from the remaining impurities has been achieved by using a size exclusion technique in the form of sucrose gradient fractionation. Note that Cav3 is predominantly in the 20% sucrose fraction, and that it is the only protein observable, albeit at a low concentration. It is encouraging to see that Cav3 is not present in the proteins that were observed at the bottom of the column (40%), which are likely aggregated proteins, thus indicating that Cav3 is likely not aggregated. As can be seen, there are no observable impurities. The sample was sent for identification by tandem mass spectrophotometry (Protein Mass Spectrometry Core Facility, Manchester University), where it was subsequently confirmed to be Cav3. Further evidence for the purity of Cav3 will come later (in Chapter 5), where the electron microscopic micrographs show a homogeneous Cav3 sample. A total of 0.02-0.03mg Cav3 was obtained from $2.5x10^9$ cells.

3.3.5. Thrombin cleavage of MAT-tag

Having successfully purified recombinant human Cav3, the small MAT-tag that was fused at the C-terminus of the recombinant protein was removed. The accompanying thrombin cleavage protocol stated that it must be complete at room temperature (22°C), for 16hours and at low (preferably zero) imidazole concentration; none of which are particularity favourable to maintaining a functional recombinant protein. To address if any of these variable could be altered, a thrombin cleavage assay was completed to address these concerns. Four variables were explored: time, thrombin concentration, temperature, buffer constitution. Reducing the amount of time required for 100% cleavage was desirable, so as to reduce the amount of time in which aggregation could potentially happen. Reducing the amount of thrombin required was also required, so as to reduce the overall cost. Establishing the optimum temperature was required, so that experiments could be planned with temperature in mind. Many of the subsequent biophysical techniques require Cav3 to be in certain buffers, so for that reason, certain buffer components were also assessed.

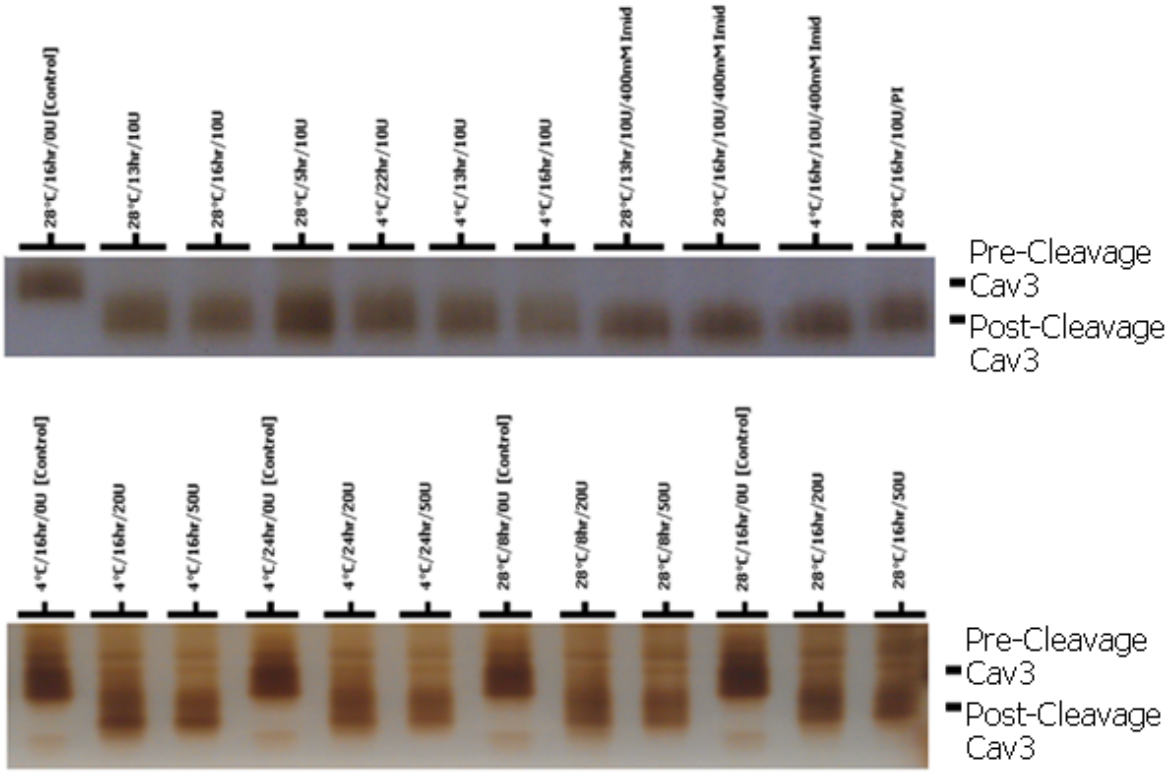

Figure 70: Optimisation of the thrombin cleavage of the MAT-tag

The partially-purified Cav3 from the HisTrap HP column elution fraction was used to optimise the cleavage conditions. A variety of cleavage conditions were explored, including different temperatures, incubation times, thrombin concentrations (U) and imidazole concentrations. Most of the conditions explored were sufficient for cleavage. Samples of the post-cleavage samples were analysed on an SDS-PAGE gel and silver stained.

As can be seen in Figure 70, thrombin cleavage was successful in all condition. Indeed, thrombin cleavage can be complete at low temperatures (4°C), high imidazole concentrations (400mM), in a short period of time (5hr), and even in the presence of protease inhibitors (cOmplete, Mini, EDTA-free protease inhibitor cocktail tablets (Roche)). Normally, having cleaved the MAT-tag, subsequent purification is required to eliminate the thrombin protease, the uncleaved Cav3 and the cleaved MAT-tags. However, given that the Cav3 yield was already very low, a further stage of purification was very undesirable as this would have reduced the Cav3 yield to below levels usable in the subsequent biophysics techniques. For that reason, despite having optimised the cleavage protocol, it was decided to keep the C-terminus MAT-tag attached, especially since there were distinct advantages to maintaining it, such as allowing electron microscopy gold-labelling (as described in Chapter 5).

3.3.6. Summary

A variety of expression, solubilisation and purification techniques have been employed in order to purify full-length recombinant Cav3. Ultimately, a combination of HisTrap HP purification and sucrose density fractionation were sufficient to purify Cav3 to homogeneity, as judged by SDS-PAGE and MALLS (see Chapter 5), though it is worth noting that these methods would not distinguish different types and levels of post-translational modifications that may be present such as palmitoylation.

Section			Variables	Outcome
Expression Optimisation			Incubation time, MOI	Optimisation: 72hr, 5MOI
Solubilisation			Buffer choice, Detergent choice	Optimisation: Tris, DDM
Purification (1st Stage)	IMAC	Ion Choice optimisation	Metal ion choice	Optimisation: Nickel ion
		NiNTA	Incubation time, Imidazole concentration	Success, but too small scale. Less control over elution conditions
		FPLC and HisTrapHP	Incubation time, Imidazole concentration, Gradient [linear/staggered]	Success. Partial purification, many impurities removed
Purification (2nd Stage)	IEX		NaCl concentration, pH, protein charge, Temperature, elution gradient	Insufficient purification
	Red agarose		Nucleotide binding capacity	Insufficient purification
	Size Exclusion	Gel filtration	Column choice	Inappropriate column available
		Sucrose Gradient Fractionation	Sucrose concentration, Gradient, Gradient volume, centrifugation speed	Success: Cav3 purified to homogeneity

Table 13: Summary of the purification methods explored

3.4. Conclusion

Here we have successfully purified to homogeneity full-length Cav3 with a C-terminus MAT-tag. The successful protocol employed a Tris-based solubilisation buffer and included the non-ionic detergent n-Dodecyl-ß-maltoside. IMAC utilising the affinity of the MAT-tag for charged nickel was employed as the first stage of purification, and the FPLC purification system was used to enable bulk purification. This eliminated many of the impurities, but many remained. Size exclusion, in the form of sucrose gradient fractionation was used as a secondary stage of purification, and this resulted in the remaining impurities being successfully removed. The removal of the MAT-tag was chosen against as the yield of Cav3 was already very low, and any further purification would have reduced the yield to levels that would not be suitable for subsequent biophysical analysis. In conclusion this report describes the first purification of full-length human Cav3.

Using IEX as a purification method did not work. There are several reasons that this approach may not have been successful: 1) lack of knowledge of the pI of the oligomeric Cav3, 2) the presence of contaminating proteins with very similar charge. Options do exist to get an accurate prediction of pI such as using isoelectric refocusing gels or using NMR to measure the individual residues pKa. However, with there being so many other methods of purification still available these options were not explored. Should the pI of Cav3 be experimentally determined at some point in the future, using IEX as a method may become a viable option.

Although *size* exclusion chromatography (gel filtration) was in part successful in terms of separating the translocase from Cav3, the column employed did not lead to the isolation of pure Cav3. This could be due to an inappropriate column choice, where the column we employed was suitable for the separation of proteins up to 8MDa. More suitable columns that could have been used include the Sephacryl S-200 or S-300 (GE Healthcare), which are more suited for separation of proteins in the ranges of 5kDa-250kDa and 20kDa-1.5MDa, respectively. However, sucrose gradient fractionation proved to be highly successful. This is a method that separates proteins based upon *density*. Size and density are not the same, for example, a large, heavy protein could fold into a compact conformation, whereas a small, light protein could adopt a loosely folded and extendable tertiary structure. Potentially, these two proteins would then be separated together *via* gel filtration, because this method separates based upon *size* i.e. the hydrodynamic volume of the protein (the space a particular protein takes up when it is in solution). In contrast, these proteins would be separated very differently *via* SGF which is based upon *density,* and not

size i.e. despite being tightly packed, the dense protein, although 'small' in volume, would migrate further due to its increased density.

The decision to leave the MAT-tag attached was a considered one. Concerns over whether its presence would interfere with structure or function were considered. However, cleavage was not an option, as the yield achieved after the lengthy purification was already very low i.e. a total of 0.02-0.03mg of Cav3 was obtained from $2.5x10^9$ Sf9 cells. Any further purification, which would have been required to eliminate the thrombin protease, the uncleaved recombinant protein and the cleaved MAT-tags, would have reduced the final yield to levels that would not be feasible. Since there is not an easy way to assess whether the Cav3 is functional there was no way to determine whether the MAT-tag would impact upon the protein structure or function. However, it should be noted that it did not prevent caveolae-like vesicles from forming in the Sf9 cells (discussed in more detail in Chapter 4), suggesting that the purified Cav3 retained function. Additional support for the decision comes from a study in which it was observed that even without the cleavage of a C-term Myc-tag and His-tag, Cav1 was still inserted into lipid membranes, and was also co-fractionated with endogenous Cav1 (Li et al., 1996c). Thus, although different tags, the two tags (as opposed to the one used here), did not seem to interfere with Cav1 function, localisation to caveolae-like vesicles or oligomerisation, thus providing evidence that the presence of a C-terminus tag does not necessarily affect the function of the protein. Finally, although anecdotal, unpublished, and for a different protein, a colleague who completed a functional assay on the protein they were studying, observed the same results both with and without cleavage of the MAT-tag (Gonzalez, P. L. Manchester University. Personal communication).

Chapter 4: Cav3 interaction with RyR, and the formation of caveolae-like vesicles

4.1. Introduction

4.1.1. Interaction with the membrane

Cav3 is already known to interact with the cell membrane, where it forms goblet-like invaginations in the cell membrane, termed caveolae (Murata et al., 1995; Rothberg et al., 1992). It is the presence of caveolin that distinguishes them from the lipid rafts and the typical plasma membrane (Glenney, 1992; Rothberg et al., 1992). The morphology of caveolae depends upon several factors, such as location within the cell and its designated function. Traditional caveolae are 50-100nm membrane invaginations, although, many different sized caveolae have been observed, ranging from 13-2000nm (Edidin, 2001; Kirkham et al., 2008; Pralle et al., 2000; Sheets et al., 1997). The wide range prediction is in part down to the technique used to determine their size. However, several other less well characterised formations exist which may have contributed to the wide ranging size predictions, for example, plasmalemmal vesicles, which reside just beneath the cell membrane on the cytosolic side, and fully internalised variants not associated with the membrane, amongst several other distinct forms (Cohen et al., 2004) (as shown in Figure 2 of the thesis introduction). Despite these explanations for the possible size range of caveolae observed, it is hard to see how a caveolae of the rather diminutive 13nm width could contain many proteins, or even more than one caveolin oligomer, given that a Cav3 oligomer would likely be larger than this. Interestingly, certain forms of caveolae form in specific cell types; for example, rosette caveolae are common in adipocytes, whereas many different states exists simultaneously in endothelial cells (Razani et al., 2002b). In addition, certain cell lines are devoid of all caveolae; for example lymphocytes (Fra et al., 1995). Furthermore, there would appear to be many different sites within the cell at which caveolae are present, suggesting that the form and location of caveolae has functional significance.

As part of a functional test to examine whether recombinant Cav1 possessed native function, Li and Co-workers investigated whether recombinant Cav1 formed caveolae. They found that ectopic over-expression of canine Cav1 (both α and β isoforms) in a heterologous cell line (Sf21) was sufficient to drive the formation of caveolae-like vesicles of 50-120nm in size (Li et al., 1996b); see Figure 71 below. This was an interesting observation given that Sf21 insect cell membranes are generally distinct to mammalian cells, in that they typically have very low cholesterol (essential to caveolae formation

(Chang et al., 1992; Murata et al., 1995; Rothberg et al., 1992; Simionescu, 1983)) content (Marheineke et al., 1998), and a different phospholipid profile (Gerbal et al., 2000). Moreover, there is growing evidence that the protein, cavin, is required for the formation, organisation and function of caveolae (Hill et al., 2008; Liu et al., 2008; Liu and Pilch, 2008); a protein that has not had a homolog yet found in insects.

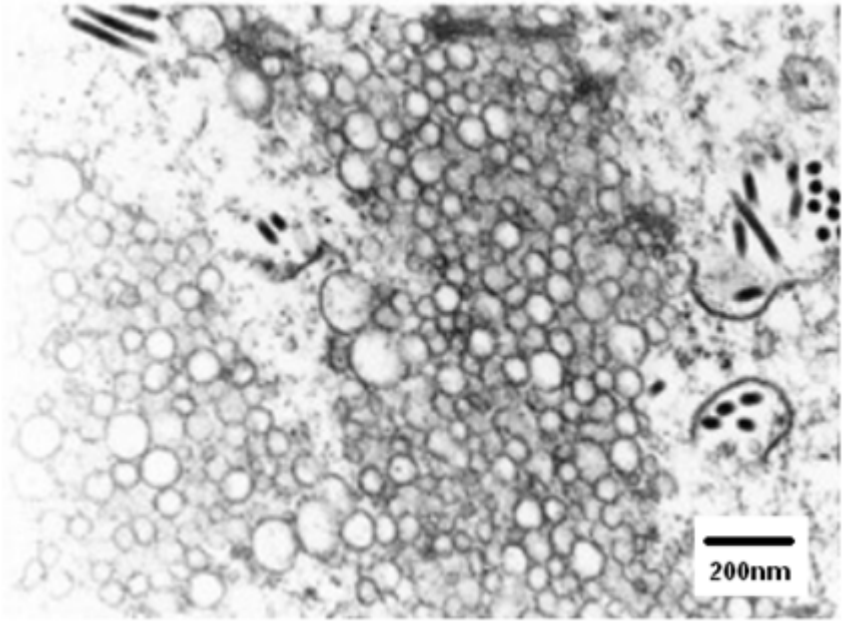

Figure 71: Example of the caveolae-like vesicles observed in the Li et al. study.
Vesicle size ranges from 50-120nm in width. The black bar-like shapes are the baculovirus. Taken from Li et al., 1996a.

Interestingly, Li and co-workers showed that over-expression of canine Cav1 induced the formation of caveolae-like vesicles in the Sf21 cell line, but not in the COS-7, 293-T, MDCK and FRT cell lines (Scherer et al., 1996; Scherer et al., 1995; Song et al., 1996b; Tang et al., 1996).

4.1.2. Interaction with other proteins

Caveolae have been shown to be involved in multiple cellular functions, including, vesicular transport, cholesterol homeostasis and signalling transduction (described in detail in the thesis Introduction). Ultimately, it is now generally accepted that caveolae provide a compartmentalised signalling environment in which signalling processes and key members of pathways are harboured, thus allowing the rapid modulation of signalling events in response to a range of stimuli intent on regulating the cell (Gonzalez et al., 2004; Razani et al., 2002b).

The list of caveolin binding partners encompass a wide range of functionally varied proteins, including membrane proteins, non-receptor kinases, enzymes, structural proteins, nuclear proteins, GPCRs and G-proteins (Balijepalli and Kamp, 2008). Interestingly, many are ion channels and/or are involved in ion regulation and EC-coupling e.g. HCN4 (Ye et al., 2008), PMCA (Darby et al., 2000; Fujimoto, 1993), Na^+/K^+-ATPase (Liu et al., 2003), $Na_v1.5$ (Vatta et al., 2006; Yarbrough et al., 2002), NCX (Bossuyt et al., 2002), β-adrenergic receptors (Balijepalli et al., 2006; Xiang et al., 2002), Muscarinic receptor M2 (Feron et al., 1999), adenosine A1 receptor (Lasley et al., 2000), Calsequestrin (Darby et al., 2000), $Ca_v1.2$ (Balijepalli et al., 2006; Daniel et al., 2001; Darby et al., 2000), $Ca_v3.2$ (Markandeya et al., 2011), NOS (Feron et al., 1996; Garcia-Cardena et al., 1996a; Garcia-Cardena et al., 1997), $K_v1.5$ (Martens et al., 2001), K_{ATP} (Davies et al., 2010; Garg et al., 2009b; Jiao et al., 2008), $K_v11.1$ (Balijepalli et al., 2007) and heterotrimeric G-proteins (Tang et al., 1996). Interestingly, many of these proteins are observed as part of specific macromolecular signalling complexes (e.g. Cav3, $Ca_v1.2$, β-adrenergic receptor, G-protein α_s, adenylyl cyclase, PKA and protein phosphatase 2a are co-localised (Balijepalli et al., 2006)). Interaction studies range from showing an actual *direct* interaction with caveolin (e.g. (Balijepalli et al., 2006)), to *morphological* (e.g. immunogold electron microscopy of caveolae in which a protein is detected e.g. (Fujimoto et al., 1992)) or *biochemical* (e.g. Pull-Down assays; e.g. (Cavalli et al., 2007)) results; the latter two forming the majority of observed interactions. Many of the above studies show a role for caveolins in directly altering ion channel activity and kinetics, as well as in the trafficking and surface expression at the membrane.

It should also be noted that caveolae should not be viewed as a static entity in which signalling molecules are indefinitely confined as it is thought that proteins can both exit or enter the caveolae depending upon their stimulation state. For example, the β_2-adrenergic receptor has been shown in cases to exit the caveolae upon stimulation (Rybin et al., 2000), whereas the B2 Bradykinin receptors are believed to enter the caveolae upon stimulation in a range of cell types (deWeerd and LeebLundberg, 1997; Haasemann et al., 1998; Sabourin et al., 2002). In contrast, some molecules appear to be permanent residents in caveolae such as the β_1-adrenergic receptor; though it is also localised in non-caveolar regions of the plasma membrane (Rybin et al., 2000). Indeed, the role of Cav3/caveolae in many of these interactions is increasingly unclear, and confused by a variety of unavoidable variables, such as cell type, the species used, and the stage of cell maturation. Regardless, many of the examples highlight the significance of caveolae localisation to signal regulation, calcium regulation and cardiovascular physiology regulation, and give an

insight into how disruption of these caveolae, and hence signalling complexes, can result in an altered channel function.

To list in detail all the putative pathways and proteins thought to associate with caveolae would not be possible here. Instead, this introduction will focus on a protein key to EC-coupling, and involved in the regulation of calcium ions, namely the Ryanodine Receptor, which has been shown to both co-localise and co-immunoprecipitate with Cav3 (Head et al., 2005; Li et al., 2006; Scriven et al., 2005; Vassilopoulos et al., 2010), and is of interest to this lab; however, no detailed information is known about the structural and regulatory basis of the interaction.

4.1.3. Putative Cav3 interacting proteins: Ryanodine receptor

Given the evidence of Cav3 presence at the sarcolemmal membrane (Rothberg et al., 1992), mature T-tubules (Head et al., 2005) and possibly even in the sarcoplasmic reticulum (Li et al., 2006), paired with the fact that each of these regions is involved in EC coupling, and that Cav3 has been shown to be associated with a range of EC-coupling related proteins (described above), it is a logical question to ask what role Cav3 is playing in these regions in terms of EC-coupling. Is it simply structural, in that it helps form these key cellular structures or, given its known role in the functional regulation of certain proteins, does it act functionally at these sites?

Arguably one of the most important proteins in EC coupling is the Ryanodine Receptor (RyR). The receptors are calcium release channels responsible for creating a rapid transient increase in cytosolic calcium, and are found in the membrane of the sarcoplasmic reticulum (SR; intra-cellular calcium stores) (Otsu et al., 1990), which are key regions involved in EC coupling. Composed of four monomeric units, each ~550kDa in size, they form a large homo-tetramer of ~2MDa (Lai et al., 1989) making them the largest known ion channel. Its protein structure determined from a combination of electron microscopy and single particle analysis (described in more detail below) shows that 80% of the protein is in the cytosol, whereas the other 20%, which contains the C-terminal region, is found within the SR membrane and SR luminal region. The channel activity of RyR is modulated by a variety of factors including ion concentrations (e.g. Ca^{2+} and Mg^{2+}), pH, phosphorylation, as well as *via* interactions with a range of different proteins and molecules found both in the cytosol (e.g. calmodulin, CaMKII, PKA and PKG) and the luminal region of the SR (calsequestrin, triadin and junctin).

Three RyR isoforms exist in humans; two of which are found predominantly within striated muscle, namely RyR1, which is primarily found in skeletal muscle (Zorzato et al.,

1990), and RyR2, which is primarily found in cardiac muscle (Otsu et al., 1990); although both have been shown to be expressed in a range of other tissue types. The third isoform, RyR3, is predominantly expressed in the brain (Hakamata et al., 1992); however, again, it is also found in many other tissue types. The proteins have different roles in certain cell types, for example, within cardiac and skeletal muscle cells the proteins play a major role in EC-coupling, whereas in other cell types, such as those of the nervous system or osteoclasts, they play a role in signal transduction (Chavis et al., 1996; Zaidi et al., 1992).

Within muscle cells, RyR1 and RyR2 have the same function as a SR-bound calcium release channel involved in EC-coupling. However, the mechanics by which they function differs between cell types. For example, skeletal muscle SR calcium release is caused as a result of the mechanical coupling of the calcium channel ($Ca_v1.1$) with the RyR1 (Rios and Brum, 1987), whereas in cardiac muscle (in which the calcium channel isoform is $Ca_v1.2$) such a physical tethering is not observed and the SR calcium release is caused by calcium-induced calcium-release (CICR) (Endo, 1977). Interestingly, the region of RyR involved in the LTCC interaction is believed to be one of the most divergent regions between the RyRs (a region termed the D2 region) (Perez et al., 2003), suggesting that although both RyR1 and RyR2 are found in muscle, are involved in EC-coupling and share a good degree of sequence similarity (65% throughout isoforms), they are different. Indeed, such functional distinction may be due to the differences between skeletal and cardiac cell types where although both cell types are striated muscle, involved in EC-coupling, contain large SR stores of calcium, release calcium from SR stores upon activation, and contain T-tubules, they are dissimilar in multiple ways, such as the cell shape, action potential initiation and length, the extent of the SR, the location and association of the SR with regards to the T-tubules, and the extent of the T-tubule system. Further distinctions between the RyR isoforms can be observed in their structures. Although they share the same overall structure akin to the four leaves of a ‘clover-leaf’, small differences do exist and it is these regions that may play a role in isoform specific function.

Knowledge of such variable areas in the structure of RyR isoforms is thanks to the success by multiple labs in the reconstruction of each of the RyR isoforms in a variety of activation states. The predominant method employed for determining the RyRs structure has been a combination of cryo-EM and single particle analysis with full-length oligomeric RyR1 (Ludtke et al., 2005; Orlova et al., 1996; Radermacher et al., 1992; Samsó et al., 2009; Samsó et al., 2005; Serysheva et al., 2005; Serysheva et al., 2008; Serysheva et al., 1995; Serysheva et al., 1999), RyR2 (Liu et al., 2005; Liu et al., 2002; Liu et al., 2004;

Sharma et al., 1998) and RyR3 (Liu et al., 2001; Sharma et al., 2000) homotetramers having had their structure determined at a resolution of up to 8Å. Further resolution improvements have been achieved for small sections of the protein, namely the first ~217 residues of the N-terminus using x-ray crystallography, which has achieved resolutions of up to 2.5Å (Amador et al., 2009; Lobo and Van Petegem, 2009). The overall structure of the homotetramer is often described as like a 'clover-leaf' on account of the approximated four-fold top-down symmetry. The transmembrane region, which contains the 'pore' through which the calcium is released, is believed to contain approximately 5-6 membrane spanning α-helices per monomeric subunit of RyR (total of 20 or 24 in the complete homotetramer) and has been shown to take on different conformations depending upon the open/closed state of the channel (Ludtke et al., 2005; Samsó et al., 2009; Samsó et al., 2005; Serysheva et al., 2008), with a shift in diameter of up to 4Å being observed between the ion gate structures of open and closed RyR1 (Samsó et al., 2009). The C-termini of RyR are thought to be within the transmembrane domain region (Bhat et al., 1997), though they are not specifically in the membrane, but are thought to be within the cytoplasm (Takeshima et al., 1989; Tunwell et al., 1996). All models show the same approximate folding conformation, although minor differences are observed in the β-strand connecting loops between the RyR1 and RyR2 isoforms.

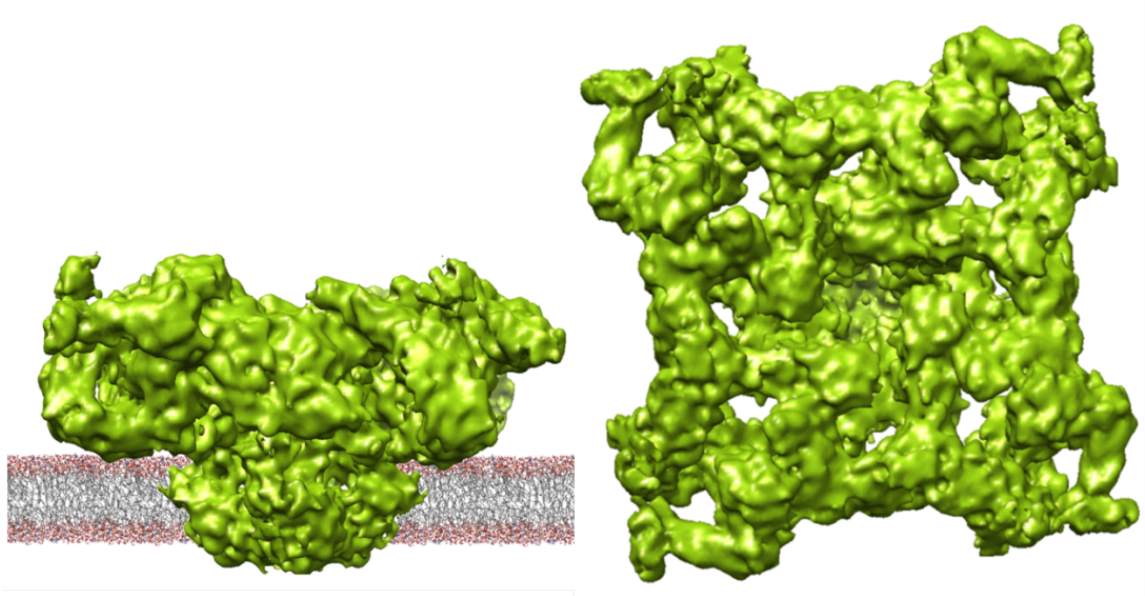

Figure 72: RyR1 structure reconstructed using cryo-EM and single particle analysis
The 3D cryo-EM map for RyR1 (accession no. 1275) (Serysheva et al., 2008) was downloaded from the EMBL European Bioinformatics Institute database (http://www.ebi.ac.uk/Databases/). **A**: proposed membrane topology of the protein. **B:** the clover-leaf fourfold symmetry. The lipid co-ordinates were downloaded from the website of Dr Scott Feller, Wabash College (http://www.lipid.wabash.edu/).

As mentioned above, the RyRs are regulated by a host of different factors, including ions, phosphorylation and a range of proteins. Perhaps the most characterised interaction in skeletal muscle is with the L-type voltage gated channel, $Ca_v1.1$, as mentioned above, though many other examples exist. For example, Ca^{2+} itself influences the RyR receptor activity *via* interactions with both its cytosolic and transmembrane regions, both directly (Meissner et al., 1986; Meissner et al., 1997) and indirectly e.g. *via* calmodulin (Maximciuc et al., 2006; Moore et al., 1999; Rodney et al., 2000; Samsó and Wagenknecht, 2002). It is thought that low levels of Ca^{2+} activate the receptor by binding to specific high-affinity sites, whereas when Ca^{2+} levels are high, the receptor is closed due to multiple less specific low affinity sites being bound by Ca^{2+} (Meissner et al., 1986; Meissner et al., 1997; Samsó and Wagenknecht, 2002). Other small molecules involved in regulating RyR activity include ATP and Mg^{2+}, which are thought to activate and inhibit RyR respectively (Laver et al., 1997; Meissner, 1984).

Another key factor that influences RyR channel activity is phosphorylation. Indeed, PKA (Xiao et al., 2006) and CaMKII (Wehrens et al., 2004) have each been shown to phosphorylate RyR. RyR has been shown to be redox sensitive, and the modification of a number of sites within RyR has been shown to have functional effects (Boraso and Williams, 1994; Stoyanovsky et al., 1997). For example, the inhibition of RyR1 channel activity by CaM is prevented by the S-nitrosylation of specific cysteine residues (Porter Moore et al., 1999; Sun et al., 2001). Indeed, this makes RyR a potential target for the deleterious effects caused by cardiac ischemia-reperfusion injury, which is often associated with elevated levels of reactive oxygen and nitrogen species.

RyR interaction with caveolae and Cav3

Interestingly, as for Cav3, RyR has been associated with a range of cardiac arrhythmic conditions and myopathic conditions. The cardiac isoform (RyR2) being associated with the arrhythmic conditions: Arrhythmogenic right ventricular dysplasia (Tiso et al., 2001) and ventricular tachycardia (Priori et al., 2001). The skeletal muscle isoform (RyR1) being associated with a range of myopathic conditions, including: central core disease (Zhang et al., 1993), minicore myopathy (Monnier et al., 2003), neuromuscular disease (Sato et al., 2008) and malignant hyperthermia (Quane et al., 1993). Both skeletal and cardiac muscle show the co-localisation of RyR with Cav3 (Head et al., 2005; Li et al., 2006; Scriven et al., 2005; Vassilopoulos et al., 2010). This relationship between RyR and Cav3 will be discussed briefly here.

RyR2: Cardiac muscle cells

It was originally thought that Cav3 only associated with T-tubules during development (Parton et al., 1997). However, a study by Head and co-workers (Head et al., 2005) used a series of different techniques to co-localise Cav3 to both the sarcolemmal membrane (i.e. the cell membrane in muscle) and the T-tubules in *adult* rat *cardiac* myocytes. The finding that Cav3 was present in both the T-tubules of adult cells, as well as the T-tubules in cardiac cells was novel, as was their observation that Cav3 was co-localised with RyR2, amongst other proteins involved in EC-coupling. Further support of a Cav3/RyR2 localisation at the T-tubules of cardiac muscle cells, comes from a study by Scriven and co-workers (Scriven et al., 2005). They showed that although Cav3 predominantly forms caveolae at the sarcolemmal membrane, there were caveolae within the T-tubules, where they co-localised with a subpopulation of RyR2. Interestingly, these co-localised RyR2 were not part of the usual dyad, but instead part of a non-dyadic subpopulation of RyRs that were predominantly found within, but near the mouth of T-tubules, suggesting that a distinct population of T-tubule-based caveolae exist which interact with RyR2. Interestingly, the presence of Cav3 at the neck of the T-tubules in association with key EC-coupling proteins has been observed by other labs. Murphy and co-workers, not only showed that Cav3 was at its greatest expression at these 'hot spots', but that it also co-immunoprecipitated with $Na_v1.4$ (Murphy et al., 2009), another channel protein involved in the cardiac action potential.

RyR1: Skeletal muscle cells

Support for a RyR/Cav3 interaction in skeletal muscle comes from a study by Vassilopoulos and co-workers (Vassilopoulos et al., 2010). They observed a Cav3/RyR1 interaction, *via* co-immunoprecipitation, in skeletal muscle from 3-4 day old mice. Interestingly, their work also suggested that there was an alternative subpopulation of caveolae that interacted with RyR at the plasma membrane; one in which Cav3/triadin and RyR1 associate at a SR/caveolae border. They go on to suggest that these distinct populations maybe involved in store operated calcium entry (SOCE). SOCE is a mechanism that replenishes depleted intracellular calcium stores by bringing extracellular calcium into the cell. Further support for this SOCE-involved sub-population of RyR/triadin/Cav3 complexes at the SR/plasma membrane border comes from the observation that over-expression of triadin resulted in reduced calcium entry in myotubes, suggesting the complex had been disrupted. Indeed, as mentioned throughout this thesis, caveolae have been shown to contain a range of calcium regulating proteins. In addition, the re-localisation of Cav3 to intracellular sites in association with triadin upon over-

expression of triadin, suggests that the disruption in this SOCE complex may indicate the mechanism by which the reduced calcium regulation occurred. In summary, these data add support for the existence of a distinct subpopulation of Cav3/RyR, as proposed by Scriven et al, (Scriven et al., 2005).

Region and location of RyR/Cav3 interaction

Although the Cav3/RyR relationship is still not fully understood, even less is known about the specifics of the protein-protein interaction. Another interesting observation from the Vassilopoulos and co-workers study (Vassilopoulos et al., 2010) was that they also found that Cav3 interacted with the *transmembrane* region of RyR. Given that this region would ordinarily be *within* the SR membrane it would suggest, that for Cav3 to have access to this region, Cav3 *is part* of the SR membrane; although this observation was not made by the authors. The only other evidence of Cav3 being present in the SR comes from a study by Li and co-workers (Li et al., 2006), who found that rabbit Cav3 was associated with detergent-resistant membrane (DRM) regions of skeletal SR, where it was associated with SERCA, indicating that the DRM regions, which were also rich in cholesterol and GM1, were likely, but not necessarily, from the longitudinal region of the SR.

It is becoming clear that there is no 'one-state' for caveolae with regards to its interaction with RyR. Indeed, it would appear that several sub-populations of RyR exist in which it associates with Cav3 (Head et al., 2005; Scriven et al., 2005; Vassilopoulos et al., 2010). The specifics of these specialised regions is yet to be elucidated, though the caveolae presence of so many proteins involved in calcium regulation e.g. $Ca_V1.2$ (Balijepalli et al., 2006), β-adrenergic receptor (Balijepalli et al., 2006; Rybin et al., 2000), or capable of regulating RyR e.g. PKA (Razani et al., 1999), CSQ (Darby et al., 2000) would point towards a potential role of caveolae in calcium handling/regulation, EC-coupling and RyR regulation.

It is also interesting that given that Cav3 appears to play a role in cardiac ischemia-reperfusion injury (CIRI) and ischemic preconditioning (Horikawa et al., 2008; Tsutsumi et al., 2008), and that RyR appears to be a potential target for the deleterious effects caused by CIRI (in that they have numerous redox sensitive residues), that maybe there is some functional significance to the co-localisation of RyR with Cav3. Indeed, multiple other proteins that are involved in cardiac ischemia-reperfusion injury (e.g. ERK1/2 (Engelman et al., 1998a) and PI(3)K) (Zundel et al., 2000) are also located to caveolae or interact with caveolins. Indeed, as discussed in the thesis introduction (section The role of caveolin in cardiac ischemia/reperfusion injury), upon CIRI, Cav3 distribution is altered and Cav1 is

down regulated (Ballard-Croft et al., 2006), and thus NOS inhibition is reduced, resulting in elevated levels of NO (Jasmin et al., 2012), which as a free radical may be involved in the irreversible modification of RyR leading to a variety of knock on effects with regards to EC-coupling. Indeed NO, derived from a range of forms (NO, NONOates, S-nitrosothiols) has been shown to alter the channel activity of both RyR1 and RyR2 by S-nitrosylation of thiol groups within the receptor, as assessed by the tritiated binding assay (a technique discussed later in this chapter) (Stoyanovsky et al., 1997).

4.1.4. Techniques available for detecting protein-protein interactions

Virtually every cellular process is governed by protein-protein interactions, thus understanding which proteins interact with which others is a key step towards improving our understanding of the living system. Indeed, knowledge of key-interactions can be exploited towards developing new therapeutic methods of dealing with disease. Given that many of the interaction claims for Cav3 to-date are *via* co-localisation alone, it is, therefore, important to dissect the specifics of these complex relationships in order to understand specifically which proteins are interacting and how. A range of techniques exist that can help give more functionally relevant quantitative information regarding interactions; the ones that are relevant to this project will be discussed here.

Pull-down assay

The pull-down assay (PDA) is a type of immunoprecipitation that can be used to help identify protein-protein interactions. The technique involves the binding of one of the potentially interacting proteins (the bait) to an immobilised surface, then incubating it with the other potentially interacting protein (the prey). Interacting partners can then be co-eluted, which can indicate a potential interaction See Figure 73.

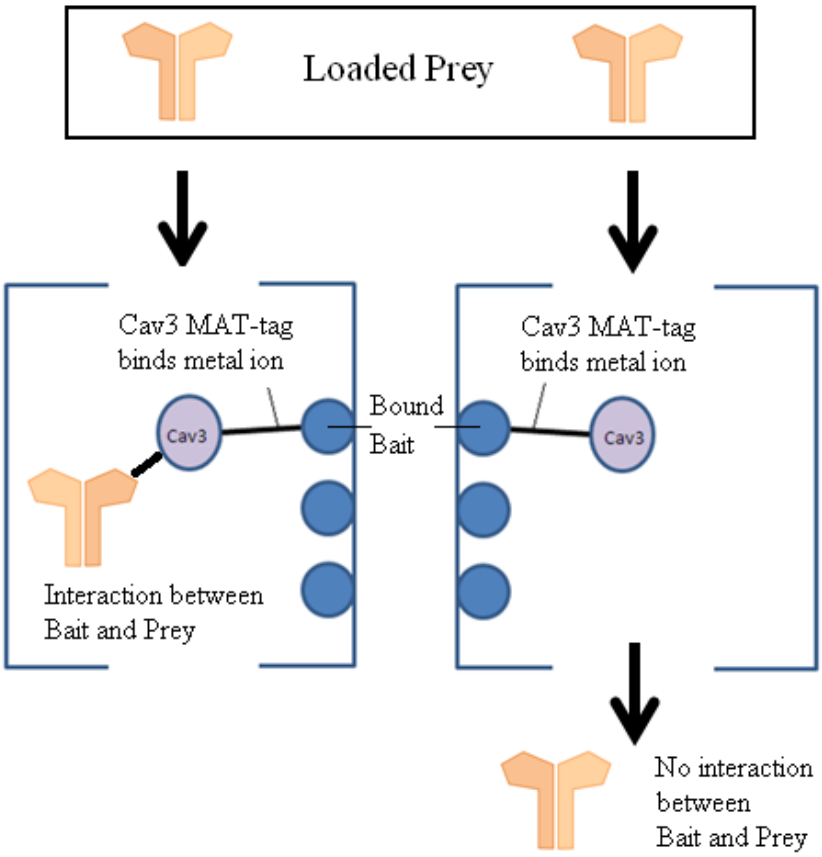

Figure 73: Outline of pull-down assay.

In brief, the bait protein (e.g. Cav3) is immobilised *via* its MAT-tag, and putative interaction partners (prey) are added. Bound proteins will be retained, whereas unbound will not be. These samples can be easily checked for the presence of proteins of interest by western blotting.

Although the PDA technique is a useful technique for identifying protein interactions, complete confidence in any predicted interaction cannot be made. For example, the assay does not readily detect transient interactions. In addition, there is the possibility that the physical interaction of the bait with the immobilised surface can, a) occlude the potential interaction sites or b) cause a conformational change, such that interaction is not possible. One further inconvenience of the PDA technique is that it does not give any information on binding constants. Thus, any findings derived *via* a PDA, should also be followed up by more thorough interaction investigation techniques.

Tritiated ryanodine binding

Ryanodine is a plant alkaloid that has a high affinity to the ryanodine receptor (Chu et al., 1990). At nano-molar concentrations ryanodine binds the receptor resulting in a semi-open state of the channel. However, micro-molar concentrations of ryanodine

completely close the channel (Meissner et al., 1986). If, however, the channel is already closed, the ryanodine cannot bind the receptor (see Figure 74).

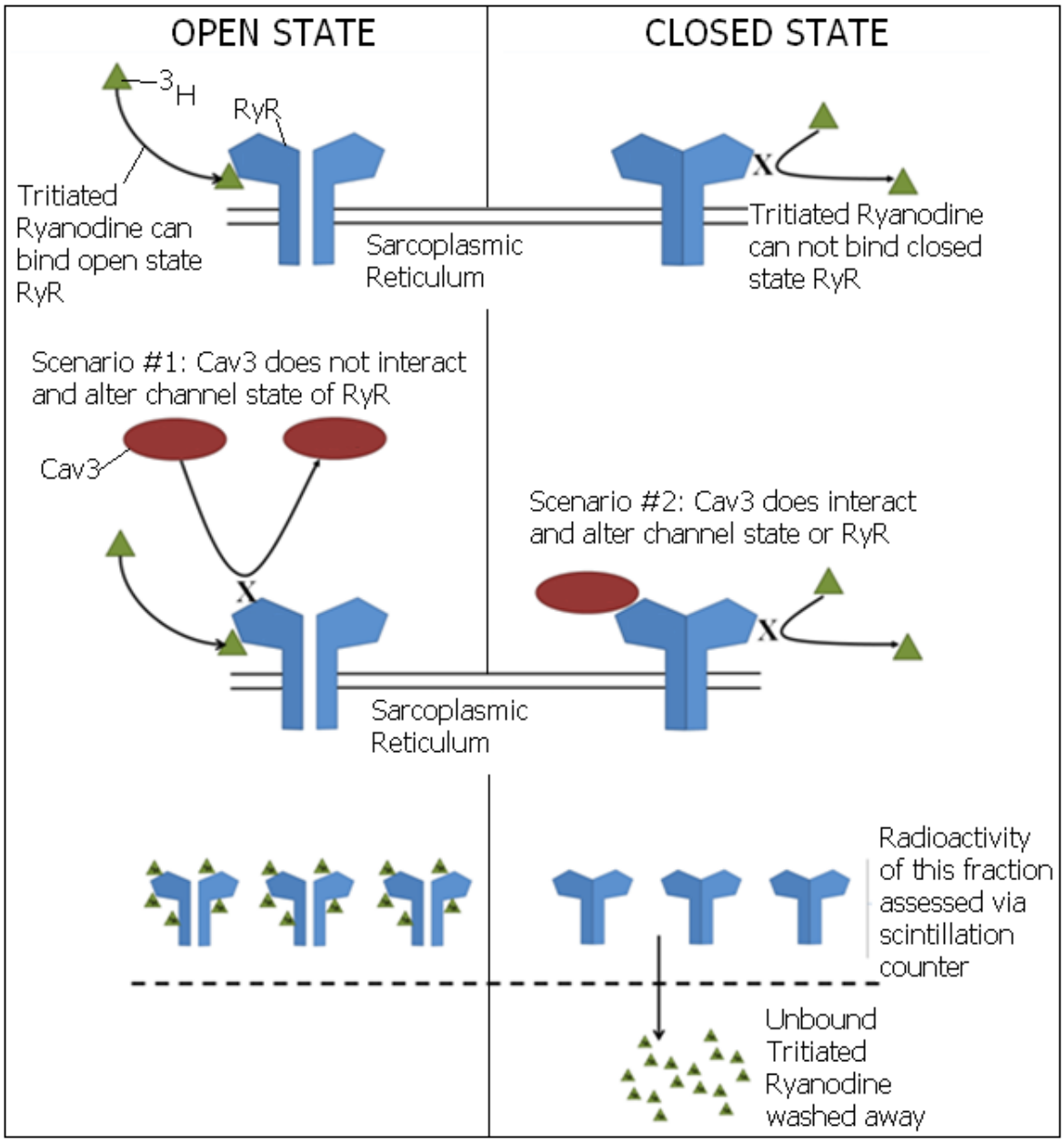

Figure 74: Outline of the tritiated ryanodine binding assay.

The tritiated ryanodine binding assay allows for the detection of the open state of the ryanodine receptor. Binding of tritiated ryanodine to the ryanodine receptor can only occur if the receptor is in an open state, thus if the receptor is in a closed state due to an interaction with a modulating protein, then it will not be able to bind. Since the ryanodine is tritiated, radioactivity levels can be readily detected, which can help give information on the open or closed state of the receptor.

This relationship between ryanodine and RyR can be exploited in order to study putative interactions between the receptor and potentially interacting partners. By

incubating the receptor with the potentially interacting protein and then adding tritiated ryanodine it is possible to monitor the amount of radioactive ryanodine bound and hence the open/closed state of the channel pore. For example, if Cav3 was incubated with RyR1 and the proteins interacted in such a way that the RyR calcium release channel fully closed, the radioactive ryanodine would not be able to be bound and all unbound ryanodine could be easily removed. If, however, the two proteins did not interact, then RyR would remain in the open state, and the radioactive ryanodine would be able to bind. Further, the stoichiometric relationship between interacting partners can also be roughly explored using this technique by altering the molar ratio of the two proteins. It should be noted that this assay would not detect any Cav3-RyR1 interaction in which channel activity was not altered i.e. if Cav3 binds RyR1, but does not affect the open/closed state of the channel.

4.1.5. Aims and objectives

The aims and objectives of this part of this thesis research were to explore the potential role of Cav3 in endogenous caveolae formation and as a modulator of RyR channel activity. Since the expression of Cav1 in Sf21 cells has been shown to induce caveolae formation, we also wanted to investigate whether infection of Sf9 cells with Cav3 would also produce caveolae. Evidence points towards a potential functional RyR-Cav3 interaction and so to investigate this further we purified RyR1 to probe Cav3-RyR1 interactions employing two approaches: Pull down assays and the tritiated ryanodine binding assay.

4.2. Materials and Methods

4.2.1. Sample preparation

Full-length Cav3, the N^{1-54} domain and the SUMO-tagged N^{1-54}domain were purified as described in the Material and Method sections of Chapters 2 and 3.

Material suppliers

Unless otherwise stated, all materials were purchased from Sigma.

4.2.2. Bioinformatics

Hydrophobicity plots and transmembrane helices were calculated using the SPLIT tool (http://split4.pmfst.hr/split/4/ (Juretić et al., 2002). Alignments were complete using ClustalW (http://www.ebi.ac.uk/Tools/msa/clustalw2/) (Larkin et al., 2007). Primary sequences were scanned for caveolin binding motifs [FWY]X[FWY]XXXX[FWY] and [FWY]XXXX[FWY]XX[FWY] (Couet et al., 1997) using ScanProsite (http://prosite.expasy.org/scanprosite/) (de Castro et al., 2006). The RyR1 (AAA60294) and the RyR2 (NP_001026.2) sequence files were acquired from the NCBI database (http://www.ncbi.nlm.nih.gov).

4.2.3. Transmission electron microscopy of thin sections of Cav3 infected Sf9 cells

Infected cells (MOI of 5) were fixed with 2.5% (v/v) glutaraldehyde in 100mM sodium cacodylate buffer (pH 7.2) for 2hr on ice. Samples were rinsed three times in 100mM sodium cacodylate buffer, and post-fixed with 1% (w/v) osmium tetroxide in cacodylate buffer, then washed 3 times in 100mM sodium cacodylate and then $_{dd}H_20$, before being en bloc stained with 1% (v/v) aqueous uranyl acetate for 1hr. Samples were washed in $_{dd}$H20 three times, then dehydrated in graded ethanol (25% (v/v), 50%, 70%, 80%, 90%, 95% - one time; 100% - three times). Samples were washed three times in propylene and embedded in propylene LV Resin for 2hr. Thin sections were cut on a Reichert-Jung Ultracut E, double stained with 2% (w/v) uranyl acetate and 0.3% (w/w) lead citrate, and examined under a FEI Biotwin TEM Microscope at an operating voltage of 100kV. Preparation of samples was completed by Samantha Forbes at the Electron Microscopy Facility, Manchester University.

4.2.4. Sarcoplasmic reticulum and RyR1 purification

Isolation of sarcoplasmic reticulum junctional terminal cisternae (JTC) from sheep skeletal muscles

The following protocol is adapted from (Chu et al., 1988) and (Meng et al., 2009). 200grams of sheep skeletal muscles were homogenised using a blender (Moulinex® Optiblend 2000) in 1L of buffer (10mM HEPES pH7, 300mM sucrose, 0.5mM EDTA). The homogenate was centrifuged for 15min at 11,000xg (Sorvall Evolution RC; SLA-1500 rotor). The pellet was discarded and the supernatant was centrifuged at 110,000xg (Beckman Optima L-90K ultracentrifuge; T70 rotor) for 60min to sediment the mixed membrane population. This was then resuspended in 200ml of buffer (10mM HEPES pH7, 650mM KCl, 300mM sucrose, 0.5mM EDTA), and then stirred at 4°C for 60min before being re-pelleted by centrifugation at 200,000xg (Beckman Optima L-90K ultracentrifuge; T70 rotor) for 60min. This was followed by re-homogenisation in 30ml buffer (10mM HEPES pH7, 650mM KCl, 300mM sucrose, 0.5mM EDTA). The re-homogenate was layered onto a sucrose gradient of 45%, 38%, 32% and 27% (w/v) sucrose steps and centrifuged at 100,000xg (Beckman Optima L-90K ultracentrifuge; SW28 rotor) for 16hrs. The 38-45% interface containing the sarcoplasmic reticulum JTC was collected, diluted twofold with buffer (10mM HEPES pH7, 300mM sucrose, 0.5mM EDTA) and re-centrifuged at 110,000xg (Beckman Optima L-90K ultracentrifuge; T70 rotor) for 60min. The pellets were resuspended in buffer (10mM HEPES pH7, 300mM sucrose), and then snap frozen in liquid nitrogen and stored at -80°C.

Purification of RyR1: Sucrose gradient fractionation of solubilised sarcoplasmic reticulum JTC

The following protocol is adapted from (Serysheva et al., 1999). The sarcoplasmic reticulum JTC (~20mg), ~1.5mg of which had been pre-labelled with [^{3}H] ryanodine, was solubilised at 2.0mg/ml in buffer (50mM MOPS pH 7.4, 185mM NaCl, 100mM EGTA, 2.0mM dithiothreitol (DTT), 2% (w/v) CHAPS/1% (w/v) soybean lecithin (SBL)) for 60min on ice. To remove the insoluble material the mixture was then centrifuged at 100,000xg (Beckman Optima L-90K ultracentrifuge; T70.1 rotor) for 30min at 4°C. The solubilised skeletal SR was layered onto a step-wise sucrose gradient (5-25% (w/v)) on top of 35% (w/v) sucrose cushion. Sucrose gradient solutions were prepared in buffer (50mM MOPS pH7.4, 185mM NaCl, 100mM EGTA, 2.0mM DTT, 0.5% (w/v) CHAPS). Sucrose gradient tubes, one of which was labelled for radioactivity, were centrifuged at 125,000xg (Beckman Optima L-90K ultracentrifuge; SW28 rotor) for 16hrs. This was followed by

fractionation into ~0.5ml portions. 100µl of every other portion was reserved for liquid scintillation counting. Another 100µl was reserved for protein assay and SDS-PAGE. All fractions were then quick frozen in liquid nitrogen and stored at -80°C. All buffers contained the following protease inhibitors: 2mM PMSF, 1µM pepstatin A, 1µM E64, 1mM benzamidine or complete mini EDTA-Free protease inhibitors cocktail tablets (Roche).

Scintillation counting

Approximately 100µl of the protein fraction was added to a scintillation vial (Pony vials, Packard Instruments) containing 4ml scintillation fluid (Ecoscint A, National Diagnostics). The vials were sealed and shaken and radioactivity measured using liquid scintillation analyser (1900TR, Packard instruments). The background radiation was subtracted from each measurement.

4.2.5. Negative stain transmission electron microscopy of RyR1

In brief, 20µl aliquots of RyR at 0.01mg/ml were negatively stained with 2% (w/v) uranyl acetate following standard protocols (Walsh et al., 2009a). Images of RyR1 were recorded on a Polara 300-kV Field Emission Gun transmission electron microscope (by Dr Ashraf Kitmitto, Manchester University) and data were collected with the microscope operated at 200kV, under cryo-negative (198K) and low dose conditions i.e.10-20$e^-/Å^2$. Micrographs of RyR1 were recorded using a 4Kx4K CCD Gatan camera with a calibrated magnification corresponding to 5.1Å/pixel at the specimen level.

4.2.6. Biophysical technique: Pull-down assay

50µl Cobalt chelate resin was loaded onto spin columns (Thermo scientific #21277). The resin was washed four times in buffer (for full-length Cav3: 25mM Tris pH7.5, 115mM NaCl, 0.075% (w/v) n-Dodecyl-ß-maltoside. For the 6xHisTag-SUMO or 6xHisTag-SUMO-N^{1-54}: 10mM Tris pH8, 150mM NaCl, 10mM imidazole, 0.03% (v/v) Triton X-100), then centrifuged at 1250xg (eppendorf Minispin plus) for 30secs. 150µg of the bait protein (Cav3, 6xHisTag-SUMO or 6xHisTag-SUMO-N^{1-54}) was loaded onto the spin column and incubated with rotation for 30mins at 4°C. Unbound bait protein was removed by centrifuging at 1250xg (eppendorf Minispin plus) for 1min. The bait-bound cobalt resin was washed five times with 400µl buffer (composition as above) then centrifuged at 1250xg (eppendorf Minispin plus). 150ug of prey protein (RyR1) was loaded onto the spin column and incubated with rotation for 1hour at 4°C. The sample was

centrifuged for 30secs at 1250xg (eppendorf Minispin plus) to remove any unbound prey. The prey-bait-bound cobalt resin was washed five times with 400µl buffer (25mM Tris pH 7.2, 150mM NaCl) then centrifuged at 1250xg (eppendorf Minispin plus). 250µl of elution buffer (25mM Tris pH 7.2, 150mM NaCl, 290mM imidazole) was added to the column then incubated for 5min at 4°C with gentle agitation. This was followed by centrifugation at 1250xg (eppendorf Minispin plus) for 30secs to collect the eluted fraction.

4.2.7. Biophysical technique: Tritium ryanodine binding assay

The channel state of RyR was assessed by measuring [9,21(n)-^{3}H] ryanodine association kinetics using a modified version of the method described by Needleman and co-workers (Needleman and Hamilton, 1997). Skeletal SR membranes (0.03mg/ml final protein concentration) corresponding to 11.4femtomoles of RyR were added to buffer (300mM KCl, 50mM Mops, 100µM $CaCl_2$, 5mM $MgCl_2$, 1mM AMP-PCP, 0.1% (w/v) CHAPS and protease inhibitors (cOmplete, Mini, EDTA-free protease inhibitor cocktail tablets (Roche)), pH7.4). Cav3 was added in molar excess (507:1) and the sample was left for 10mins. 20nM [^{3}H] Ryanodine was then added to the sample, and the sample was incubated for 100min. 100µl aliquots were filtered through a Millipore vacuum filtration apparatus fitted with Whatman GF/F glass fiber filters (pre-soaked in 2% (v/v) polyethyleneimine). Filters were washed 5 times with ice-cold buffer (10mM Mops pH7.4, 300mM KCl, 100µM $CaCl_2$). Filters were added to scintillation tubes containing 4ml scintillation fluid (Ecoscint A, National Diagnostics) and shaken for 60min. Radioactivity was measured by liquid scintillation counting using a 1900TR liquid scintillation analyser. All experiments where done in triplicate. Non-specific binding experiments were also conducted using an excess of cold ryanodine (non-tritiated), and this radioactivity was subtracted from all test cases.

4.3. Results and Discussion

4.3.1. Caveolae formation in Sf9 cells

Previous reports using Sf21 cells for the production of canine Cav1 protein reported that protein over-expression led to the formation of caveolae with a size and density comparable to those observed in mammalian cells (Li et al., 1996b). This was interesting for a number of reasons. Firstly, the presence of caveolae suggested that the recombinant protein had some native function, despite being in a non-native host. Secondly, caveolae formation was achieved despite the fact that the presence of cholesterol, which is essential for caveolae formation, is considerably lower in Sf9/Sf21 insect cells than in mammalian cells (Marheineke et al., 1998). Thirdly, no evidence exists for the expression of Cavin, another protein thought to be essential to caveolae formation (Hill et al., 2008; Liu et al., 2008; Liu and Pilch, 2008), in Sf21 cells.

In order to investigate whether over-expression of human Cav3 in Sf9 cells would similarly result in the formation of caveolae, infected cells were examined by transmission electron microscopy. In brief, after 72hours incubation at 28°C Cav3-infected cells were pelleted and fixed following standard protocols described above (see Materials and Methods section Transmission electron microscopy of thin sections of Cav3 infected Sf9 cells) and thin sections were prepared and examined by TEM.

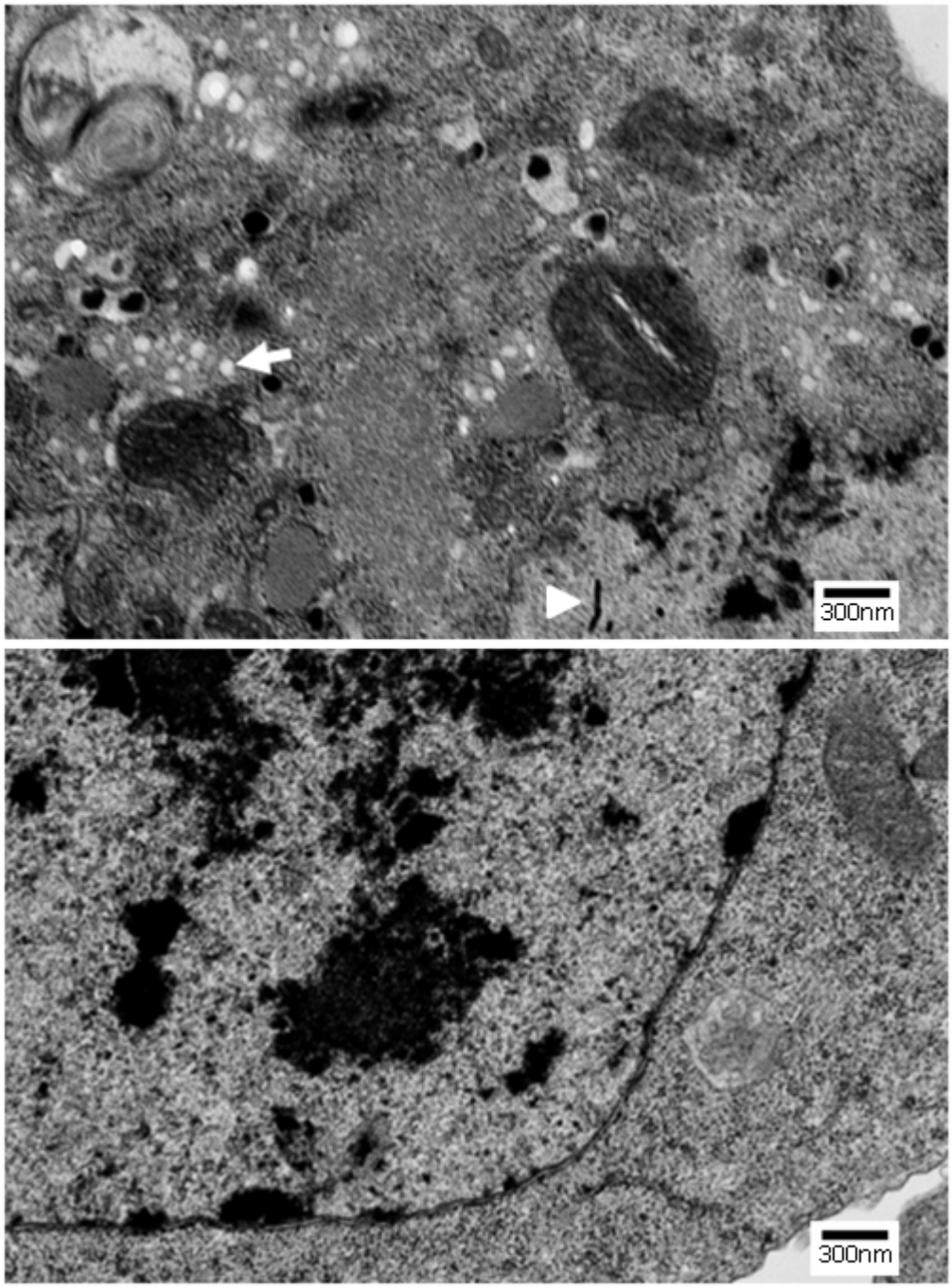

Figure 75: TEM image of caveolae formation in Sf9 cells

Electron micrograph of a thin section of a Sf9 cell infected with Cav3 illustrating formation of caveolae between 60-110nm in width (top), and an uninfected control Sf9 cell (bottom). Sf9 cell samples were fixed with glutaraldehyde, post-fixed with osmium tetroxide, and stained with uranyl acetate and lead citrate. Arrow: example of caveolae-like vesicles. Arrow heads: the baculovirus that carries the Cav3 gene.

As can been seen in Figure 75, caveolae-type vesicles 60-110nm in diameter are clearly apparent which would suggest that the expressed Cav3 protein was functional. It was noted, however, that although the caveolae-like vesicles were clearly apparent Cav3

(Figure 75, arrows), expression did not induce 'hundreds' of these vesicles per cell as described for Cav1 (Li et al., 1996b). Since Sf9 cells are a subclone of Sf21 cells and considered virtually indistinguishable it may be that the prevalence of caveolae is dictated by the caveolin isoform or may reflect the level of Cav3 protein expression. Indeed, it has previously been shown that different isoforms of Cav1 (α and β) are preferentially associated with morphologically distinct caveolae that locate to different positions within the cell (Fujimoto et al., 2000). Further, given the relatively low yields of protein (approximately 30μg of purified Cav3 protein was isolated from $2.5x10^9$ Sf9 cells) the latter maybe a possible explanation, although levels of Cav1 expression were not reported by Li and co-workers (Li et al., 1996b). As for Li and co-workers, the control uninfected Sf9 cells did not show any such caveolae-like vesicles Figure 75 (bottom).

The caveolae are predominantly intracellular and not at the membrane. Although some examples of caveolae were found close to the plasma membrane, the examples shown in Figure 75 appear to have accumulated in the intracellular region of the cell. One possibility for this is that the insect membrane may not be able to integrate the human caveolin based caveolae. Indeed, species differences do exist with regards to the sterol/lipid composition of the membrane, and cholesterol levels can influence the rate at which the Golgi produce caveolae (Pol et al., 2005). However, caveolae formation has been show to occur in a variety of different species in which the sterol/lipid composition differs (Rietveld et al., 1999). Moreover, the accumulation of intracellular caveolae here indicates that the Golgi has successfully produced the caveolae, so Golgi involvement may not be the cause of the intracellular accumulation. Another possibility is that the Sf9-specific mechanisms involved in the transportation of proteins/complexes to the membrane cannot keep up with the rate at which the caveolin oligomers are being produced. Indeed, pools of recently formed caveolin are found located internally near the Golgi apparatus (Luetterforst et al., 1999). It could also be possible that they are simply not being transported to the membrane due to incorrect targeting. For example, the intracellular localisation may be due to the phosphorylated state of the S53 residue, which if phosphorylated maintains the complexes intracellularly (Kirkham et al., 2008) i.e. the native Sf9 kinases may be phosphorylating this residue and preventing its movement to the membrane. Another explanation may be the way in which the section has been cut i.e. this 'slice' may actually be through the plasma membrane and this view is orthogonal to the plane and thus gives an impression of being intracellular but are in fact invaginations of the surface membrane. The exact mechanism behind the formation of caveolae is not understood; for example, one theory is that caveolin oligomers are produced by the Golgi

and that these oligomers accumulate at the plasma membrane where they form caveolae in the membrane (Fra et al., 1995). An alternate theory is that the Golgi complex itself produces the complete caveolae that are then transported to the membrane and inserted (Tagawa et al., 2005). Clearly, more research on this mechanism needs to be undertaken.

Another interesting observation is that the caveolae shown here and also by Li and co-workers are rather small, when you consider the range of caveolae size predictions that have been claimed (26-2000nm). It could be speculated that the lower concentration of cholesterol and the absence of Cavin, or the specific cell type is responsible for these rather small caveolae.

4.3.2. Interaction between Cav3 and RyR1

The observance of caveolae like structure suggests that the Cav3 isolated here is functional. To investigate this further a series of experiments were devised in order to investigate the functional relationship between Cav3 and the Ryanodine receptors.

Bioinformatics

As discussed in the thesis introduction, knowledge of the caveolin scaffolding region has been used to scan for other potentially interacting proteins. From the interacting proteins identified two Caveolin Binding Motifs (CBM) were found (Couet et al., 1997): [F/W/Y]X[F/W/Y]XXXX[F/W/Y] and [F/W/Y]XXXX[F/W/Y]XX[F/W/Y]. It is worth pointing out that the CBM sequence consists of a series of large hydrophobic residues, which is also a feature shared with membrane-anchors, which are one means by which certain proteins *associate* with the membrane. Given that Cav3 is membrane bound, it is possible that the prevalence of this CBM sequence in putative interacting proteins is, in fact, due to a need for membrane location (in this case caveolae), and not necessarily a sign of Cav3 interaction. Despite this concern, these CBM have since been used to discover other potentially interacting proteins (Alioua et al., 2008). We examined the primary sequence of both RyR1 (NCBI, AAA60294) and RyR2 (NCBI, NP_001026) for CBM using ScanProsite (http://prosite.expasy.org/scanprosite/), finding that RyR1 has six CBM, five of which in were in the transmembrane region. RyR2 has nine in total, six of those being at the same site as those found in RyR1 plus 3 additional ones (7 of the 9 were found in the TM). None of the observed CBM mapped to known interaction sites within RyR1 or RyR2 (see Lanner for a review of RyR interaction sites (Lanner et al., 2010)), except for the ones within sites that have been shown to interact with Cav3 (Vassilopoulos et al., 2010), discussed below.

#1	(RyR1)1431-1438: YyYsvrvF (RyR2)1426-1433: YyYsvriF ******:*	Located to Cytosolic Region
#2	(RyR1)4706-4714: FpsnyWdkF (RyR2)4640-4648: FpnnyWdkF **.******	Located to Transmembrane Region
#3	(RyR1)4844-4851: YlYtvvaF (RyR2)4779-4786: YlYtvvaF ********	
#4	(RyR1)4846-4854: YtvvaFnfF (RyR2)4781-4789: YtvvaFnfF **********	
#5	(RyR1)4851-4858: FnFfrkfY (RyR2)4786-4793: FnFfrkfY ********	
#6	(RyR1)5009-5017: YqercWdfF (RyR2)4944-4952: YqercWefF ******:**	

Figure 76: Aligned CBM identified in both RyR1 and RyR2.

Of the nine individual caveolin binding motifs identified, six were common to both RyR1 and RyR2. These motifs were aligned to show the degree of sequence homology. Asterisks indicate identical match. Colons indicate a strongly similar match. Full stops indicate a weakly similar match. Five of the motifs were located to the region of the ryanodine receptor termed the transmembrane region. One was located in the cytosolic region of RyR. Capitalised letters indicate key regions in the motif. Numbers denote the residues. All alignments were completed using ClustalW (http://www.ebi.ac.uk/Tools/msa/clustalw2/).

RyR1 and RyR2 share 65% sequence similarity, and as can be seen in Figure 76, the six shared motifs show considerably sequence homology. Interestingly, the three additional CBM in RyR2, shared very little sequence homology with the corresponding region within RyR1 (see Figure 77). Therefore, these additional RyR2 CBM sites may represent unique binding sites for Cav3 in the cardiac isoform of RyR (RyR2).

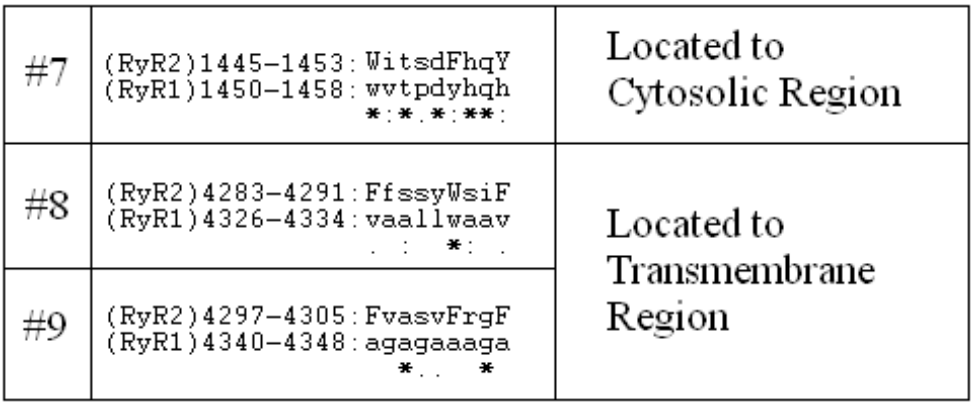

Figure 77: Aligned RyR2 CBM with corresponding RyR1 sequence.
Three additional caveolin binding motifs were identified in RyR2 alone. These motifs were aligned with the corresponding sequence in RyR1 to show the lack of sequence homology. Asterisks indicate identical match. Colons indicate a strongly similar match. Full stops indicate a weakly similar match. 'Space' indicates no match. Two of the motifs were located to the region of the ryanodine receptor termed the transmembrane region. One was located in the cytosolic region of RyR2. Capitalised letters indicate key regions in the RyR2 motifs. Numbers correspond to the residue number. All alignments were completed using ClustalW (http://www.ebi.ac.uk/Tools/msa/clustalw2/).

The observance of so many CBM within the transmembrane region (residues ~4026-5032 in RyR1, ~3974-4967 in RyR2) is interesting given that sections of this region of RyR1 (specifically residues 4450-5032) have previously been shown to interact with Cav3 (Vassilopoulos et al., 2010). However, despite the Vassilopoulos study referring to this region as the transmembrane region, this definition requires further elucidation. Cryo-EM studies have shown that this transmembrane 'foot' is ~7nm in depth, which makes it thicker than the SR membrane (Serysheva et al., 1995). Thus, portions of the region termed the transmembrane region are not necessarily completely membrane bound, and that regions are also present in both the cytosol and within the SR lumen. Indeed, RyR are known to interact with a range of SR luminal proteins (Guo and Campbell, 1995; Györke et al., 2009; Wei et al., 2009). Unfortunately, little is known about the specific structure of this region; indeed, the volume has been predicted to contain between 16-40 transmembrane α-helices (4-10 per subunit) (Ludtke et al., 2005; Radermacher et al., 1994; Samsó et al., 2009; Samsó et al., 2005; Serysheva et al., 2008; Serysheva et al., 1995; Takeshima et al., 1989; Tunwell et al., 1996), though it is now commonly thought to be between 24 and 32 (Samsó et al., 2005). To correlate the identified CBM (those shared by both RyR1 and RyR2) to the regions within the RyR transmembrane region, we calculated

the hydrophobicity of this region as well the likelihood of α-helices to form within this region.

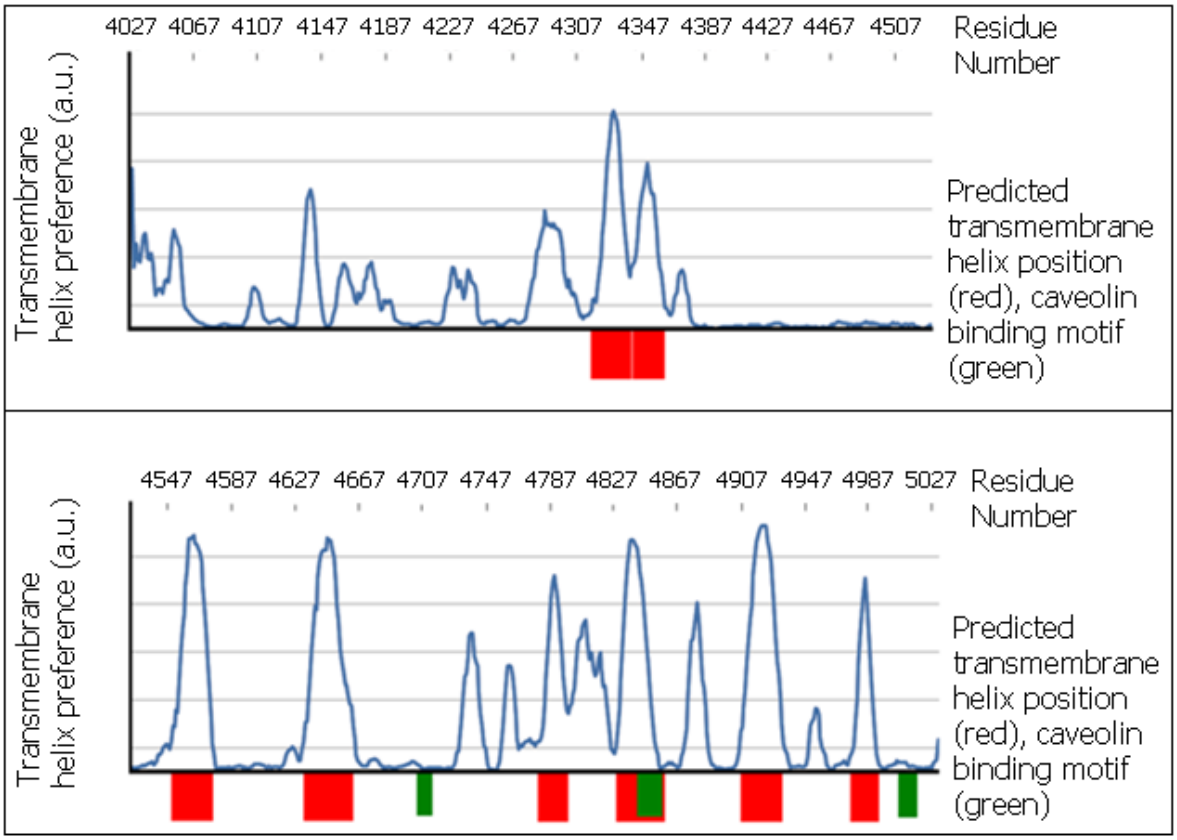

Figure 78: Predicted regions of transmembrane α-helix and location of CBMs in the transmembrane region of RyR1.

The propensity to form α-helices within the transmembrane region of RyR1 was predicted using the SPLIT tool (http://split4.pmfst.hr/split/4/). The blue traces show the regions most likely to adopt helical conformation. Those regions that are also predicted to form helices within the membrane are highlighted in red. The locations of the CBMs are highlighted in green. Note that eight helical regions are predicted, which fits with the prediction of between 4-10 mentioned above. Also note that two of the CBMs (corresponding to #2 and #6) are located to regions that are not predicted to be within the membrane or to form α-helical structures. The other three CBM (#3, #4 and #5) are all located in close proximity to each other within a region predicted to be both α-helical and part of the membrane. The image has been split into two sections in order to fit on the page.

As can be seen in Figure 78, two of the CBM identified (#2 and #6) are located to regions that are not likely within the membrane, whereas, the other three CBM (#3, #4, #5) are located in a site that is both predicted to be an α-helix and is predicted to be within the membrane. The two additional CBM that were located within the transmembrane region of the cardiac isoform RyR2 (#8, #9), but not RyR1, were located in a region that was

predicted to be both helical and within the membrane in both of the RyR isoforms (see Figure 79).

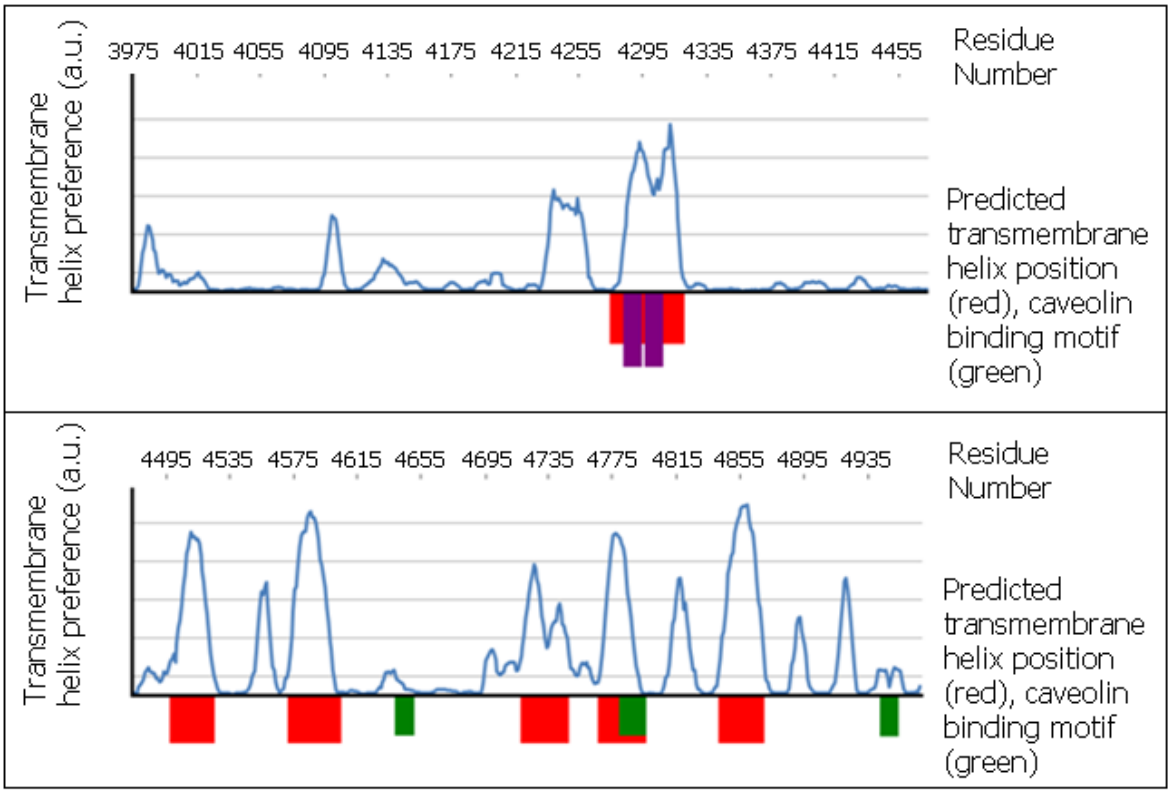

Figure 79: Predicted regions of transmembrane α-helix and location of CBMs in the transmembrane region of RyR2.

The propensity to form α-helices within the transmembrane region of RyR1 was predicted using the SPLIT tool (http://split4.pmfst.hr/split/4/). The blue trace shows the regions most likely to adopt helical conformation. Those regions that are also predicted to form helices within the membrane are highlighted in red. The location of the CBMs shared by both RyR1 and RyR2 are highlighted in green. The CBM that are unique to RyR2 are shown in purple. Note that six helical regions are predicted, which fits with the prediction of between 4-10 mentioned above. Also note that, as for RyR1, two of the caveolin binding motifs (corresponding to #2 and #6) are located to regions that are not predicted to be within the membrane or to form α-helical structures. Also as for RyR1, the other three CBM (#3, #4 and #5) are all located in close proximity to each other within a region predicted to be both α-helical and part of the membrane. In addition to the CBM in RyR1, two additional CBM are located (purple), and these are also located in close proximity to each other within a region predicted to be both α-helical and part of the membrane.

The location of the helical content and likely transmembrane regions within RyR2 (Figure 79), show a considerable overlap with those in RyR1. However, two additional CBM are located within the transmembrane region of RyR1. Interestingly, despite the fact

that the sequence within this region is shown to be quite distinct (see Figure 77) between the two RyR isoforms, and that CBM are only identified in RyR2, transmembrane α-helices are still predicted in both isoforms.

Thus, it would appear that potential sites of interaction between Cav3 and the region termed the transmembrane region of both RyR1 and RyR2 may be within both the membrane as well as externally (be that in the cytosol or the lumen of the SR). Unfortunately, the nature of the hydrophobicity and secondary structure algorithms do not allows us to identify which side of the membrane the CBMs are located on. Further, because a high resolution structure is not available for either RyR it is not possible to pin point the sites of the non-transmembrane region CBMs (#1, #7). Despite this, encouraged by the observance of multiple caveolin binding motifs within RyR, a series of interaction studies were devised to explore this potential relationship further.

Purification of junctional sarcoplasmic reticulum and RyR1

Previous efforts in our lab employing multiple techniques (Sharma et al., 2006; West et al., 2002) to purify the cardiac ryanodine receptor isoform, RyR2, resulted in very poor yields of the channel with poor quality EM images of the purified protein due to the presence of high concentrations of lipid (added to stabilise the receptor). However, the purification of the skeletal muscle isoform, RyR1, was more successful. Although the initial intention of this part of the project was to investigate the interaction between Cav3 and the cardiac isoform of RyR (RyR2), this was not possible. Thus, the interaction of the skeletal isoform (RyR1) with Cav3 was explored given that Cav3 is expressed in both cardiac and skeletal muscle cells. As described in the Materials and Methods, a protocol was developed based upon previous RyR1 purification protocols (Chu et al., 1988; Meng et al., 2009; Serysheva et al., 1999), to purify both the junctional sarcoplasmic reticulum (jSR) membranes and RyR1.

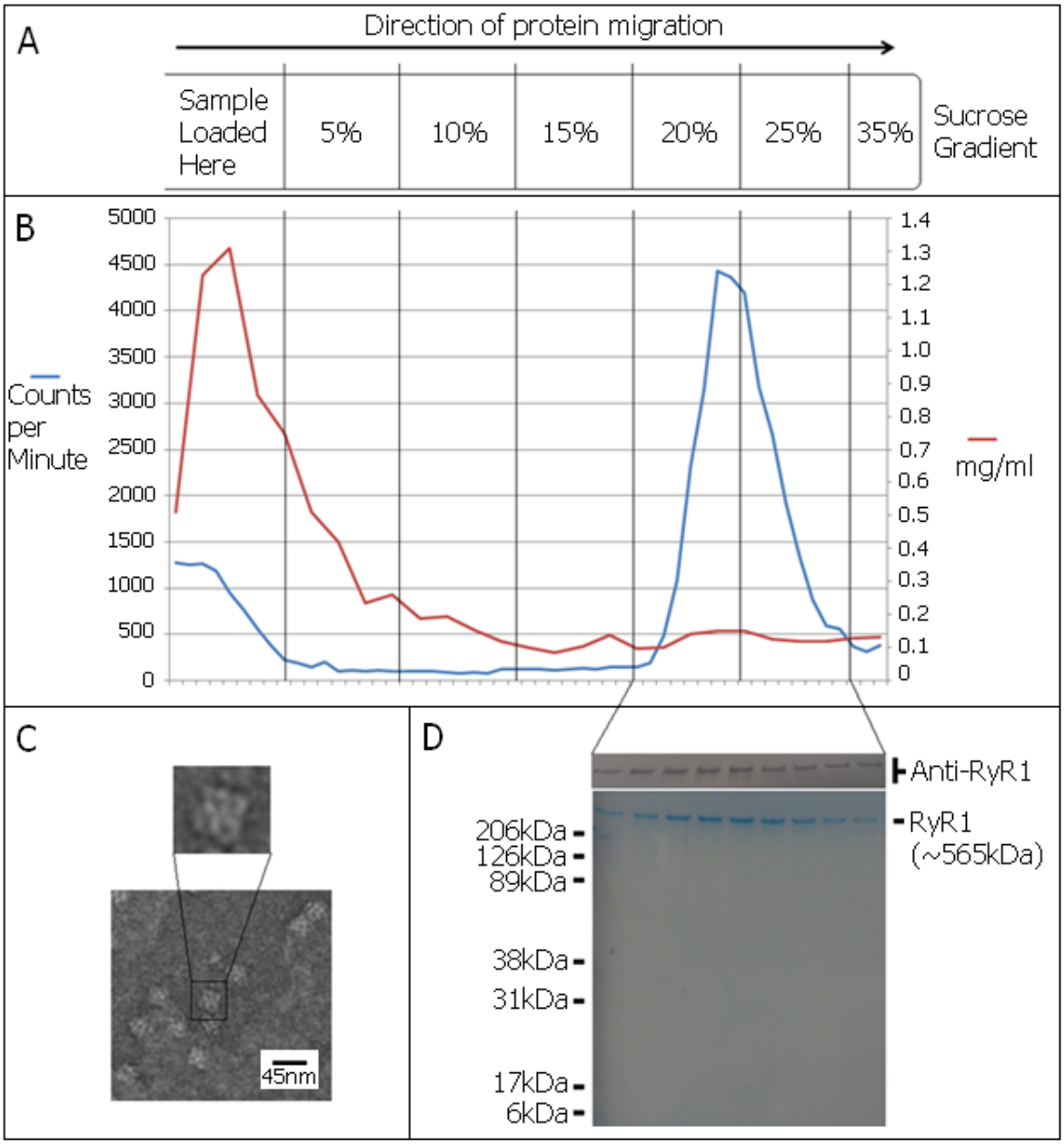

Figure 80: Purification of RyR1 using a sucrose step gradient.

A: Sucrose gradient fractions showing the percent of sucrose used in the gradient. **B:** Radioactivity profile (counts/min, blue) and the protein concentration (mg/ml, red). The radioactivity shows where the RyR1 is present. Note that peak CPM (and hence RyR1) is found at the 20/25% sucrose fractions. Also note that the majority of the total protein (measured in mg/ml) is present at the start of the sucrose gradient. **C:** Negative stained electron microscopy image showing sample of the purified RyR1. Inset is a RyR1 oligomer. Note the homogeneity of the sample. **D:** Western blot with an anti-RyR1 antibody shows the presence of RyR1 (top) and the Coomassie staining shows homogeneity of RyR1 (bottom).

As can be seen in Figure 80 (panel C, D), the purification of RyR to homogeneity was successful. Pure RyR1 (panel D) was obtained from the 20/25% sucrose interface, and the yield was approximately 0.1mg/ml. To examine the purity of the sample further an aliquot of the peak fraction was negatively stained and examined by TEM. The field of particles shown in panel C illustrate that the RyR1 is pure and that the receptor exhibited a characteristic 'four-lobed' appearance indicative of a homo-tetramer. The RyR1 homotetramers can be seen to measure ~30x30nm in agreement with previous reports (Radermacher et al., 1994; Serysheva et al., 1995).

Cav3 presence in the junctional sarcoplasmic reticulum

Although, the presence of Cav3 in skeletal muscle cells is known to be predominantly at the plasma membrane (Hagiwara et al., 2002), and the developing T-tubule system (Parton et al., 1997), it has also been reported that Cav3 co-localises with the Ganglioside M1 and SERCA in detergent resistant regions of the sarcoplasmic reticulum of rabbit skeletal muscle (Li et al., 2006). The presence of Cav3 in the SR is currently incompletely understood. However, the co-localisation of SERCA and Cav3 indicates that it may be involved in calcium regulation. To investigate whether the SR fractions purified here (i.e. the fraction that was ultimately used to further purify RyR1) also expressed Cav3, immunostaining for Cav3 in the SR fraction was undertaken.

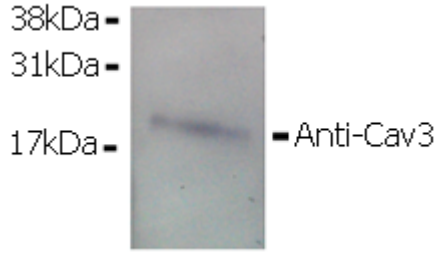

Figure 81: Cav3 expression in the jSR of skeletal muscle.
Junctional terminal cisterna of sarcoplasmic reticulum were treated to 5XSDS sample buffer and then analysed *via* SDS-PAGE. Western blotting using an anti-Cav3 antibody was completed on the sample. Note the presence of Cav3 in the junctional terminal cisterna of sarcoplasmic reticulum.

As can be seen in Figure 81, in agreement with Li and co-workers study (Li et al., 2006), Cav3 expression was detected in the SR fraction. The protocol used in this thesis included the purification of intact SR, then the separation of the junctional SR regions from the longitudinal SR regions *via* the use of KCl to break them apart, then separation of the two regions by density centrifugation; it is important to note that the lipid and protein make

up of these two regions is distinct. For example, RyR is predominantly at the junctional region, where it interacts with the membranes, whereas SERCA is predominantly in the longitudinal region, where it is involved in the re-uptake of calcium. In our study, only the junctional SR was examined for Cav3 expression (Figure 81), where it was detected. However, Li and co-workers purified SR, and then used 1% (v/v) Triton X-100 to solubilise the SR, resulting in detergent-resistant membrane (DRM) regions and detergent-solubilised membrane (DSM) regions. These two regions were then separated by density centrifugation, finding Cav3 within the DRM regions co-localised with SERCA, which would imply (given the presence of SERCA) that the DRM regions represent regions from the longitudinal SR, not the junctional SR. Therefore, it may be that Cav3 is actually ubiquitous to *both* junctional and longitudinal regions. We did not check longitudinal SR for Cav3 expression and future work should address this issue.

Pull-down assay

Since Cav3 was present in the jSR membrane preparations the next logical step was to investigate whether Cav3 could directly interact with the ryanodine receptor. Since both Cav3 and RyR1 had been purified an assay was developed to test whether full-length Cav3 could bind purified RyR1. Since Cav3 has a C-terminal MAT-tag the purified sample was applied to a cobalt-chelate resin column to immobilise the protein. The matrix was then washed with buffer (identical to the RyR1 buffer) to remove any unbound Cav3. Purified RyR1 was then applied to the cobalt-Cav3. The agarose beads were washed to remove any unbound protein and then SDS sample buffer added and then centrifuged. Aliquots were taken for analysis by both 5% (to detect RyR1) and 12% (to detect Cav3) SDS-PAGE gels with western blotting using anti-RyR1 and anti-Cav3 antibodies.

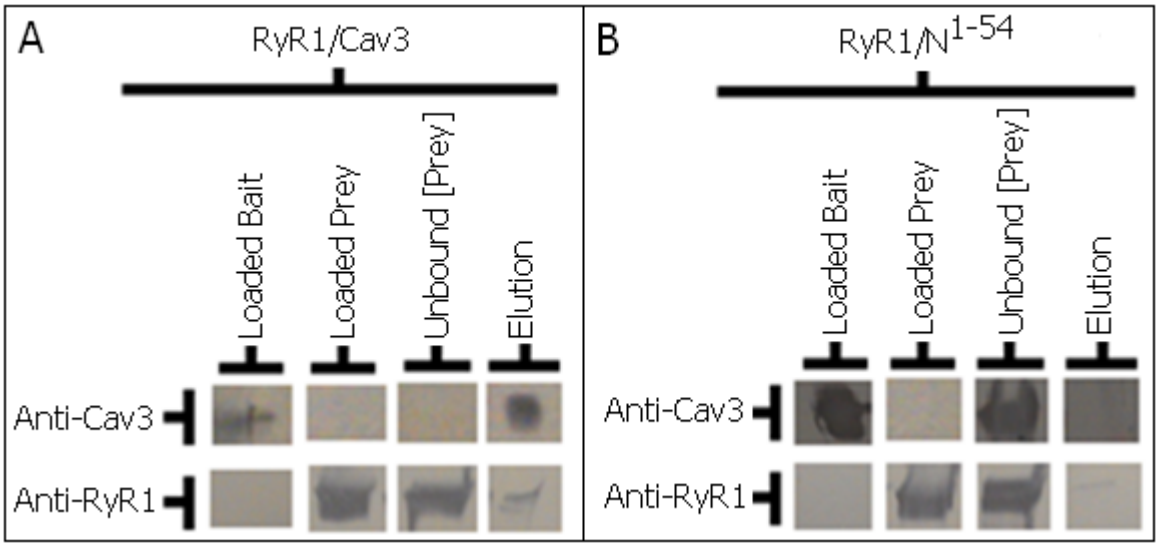

Figure 82: Pull-down assay: RyR1 and Cav3/ N^{1-54} domain.

A: The fractions obtained from the co-immunoprecipitation of Cav3 (BAIT) and RyR1 (PREY) were examined by SDS-PAGE/western blotting using two different antibodies, one raised against Cav3 (abcam, ab2912) and one raised against RyR1 (abcam, ab2868). Cav3 can be seen to co-elute with RyR1. **B:** The fractions obtained from the co-immunoprecipitation of the N^{1-54} domain (fused to 6xHisTag and SUMO-tag) domain (BAIT) and RyR1 (PREY) were examined by western blotting using two different antibodies (as above). Note that the bound N^{1-54} domain is stripped from the immobilised cobalt upon addition of RyR1.

As can be seen in Figure 82, there appears to be co-immunoprecipitation of Cav3 and RyR1 (panel A, Elution), indicating a putative interaction between Cav3 and RyR1. To examine which domain of Cav3 might be involved in binding to the RyR1 the experiment was also completed using the N^{1-54} domain (expressed with an N-terminal His-tag and SUMO protein). As with the full-length Cav3, the N^{1-54} domain was immobilised on a cobalt-chelate resin column. Inspection of Figure 82 (panel B) finds that the loading of the RyR1 prey has stripped the N^{1-54} domain fusion protein from the immobilised cobalt. One possibility for the observation could be that RyR1 and the N^{1-54} domain fusion protein interact in such a way that N^{1-54} domain's preferential binding to RyR1 disrupts the binding of the N^{1-54} domain fusion protein to the immobilised cobalt; thus resulting in both proteins being found in the unbound fraction, as opposed to the expected elution fraction. One other possibility is that the DTT present in the RyR1 buffer (2mM DTT), which is a reducing agent, has disrupted any interaction of the domain with the cobalt, resulting in the domain being found in the unbound fraction. However, it is important to remember that the N^{1-54} domain included a N-terminus His-Tag and SUMO fusion protein and thus it cannot be determined whether there may have been involvement of the SUMO tag and not N^{1-54} domain. To address the possibility that it was the SUMO protein that was responsible for the observed interaction with RyR1 a repeat experiment was conducted using the 6xHis-tag-SUMO (without N^{1-54} domain), as a control (see Figure 83).

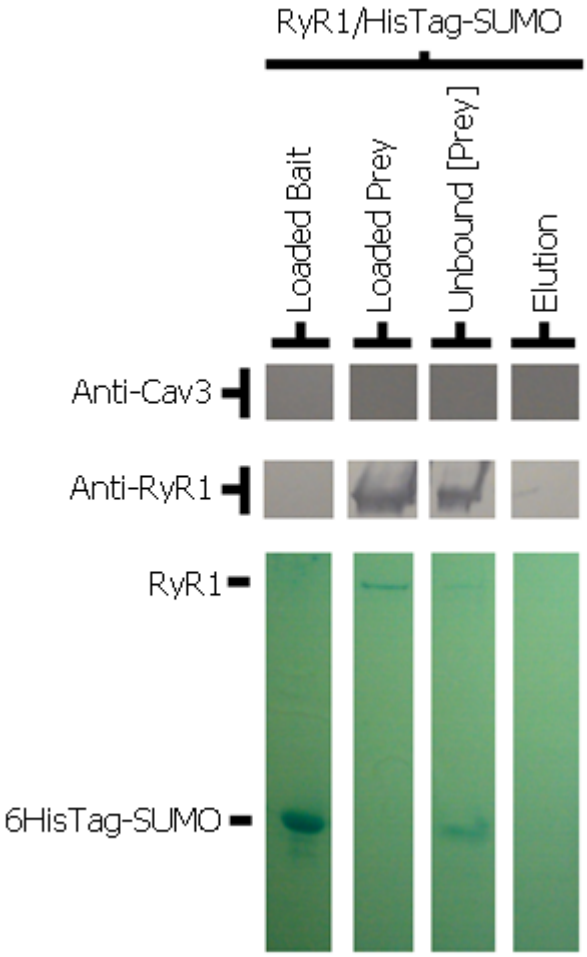

Figure 83: Pull-down assay: RyR1 and 6xHisTag-SUMO.
The fractions obtained from the Pull-down assay of 6xHisTag-SUMO (BAIT) and RyR1 (PREY) were examined by both western blotting (both anti-Cav3 and anti-RyR1) and Coomassie staining. As confirmed by the anti-Cav3 antibody, no Cav3 was present in either the bait or prey fractions, as expected. The Coomassie stained gel shows that the 6xHis-tag-SUMO protein was present in the unbound Prey fraction.

As can be seen, a similar result was observed (to that when N^{1-54} was included), in that the BAIT was stripped from the resin, indicating that the observed interaction was likely due to an interaction between the 6xHis-SUMO protein (and not the N^{1-54} domain) and RyR1. The method calls for a 1hour incubation of the PREY with the BAIT; it is possible that this incubation is too long, and that it is resulting in the BAIT being removed from the immobilised cobalt. Unfortunately, it was not possible to complete the pull-down assay using the cleaved N^{1-54} domain alone, as the nature of assay requires the BAIT protein to be bound to the immobilised cobalt.

With regards to the region in RyR that may be involved in the interaction, previous studies have shown that the last 582 residues of RyR1, which correspond to a region within

the transmembrane region of RyR1, have been shown to interact with Cav3 (Vassilopoulos et al., 2010). Unfortunately, no further information on the region within RyR1 or Cav3 that were involved in the interaction was discerned. However, having scanned the RyR1 sequence for CBMs here, we have found that RyR1 has six CBMs within it, five of which are found in the transmembrane region. Thus, it may be that the region within RyR1 involved in this interaction involves the transmembrane region of RyR1, thus supporting the likelihood of a SR associated Cav3.

Tritium ryanodine binding assay

To further investigate a putative interaction between Cav3 and RyR1 a functional assay employing ^{3}[H] ryanodine was investigated. The jSR fraction containing RyR1 was incubated with Cav3, and then ^{3}[H] ryanodine was added. The amount of radioactive ryanodine that bound was detected by measuring the radioactivity of each sample *via* the use of a scintillation counter. The level of radioactivity detected between samples gives an indication of the open/closed state of the RyR channel pore; and hence information on a potential interaction. A high radioactivity indicates that ^{3}[H] ryanodine has bound RyR, whereas, a low radioactivity indicates that ^{3}[H] Ryanodine was unable to bind. Thus, the assay allows for the detection of the open state probability of the RyR upon addition of potential binding partners and is hence indicative of an interaction. It should also be noted that the contribution of the Cav3 found within the jSR fraction (see Figure 81) should not have affected the results observed here, because the same jSR fraction was used for all assays, thus the effect of the presence of native sheep Cav3 in the control will be constant.

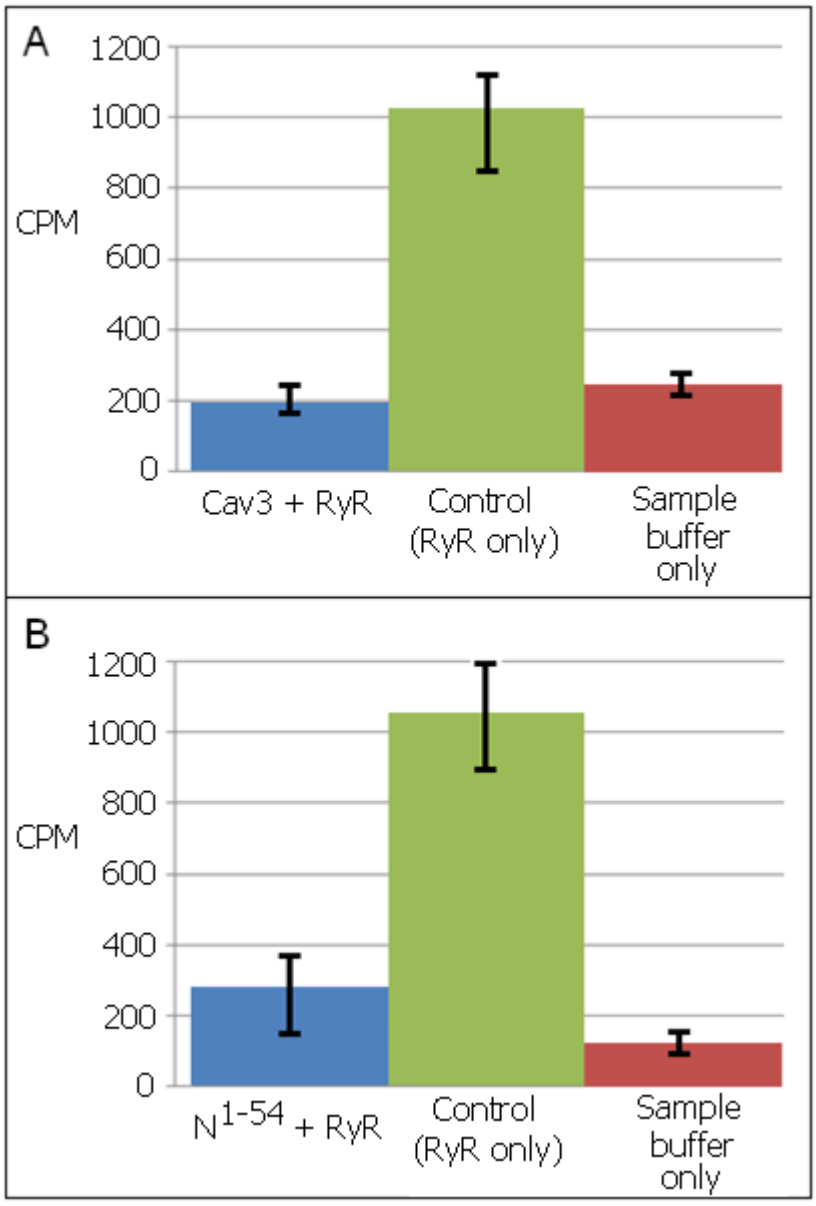

Figure 84: Tritium ryanodine binding assay.

Analysis of the RyR1 channel open state in response to the addition of Cav3 and N^{1-54} to jSR membranes. Method adapted from Needleman and Hamilton (Needleman and Hamilton, 1997). Y-axis represents radioactivity in counts per minute (CPM). **A:** Full-length Cav3 was added to the jSR membranes at a molar ratio of 507:1 (Cav3:RyR1). The green column shows ryanodine binding in the absence of Cav3, the blue column when Cav3 has been added and the red column the effects of the sample buffer. **B:** Tritiated ryanodine binding to jSR membranes before and after addition of the Cav3 N^{1-54} domain; added for a molar ratio of 507:1 (N^{1-54}:RyR1). Although there appears to be a considerable reduction in the open state probability of RyR1 upon the addition of either Cav3 or N^{1-54}, a similar large drop in CPM is observed when Cav3 or N^{1-54} buffer is added. Assays were complete in triplicate. Bars represent the range of results observed.

The ^{3}[H] ryanodine binding assay is an indirect measure of the open probability of the channel with an increase in ligand binding considered to be an indicator of increased channel activity whereas a reduction in binding suggests that the channel has been inactivated. Upon initial inspection it appeared that both Cav3 and the N^{1-54} domain had a significant impact upon ^{3}[H] ryanodine binding to the jSR (RyR1) membranes, leading to an approximate 80% reduction which would suggest that Cav3 binding has led to inactivation of the channel and also reinforces the biochemical data indicating a direct interaction (see Figure 82). Attempts were made to test whether the effects of Cav3 were dose-dependent and a series of RyR1:Cav3 combinations were tested at varying molar ratios (data not shown). However, there was no clear correlation between Cav3 concentrations relative to RyR1 density. Control experiments were devised, whereby the Cav3 or N^{1-54} buffer (20mM Tris pH7.5, 115mM NaCl, 0.02% (w/v) n-Dodecyl-ß-maltoside, ~20% (w/v) sucrose, plus protease inhibitors; and 10mM Tris pH8, 150mM NaCl, 10mM imidazole, 0.03% (w/v) Triton X-100 respectively) was added without the protein (Cav3 or N^{1-54}) to the jSR membranes, and the binding assay was conducted (Figure 84; Red bars). However, as can be seen from the figure, the buffers resulted in a similar reduction to ^{3}[H] ryanodine binding, indicating that the observed reduction in RyR channel pore open state was as a result of the addition of the buffer, and not *via* a interaction between Cav3 (or N^{1-54}) and RyR1.

How exactly the buffer causes a reduction in the open probability of the channel, as judged by ^{3}[H] ryanodine binding is not entirely clear. One possible reason may be due to the detergent in the Cav3 and N^{1-54} sample's buffer. Although the detergents were close to the CMC they may have led to partial solubilisation of the jSR membrane. Indeed, if the assumptions made about Li and co-worker's detergent-solubilised membrane (DSM) equating to the jSR are correct (Li et al., 2006), then this region would be susceptible to the addition of detergent. It is unlikely that there would be complete solubilisation of RyR1 although if a population or RyR1 was released from the bilayer then the solubilised RyR (once housed within the jSR), would be eliminated during the filtering stage of the experiment (note that individual proteins, but not intact jSR, could pass through the filter paper used), thus taking any potentially bound ^{3}[H] ryanodine with it. Another possibility could be that partial solubilising of the SR could potentially release other proteins from within the jSR, or that are bound to the RyR1, that upon binding to or dissociation from the RyR1 channel modulate the open and closed state of the channel. In addition, partial solubilisation of the jSR may have lead to conformational changes in RyR1 which resulted in a closed channel.

Unfortunately, removal of n-Dodecyl-ß-maltoside (by dialysis) from the Cav3 sample was not an option, as this detergent was present to provide stability to Cav3. Thus, given the unavoidable issue with regards to the buffer, it remains unclear as to whether Cav3 interacts with the RyR calcium release channel. To study this further, one approach could be to create artificial proteoliposomes in which both RyR and Cav3 are present. The creation of proteoliposomes would entail that detergents are removed, thus removing this potentially contributing factor. It should also be noted that the results observed here do not necessarily imply that there is no interaction or effect upon channel activity, merely that either: a) the putative cytosolic CBM in RyR1 is occluded, b) the solubilised Cav3 cannot access the transmembrane CBMs and thus this assay may not be appropriate, or c) there is an interaction, but no effect upon open channel activity. For example a Cav3-RyR1 interaction may be important for localisation of RyR1 to different regions of the SR and/or act as a scaffold to bring other regulatory molecules in close proximity to RyR1.

4.4. Conclusion

An intriguing observation from this study was that over-expression of human Cav3 appeared to induce caveolae formation in agreement with Li and co-workers (Li et al., 1996b). Although, since we did not conduct any labelling we cannot conclusively say that the 'vacuoles' that we see are definitely Cav3. However, encouragingly, as for Li and co-workers (Li et al., 1996b), examination of control un-infected Sf9 cells did not find these types of vesicles and would suggest that they are formed as a result of over-expression of Cav3. In the Li study, they also reported that the vesicles were not observed in the control cells that do not possess Cav1. There also remains the possibility that these vesicles are, in fact, a cellular defensive response of Sf9 to the high concentrations of baculovirus present. The Li paper (Li et al., 1996b), claims to confirm the presence of Cav1 in the caveolae by immunostaining. However, even the presence of Cav1 does not beget the assumption that they are involved in this formation process. Instead, they may be present due to another cellular process trying to cope with the over-expression of a non-native protein. Furthermore, the claim that Cav1 causes the vesicle formation is not a direct observation. They purified what they claimed was the vesicle/caveolae fraction then completed immunostaining upon this fraction. There is no guarantee that what they purified *via* their purification techniques were the vesicles they observed *via* EM. Indeed, the sheer number of their Cav1, due to its over-expression, would likely mean that Cav1 would be unavoidably present in all the fractions derived during lysis. Thus, although it would be very tempting to say that the vesicles observed *are* caveolae, and that they *are* formed by Cav3, caution must be expressed. It can only really be claimed that the presence of the vesicles is associated with the over-expression of Cav3. The intricacies of this relationship require further elucidation. However, the presence of these putative 'caveolae' is intriguing since it opens up a host of further questions such as the importance of both cholesterol and cavin in caveolae formation.

Another potentially interesting avenue would be to see if Cav3 undergoes palmitoylation, glycosylation or phosphorylation, as this would give further information on the potential localisation and function of the recombinant Cav3, which, in turn, could give further information on any potential interactions, caveolae formation or membrane association.

It has been previously shown that Cav3 can form part of the SR membrane in rabbit skeletal muscle (Li et al., 2006), and this is something that we also observed here for sheep skeletal muscle. The specific region of the SR in which we observed Cav3 was the *junctional* terminal cisterna, which likely differs from that of the Li and co-workers study

(Li et al., 2006), in which they found it within what likely equates to the *longitudinal* fraction (note this observation of the specific SR location was not made by the researchers, but is inferred here by the high concentration of SERCA, cholesterol and GM1 – all markers of the longitudinal SR – within their purified detergent-resistant SR fraction). One possibility for the observed presence of Cav3 in both the junctional and longitudinal regions of Cav3 is that neither of the purification protocols (Li's or ours) resulted in 100% resolution of the junctional/longitudinal and DSM/DRM regions; thus, Cav3, whichever fraction it is associated with, was detected by the highly sensitive technique that is western blotting. Regardless of the specific region of the SR in which Cav3 is (indeed, it may be ubiquitous to all regions of the SR), the finding of Cav3 in the junctional SR by us, and the finding of Cav3 in DRM regions of SR associated with SERCA (Li et al., 2006), plus the finding that Cav3 interacts with specifically the transmembrane region of RyR (Vassilopoulos et al., 2010), all suggest that, indeed, Cav3 is part of the SR membrane. To investigate further the specific region of the SR in which Cav3 is present, future studies could test for the presence of markers for independent regions of the membrane in order to identify the specific region of the SR in which Cav3 is located.

The intriguing observance of a direct interaction of Cav3 with RyR1 in skeletal muscle (Vassilopoulos et al., 2010), suggested a potentially functional relevance of Cav3's location at, or in, the SR membrane, with regards to RyR1 function. A bioinformatics approach to analysis here, employing both hydrophobic region and secondary structure prediction algorithms led to the identification and approximated location of putative caveolin binding motifs within both RyR1 and RyR2; the majority of which were located to the transmembrane region of RyR. Co-precipitation methods showed that RyR1 bound to immobilised full-length Cav3, but not to the N-terminal domain (N^{1-54}), which may support the concept that it is the transmembrane regions of RyR1 that are involved in a Cav3/RyR1 interaction and thus more likely that it is the more hydrophobic domains of Cav3 (i.e. not the cytosolic N^{1-54} region) that associate with RyR1. The results from the ^{3}[H] ryanodine binding assay were inconclusive due to the interference from the buffer employed. Future work would be directed towards exploring biophysical techniques such as surface plasmon resonance to examine Cav3-RyR1 interactions. Although RyR1 could be purified in amounts suitable for these types of studies, yields of Cav3 were very low as described in Chapter 3. Improvement of yields would increase the scope for experimental approaches for studying interactions, with techniques such as SPR providing more quantitative data such as association/dissociation, rate constants and equilibrium constants.

Chapter 5: 3D structure of Caveolin-3

5.1. Introduction

The molecular analysis of the structure and topology of full-length Cav3 has not been achieved for a variety of reasons, leading one researcher to describe it as "*having an obstinately uncooperative attitude toward authority*" (Razani et al., 2002b). Indeed, we have also encountered its recalcitrant nature during the course of this PhD work. However, despite the many hurdles, the successful purification of recombinant human Cav3 has been achieved. In this chapter, we describe for the first time the 3D structure of a recombinant human Cav3 oligomer. Given the low yields of Cav3 (see Chapter 3), its hydrophobic nature, size (i.e. oligomer ~220 kDa) and need for detergents, transmission electron microscopy (TEM) combined with image analysis methods were selected as the most appropriate approach for structural studies.

5.1.1. Transmission electron microscopy

The observation by de Broglie in 1924 that electrons behaved like particles, in that they have waveform, made the field of electron microscopy (EM) possible. Electrons possess a much smaller wavelength than light leading to higher attainable resolutions, some 100-fold greater compared to that of the then light microscopes. Despite this, the resolution that can be achieved by transmission electron microscopy (TEM) is still less than methods such as X-ray crystallography and NMR due to factors such as radiation damage and low sample contrast. In brief, TEM typically involves heating a filament (e.g. a tungsten or lanthanum hexaboride thermionic emitter) such that it emits excited electrons that are then accelerated and focused into a monochromatic beam. The development of the field emission gun (FEG) has provided an alternative to the thermionic emitter, generating a more focussed collimated beam of electrons, and has allowed microscopes to be operated at voltages up to 400keV. The result is an improved signal:noise ratio and ultimately an increased theoretical resolution, as well as allowing for thicker samples to be examined. The microscope used in this PhD thesis used a FEG. The electron beam interacts with the specimen/sample inserted *via* the stage. Many different types of electron scattering can occur, including a range of specific collisions as well as near collisions of the incident electrons with the components of the sample, such as the electrons of its K- and L-shells, and those in the valence band, as well as the surrounding plasmon. Direct collisions occur when the incident electron collides with the atomic nuclei of the sample; however, these interactions are relatively rare. Much more common are electrostatic deflections, which

include where there are collisions of the incident electrons with the electrons of the sample. In addition, due to the sample being ultra-thin (electron transparent), many electrons simply pass through the sample without any interaction or change in trajectory.

These interactions can be defined as either *inelastic* collisions, or elastic collisions. Inelastic collisions are when there is a loss of energy that occurs upon the interaction of the incidental electron and its collision partner electron. This energy transfer results in a shift to a longer wavelength and a reduced angle of deflection/scattering for the incident electron. However, because the amount of energy transferred is both variable and random, when the electron reaches the imaging device the amount of energy and the angle of incidence is unknown resulting in the generation of noise. The majority of these interactions are captured by the objective aperture because they are generally deflected through small angles; because of this, images often have a high noise to signal ratio. Elastic interactions occur when the incident electrons pass close to the atomic nuclei, but do not collide, resulting in no energy loss. However, due to the positive charge of the atomic nuclei the trajectory of the electron is altered, with the angle of change being defined by how close the electron passes as well as the atomic number of the atomic nuclei. Many of these electrons are subsequently deflected through large angles and many are often not detected by the objective aperture. Due to no energy transfer occurring, the angle of incidence can be calculated (due to law of conservation of momentum), and these unaltered short wavelengths of high velocity can provide the high resolution data.

An objective aperture located in between the sample and the imaging platform determines those deflected electrons that contribute to the image (termed the back focal plane), and thus the contrast. The resultant selected diffracted electrons are magnified and focused onto an imaging device, which records the intensity and specific diffraction condition of the electron wavelength. The image can then be stored digitally using a charge-coupled device (CCD). An alternative method to digital storage is to store images on film; indeed, it is only relatively recently that CCDs have become available. The microscope used in this PhD thesis used CCD. A summary of the concept is shown in Figure 85. There are several different approaches to structural studies using TEM; electron tomography of tissue sections, electron crystallography whereby protein is organised into 2D arrays one molecule thick, and single particle analysis. Single particle analysis of Cav3 has been employed in this thesis work and so will be the focus of this chapter.

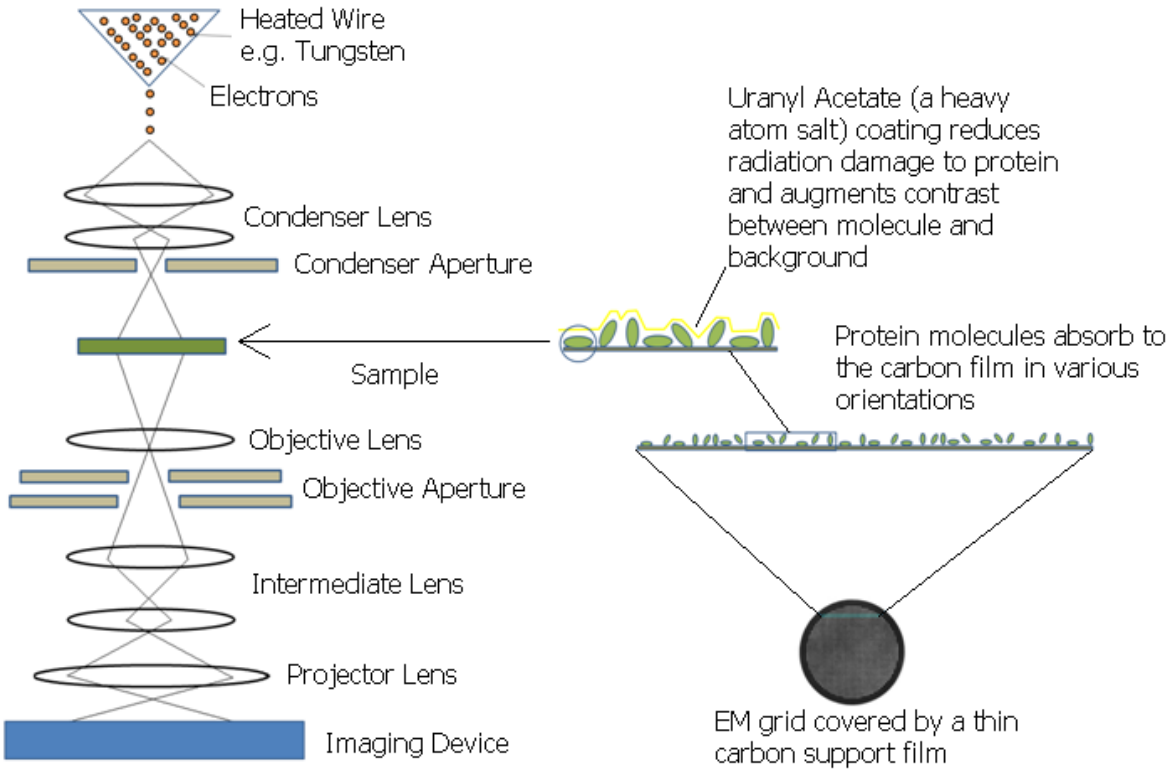

Figure 85: Brief overview of transmission electron microscopy.

5.1.2. Contrast and negative stain.

One of the factors that limit the resolution of an EM image is the lack of contrast. Contrast is defined as the ratio of the luminance between the darkest and lightest areas. If all electrons made it through to the imaging platform, then no contrast would be observed. However, by increasing the scattering of the electrons, it is possible to increase the contrast. The contrast is specifically determined by the inherent contrast within the sample being analysed, which is dictated by the average atomic number of the sample, where a low atomic number average has low contrast. Due to the inherently low contrast afforded by biological specimen (due to the low average atomic number resultant of being made up predominantly of hydrogen [atomic number 1], carbon [atomic number 6], nitrogen [atomic number 7], oxygen [atomic number 8]), the contrast observed is low, as incident electrons are not scattered as much. One way of increasing the contrast is to use metal stains. For the study of proteins in solution, uranyl acetate (an acetate salt of Uranium) is a commonly employed stain, which due to its high average atomic number of 92 leads to an increase in electron scattering and the subsequent filtering out of these wide-scattered electrons *via* the aperture, resulting in high contrast. Naturally, by eliminating these wide-angular deflecting electrons, high resolution information is lost at the cost of this increase contrast. This is not usually a problem, as high resolution structures are generally not obtainable from un-ordered protein when using negative stains as the maximum resolution

obtainable is limited by the grain size of the metal stain, which is approximately in the region of 20Å. Therefore, ultimately, more contrast is desirable in order to have the clear defined edges to the particle images. However, a drawback of negative staining is that there can sometimes, though not necessarily always, cause distortion e.g. flattening of the structure. Therefore, another approach to sample preparation aimed at preserving the sample in the microscope vacuum is to use frozen-hydrated (cryo) protein, i.e. no heavy metal stains are used. In brief, a thin layer of the sample is frozen in a hydrated state (vitrified) by immersion in liquid nitrogen or ethane whilst in a buffer that is optimised for protein stability, allowing them to be viewed in their native, non-distorted form. However, this comes at the cost of low contrast. In addition, preparing samples for cryo-EM is technically demanding and can require considerable protein to optimise e.g. protein loading and ice thickness. Although this approach was tested for Cav3 the yields of the protein were too low for sufficient optimisation at this stage of the project and thus negative staining methods were employed. Given that there are no structures for Cav3 this approach also seemed sensible for generating images with a high signal:noise.

5.1.3. Single particle analysis

One of the techniques developed over the last 20 years to extract structural information from non-ordered protein samples is single particle analysis (SPA). The individual protein particles have a low signal:noise ratio and SPA methods were developed to extract structural data by selecting thousands of individual protein molecules with the aim of increasing the signal-to-noise ratio. SPA has been becoming an increasing viable option as improvements in computer processing power have happened. In brief, the concept of SPA works by aligning multiple images of individual particles. Due to the fact that the samples features will be constant, and the noise random, by aligning many images, the true features are reinforced and the noise is reduced. There are many stages to the SPA 3D reconstruction process; a few of the more relevant key features will be briefly discussed here.

5.1.4. Image processing

A range of different software has been developed for 3D structure reconstruction based upon single particles; for example, IMAGIC (van Heel et al., 1996), SPIDER (Frank et al., 1996) and EMAN (Ludtke et al., 1999). This introduction will focus upon the software suite, EMAN. EMAN is a collection of tools designed for processing TEM images in order to derive high resolution single particle constructions and has been

specifically designed for analysing electron micrographs. In addition, it is free to the academic community, making it a popular choice for structural studies. There are two main approaches to reconstructing a 3D structure from single particles: Random conical tilt and angular reconstitution. The method employed in this thesis work used angular reconstitution and thus is described below.

The digitised micrographs obtained from TEM shows many different views of the protein. It is these different 2D views that are essential to the 3D reconstruction process. The process is underlined by the concept of the *common line projection* that states that *"two different two-dimensional (2D) projections of the same three-dimensional (3D) object always have a one-dimensional (1D) line projection in common"*. Knowledge of the angles associated between these 1D projections is used to calculate the relative Euler angle orientations, and thus how the images relate to one another, and from this a 3D projection of the protein is developed (Van Heel, 1987). This process is greatly aided if the protein possesses symmetry. If not, at least three different projections are required to solve the orientation problem. In certain circumstances preferred orientations of the protein on the grid can occur that can skew the analysis. In these instances the use of random conical tilt can enable alternative views (i.e. the ones not captured due to the proteins preferred orientation on the grid) to be captured (Radermacher, 1988).

Once collected, these particles need to be 'boxed' out to create a separate file in which the 'single' particles are present. The boxing process can be done *via* both automated and manual means using software called BOXER, which can also be used to normalise the image. Once these single particles have been selected they are used as the starting point for the 3D reconstruction process.

5.1.5. Contrast transfer function correction

In EM there are two components of image formation: Phase and amplitude contrast with phase being the more dominant component. The contrast transfer function (CTF) is the modulation of the amplitude and phase of the electron diffraction pattern (Fourier transform) that limits the resolution of image. The CTF is the result of a combination of factors such as defocus, spherical aberration and temporal/spatial coherence of the electron beam. Without correcting for the CTF, the resolution of the image is limited to the first phase reversal (zero crossing), because when the CTF crosses zero on the x-axis, the phase of the contrast is flipped, i.e. black becomes white, and white becomes black. Fortunately, EMAN allows for the correction of the shifts in the phase and amplitude of the CTF, thus

allowing the use of the corrected data to increase the resolution of the image and ultimately the 3D model.

Due to the low contrast data in biological specimens, images are often intentionally taken through a range of defocus values (underfocus) in order to increase the contrast. This is particularly the case for unstained cryo-specimens. By acquiring images at a range of different focuses, information that would otherwise be lost at the phase shift (termed 'zeroes', where the wavelength crosses the x-axis) can be acquired. Although this increase in contrast can ultimately help increase the resolution of the final image, corrections for the defocusing have to be accounted for in order to ensure that all images are 'in-phase' relative to each other. However, it is often argued that CTF correction is not actually required for negative stained datasets (Adair et al., 2008; Stagg et al., 2006) since the resolution limit is restricted by the grain size of the metal stain i.e. the additional high resolution data obtainable by correcting for the CTF is beyond the resolution limit of analysis. Moreover, there is evidence that suggests correcting for amplitude can actually introduce artefacts, and generate noise (Stagg et al., 2006). For this reason, correction for phase alone is often preferred (Adair et al., 2008). However, it is good practice to correct for CTF anyway. A summary of the CTF concept can be seen in Figure 86 below).

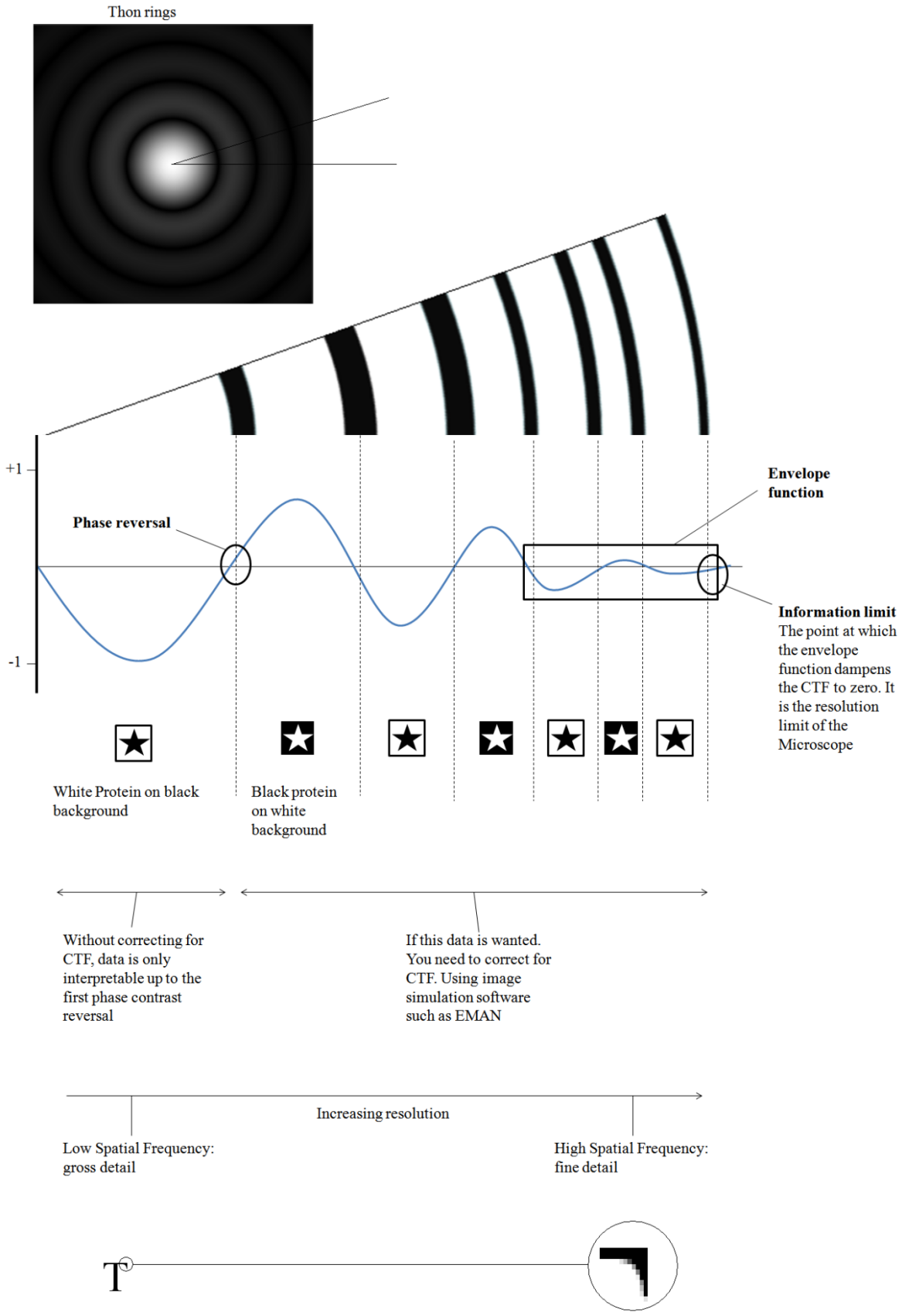

Figure 86: Summary of the contrast transfer function illustrating the effects of amplitude and phase on the resolution of the image.

The contrast transfer function modulates both the phase and the amplitude of the image. However, both can be corrected for using image reconstruction software such as EMAN.

The information at the 'zeros', where the phase reversal occurs does not provide any information. By capturing images at a range of 'defocuses', information can be obtained for these 'zero' regions. However, this defocusing needs to be corrected for such that all the images are relative to each other. To use the high spatial frequency data (high resolution) correction for the phase flips and the amplitude changes must be complete. If this is not done, only the data up until the first phase flip can be used; this, however, only contains low spatial frequency data (low resolution). Note the extra detail afforded by an increased resolution.

5.1.6. Filtering

Once the images have been corrected for the CTF, there is the option of filtering. Multiple types of filtering exist, such as low-pass filtering, which reduces the contribution of high spatial frequencies resulting in a smoother image; high-pass filtering, which reduces the contribution of the low spatial frequencies resulting in enhanced sharpness; and band-pass filtering which is a combination of both and can simultaneously sharpen the image and reduce the associated noise. The concept is best understood by examining a real example, see Figure 87.

Figure 87: Example of how filtering can affect the image.
The filtering of specific frequencies can affect the image's smoothness and sharpness, which can help accentuate certain features to aid further analysis.

5.1.7. Alignment and classification

Two important stages in the reconstruction process are alignment and classification. To understand these processes it is important to consider that: 1) the orientation of each protein on the grid, and hence the digitised image, present as a range of different 2D views, 2) these 2D views can be described in terms of their Euler angles, which are directional angles used to describe the orientation of an object in space around a common centre, 3) 3D reconstruction of structure is based upon recombining these 2D projections together.

Given the large number of proteins present, many different views are provided. The sheer number of proteins present ensures that common views are repeated; these repeated views are termed ‘classes’, from which class averages are derived, and are essential for producing a reliable 3D construction. However, before any class averages can be defined, centring and alignment of the particles needs to be undertaken. Alignment involves the elimination of in-plane rotational degrees of freedom allowing the particles to be in the same ‘view’ i.e. the particle’s structural features appear in the same position, hence ‘aligned’. If a known 3D model already exists, then this structure can be used to help align the particles, as well as build up the classes; however, there are a number of problems with this approach. Firstly, if the structure is incorrect or in an alternate conformation, then an incorrect bias is introduced into the reconstruction. Secondly, most proteins do not have a structure available. The alternative to using a known structure is to do a ‘reference-free’ alignment, which involves an iterative process of cross correlation that measures the similarity between two particles.

If the sample is homogenous, all of the selected particles will fit into one of the many classes; a stage termed classification. From this, class averages can be determined, resulting in a higher signal-to-noise of the averaged imaged compared to the individual raw images. It is from these class averages that a preliminary 3D structure can be reconstructed. The whole process is iterated several times until a reliable preliminary model is achieved. A summary of the alignment, classification, and reconstruction process is summarised in Figure 88.

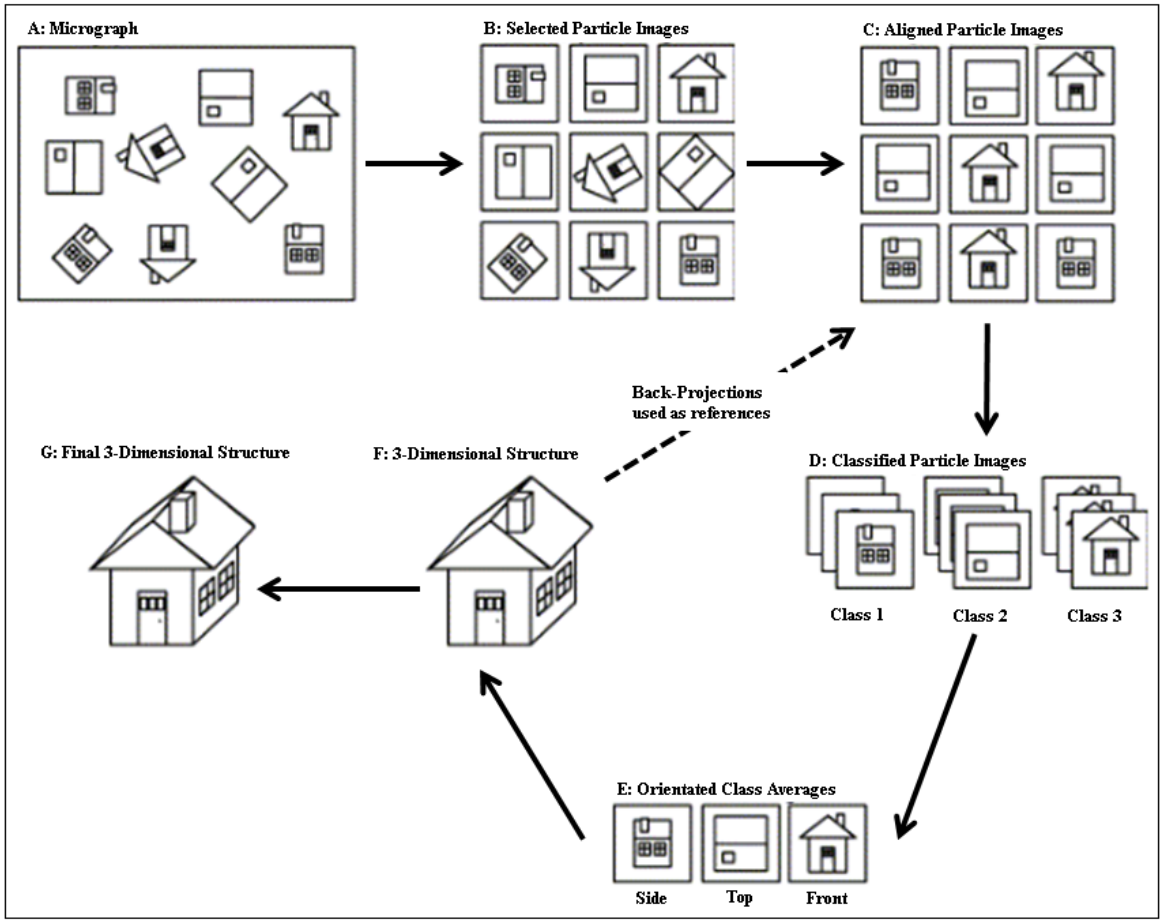

Figure 88: A summary of the alignment, classification, and reconstruction process. **A:** A micrograph contains many different orientations of the same molecule. **B:** Individual particles are picked using boxer. **C:** These particles are centred and aligned to a common view (in this example, 3 views). **D:** Particles are aligned to derive classes based upon unique views (in this example, 3 classes). **E:** Orientated class averages are derived based upon these unique views (in this example, 3 class averages). **F:** A 3D model is derived based upon the combination of the class averages. This process (C-D-E-F) is repeated multiple times, allowing the class averages and subsequently the prediction of a final 3D model (**G**) to improve resolution and accuracy. Adapted from (Thuman-Commike, 2001).

5.1.8. 3D model calculation

Each of the class averages has a unique Euler angle reference, or projection. Knowledge of these angles allows the construction of an initial 3D model using a 'back-projection' algorithm. Once a preliminary model has been created, it can then be 're-projected' (see Figure 89 for pictorial depiction of the back-projection and re-projection concept) at the unique Euler angles that correspond to the class averages. These new projections will differ slightly to the original class averages as the 3D model is not simply images patched together from unique views, but instead '*constructed'* based upon the

unique views. These new projections (based on the 3D model) are then used as averages to re-classify the raw data set. The new class averages are then employed to generate a new 3D model. This updated preliminary 3D model is then re-projected and this time the *entire dataset* is aligned with the projections, termed a multi-reference alignment, and new class averages are derived. These new class averages are used to predict a new 3D model. This process (from the introduction of the entire dataset onwards) is then iterated multiple times. The process continues until the 3D model converges as judged by the Fourier shell correlation, as described below.

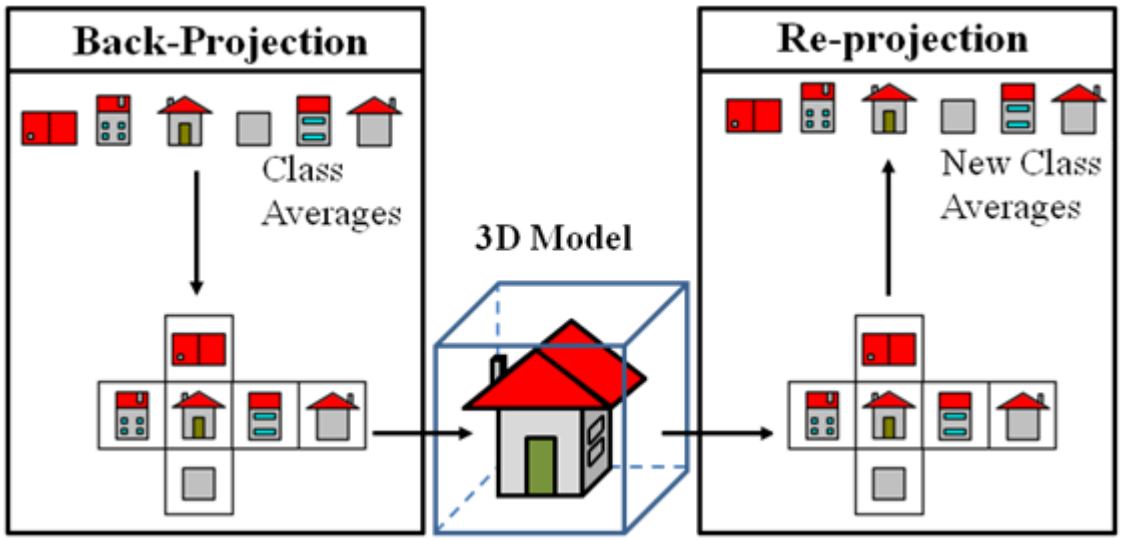

Figure 89: Cartoon explaining the concept of back-projection and re-projection. Only six projections are considered in this example here. In reality, many more are considered.

5.1.9. Analysis of the 3D model

The quality of the reconstruction should be evaluated for a number of reasons; for example, 1) to check each iteration of the 3D model to determine when the models converge and thus the structure has 'stabilised', and 2) to assess the resolution of the final model. To achieve this, the Fourier shell correlation (FSC) must be calculated. The FSC is the normalised cross-correlation coefficient between two models; basically, each model created will have a specific Fourier space unique to it, and these can be compared between models generated between, for example, each iteration. To assess whether the final model is accurate, the dataset can be randomly split into two separate groups and each dataset used to develop a model (Bottcher et al., 1997). The FSC of the resultant two models can then be calculated to see if the same model is produced. Many publications quote a FSC of 0.5 as sufficient to show an accurate prediction (Bottcher et al., 1997). An estimation of the resolution limit is taken to be the resolution where the FSC value falls below 0.5.

5.1.10. Aims and objectives

The 3D structure of Cav3 is currently not known. Clearly the area of caveolin structure needs more research; indeed, research from the 90's still predominant the canon, and much of the current prediction of its conformation has been inferred based upon a series of experiments that have either a) focused on an isolated section of the protein, or b) biophysical analysis of its properties, i.e. no direct observation of Cav3 structure has been previously achieved. As described in Chapter 3, a method has been developed during this PhD that has resulted in the purification of homogenous recombinant human Cav3. This chapter develops the work further by employing multi-angle laser light scattering and native gel electrophoresis to investigate the molecular mass of the purified Cav3. The next logical step was to further characterise Cav3 to determine the first 3D structure for this unique protein.

5.2. Materials and Methods

5.2.1. Sample preparation

Full-length Cav3 and the N^{1-54} domain were purified as described in the Materials and Methods sections of Chapters 2 and 3.

5.2.2. Non-denaturing gels (Native)

Sample buffer (312mM Tris-HCl, 50% (v/v) glycerol (Fisher Scientific), 0.05% (w/v) bromophenol blue) was added to each sample at a ratio of 4:1 (protein:sample buffer) for visualisation and to aid with gel loading. 15% acrylamide concentration running gels were made (1x0.75mm) using 6.3ml $_{dd}H_20$, 7ml 1.5M Tris-HCl pH8.9, 13.9ml 30% acrylamide/0.8% bisacrylamide solution (National Diagnostics – Ultrapure ProtoGel) (v/v), 100µl 10% (w/v) ammonium persulphate, 23µl TEMED (Bio-Rad). 5% stacking acrylamide concentration gels were made using 12.8ml $_{dd}H_20$, 4ml 0.5M Tris-HCl pH6.8, 1.5ml 30% acrylamide/0.8%bisacrylamide solution (National Diagnostics, Ultrapure ProtoGel) (v/v), 15µl TEMED (Bio-Rad), 150µl 10% (w/v) ammonium persulphate. 5% acrylamide concentration running gels were also made by altering the ratio of acrylamide accordingly. Gels were completed at 4°C.

5.2.3. Western blotting

Western blots were carried out as outlined in the Materials and Methods section of Chapter 2.

5.2.4. Light scattering

Samples were sent to the Manchester University Biomolecules Core Facility for multi-angle laser light scattering (MALLS) analysis. Samples of purified recombinant protein were applied to a Superose 6 column 10/300GL (from GE Healthcare) running at a flow rate of 0.75ml/min in Tris buffer (for full-length Cav3: 25mM Tris pH7.5, 115mM NaCl, 0.075% (w/v) n-Dodecyl-ß-maltoside. For N^{1-54}, 10mM Tris pH8, 150mM NaCl, 0.03% (v/v) Triton X-100). Samples eluting from the column passed through an in-line DAWN HELEOS-II laser photometer (laser wavelength 658nm) and an Optilab rEX refractometer with a QELS dynamic light scattering attachment (Wyatt). Light scattering intensity and eluant refractive index (concentration) were analysed using ASTRA v5.3.4.13 software to give a weight-averaged molecular mass (Mw).

5.2.5. Incorporation of Cav3 into large uni-lamellar vesicles

Large uni-lamellar vesicles consisting of DOPE:DOPG:DOPC at a 2:1:1 ratio were prepared as described by Geertsma and co-workers (Geertsma et al., 2008). In brief, lipids (DOPE, 1,2-Dioleoyl-sn-glycero-3-phosphoethanolamine, Sigma 42490; DOPG, 1,2-Dioleoyl-sn-glycero-3-phospho-rac-(1-glycerol) sodium salt, Sigma P9664; DOPC, 1,2-Dioleoyl-sn-glycero-3-phosphocholine, Sigma P6354), were solubilised in diethyl ether and then dried. Lipids were resupended in 25mM Tris pH7.4, 115mM NaCl to a final concentration of 20mg/ml and sonicated (six cycles of 15seconds) on ice under a gentle stream of N_2 gas to create small uni-lamellar vesicles (SUVs). To fuse the SUVs into large multi-lamellar vesicles (LMV), the SUVs were flash frozen in liquid nitrogen and thawed at room temperature for 20mins, three times. The LMVs were passed through an extruder (400nm polycarbonate filter) 11 times to form large uni-lamellar vesicles (LUVs), which were then diluted to 4mg/ml in 25mM Tris pH7.4, 115mM NaCl, and the glycerol content adjusted to 20% (v/v) in order to stabilise them. The LUVs were titrated with Triton X-100, until a midpoint between membrane saturation and solubilisation was reached (as judged by measuring the optical density at 540nm). Purified Cav3 was added to the destabilized LUVs at mass ratio of 1:75 (Cav3:lipid) at 4°C. The sample was incubated for 15minutes at 4°C. Biobeads SM-2 polystyrene beads (Bio-Rad, cat. no. 152-3920) were added at 20mg biobeads per 500µl protein-liposome suspension and the sample incubated for 30min at 4°C. Additional biobeads were added after 1hour, 8hours and 10hours, before removal of the biobeads. The proteoliposomes were diluted 10x (lipids at 4mg/ml and protein at 1.5mg/ml) via the addition of 25mM Tris pH7.4, 115mM NaCl. The sample was centrifuged at 267,000xg for 20mins at 4°C to collect the proteoliposomes, which were then diluted to a range of different concentrations suitable for further analysis. Samples were prepared for transmission electron microscopy following the protocol described in Chapter 4, section Negative stain transmission electron microscopy of RyR1.

5.2.6. Transmission electron microscopy and 3D structure analysis of purified Cav3

Micrograph images of Cav3 (at 0.01mg/ml) were recorded by Dr Richard Collins (Electron Microscopy Facility, University of Manchester) as described in the previous chapter (Chapter 4, Materials and Methods, section Negative stain transmission electron microscopy of RyR1). Each micrograph was examined using the CTFIT program within the EMAN package (Ludtke et al., 1999) to determine the degree of underfocus; only those images between 0.5–1.8µm defocus were included in the 3D reconstruction. Any

astigmatised images were discarded. Cav3 particles (5643) were selected using the GUI Boxer software into a 64x64 pixel (320Åx320Å) box. The contrast transfer function (CTF) was determined for each image using CTFIT (part of the EMAN software) with images corrected for phase (Adair et al., 2008).

Classification of the particles, after centring and translational and rotational alignment, produced a set of unbiased reference-free class averages showing different orientations of Cav3. A 3D model was iteratively refined applying C9 symmetry. The EMAN software employs a projection matching routine whereby uniformly distributed orientations back-projections of the preliminary 3D model are used as references for classification of the raw dataset, with the class averages from this step used to construct a new 3D model. Refinement was carried out with an angular interval of 5° generating 85 separate classes containing between 44 and 163 particles per class. Convergence, i.e. stabilisation of the 3D structure, was monitored by examining the Fourier shell correlation (FSC) of the 3D models generated from each iteration. To assess the resolution of the final 3D volume of Cav3 the dataset is randomly split into two with a volume calculated for the two sub-sets. Following established procedures (Bottcher et al., 1997) the resolution is estimated by the Fourier shell correlation coefficient (FSC). An estimation of the resolution limit is taken to be where the FSC value fell below 0.5. All the Cav3 3D maps and models are displayed using the Chimera software (Pettersen et al., 2004). An outline of the process is shown in Figure 90.

Contour-delineated class averages were generated using the SPIDER software contouring function (Frank et al., 1996).

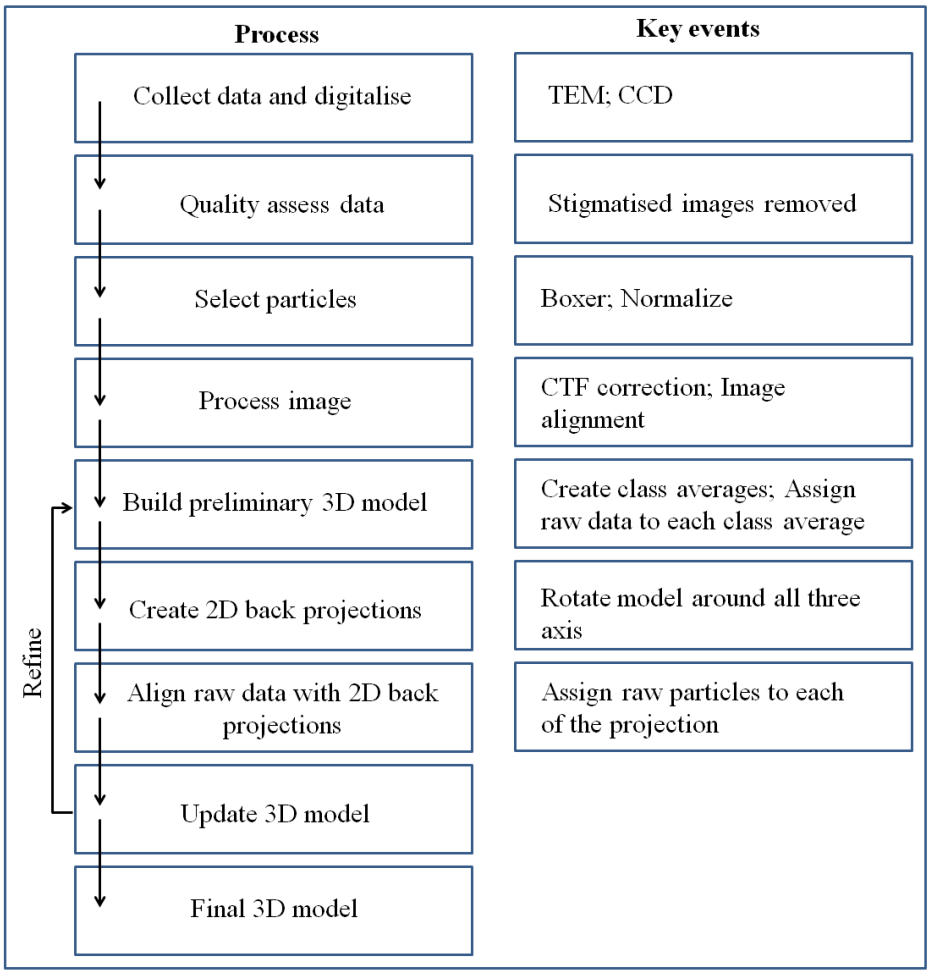

Figure 90: 3D reconstruction process

5.2.7. Symmetry analysis

Cross correlation coefficient

To investigate the symmetry of the purified Cav3 oligomer rotational cross-correlation analysis of reference-free class averages of Cav3 was carried out using the SPIDER software (Frank et al., 1978; Frank et al., 1996; Frank et al., 1981). The class averages of the raw Cav3 data determined using the EMAN command refine2d.py were converted into SPIDER format. A class average presenting a circular view of the complex was selected and rotated around the z-axis in increments including those corresponding to C3, 4, 5, 6, 7, 8, 9, 10, 11, 12, 13, 14 symmetries (e.g. 26°, 28°, 33°, 36°, 40°, 45°, 51°, 55°, 90°, 120° etc) through 360°, after centring and applying a mask to the 2D class average. Each of the rotated 2D images was compared to the original un-rotated class average using the SPIDER command CC C. The cross-correlation coefficient was plotted against the angle of rotation.

Oval Plot

In a separate approach a circle was positioned equi-circumferenced approximately

in the middle position of the outer ring of protein density. Using Oval Plot (ImageJ) the grey scale intensities were plotted as a function of angle.

5.2.8. Labelling the C-terminus of Cav3

The presence of the C-terminal MAT-tag allowed labelling of the Cav3 C-terminus using NiNTA gold (Nanoprobes Inc). Following a previously described protocol (Walsh et al., 2009a; Walsh et al., 2009b) an aliquot of purified Cav3 was incubated for 3hours with NiNTA-gold. Samples were negatively stained and examined in a Tecnai 12 Biotwin TEM at an operating voltage of 100kV. More than 100 gold-labelled Cav3 complexes were selected and subjected to reference free-class averaging (refine2d.py, EMAN software).

5.2.9. Segmentation

Segmentation of the nonamer into potential monomers was completed using Segger, which is an extension to the UCSF Chimera software, following the instruction at http://ncmi.bcm.edu/ncmi/software/segger/docs_segmenting.

5.2.10. Bioinformatics

Secondary structure prediction was made using both PSIPRED (version 2.6 http://bioinf.cs.ucl.ac.uk/psipred/) (Jones, 1999), and JPred (http://www.compbio.dundee.ac.uk/www-jpred/index.html) (Cole et al., 2008), both of which utilise position specific iterated blast searches and neural networks to predict secondary structure. Kyte-Doolittle hydrophobicity plots (Kyte and Doolittle, 1982) and Hopp-Woods hydrophilicity plot (Hopp and Woods, 1981) were plotted using the tool available at http://www.vivo.colostate.edu/molkit/hydropathy/. The helical plotting tool available at http://rzlab.ucr.edu/scripts/wheel was used to plot the helical wheel.

5.3. Results and Discussion

5.3.1. Structure determination of full-length Cav3

Oligomerisation and size

Native gel electrophoresis

There are multiple and conflicting claims for the size of caveolin oligomers e.g. (Li et al., 1996c; Monier et al., 1995; Sargiacomo et al., 1995; Tang et al., 1996), with predictions ranging from 200 to 600kDa. Many of these predictions are for Cav1, not specifically Cav3. In order to characterise the oligomeric form of Cav3 purified here we first employed non-denaturing (native) gel electrophoresis; a technique for protein separation that is performed in the absence of the detergent, SDS, and at 4°C, to maintain the protein in its native oligomeric conformation.

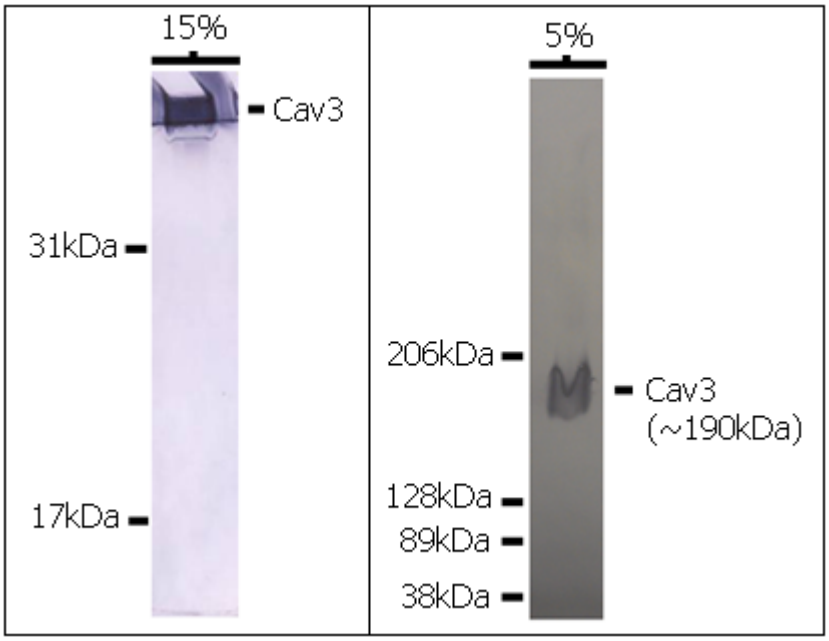

Figure 91: Native gel electrophoresis of purified Cav3.
Samples were run on 15% (A) and 5% (B) native gels with Cav3 detected by western blotting using an anti-Mat-tag antibody. **A:** A 15% gel of Cav3 illustrating that no low molecular mass monomers of Cav3 are detected. The band at the top of the well suggests that native Cav3 was too large to enter the gel indicating that Cav3 is likely in its large oligomeric form. **B:** When ran on a 5% gel Cav3 migrated as a smeared band at approximately 190kDa.

The native gels shown above illustrate that Cav3 forms a high molecular weight polymer that is approximately 190kDa, which suggests that the cell lysis protocol and the

purification protocol have maintained Cav3 in an oligomeric state. The Cav3 band can be seen to be smeared providing a rough idea of the molecular mass of the oligomer.

Unlike SDS-PAGE, where mass alone dictates protein migration, migration during native gel electrophoresis is dictated by multiple variables: size, shape, and native charge. Therefore, the prediction of 190kDa mass will be only approximately correct. For a more accurate determination of the Cav3 oligomer molecular mass we employed multi-angle laser light scattering (MALLS).

Multi-angle laser light scattering

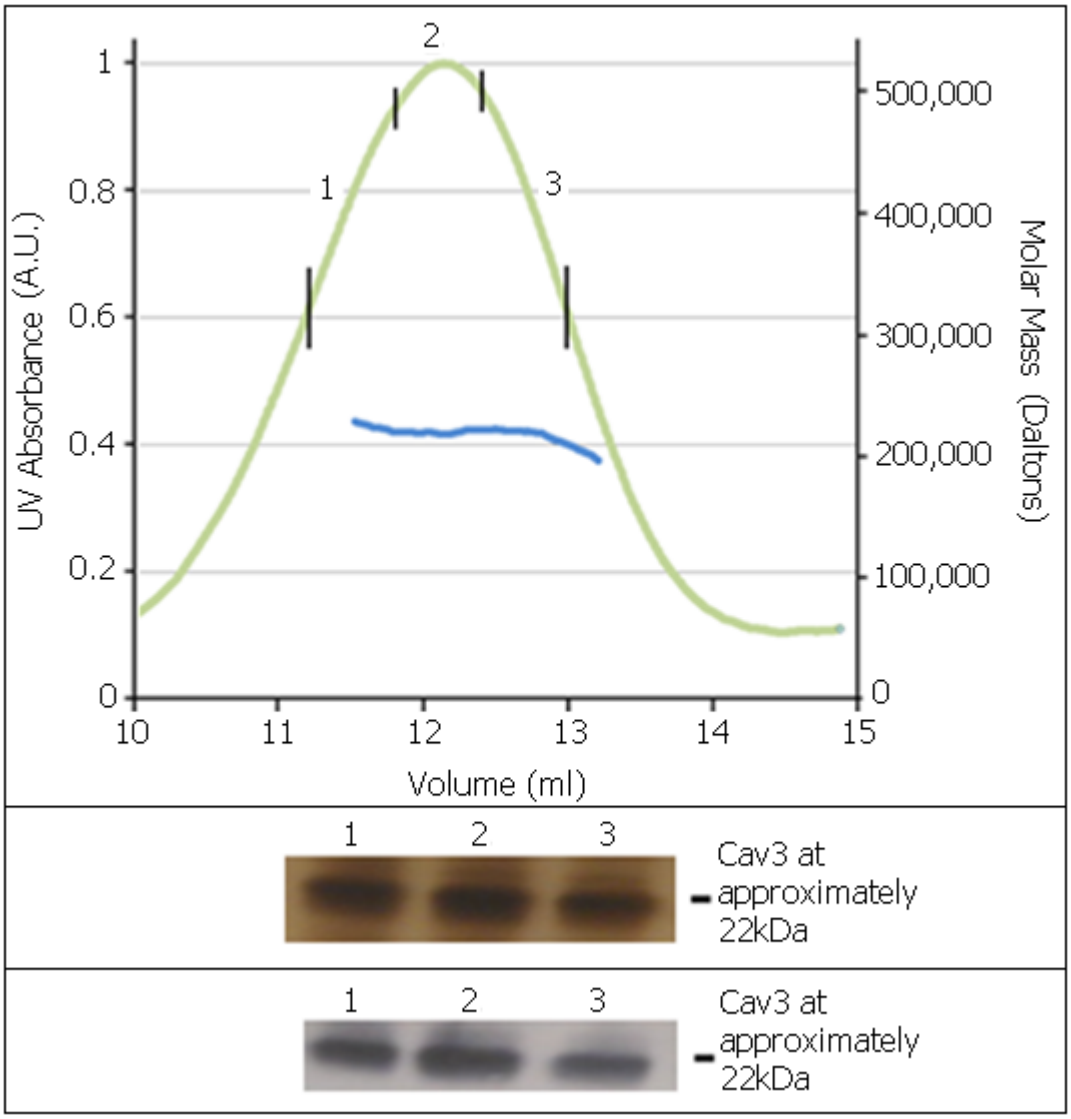

Figure 92: Multi-angle laser light scattering of Cav3.
Multi-angle laser light scattering of the soluble Cav3. **A**: the UV trace (green) shows the elution profile of Cav3. The measured molecular mass (blue) shows that Cav3 eluted as a 200-220kDa protein, indicating that Cav3 is in an oligomeric form. **B**: Samples of the peak fraction were analysed by SDS-PAGE and silver stained to confirm the presence of Cav3.

C: Western blotting (anti-MAT-tag) confirmed the presence of Cav3. The numbers denote fractions.

The purified Cav3 eluted in a protein peak with a corresponding molecular mass of 200–220kDa as shown in Figure 92 indicating that it is in its oligomeric form. Given that Cav3 is a membrane protein, part of this mass prediction will likely include the contribution of the detergent. Previous reports suggest that a detergent can contribute a factor of between 0.3-1.5 to the observed mass of a protein (Gennis, 1989). During this PhD, Cav3 was regularly observed to migrate at approximately 22kDa, suggesting that the 200-220kDa observed here via MALLS is composed of either 9 or 10 monomeric subunits. However, migration on SDS-PAGE is not exact. The theoretical monomeric size of Cav3 is approximately 19kDa, therefore making, for example a 9-mer (as we believe it is, and is discussed in more detail in the subsequent section – symmetry), 171kDa. This suggests that the detergent has contributed a factor of approximately 0.2 to 0.3 to the mass observed by MALLS. This figure is at the lower end of the estimation made by Gennis; however, given that only a portion of Cav3 is believed to be associated with the membrane, then a limited amount of bound detergent is perhaps not unexpected.

As outlined in the introduction to this thesis, there are multiple different reports for the size of caveolin oligomers ranging from 200 to 600kDa. The evidence would seem to point towards the likelihood of a range of different sized oligomers existing, and that the varied experimental isolations employed have isolated different forms; indeed, many different cell lines (CoS-7, MDCK, *E.coli*, Sf9), species sources (human, dog, rat, monkey), caveolin isoforms (Cav1, Cav2, Cav3) and tissue types (e.g. lung, kidney, skeletal muscle) have been studied. Further, many different purification strategies have been employed. The possibility that different isoforms of caveolin, in specific tissue and cell types may oligomerise differently is interesting; indeed, as described in the thesis introduction, reports of isoform specific hetero-oligomerisation and homo-oligomerisation (Scheiffele et al., 1998; Scherer et al., 1997; Song et al., 1997; Volonte et al., 2008) highlight the potential difference pertaining to oligomerisation mechanisms that exist between the different isoforms. Interestingly, despite the range of oligomers sizes reported, the repeated presence of 200kDa, 400kDa and 600kDa forms, may point to the possibility of multiple oligomers forming higher-order oligomerisation, with the 200kDa oligomer being the primary subunit. It is, therefore, intriguing that the Cav3 oligomer isolated here has been determined to be 200-220kDa. Indeed, as mentioned in the introduction to this chapter, the figures within the Tang *et al.,* paper clearly show that the rat Cav3 isolated *via*

sucrose gradient fractionation migrated predominantly to the same fraction as the 200kDa marker (Tang et al., 1996). In addition, they also observed a trace amount of a 443kDa protein oligomer, which was not observed here.

Individual fractions of the sucrose gradient in which Cav3 was purified here were independently analysed by multi-angle laser light scattering and *via* TEM with only the 200-220kDa oligomeric form ever being observed. The isolation of a single oligomeric form of Cav3 was encouraging to advance these studies to investigate the structure.

3D structure of Cav3

Characterisation of sample

Very little is known about caveolin structure for any of the isoforms, particularly Cav3. The current predicted conformation and membrane topology of caveolin oligomers has not been experimentally determined, but instead has been inferred from a series of smaller less structurally focused experiments. Certain regions have received structural characterisation; however, many of these have been on small isolated regions. To date, there has not been an experimental structural characterisation for the complete full-length Cav3 oligomer.

An aliquot of the peak fraction of purified Cav3 was negatively stained and examined by transmission electron microscopy with an example area of a field of Cav3 particles shown Figure 93. As can be seen from the micrograph, the sample is relatively homogeneous in agreement with the biochemical data identifying only one oligomeric form of Cav3.

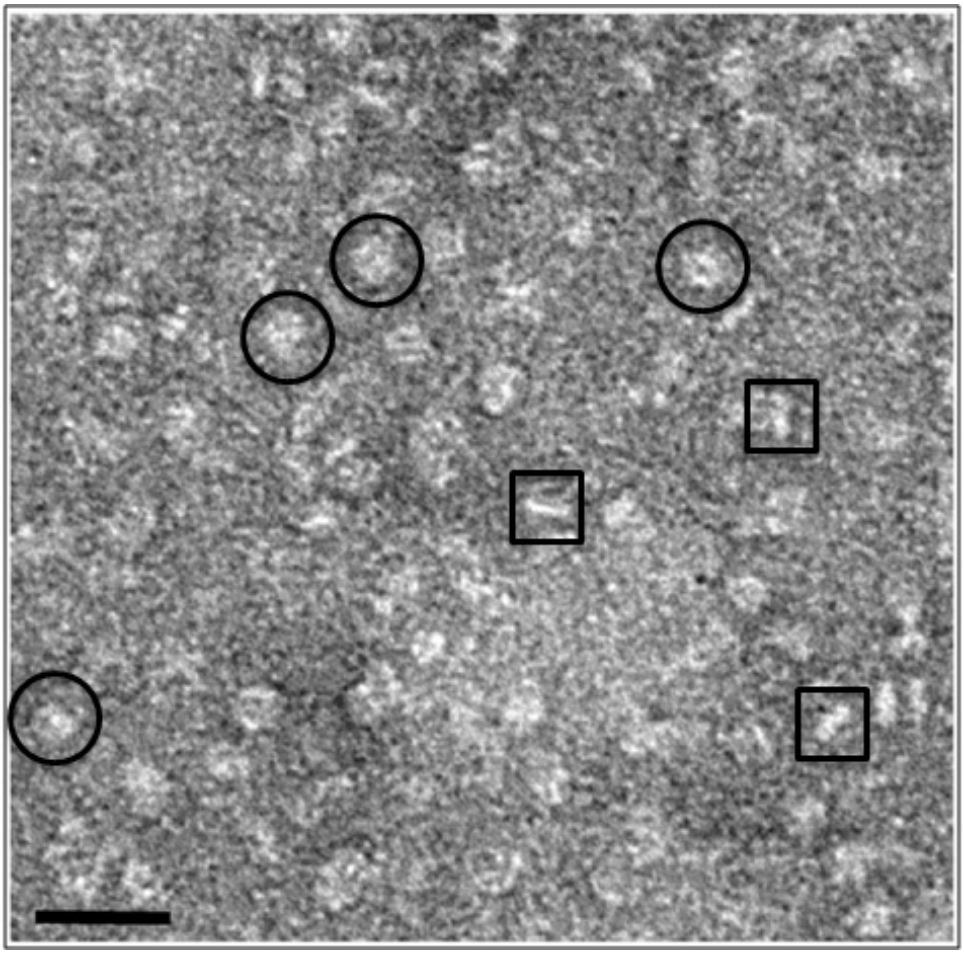

Figure 93: An example area from a micrograph of negatively stained Cav3.
An aliquot of the peak fraction of purified Cav3 was negatively stained (2% w/v uranyl acetate) and examined by transmission electron microscopy. Protein is visualised as the white densities. Several distinct views of Cav3 are present including a circular-shaped complex ~120-150Å in diameter (circled particles) and rod shaped particles measuring 120–150Å in length and ~35-50Å thick (boxed). It can also be seen that purified Cav3 forms a mono-disperse homogeneous population of particles. Bar= 50nm.

As can be observed in Figure 93, negatively stained Cav3 was both mono-disperse and showed multiple and distinct views of the complex; both of these factors are encouraging for single particle analysis using the angular reconstitution method.

Cav3 oligomers were selected from the micrographs and the dataset was CTF corrected, centred and aligned employing established programmes within the EMAN image processing software suite (Ludtke et al., 1999). Random conical tilting was not required as reference-free class averaging of the raw dataset revealed that a range of orientations of Cav3 oligomers had been captured (see Figure 94, panel A), and a good coverage of the 3D space was achieved, as shown in the Euler Triangle (Figure 94, panel B), thus 3D reconstruction using the common-lines method was achievable.

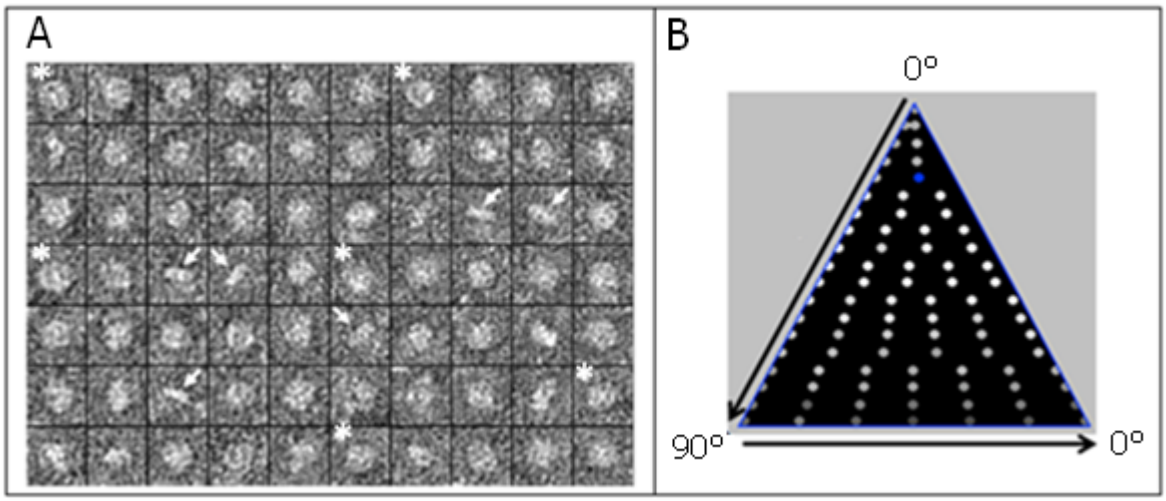

Figure 94: A montage of selected raw particles used in the 3D reconstruction and the asymmetry triangle illustrating good sampling of a range of different orientations of the Cav3 oligomer.

Many different orientations of the same particle exist. **A:** The asterisks highlight particles with a distinct circular shape, ~160-170Å in diameter with a central density; arrows point to Cav3 complexes that are rod-shaped. **B:** The asymmetry triangle represents the Euler angle distribution of the class averages. The positioning of the dot represents a unique combination of Euler angles (ϕ, θ, and ψ), and the intensity of the dot indicates the number of particles used in that class average. As can be seen, a good coverage of three-dimensional space was achieved by sampling over a range of Euler angles.

Reference-free class averaging (#particles in class average=85) generated distinct orientations of the Cav3 complex. Three of the more distinct views (circular and rod-shaped views of the complex) are shown in Figure 95.

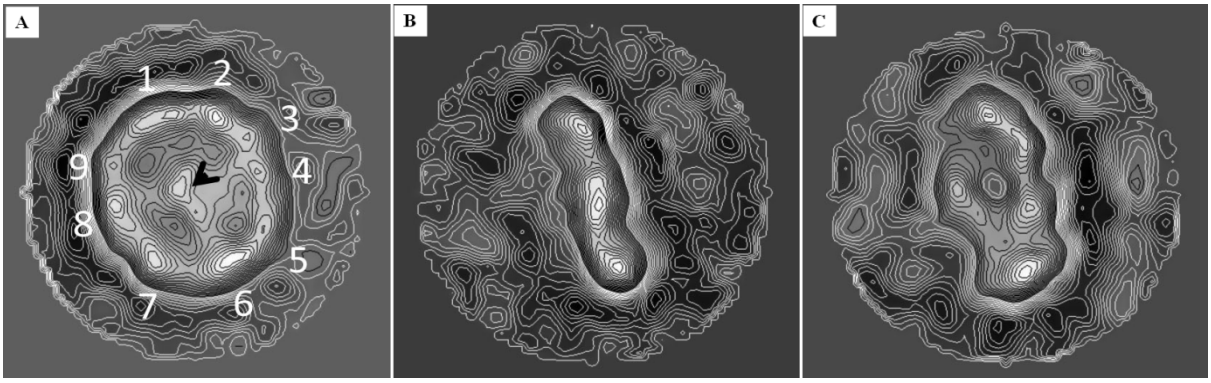

Figure 95: Contoured projection maps of three reference-free class averages of Cav3.

A: A contoured projection map of a reference free class average (#particles in class average=108) of Cav3 exhibiting a ring of protein resolved into nine domains (numbered 1 to 9) with a diameter of ~165Å surrounding a central region of density indicated by the

arrow head. **B:** Class average (#particles in class average=106) of Cav3 that is rod-shaped ~165Å long and ~40Å thick. **C:** This class average (#particles in class average=96) shows a partial side-view of the complex. Box size = 326x326Å.

Figure 95 (panel A) shows an example reference-free class average presenting the circular view of Cav3 seen in the raw images. The protein density, which is white under negative staining conditions, can be seen to form a ring around the perimeter of the complex with an overall diameter of ~165Å. The outer rim of protein in this view is connected to a central density. Interestingly, the outer perimeter of the image appears to be resolved into nine protein domains, which may suggest that the oligomer is composed of nine individual monomeric subunits; a figure that fits with the mass determination of a Cav3 oligomer of 200-220 kDa evidenced by the MALLS data above. Panel B shows what appears to be a rod like class average, which likely represents a side view of the protein in panel A. Panel C shows what is likely a partially tilted side-view of panel B.

Symmetry

To investigate Cav3 oligomerisation, rotational cross-correlation analysis was employed to determine the symmetry features of the raw particles. A reference-free class average corresponding to a circular view of the complex was rotated in increments about the z-axis as described in the Materials and Methods (section Symmetry analysis – Cross correlation coefficient). Cross-correlation of each of the rotated images with the original un-rotated 2D average found regular peaks at 40 degree intervals as displayed in Figure 96, which would correspond to a complex with a nine-fold rotational symmetry.

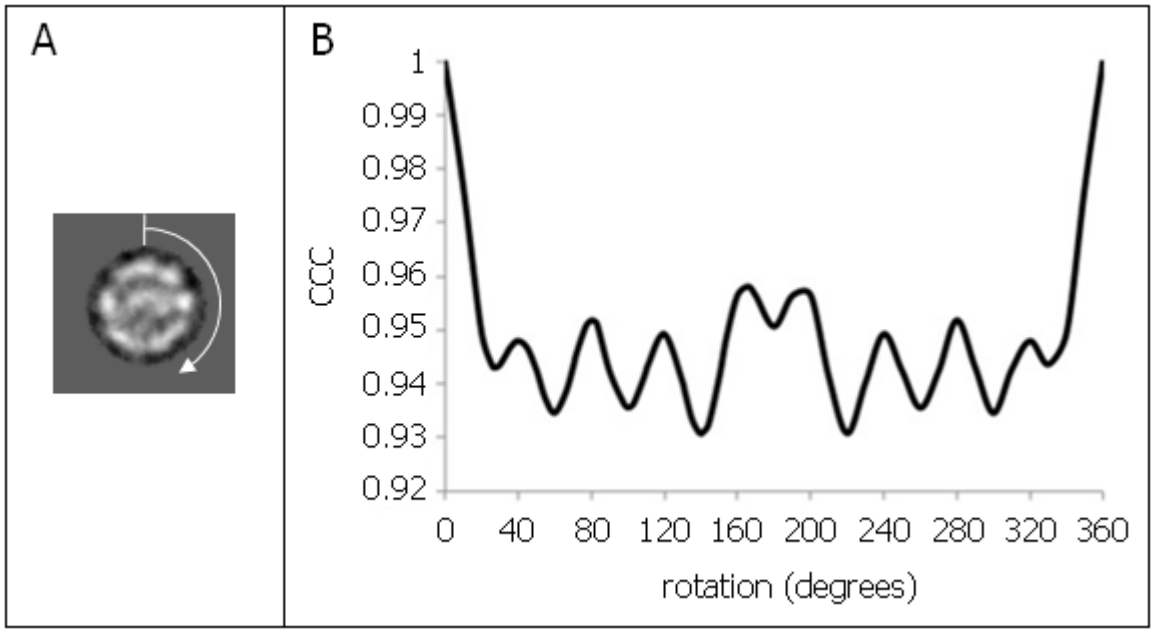

Figure 96: Symmetry determination of Cav3 - Correlation coefficient plotted against the angle of rotation.

A: To investigate the symmetry of the purified Cav3 oligomer, rotational cross-correlation analysis of reference-free class averages of Cav3 (#particles in class average=91) was carried out using the SPIDER software (Frank et al., 1996). A class average presenting a circular view of the complex was selected and rotated around the z-axis in increments including those corresponding to C3, 4, 5, 6, 7, 8, 9, 10, 11, 12, 13, 14 symmetries (i.e. 120°, 90°, 72°, 60°, 51°, 45°, 40°, 36°, 33°, 30°, 28°, 26° respectively) through 360 degrees. **B**: Each of the rotated 2D images was compared to the original un-rotated class average and the cross-correlation coefficient plotted against the angle of rotation.

As can be seen in Figure 96, clear peaks of high correlation were identified at 40 degree intervals, which would correspond to a complex with C9 symmetry. In order to support the suspected C9 symmetry, a further test, using Oval plot (an ImageJ plugin) (Abramoff et al., 2004), was completed on the reference-free class average, a circle was positioned equi-circumferenced roughly in the middle position of the outer ring of protein density. The greyscale and intensities were plotted as a function of angle.

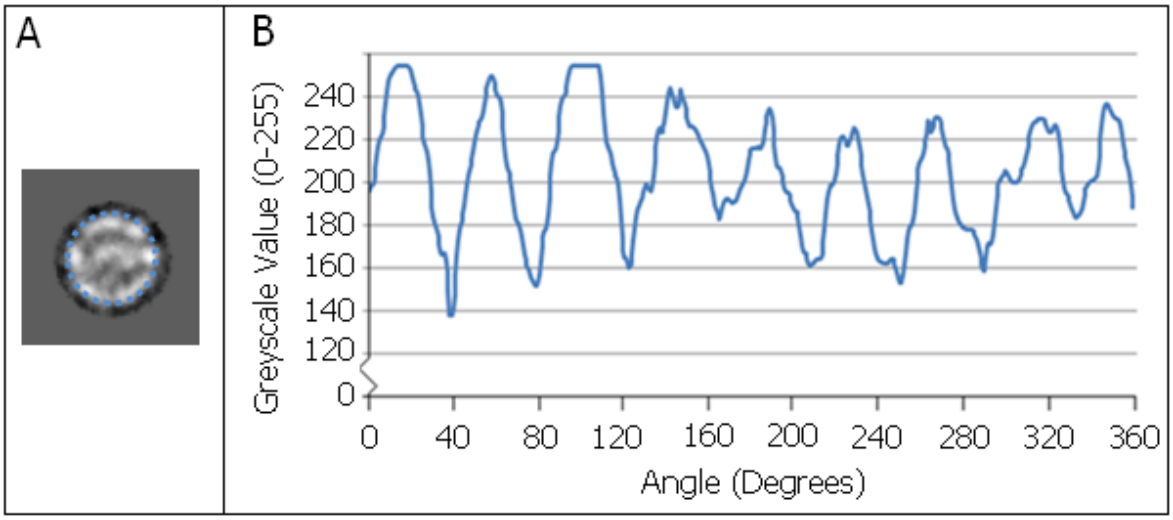

Figure 97: Symmetry determination of Cav3 – Oval plot

A: To investigate the symmetry of Cav3, the greyscale was measured along the perimeter of a circle (dashed blue ring) placed upon a reference-free class average (#particles in class average=91). **B:** The greyscale value was plot as a function of angle. Peaks of white were observed at approximately 40° intervals.

As can be seen in Figure 97, nine grey scale intensity peaks were also observed at roughly 40 degree intervals which would be again consistent with a protein exhibiting nine-fold rotational symmetry.

Final 3D volume of Cav3

Given that the biochemical data indicated that the Cav3 complex had an approximate molecular mass of 200-220kDa, coupled with the symmetry analysis, it seemed reasonable to refine the 3D structure using C9 symmetry producing a final model that is shown in Figure 98.

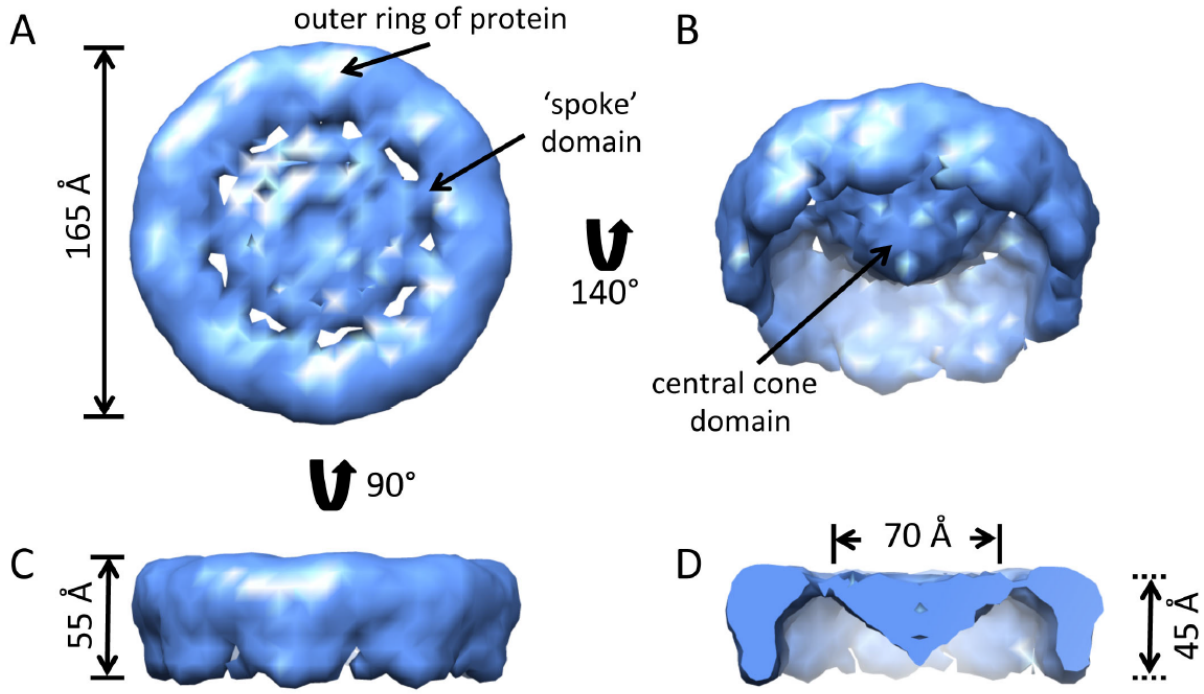

Figure 98: Final 3D volume of Cav3 refined in C9 symetery.
The 3D structure of Cav3 is toroidal in shape with a diameter of ~165Å refined in C9. The orientation of the complex in (**A**) reveals what we have termed the base of the Cav3 complex showing that it is formed by an outer ring of protein ~40Å wide. The outer protein rim is connected to a central density domain *via* 'spoke-like' bridging densities. **B:** Rotation of this view 140° about the x-axis presents a partial view of the underside of the complex providing details of the interior of the oligomer showing that the central protein density extends away from the base of the complex and is 'cone-shaped' in appearance, revealing that the complex is bowl-shaped. **C:** A side-view (orthogonal to the orientation in panel A) illustrating that the overall height of the Cav3 nonamer is ~55Å and that the upper surface (base) of the complex is relatively flat. **D:** Removal of the front portion of the complex when viewed from the side reveals the dimensions of the central 'cone' density with a base of ~70Å diameter and height of ~45Å. The surface of the model has been rendered to encompass a complex of 220kDa.

Presented in Figure 98 is the 3D volume of Cav3 refined with C9 symmetry applied. The Cav3 oligomer can be seen to be toroidal in shape (panel A) with an outer rim of protein connected to a central domain *via* spoke-like densities (panel A). The interior of the complex (panel B) shows features of a central 'cone-shaped' density that is approximately 45Å in depth and 70Å wide (panels D). The outer rim of the volume extends approximately 55Å downwards from what appears to be a relatively flat base (panel C).

Resolution and reliability of the 3D Cav3 model

The resolution of the final 3D model was analysed using Fourier shell correlation. The particle dataset was randomly split into two separate sub-sets with a volume calculated for the two sub-sets following established procedures (Bottcher et al., 1997).

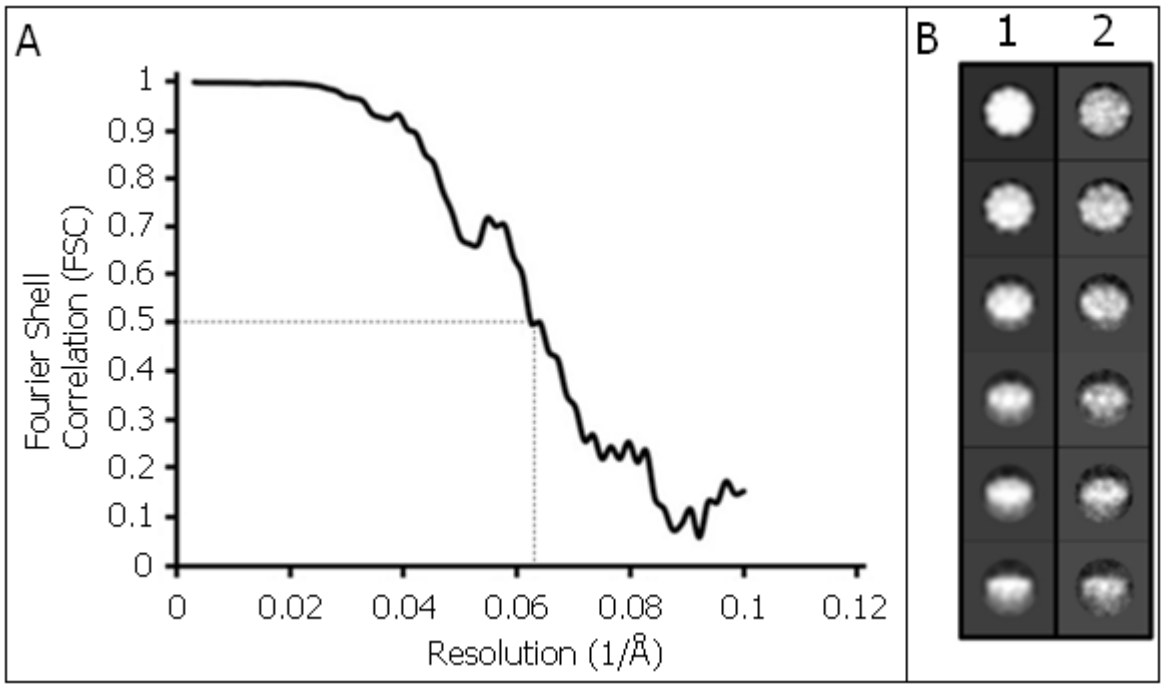

Figure 99: Fourier shell correlation plot.

A: Fourier shell correlation plot illustrating that at a cut-off of 0.5 the resolution of the Cav3 nonamer is ~17Å. **B:** Column 1 presents back-projections of the final 3D volume with the corresponding class-averages in column 2. A comparison of the images in each row finds a good correlation between the two (box size 326x326Å).

A Fourier shell correlation plot (FSC) is shown in Figure 99 (panel A) illustrating that the resolution estimate of the 3D C9 EM Cav3 volume approaches ~17Å and thus is at the limit for negative staining. A good correlation between projections of the final 3D volume and class averages can be seen in Figure 99 (panel B). The nine-lobes forming the outer ring are discernible in the class averages (e.g. top three rows) as well as the central density. Furthermore, the side views in the bottom two rows show a good match to the reference-free class average shown in Figure 95 (panel B) illustrating that the features of the raw data (Figure 94), reference free-class averages (Figure 95), and the back-projections of the final 3D model of Cav3 (Figure 99) are robust.

The C-terminal domains of Cav3 form the central cone-shaped density

Following established methods (Walsh et al., 2009a) the purified Cav3 was incubated with NiNTA-gold (~1.8nm diameter). The Cav3 was expressed with a C-

terminal MAT-tag, which if sterically exposed within the oligomeric structure would bind the NiNTA-gold conjugate. The Cav3 sample was incubated with the NiNTA-gold and an aliquot taken for negative staining and examination by TEM. Under these conditions the electron dense gold is visualised as a black density whereas the protein is white. The position of the bound gold will therefore give an indication of the position of the C-terminal domain within the 3D volume.

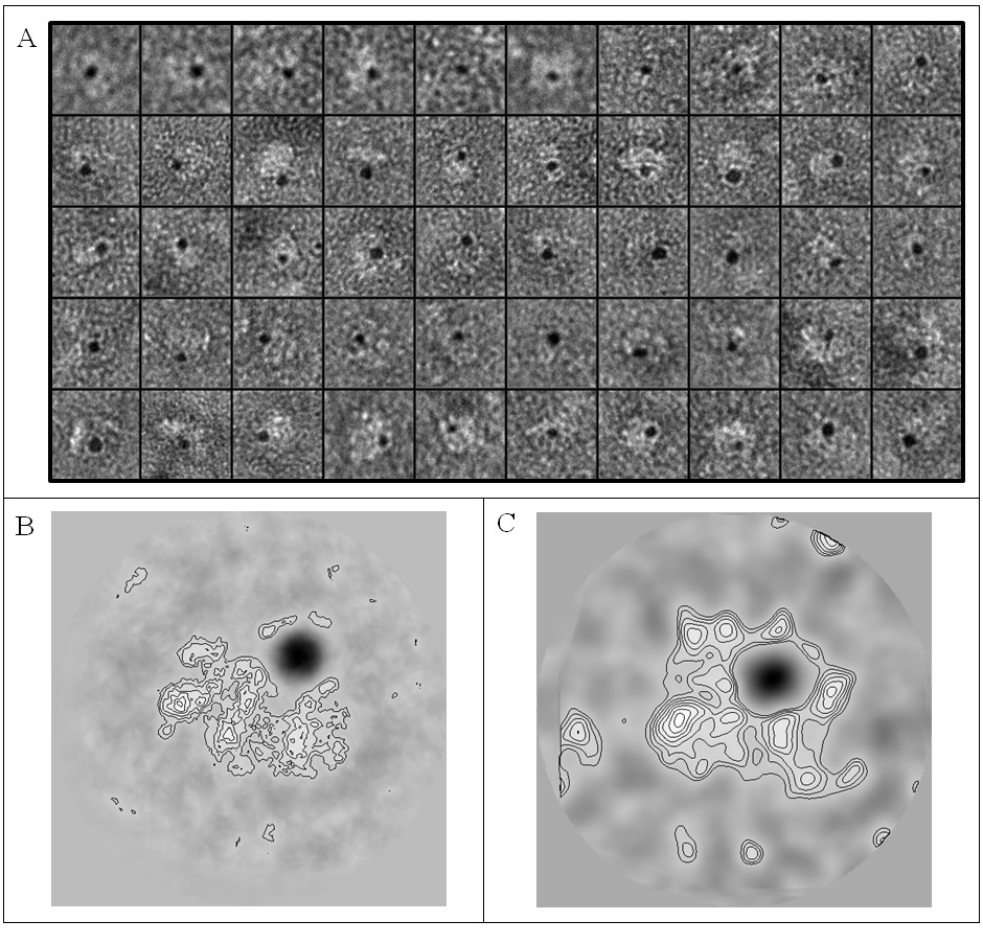

Figure 100: Labelling of the C-terminal domain of Cav3 indicates that it forms the central cone density within the 3D EM volume.

A: A montage of negatively stained Cav3 oligomers after incubation with NiNTA-gold. The presence of a MAT-tag at the C-terminus of Cav3 binds the NiNTA-gold conjugate. The gold is visualised under these conditions as electron dense (black) particles. The Cav3 protein (white) is decorated with only one NiNTA-gold conjugate. The diameter of the gold is ~1.8nm and thus in some of the examples it appears that more than one label is binding as the electron dense particle is ~4nm. However, this would indicate that the binding sites are juxtaposed within the EM volume. **B:** A class average (#particles in class average=14) showing the rod-shaped view of Cav3 with a gold particle bound to the side. **C:** A class average (#particles in class average=20) of a partial side view illustrating that the gold conjugate is bound towards the centre of the complex. Box size=322x322Å.

Inspection of the individually labelled complexes finds that the electron dense gold particle ranges in diameter from ~2 to 4nm. Since a single gold colloid is ~1.8nm this would suggest that there is a cluster of several gold-conjugates i.e. binding very closely to each other within the Cav3 oligomer. More than 100 gold-labelled Cav3 complexes were selected and subjected to reference-free class averaging. Two distinct class averages composed of 14 and 20 particles were identified, as shown in Figure 100 (panel B and C respectively). The projection map in panel B shows a rod-shaped side view of the complex with the gold label positioned above the protein density approximately over the centre of the long axis (~165Å in length). Panel C is a partial side-view again revealing a single gold domain ~45Å in diameter and thus likely corresponds to more than one bound gold particle.

If the C-terminal domain formed part of the outer rim of protein then it might be expected to observe Cav3 oligomers with multiple gold particles bound around the perimeter of the complex (depending upon the orientation of the oligomer and binding efficiency); instead, we find a single cluster above the centre of the complex suggesting that the C-terminal domains of each monomer unit are located within the central cone region. Given that the C-terminus is predicted to be relatively hydrophobic (as shown in the hydrophobicity plot below – see Figure 102, panel C), as well as housing three palmitoylation sites, it is perhaps not surprising that these domains cluster together. Therefore, this structure provides the first evidence for the C-terminal regions associating to form a domain at the *centre* of the complex i.e. pointing inwards rather than outwards as often proposed in images of predicted caveolin oligomer structure e.g. (Schlegel et al., 1998; Song et al., 1997). Significantly, regions within the C-terminal domain have previously been shown to interact with each other (Song et al., 1997); however, in that study, the researchers concluded that this interaction is likely involved in high-order oligomerisation i.e. the interaction of oligomer with oligomer. Here, our findings would suggest that that the interaction is likely involved in individual oligomer formation.

The Cav3 monomer position within the nonameric model

Although we have determined that the Cav3 oligomer purified and structurally characterised here is likely composed of nine individual monomers, with the C-terminus in the centre of the structure. Due to the low-medium resolution afforded by EM, it is not possible to determine any secondary structure features. However, an attempt to 'segment' the 3D model into the sections to represent the individual monomers using an USCF

Chimera plugin called Segger was utilised, in order to roughly predict the volume corresponding to an individual monomer (see Figure 101).

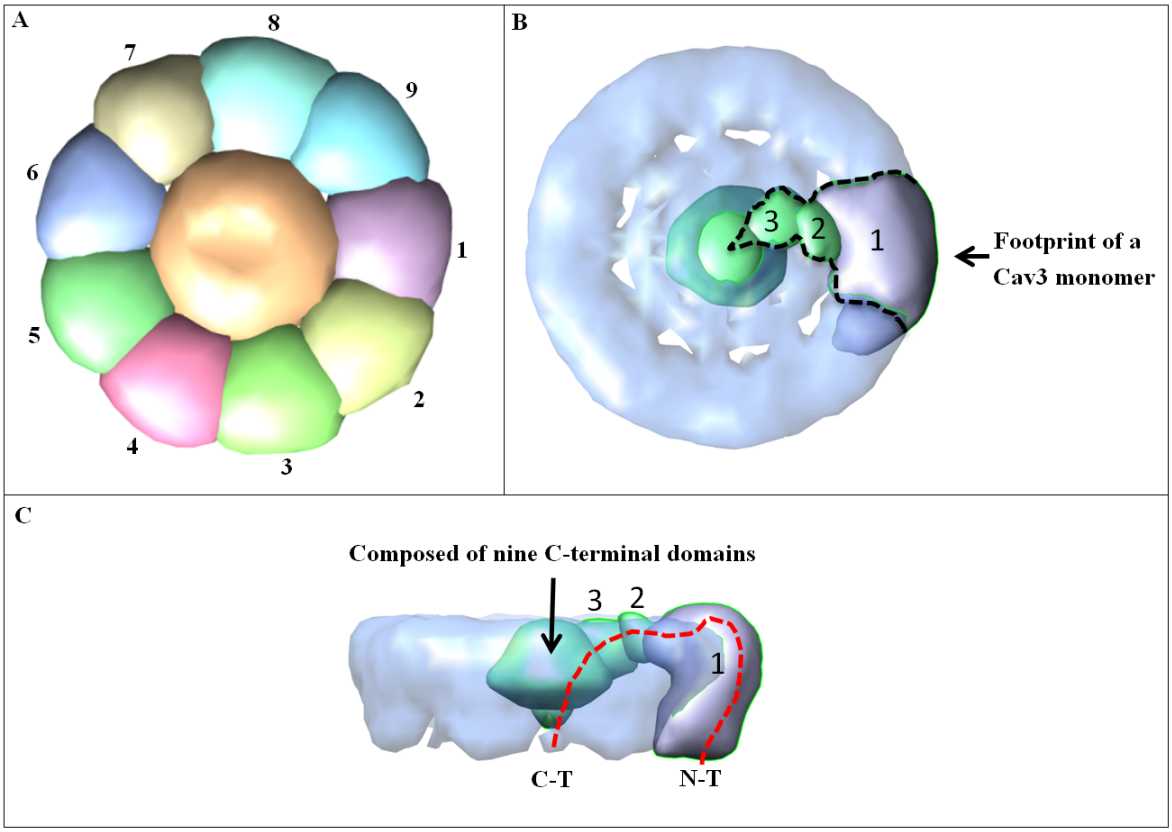

Figure 101: Predicted monomer position within the 3D Cav3 nonamer model.
A: The outer ring of the complex and the bridging unit were segmented into nine separate domains. Segger could not completely computationally resolve the central cone domain. **B:** Segmentation of the Cav3 nonamer (light blue, transparent) into nine protein domains using Segger allowed the approximate identification of a monomer of Cav3 (green and purple regions; opaque). The central cone region is shown in turquoise. The outer rim region is shown in purple (labelled 1). The domain that bridges these two regions is shown in green (labelled 2, 3). The dashed black line outlines the footprint of a monomer. **C:** A side view of **B**, in which the possible position and orientation of the proteins N- and C-terminal (N-T, C-T) domains has been highlighted (dashed line, red).

Segmentation of the nonamer into approximate monomeric volumes allows an approximate delineation of the volume occupied by an individual monomer. For example, knowing that the C-terminus is found centrally, and that the bridging region is sufficient for a single pass of protein alone, indicates that the N-terminus is likely within the outer rim domain.

Membrane topology

Cav3 is an unconventional membrane protein, in that it does not completely pass through the membrane, but instead only partially passes through, resulting in both the N- and C-terminus being cytosolic (Dietzen et al., 1995; Dupree et al., 1993; Sargiacomo et al., 1995). To investigate the possible orientation of our model in the membrane, the secondary structure of Cav3 was first predicted. Knowledge of the secondary structure can assist in determining the likely topology of a protein. For example, α-helices are generally associated with membrane spanning regions. A variety of different secondary structure prediction algorithms exist. We employed the PSIPred prediction algorithm here.

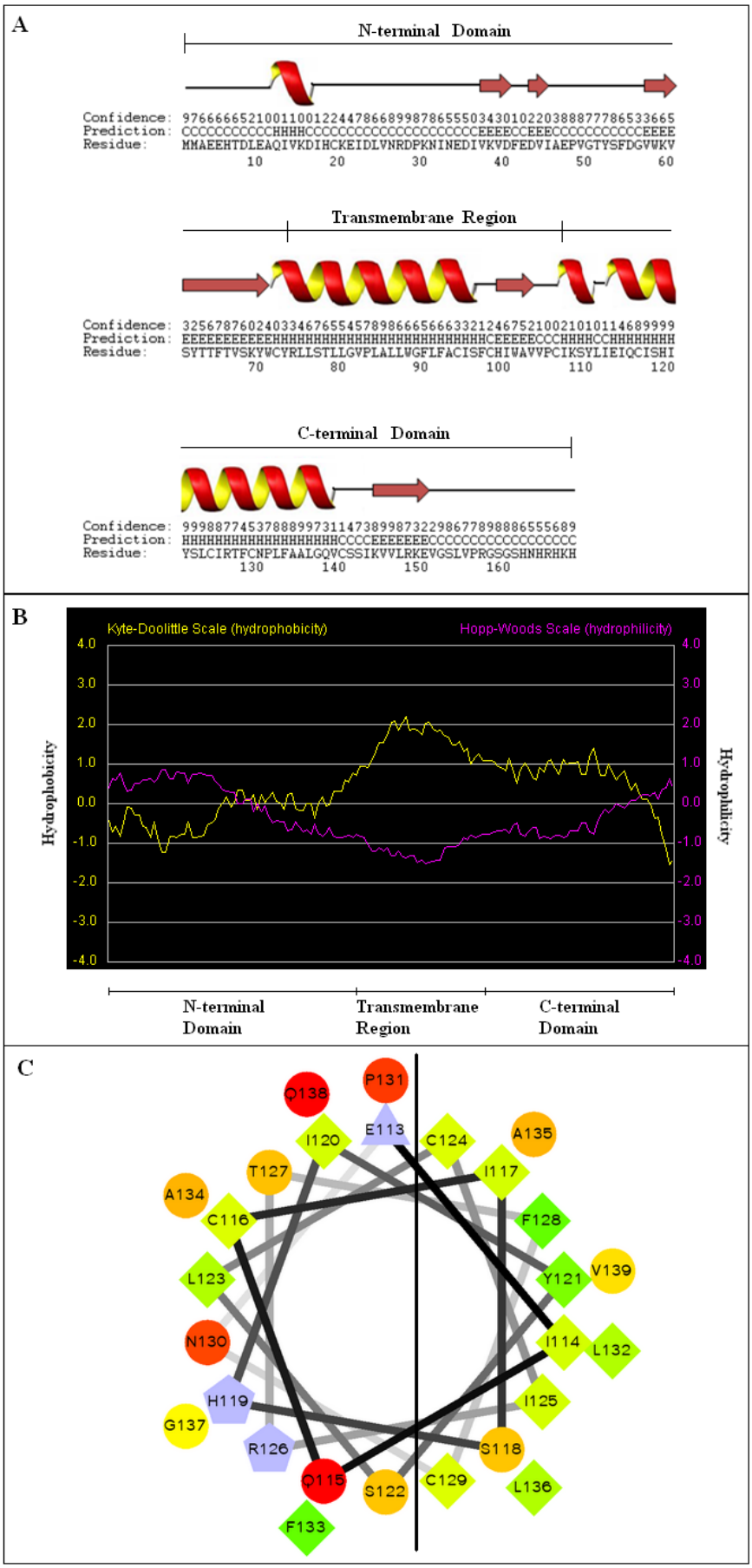

Figure 102: Secondary structure and hydrophobicity prediction of Cav3.

A: Secondary structure was predicted using PSIPred. Note the presence of two predicted α-helices each over 25 residues long. The first helix (72-97) is within the region believed to be inserted in the membrane. The second helix (113-139) forms part of the C-terminal region and contains two of the three palmitoylation groups involved in membrane association. **B:** Kyte-Doolittle hydrophobicity plot (yellow) (Kyte and Doolittle, 1982) and Hopp-Woods hydrophilicity plot (pink) (Hopp and Woods, 1981) showing that the predicted transmembrane region is, as expected, the most hydrophobic region within the protein (and least hydrophilic), thus it is the region most likely to be inserted into the membrane. In contrast, the proximal end of the N-terminal domain, and the distal end of the C-terminal domain are predicted to be more hydrophilic than hydrophobic, indicating that they are not likely to be inserted into the membrane. **C:** Helical plot for the region corresponding to the predicted second α-helix (residues 113-139) used to illustrate the 3D arrangement of residues within α-helices that would not necessarily be adjacent in random coil conformation. Note the clustering of hydrophobic residues on the righthand side (green, light green), and the clustering of hydrophilic residues on the left hand side (Red, orange, yellow). Helical plotting tool available at http://rzlab.ucr.edu/scripts/wheel.

The region proposed to form part of the transmembrane is believed to be either 53-107 or 75-107. This prediction has not been experimentally derived, but has instead come from a combination of secondary structure prediction/determination and knowledge of other key areas and their functions. Prediction of secondary structure based upon primary sequence can differ between algorithms, therefore, we employed both PSIPred and JPred here (only PSIPred data is shown here) to predict protein structure. PSIPred found that two α-helices of over 25 residues in length were predicted. The first helix (residues 72-97) is at the approximate region predicted to be within the transmembrane. In addition, previous NMR experiments for Cav1 that have shown that residues 97-129 (equivalent to 70-102 in Cav3) supports the presence of this α-helix (Lee and Glover, 2012). The second helix (113-139) is at the approximate location of the C-terminal membrane attachment domain (residues 108-123), and is known to contain two of the palmitoylated residues involved in membrane association. All other regions are predicted to be random coil or β-sheet. JPred predictions generally supported PSIPred predictions, although they extended the extent of the first α-helix proximally to residue 55 (not shown), which would support the evidence for an amphipathic α-helix associating, but not inserting into the membrane, as suggested by Kirkham and co-workers (Kirkham et al., 2008). Despite this difference, the two prediction methods generally showed a similar prediction.

As expected, hydrophobicity and hydrophilicity plots predict a region of notably higher hydrophobicity corresponding to the region of Cav3 believed to be the transmembrane region (Figure 102, panel B). Interestingly, the proximal region of the C-terminal domain that is predicted to form an α-helix is also predicted to be relatively hydrophobic in nature, suggesting that it may be membrane associated. A helical plot for this region (panel C) finds that the hydrophobic residues cluster on one side of the helix, whereas, the more hydrophilic residues are on the opposite side, suggesting that this region is more likely *associated* with the membrane rather than inserted. This is plausible, given the presence of palmitoylation groups in this region.

In summary, although the exact region thought to make up the transmembrane region is not known, the general consensus is that it is somewhere between residue 53 and 107 and contains regions that both insert or associate with the membrane. The predicted presence of an α-helix here i.e. the first helix at 72-97 (Figure 102) fits well with the consensus view, as well as the NMR structural studies by Lee and Glover (Lee and Glover, 2012). It is therefore likely that this first α-helix is inserted into the membrane. The second predicted helix (113-139) forms at the proximal region of the C-terminus, a region believed to be involved in membrane association, and which contains two of the palmitoylation groups believed to be involved in membrane association. It is possible that this helix equates to the bridging region shown in Figure 101 (panel A, green), and that it associates with the membrane in an amphipathic manner.

Incorporation of Cav3 into large uni-lamellar vesicles

To further investigate the orientation of the Cav3 oligomer within the lipid membrane, Cav3 was reconstituted into large uni-lamellar vesicles (LUVs).

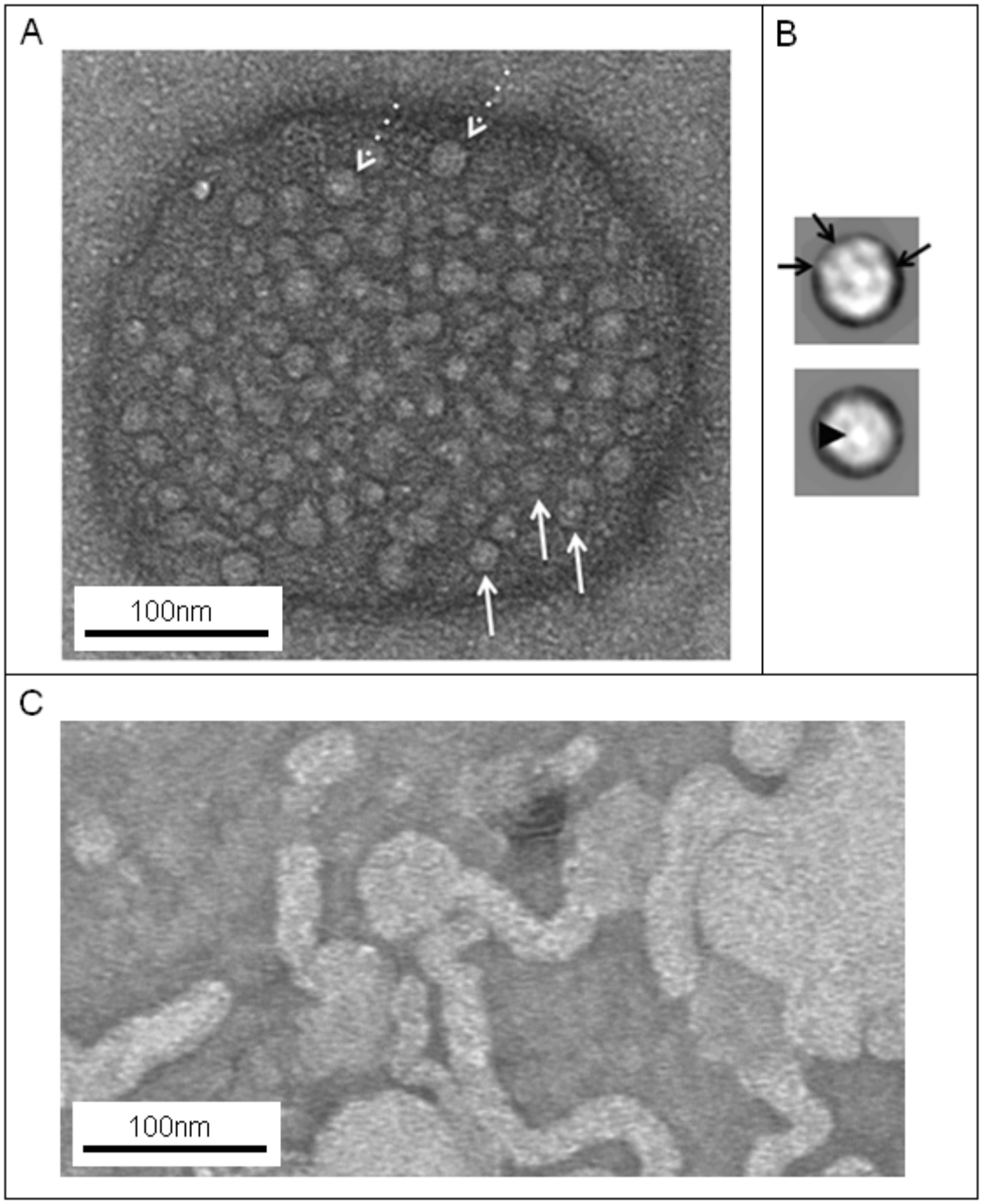

Figure 103: Reconstitution of Cav3 into large uni-lamellar vesicles.

Cav3 was reconstituted into large uni-lamellar vesicles (LUVs) at a mass ratio of 1:75 (Cav3:Lipid) following a modified version of the protocol described by Geertsma (Geertsma et al., 2008). **A**: A sample proteoliposome measuring ~300nm in diameter. Note the presence of multiple Cav3 oligomers within the vesicle (white arrows; ~166Å in diameter). Dashed white arrows indicate slightly larger complexes (~200Å) that were occasionally observed which may have formed as a result of the reconstitution process. **B**: Reference-free class averages (top, #particles in class average=44; bottom, #particles in class average=54) showing circular views of Cav3. Black arrows indicate what appear to be feet like projections. Black arrowheads point to a central density that is likely the C-

terminal cone. **C:** Control LUVs created using the same protocol, but without the addition of Cav3. A range of different shapes and sizes of vesicles were formed with branches extending outwards.

As can be seen in Figure 103 (Panel A), Cav3 has been successfully reconstituted into LUVs. These vesicles are spherical in shape and bear no resemblance to the control lipids in which Cav3 is not present (Figure 103, Panel C). The control lipids display a range of different shapes and orientations including globular and thread like branches, none of which were observed when Cav3 was present. Cav3 predominantly displays a circular view, suggesting that Cav3 orientates itself into the vesicle in a consistent orientation. The dimensions of the circular view fit well with the circular view of our proposed model described in Figure 98. Furthermore, the class averages (Figure 103, panel B), show what appear to be 'feet' like projections (arrows) that extend beyond the bilayer, and a central density akin to the central cone (arrowhead) described above (Figure 98, panel B and D). Thus suggesting that the Cav3 oligomer has inserted into the membrane via the region we have termed the base (Figure 98, panel A).

The complete reconstitution (note that no Cav3 oligomers are present outside the vesicles) further supports Cav3's membrane specificity. Interestingly, however, the vesicles did not contain cholesterol, suggesting that Cav3 inserted into the membrane in a cholesterol-independent manner. Further, the complete presence of spherical vesicles, and the absence of any thread like lipid structures in the LUVs in which Cav3 has been reconstituted suggests that the Cav3 isolated here is physiologically active and capable of both interaction with lipids as well as causing structural changes in lipid morphology. These findings are interesting in terms of the role of Cav3 in caveolae biogenesis and will form the basis of future work.

Based upon the identification of the C-terminal domains as forming the central cone region *via* gold labelling (Figure 100); the hydrophobicity/hydrophilicity plots (Figure 102, B); the likely position of the two helices i.e. the likely transmembrane helix and the putative C-terminal membrane-associated α-helix; and the observations from the proteoliposome reconstitution experiments Figure 103, we propose an orientation of the Cav3 EM volume with respect to the lipid bilayer shown in Figure 104 that places both the C- and the putative N- terminal domains of each contributing monomer within the cytoplasm.

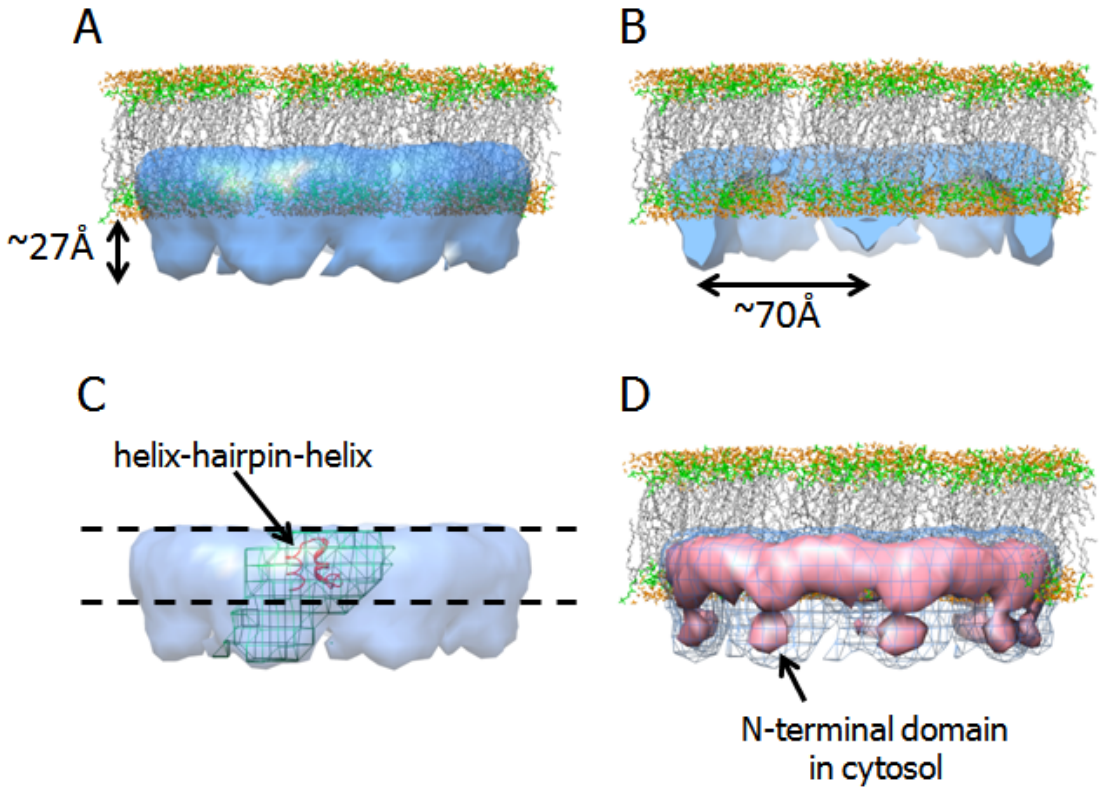

Figure 104: Modelling of the Cav3 nonamer in the context of the lipid bilayer and identification of structural domains.

A: A lipid membrane has been modelled with the Cav3 EM volume placing a portion of the structure to span a monolayer and placing both the N- and C-terminal regions within the cytoplasm. When the structure is positioned this way, approximately half of the complex is extended beyond the membrane. The N-terminus extends beyond the bilayer by ~27Å. **B:** Removal of the front portion of the complex reveals the interior of the oligomer, showing that the base of the central 'cone' density would also be submerged within the lipid layer, but that the apex (~14Å) extends into the cytoplasm so that the hydrophilic N- and C- terminal domains in the Cav3 oligomer are positioned ~70Å apart. **C:** To get a sense of scale, a single helix-hairpin-helix (HhH) motif (extracted from 2BGW, chain A 194-223; note there is no relationship with Cav3) has been crudely modelled within the monomer volume suspected to form the transmembrane region. The dashed lines indicate the putative position of a monolayer of lipid. **D:** Cav3 nonamer displayed at two thresholds. The blue mesh encapsulates a volume corresponding to an oligomer of ~220kDa with the pink surface representation showing the oligomer at a higher threshold illustrating that the outer ring of protein can be resolved into two domains; an upper ring, with nine separate globular 'feet', which we suggest may represent the N-terminus. The lipid co-ordinates were downloaded from the website of Dr Scott Feller, Wabash College (http://www.lipid.wabash.edu/).

The 3D volume is positioned so that it resides within a monolayer and does not completely cross the membrane in agreement with previous studies (Dupree et al., 1993; Monier et al., 1995; Sargiacomo et al., 1995). The predicted membrane topology places a portion of both the central density and the outer rim within the lipid environment which would agree with the predicted locations of the α-helices, and that the C-terminal domain is palmitoylated and thus likely to be hydrophobic and associating within the lipid bilayer. It also fits well with the observed orientation of Cav3 in the LUVs. In order to provide a perspective as to how the internal structure of Cav3 can be correlated to the features of the EM map as well as get a sense of scale, a helix-hairpin-helix (HhH) motif has been approximately positioned within the model at the region tentatively assigned to be the transmembrane region. In addition, as can be seen in Figure 104 (panel D) when the threshold of the model is increased the outer ring of protein is resolved into two domains with nine small spherical densities, we have termed 'feet' extending into the cytoplasm. We propose that the 'feet' correspond to the hydrophilic N-terminal domains of each contributing Cav3 monomer, which would be consistent with the proposed orientation within the membrane. Incidentally, the presence of these regions suggests that there has not been significant flattening of the structure due to the negative stain.

Cav3 interactions and the scaffolding domain

The presence of the N-terminal domain in the outer rim, as well as the likely exposure of the N-terminus as shown in Figure 104 (panel D) agrees well with studies identifying this region as being important for mediating interactions with a host of proteins. For example, recent studies have shown that the voltage-gated calcium channel $Ca_v3.2$ (α_{1H}) associates with Cav3 *via* the N-terminal tail (amino acids 1-54) (Markandeya et al., 2011). However, other regions with the N-terminal domain, namely the scaffolding domain are more commonly predicted sites of interaction e.g. for eNOS (Bucci et al., 2000; Garcia-Cardena et al., 1997; Ju et al., 1997; Michel et al., 1997), K_{ATP} (Davies et al., 2010), G-proteins and Src family tyrosine kinases, (Couet et al., 1997; Li et al., 1996a; Okamoto et al., 1998). Discussed in more detail in the thesis introduction. Although we can predict the likely positions of the C-domain region, the TM region and the N-terminus region, we cannot confidently predict the inner layout of the N-domain region, thus we cannot say whether the scaffolding domain (55-74) is exposed on the external side of the nonamer or concealed on the internal side of the N-terminal domain.

One protein relevant to this PhD, which has been shown by co-immunoprecipitation to interact with Cav3 (Li et al., 2006; Scriven et al., 2005;

Vassilopoulos et al., 2010) and by us here, and has been discussed in more detail in the previous chapter (Chapter 4), is the ryanodine receptor (both RyR1 and RyR2). Further, the last 582 residues of RyR1, which correspond to a region within the transmembrane region of RyR have been shown to interact with Cav3 (Vassilopoulos et al., 2010). Unfortunately, no further information on the region within Cav3 that was involved in the interaction was discerned. Interestingly, as discussed in the previous chapter (Chapter 4), having scanned the RyR sequence (both isoforms 1 and 2) for caveolin binding motifs here, we have found that RyR2 has nine caveolin binding motifs within it, eight of which are found within the transmembrane region (RyR1 had six motifs, of which five were in the region predicted to be the transmembrane region). Given that the scaffolding region is the region involved in many of caveolin's interactions, we have crudely modelled the N-terminal region of Cav3 in proximity to the transmembrane region of RyR within the sarcoplasmic reticulum membrane (Figure 105, A). Further, evidence exists of both sarcolemmal membrane and T-tubule sites of Cav3, and caveolin binding motifs were observed in the cytosolic portion of RyR. Therefore, this possible orientation (Figure 105, B) has also been modelled.

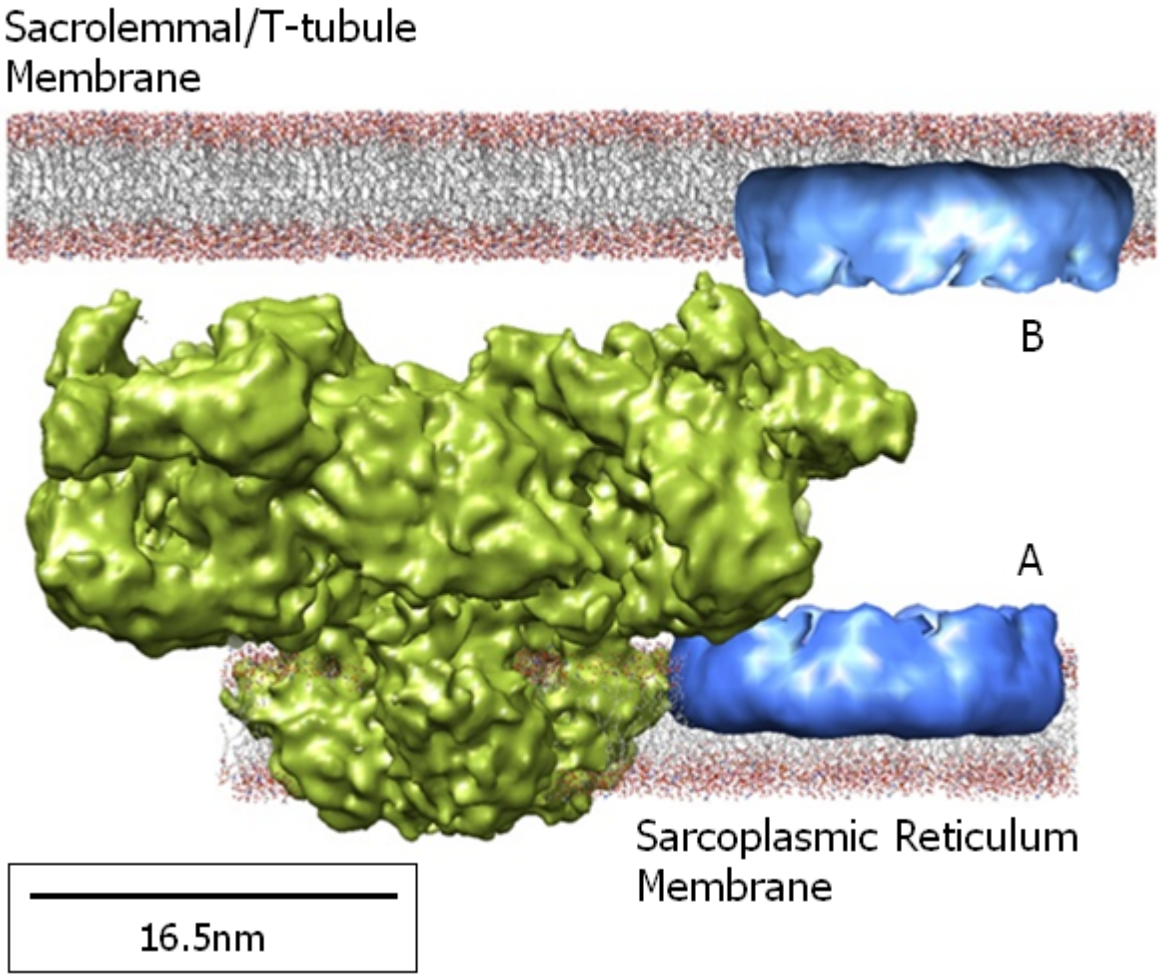

Figure 105: Possible membrane topology and interaction of Cav3 scaffolding domain with RyR1.

Model of the Cav3 nonamer (blue) with the cryo-TEM structure of human RyR1 (green) (Serysheva et al., 1995) relative to both the sarcolemmal membrane/T-tubule (top) and the sarcoplasmic membrane (bottom). The orientation of the RyR1 structure with respect to the Cav3 nonamer within both membranes is purely hypothetical. **A:** The topology within the sarcoplasmic reticulum places the RyR1 transmembrane domain, within in which there are five caveolin binding motifs close to the region suggested here to correspond to the Cav3 N-terminal domain, the most likely candidate region for interaction (bottom). **B:** The two proteins have also been modelled with each protein in a different membrane. The N-terminal region of Cav3 has been placed in close proximity to the clamp region of RyR1, which is a region believed to interact with multiple modulating proteins. The lipid co-ordinates were downloaded from the website of Dr Scott Feller, Wabash College (http://www.lipid.wabash.edu/).

The model in Figure 105 allows a comparison of the dimensions and organisation of the Cav3 EM volume and the cryo-TEM structure of human RyR1 (Serysheva et al., 1995). As can be seen, our predicted sarcoplasmic reticulum membrane topology of Cav3 (Figure 105, A) fits with the known topology of RyR1, allowing the RyR1 transmembrane region - the region which has been shown to interact with Cav3 (Vassilopoulos et al., 2010) and within which we identified 5 caveolin binding motifs - and the N-terminal domain of Cav3 i.e. the region most likely to interact with other proteins, to be in close proximity to one another.

Although our findings here would suggest the presence of Cav3 in the sarcoplasmic reticulum membrane (see Chapter 4), having not checked for markers of sarcolemmal and T-tubule membrane, there remains the possibility that incomplete separation of the sarcoplasmic reticulum from other non-sarcoplasmic reticulum regions may have occurred. Indeed, although there is support for a Cav3 presence at the SR (Li et al., 2006), there is much more evidence for its presence at the plasma membrane. That is not to say that Cav3 is *not* present in the sarcoplasmic reticulum, but instead that further work needs to be done on this area to establish whether Cav3 is found in the sarcoplasmic reticulum; and if so, what the functional significance of its presence there is. Given that Cav3 is known to be present in the sarcolemmal membrane, we have also crudely modelled how these two proteins may orientate with regards to Cav3 presence in the sarcolemmal membrane (Figure 105, B). The Cav3 model's position, although purely theoretical, has been placed where it is, out of respect for symmetry, the size of the cleft between the sarcoplasmic reticulum and T-tubules, and based upon knowledge of putative interaction sites within

both proteins (Meng et al., 2009; Sharma et al., 2006; Sheridan et al., 2006; Wagenknecht et al., 1997).

The proposed Cav3 membrane topology outlined in this chapter places the N-terminal domain (the region that houses the scaffolding domain) on the external side of the protein, providing a potential view of how Cav3 oligomers may provide compartmentalisation of signalling processes with the potential to bind multiple proteins in close proximity. Certainly the specifics of any such interactions need further elucidating. Indeed, as well as functional studies to detect the specific interacting regions within the Cav3 oligomer responsible for an RyR1 interaction, higher resolution models of Cav3 are required in order to pin point such interacting regions within the oligomer with more confidence.

Association of two oligomeric complexes

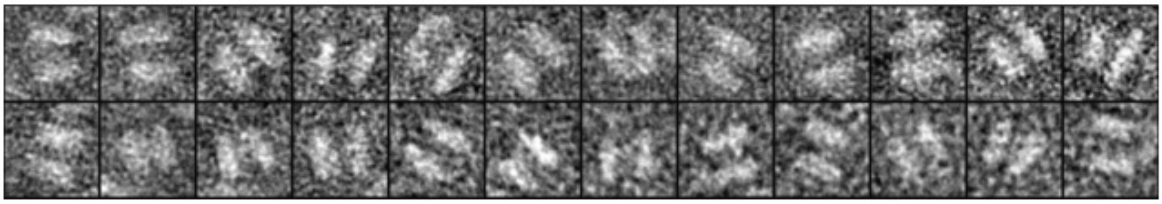

Figure 106: Association of two oligomeric complexes.
Raw particle images of two of the complexes in close proximity to one another.

Although not very prevalent, the association of two oligomeric complexes was occasionally observed (Figure 106). However, although not likely physiologically relevant (given the proposed orientation) it is possible that this represents the association of the hydrophobic base domains. These larger complexes were not detected by either light scattering (Figure 92) or native gel electrophoresis (Figure 91), and are therefore likely to represent a very minor population only picked up by EM, or have formed as a result of glow discharging the EM grid and negative staining procedures. Nonetheless, such potential for oligomer-oligomer association lends support to the claims that caveolin oligomers can combine to together to form high-order multi-oligomeric complexes (Song et al., 1997). Further, an increase in the NaCl concentration resulted in even fewer of these oligomer-oligomer complexes being observed, indicating that this interaction may have been an electrostatic interaction. It should be noted that these oligomer-oligomer complexes were rarely observed and not selected during the particle selection phase of the 3D reconstruction.

5.3.2. 3D structure determination of the N^{1-54} domain

As described in Chapter 1, we successfully purified the first 54 residues of the N-terminal domain (termed N^{1-54}). This region contains approximately half of the previously suspected oligomerisation domain. In order to explore both the size and the structure of this region, a combination of native gel electrophoresis, transmission electron microscopy and multi-angle light laser scattering was undertaken.

Characterisation of sample

An aliquot of the purified N^{1-54} was negatively stained and examined by transmission electron microscopy with an example area of a field of N^{1-54} particles shown in Figure 107.

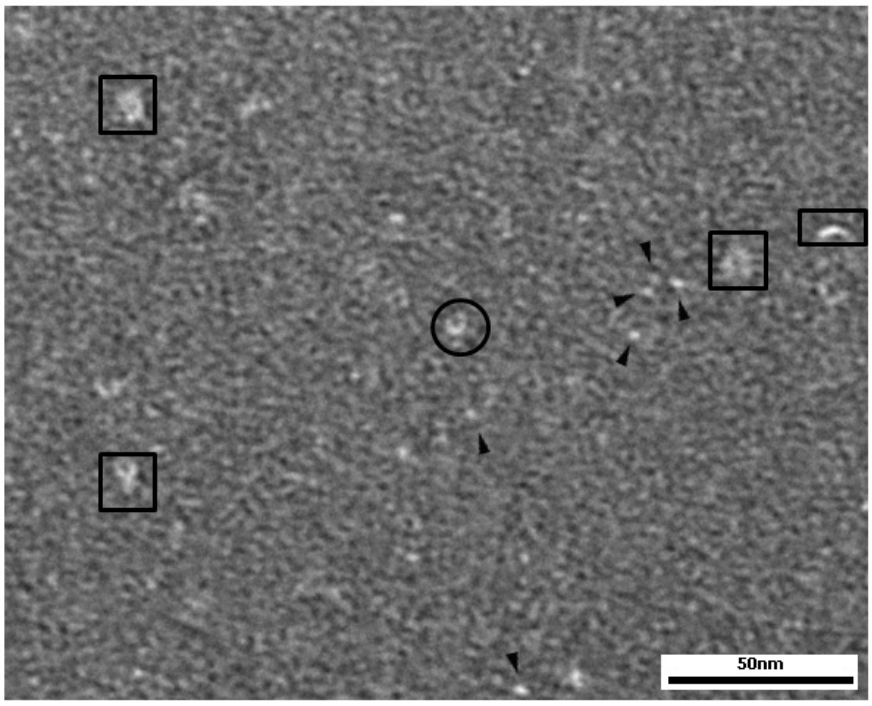

Figure 107: An example area from a micrograph of negatively stained N^{1-54}.
An aliquot of the purified $N1^{1-54}$ was negatively stained and examined by transmission electron microscopy. There is a heterogeneous mix of particle sizes: Particles 2-3nm (20-30Å) across (arrow heads), particles that are ~9 x 3nm (90 x 30Å) in size (rectangle box), and some larger complexes that are between 6 and 10.5nm (60Å x 105Å) in diameter (squares). This would suggest that some degree of oligomerisation has possibly occurred, but such a wide range of different sizes prevents single particle analysis. Given the mass of N^{1-54} monomers existed at 5-6kDa, it is unlikely that they would be observed by TEM.

As can be observed in Figure 107 negatively stained N^{1-54} is heterogeneous with a range of particle sizes. N^{1-54} monomers would be expected to be approximately 5-6kDa in

size, and thus they would not likely be discernible by TEM. The observation of multiple different size and shaped N^{1-54} particles can be interpreted in several ways. Firstly, it is possible that a portion of the N^{1-54} region is involved in Cav3 oligomerisation, but that additional domains/full-length protein are required for the formation of a stable oligomer and that the region 55-151 may have a role in determining the number of monomers that form an oligomer. Secondly, the presence of only a section of the oligomerisation domain may result in multiple polymerisation patterns. There also remains the possibility that the sample is aggregated. In order to characterise the purified N^{1-54} sample non-denaturing (native) gel electrophoresis was employed.

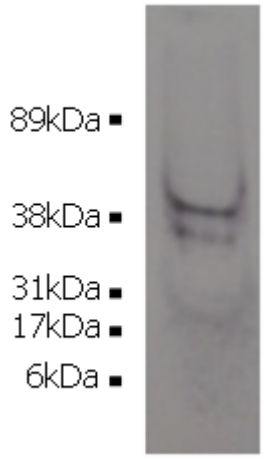

Figure 108: Native gel electrophoresis of purified N^{1-54}.
Purified N^{1-54} was analysed on a 15% native gel and western blotted using an anti-Cav3 antibody to detect the presence of the protein. Multiple bands corresponding to N^{1-54} were observed, migrated at approximately 45kDa, 36kDa and 20kDa. The most prominent band is at ~45kDa.

When examined under denaturing conditions (SDS-PAGE), the $N1^{1-54}$ is found to be 5-6kDa (as discussed in Chapter 2). However, when analysed by native gel electrophoresis, multimers of N^{1-54} are observed that are between 20-45kDa in size. Interestingly, it can be seen that no monomeric N^{1-54} was observed. It would seem that N^{1-54} is likely either in multiple conformations, or that it is aggregated. It is intriguing that an oligomer of ~45kDa would roughly correspond to the mass of nine N^{1-54} domains at 5kDa each. Multiple attempts were made to analyse the molecular mass of purified N^{1-54} by multi-angle laser light scattering. However, although multiple peaks were observed that indicated that the protein was not aggregated, light scattering data did not retrieve any information on the sizes associated with the multiple elution peaks.

Given the success with the full-length Cav3 protein structural studies, and that the N^{1-54} was heterogeneous and not suited to single particle analysis methods, attempts to structurally characterise the $N1^{1-54}$ domain were beyond the time constraints of this PhD.

5.4. Conclusion

We report here the first medium/low resolution 3D structure for human Cav3. The biochemical characterisation (multi-angle laser light scattering) coupled with the image analysis suggest that nine Cav3 monomers self-associate to form a homo-nonameric arrangement. The 9-fold symmetric 3D Cav3 volume is toroidal ~16.5nm in diameter and 5.5nm thick. The Cav3 structure is characterised by an outer rim of protein that is connected to a central 'cone-shaped' domain by narrow spoke-like densities, termed here a bridging unit. Labelling studies determined that the C-terminal domain of each contributing monomer unit forms the central cone density. Further, a combination of lipid reconstitution studies and bioinformatics has helped orientate this structure within the membrane, placing both the C-terminus and the likely N-terminus within the cytosol.

The central cone is composed of the C-terminus from each contributing Cav3 monomer, with the *proximal* region of the C-terminal domain likely forming the bridging unit that connects the central cone to the outer domain. The outer section of the nonamer is likely composed of both the TM region and the N-terminal domain, with the TM region at the base of the rim. The 'feet' of the structure would appear likely to be the exposed N-terminus. Given this, the approximate position of the scaffolding domain can be proposed, but whether it is exposed (external) or concealed (internal) cannot be confidently predicted. The reconstitution studies provide support for the interpretation of the 3D Cav3 structure with respect to the lipid bilayer. The clearly defined circular view, and feet domain and central cone would suggest that these regions extend beyond the lipid.

Previous reports have identified a number of regions thought to contain the transmembrane region (Kirkham et al., 2008; Lee and Glover, 2012; Monier et al., 1995; Parton et al., 2006). However, the specific regions believed to be membrane associated vary from experiment to experiment. Regardless of the specific regions that are membrane bound, our modelling here of the 3D Cav3 structure agrees with the previous claims that N- and C- termini are external to the membrane, and it also places the transmembrane domain in the base region of the model. The presence of the palmitoylation sites in the C-terminal domain (predicted to form α-helix at the bridging unit here) fits well with the interpretation of the 3D Cav3 structure, suggesting that the region of the C-terminal domain immediately following the putative transmembrane domain is also associated with the membrane. Further, the lipid reconstitution results would seem to support this topological modelling.

The region termed the scaffolding domain, which is believed to be involved in the majority (but not all) of protein-protein interactions, is proposed to be at the N-terminal

domain at the inner surface of the membrane leaflet (but not entering the membrane); in addition, some studies have suggested it is membrane associated (Arbuzova et al., 2000), possibly *via* an amphipathic helix (Kirkham et al., 2008). The identification of a globular domain that extends from the outer rim of protein into the cytosol in the Cav3 structure would be compatible with this region being formed in part by the scaffold domain, which is exposed to facilitate interactions with other proteins. Given the promiscuous role in protein-protein interactions that Cav3 plays, there remains the possibility that the exposed nature of this region is variable, depending upon other factors, such as the location of the complex or its association with other proteins.

The currently predicted site of caveolin oligomerisation is within the N-terminal domain region (corresponding to residues 34-74); a region termed the oligomerisation domain. However, the organisation of the Cav3 3D volume here would suggest that the C-terminal domains are also involved in the oligomerisation process, due to their close proximity. In addition, the structure may also imply that there are multiple regions within the N-terminal domain involved in oligomerisation; a high resolution structure is required for a more in-depth analysis. However, studies of the N^{1-54} domain described here do show that this region is also possibly involved in oligomerisation as indicated by the range of complex sizes observed by both native gel electrophoresis and transmission electron microscopy. As described in Chapter 2, expression and purification of the N^{1-54} domain lead to high protein yields and thus future avenues of study might include using size exclusion chromatography to separate out the different N^{1-54} oligomers. The isolation of a homogenous population of N^{1-54} oligomers would then permit techniques such as NMR or crystallisation methods e.g. X-ray crystallography or 2D crystallography methods to be employed.

It is likely that Cav3 is a highly flexible molecule given that one of the primary functions of the protein is to 'bend' the surface membrane. The Cav3 oligomer particles used here in the 3D reconstruction process have been solubilised away from the cell membrane with the detergent micelles substituting for the lipid environment. Therefore, the outer rim domain is also likely to be composed of detergent. Caveolin's interaction with the membrane is believed to underpin caveolae formation (Glenney, 1992; Rothberg et al., 1992). Experiments here in which Cav3 was reconstituted into large uni-lamellar vesicles found that cholesterol was not required for insertion of Cav3 into the membrane, suggesting that Cav3 can insert into the membrane in a cholesterol–independent manner. Future work should be aimed at improving protein yields for 2D crystallisation reconstitution studies, in which Cav3 could be inserted into a range of artificial membranes

of varied composition (Rigaud et al., 1998) (Geertsma et al., 2008). Determining the structure of Cav3 inserted into varied lipid membranes may help shed some light on which specific regions are involved in any possible conformational change or membrane insertion.

The structure of Cav3 presented here is the first and only 3D volume for any caveolin. The structure provides insights as to the organisation of the Cav3 oligomer that both supports and conflicts with many of the previous claims on Cav3 structure. There are a variety of different reasons for why, for example, 1) this study involved Cav3, not Cav1, which most previous work has been completed on, 2) the previous structural studies, of which there are very few (Fernandez et al., 2002; Lee and Glover, 2012), have focused on small sections of the protein, 3) A variety of different cell types have been used to express caveolin, some of which may not be able to process the protein in the correct form. It would be interesting to examine whether the baculovirus expression system used here has led to post-translational modifications of Cav3, with future work examining the impact any post-translational modifications such as palmitoylation and phosphorylation have upon both function and structure.

A limitation of the 3D Cav3 structure is the lack of high resolution features; although the final resolution of the map is at the limit of negative staining. An alternative to negatively staining the sample is to use cryo-TEM. Several attempts were conducted to try and examine unstained Cav3 by this approach, but difficulties were encountered with no or little protein found in the grid holes or carbon filament surrounding the holes. Given the relatively low yields obtained for the purified Cav3, this meant that cryo-EM was not feasible within the time frame of this project. As mentioned, another technique that would potentially shed some light on the membrane topology of Cav3 as well as any potential conformation changes that occur upon membrane insertion would be 2D crystallisation. Indeed, success has been had in reconstituting Cav3 into proteoliposomes here. The advantage of this approach would be that it would provide more information as to the domains of Cav3 that inserted into the membrane and those extending into the external milieu, the effect of the lipid composition of the membrane required for Cav3 insertion, as well as to help identify the key requirements for caveolae formation. Indeed, given that Cav3 is clearly a flexible protein (as highlighted by how it invaginates the membrane), it is quite feasible that a conformational change upon membrane association could occur. However, again, to develop an appropriate reconstitution protocol for 2D crystallisation, higher yields of Cav3 are required and thus future work would focus upon improving protein expression.

Chapter 6: Conclusion

This thesis describes the successful methodological development of expression systems for both the full-length Cav3 and the first 54 residues (termed N^{1-54}) of Cav3, which represents a section of the N-terminal domain containing the caveolin signature motif, a site of phosphorylation and a portion of the proposed oligomerisation domain. The *E.coli* expression system successfully expressed the N^{1-54} domain, whereas the baculovirus system was used to express full-length Cav3 in Sf9 cells. A variety of purification strategies have been explored in order to obtain the purified protein and the domain. The skeletal ryanodine receptor was also purified, from sheep hind leg calf muscle, and both full-length Cav3 and the N^{1-54} domain were characterised in terms of an interaction with the skeletal ryanodine receptor (RyR1). In addition, the structure of full-length Cav3 has been determined by employing a combination of transmission electron microscopy and single particle analysis.

A perpetual hurdle throughout this thesis has been the quantity of Cav3 that can be obtained. Indeed, such low yields have limited the range of biophysical techniques that could have been employed to characterise it, both in terms of function and structure. Many different expression systems exist that could be explored in order to improve yields of Cav3. However, the choice of system is limited by a wide range of factors, including the maintenance of native protein state, cost and time-scale. *E.coli* is one of the most optimum systems for obtaining high yields. However, given the prokaryotic setting for the expression of a eukaryotic protein it is understandably not the best choice for obtaining native functional forms of a membrane protein. In contrast, mammalian cell lines which would likely provide the most native version of Cav3 are both costly and often not suitable for large scale expression. One expression system that could possibly be explored is yeast. The yeast expression system is capable of producing both high yields and eukaryotic post-translational modifications (PTMs) more similar to mammalian PTMs, see (Romanos et al., 1992).

Future work might also focus upon optimising and purifying domains of Cav3 (described in Chapter 2). Isolating distinct regions of Cav3, each thought to be involved in a different part of Cav3 function would allow for the further dissection of the specific regions responsible for the proteins function and determination of those regions involved in protein-protein interactions. Other developments of this thesis work would be the use of the Sf9 system to express disease-associated mutant forms of Cav3 in order to assess the effect on the formation of caveolae. In addition, given the success with the proteoliposome reconstitution studies, mutant forms of Cav3 could be assessed for their effect on

membrane association and caveolae formation using this system. The effects of single point mutations upon oligomer formation would also be another logical step to advance this thesis work.

The evidence in both the literature and here suggest an interaction between RyR1 and Cav3, possibly via the transmembrane region of the RyR1. It would be very interesting to see which specific regions within both Cav3 and RyR are responsible for any interaction, and to examine whether it is specifically the caveolin binding motif regions that we have identified in RyR1 or the scaffolding domain of Cav3. Although native RyR has been employed in this study, future work could focus on the expression of recombinant RyR1 and RyR2. Given the size of a RyR homotetramer (2MDa) and the complex quaternary and tertiary organisation this would be a major undertaking with only a few reports of the successful expression and purification of the recombinant receptor e.g. (Zhao et al., 1999) and (Liu et al., 2004). Further, specific isolated domains of RyR could be expressed e.g. (Stewart et al., 2003). In order to elucidate the specifics of any Cav3 interaction, techniques such as surface plasmon resonance could provide both information on interactions as well as data on the association/dissociation, rate constants and equilibrium constants.

Another protein key to EC-coupling, with which Cav3 has been shown to associate, is $Ca_v1.2$. Further, we have identified that the primary sequence of $Ca_v1.2$ contains caveolin binding motifs within it (data not shown), suggesting a possible functional significance of their observed association. Indeed, the functional characterisation of the interplay between Cav3, RyR and Cav1.2, and how this relationship pertains to EC-coupling is an area that needs to be addressed further. Indeed, the expression of Cav3 mutations in myocytes have been shown to result in abnormal calcium handling and disorganised localisation of both RyR and L-type voltage gated calcium channels (Couchoux et al., 2007; Ullrich et al., 2011). Does Cav3 play a structural role, providing a potentially regulatable framework through which Cav1.2 can interact with its ultimate effector, RyR?; or given the role of Cav3 as a direct negative regulator of protein function does it play a functional role in directly regulating either of these proteins? Answers to these questions will no doubt contribute towards the understanding of both the molecular mechanics of Cav3 function, and what role Cav3 plays in the formation and function of specialised macromolecule signalling complexes.

Evidence provided here suggests that insertion of the caveolin complex into lipid membranes occurs. This indicates that the purified caveolin complex has maintained the ability to bind lipid as well as alter its morphology, both of which suggest that the isolated

caveolin oligomer is physiological active. The observance of a change in morphology from relatively random lipid morphology to a consistently spherical shape in which the caveolin oligomers appear to form a net-like complex, possibly underlies its role in inducing membrane curvature and ultimately caveolae formation. The orientation of the caveolin complex within in the proteoliposome, with what appears to be the N- and C-terminus tails on the outside, perhaps suggests a mechanism by which the N-terminal interaction sites are exposed to cytosolic interaction partners.

Conflicting with our net-like caveolin structure are images of caveolae from rapid-freezed deep-etched fibroblasts and endothelial cells, which appear to show 'daisy-chain like' striations upon the surface of caveolae (Rothberg et al., 1992; Shaul and Anderson, 1998). It is hard to imagine how a protein of 9-fold symmetry, which likely has multiple high-order oligomerisation points within it, could form such linear structures. Perhaps, upon physiological membrane association, or initial higher order oligomeric interactions within the native environment, conformational changes occur in the oligomers such that multiple interactions sites become unavailable. Such an explanation may explain the daisy-chain like formations, where individual threads do not seem to clearly interact. Alternatively, it may be that such threads are simply one type of higher order formation of caveolin oligomers, or they may be unique to certain cell types, caveolin isoforms, etc. Note that the reports of such striations have been in fibroblasts and endothelial cells alone. Many other possibilities exist for the differences observed between the proteoliposomes here and the striated structures observed by Rothberg and co-workers, and Shaul and Anderson, not least the absence of any other proteins, or cholesterol in our sample. Indeed, caveolin, as has been discussed in this thesis, interacts with many other proteins. It maybe that upon interaction with other proteins, such as PTRF or flotillin, or lipids such as cholesterol, that conformational changes occur within the caveolin complex such that a number of the high-order interaction sites are occluded, preventing a mesh-like network of oligomers forming. Indeed, this area is not clear and further work is required to finely dissect the mechanics by which caveolins oligomerise at a higher level.

The model provided here is the first 3D structure of any caveolin, and thus provides a benchmark upon which others can hopefully build. The limits imposed by the low resolutions on the interpretation of the model are acknowledged here; though we believe our attempts to interpret the model beyond the limitations imposed by resolution are both scientifically justified and logical. Indeed, higher resolution structural information is to be readily welcomed in this area, in order to validate our calculations of symmetry, segmentation and topological orientation. Although the data here points towards a

nonamer, this interpretation is always going to be limited by the resolution of the model. However, some confidence in the overall structure can be taken as models refined using C^7 and C^{10} symmetry showed the same overall carousel-like structure, where the C-terminal domains formed a central cone, and the N-terminal regions formed an outer rim of protein which possessed feet like entities. Should the yields of Cav3 or the N^{1-54} domain be improved, many more structural techniques become available; for example, X-ray crystallography and NMR. The resolution that is possible with these approaches could potentially provide near atomic resolution. Important information such as the position of specific regions of Cav3 within the structure need to be addressed. For example, where exactly is the scaffolding domain within the model? Which regions are involved in the oligomerisation process? How are monomeric subunits delineated within the oligomeric model? What, if any, conformational changes occur upon membrane association, or interaction with other proteins e.g. RyR1, or molecules such as cholesterol? How does the structure change when mutant forms of Cav3 are expressed? Answers to such questions would aid in both our understanding of any potential interaction in these regions, as well as highlight the possible mechanics behind when things go wrong in disease states.

Clearly, much is still to be learned about the complex role of Cav3 and caveolae. With such a vast myriad of putative interacting partners, and so many proposed roles, it is perhaps understandable why this protein remains so enigmatic and hard to pin down, to its researchers.

VIII References

Abramoff, M. D., Magelhaes, P. J., and Ram, S. J. (2004). Image Processing with ImageJ. *Biophotonics International* **11**, 36.

Adair, B., Nunn, R., Lewis, S., Dukes, I., Philipson, L., and Yeager, M. (2008). Single Particle Image Reconstruction of the Human Recombinant Kv2.1 Channel. *Biophysical Journal* **94**, 2106.

Alioua, A., Lu, R., Kumar, Y., Eghbali, M., Kundu, P., Toro, L., and Stefani, E. (2008). Slo1 Caveolin-binding Motif, a Mechanism of Caveolin-1-Slo1 Interaction Regulating Slo1 Surface Expression. *Journal of Biological Chemistry* **283**, 4808-4817.

Allred, D. C., and Mohsin, S. K. (2000). Biological Features of Premalignant Disease in the Human Breast. *Journal of Mammary Gland Biology and Neoplasia* **5**, 351.

Amador, F. J., Liu, S., Ishiyama, N., Plevin, M. J., Wilson, A., MacLennan, D. H., and Ikura, M. (2009). Crystal structure of type I ryanodine receptor amino-terminal β-trefoil domain reveals a disease-associated mutation "hot spot" loop. *Proceedings of the National Academy of Sciences* **106**, 11040-11044.

Andersen, O. S., and Koeppe, R. E. (2007). Bilayer Thickness and Membrane Protein Function: An Energetic Perspective. *Annual Review of Biophysics and Biomolecular Structure* **36**, 107-130.

Anderson, H. A., Chen, Y., and Norkin, L. C. (1996). Bound simian virus 40 translocates to caveolin-enriched membrane domains, and its entry is inhibited by drugs that selectively disrupt caveolae. *Molecular Biology of the Cell* **7**, 1825-34.

Aoki, S., Thomas, A., Decaffmeyer, M., Brasseur, R., and Epand, R. M. (2010). The Role of Proline in the Membrane Re-entrant Helix of Caveolin-1. *Journal of Biological Chemistry* **285**, 33371-33380.

Aravamudan, B., Volonte, D., Ramani, R., Gursoy, E., Lisanti, M. P., London, B., and Galbiati, F. (2003). Transgenic overexpression of caveolin-3 in the heart induces a cardiomyopathic phenotype. *Human Molecular Genetics* **12**, 2777-2788.

Arbuzova, A., Wang, L., Wang, J., Hangyás-Mihályné, G., Murray, D., Honig, B., and McLaughlin, S. (2000). Membrane Binding of Peptides Containing Both Basic and Aromatic Residues. Experimental Studies with Peptides Corresponding to the Scaffolding Region of Caveolin and the Effector Region of MARCKS *Biochemistry* **39**, 10330.

Atwell, S., Adams, J. M., Badger, J., Buchanan, M. D., Feil, I. K., Froning, K. J., Gao, X., Hendle, J., Keegan, K., Leon, B. C., Müller-Dieckmann, H. J., Nienaber, V. L., Noland, B. W., Post, K., Rajashankar, K. R., Ramos, A., Russell, M., Burley, S. K., and Buchanan, S. G. (2004). A Novel Mode of Gleevec Binding Is Revealed by the Structure of Spleen Tyrosine Kinase. *Journal of Biological Chemistry* **279**, 55827-55832.

Babitt, J., Trigatti, B., Rigotti, A., Smart, E. J., Anderson, R. G. W., Xu, S., and Krieger, M. (1997). Murine SR-BI, a High Density Lipoprotein Receptor That Mediates Selective Lipid Uptake, Is N-Glycosylated and Fatty Acylated and Colocalizes with Plasma Membrane Caveolae. *Journal of Biological Chemistry* **272**, 13242-13249.

Balijepalli, R. C., Delisle, B. P., Balijepalli, S. Y., Foell, J. D., Slind, J. K., Kamp, T. J., and January, C. T. (2007). Kv11.1 (ERG1) K+ channels localize in cholesterol and sphingolipid enriched membranes and are modulated by membrane cholesterol. *Channels (Austin)* **1**, 263-72.

Balijepalli, R. C., Foell, J. D., Hall, D. D., Hell, J. W., and Kamp, T. J. (2006). Localization of cardiac L-type Ca2+ channels to a caveolar macromolecular signaling complex is required for beta(2)-adrenergic regulation. *Proceedings Of The National Academy Of Sciences Of The United States Of America* **103**, 7500-7505.

Balijepalli, R. C., and Kamp, T. J. (2008). Caveolae, ion channels and cardiac arrhythmias. *Prog Biophys Mol Biol* **98**, 149-60.

Ballard-Croft, C., Locklar, A. C., Kristo, G., and Lasley, R. D. (2006). Regional myocardial ischemia-induced activation of MAPKs is associated with subcellular redistribution of caveolin and cholesterol. *American Journal of Physiology - Heart and Circulatory Physiology* **291**, H658-H667.

Balligand, J. L., Kobzik, L., Han, X. Q., Kaye, D. M., Belhassen, L., Ohara, D. S., Kelly, R. A., Smith, T. W., and Michel, T. (1995). Nitric Oxide-Dependent Parasympathetic Signaling Is Due To Activation Of Constitutive Endothelial (Type-Iii) Nitric-Oxide Synthase In Cardiac Myocytes. *Journal Of Biological Chemistry* **270**, 14582-14586.

Banerjee, I., Fuseler, J. W., Price, R. L., Borg, T. K., and Baudino, T. A. (2007). Determination of cell types and numbers during cardiac development in the neonatal and adult rat and mouse. *American Journal of Physiology - Heart and Circulatory Physiology* **293**, H1883-H1891.

Barouch, L. A., Harrison, R. W., Skaf, M. W., Rosas, G. O., Cappola, T. P., Kobeissi, Z. A., Hobai, I. A., Lemmon, C. A., Burnett, A. L., O'Rourke, B., Rodriguez, E. R., Huang, P. L., Lima, J. A. C., Berkowitz, D. E., and Hare, J. M. (2002). Nitric oxide regulates the heart by spatial confinement of nitric oxide synthase isoforms. *Nature* **416**, 337-340.

Barrantes, F. J. (2002). Lipid matters: nicotinic acetylcholine receptor-lipid interactions (Review). *Molecular Membrane Biology* **19**, 277-284.

Bers, D. M. (2002). Cardiac excitation-contraction coupling. *Nature* **415**, 198-205.

Bertani, G. (1951). Studies on lysogenesis. I. The mode of phage liberation by lysogenic Escherichia coli. *J Bacteriol* **62**, 293-300.

Betz, R. C., Schoser, B. G. H., Kasper, D., Ricker, K., Ramirez, A., Stein, V., Torbergsen, T., Lee, Y. A., Nothen, M. M., Wienker, T. F., Malin, J. P., Propping, P., Reis, A., Mortier, W., Jentsch, T. J., Vorgerd, M., and Kubisch, C. (2001). Mutations in CAV3 cause mechanical hyperirritability of skeletal muscle in rippling muscle disease. *Nature Genetics* **28**, 218-219.

Bhat, M. B., Zhao, J., Takeshima, H., and Ma, J. (1997). Functional calcium release channel formed by the carboxyl-terminal portion of ryanodine receptor. *Biophys J* **73**, 1329-36.

Biederer, C. H., Ries, S. J., Moser, M., Florio, M., Israel, M. A., McCormick, F., and Buettner, R. (2000). The Basic Helix-Loop-Helix Transcription Factors Myogenin and Id2 Mediate Specific Induction of Caveolin-3 Gene Expression during Embryonic Development. *Journal of Biological Chemistry* **275**, 26245-26251.

Billington, R. A., Bak, J., Martinez-Coscolla, A., Debidda, M., and Genazzani, A. A. (2004). Triazine dyes are agonists of the NAADP receptor. *British journal of pharmacology* **142**, 1241-6.

Bist, A., Fielding, P. E., and Fielding, C. J. (1997). Two sterol regulatory element-like sequences mediate up-regulation of caveolin gene transcription in response to low density lipoprotein free cholesterol. *Proceedings Of The National Academy Of Sciences Of The United States Of America* **94**, 10693-10698.

Blair, A., Shaul, P. W., Yuhanna, I. S., Conrad, P. A., and Smart, E. J. (1999). Oxidized low density lipoprotein displaces endothelial nitric-oxide synthase (eNOS) from plasmalemmal caveolae and impairs eNOS activation. *Journal Of Biological Chemistry* **274**, 32512-32519.

Bonuccelli, G., Casimiro, M. C., Sotgia, F., Wang, C., Liu, M., Katiyar, S., Zhou, J., Dew, E., Capozza, F., Daumer, K. M., Minetti, C., Milliman, J. N., Alpy, F., Rio, M.-C., Tomasetto, C., Mercier, I., Flomenberg, N., Frank, P. G., Pestell, R. G., and Lisanti, M. P. (2009). Caveolin-1 (P132L), a Common Breast Cancer Mutation, Confers

Mammary Cell Invasiveness and Defines a Novel Stem Cell/Metastasis-Associated Gene Signature. *The American Journal of Pathology* **174**, 1650.

Boraso, A., and Williams, A. J. (1994). Modification of the gating of the cardiac sarcoplasmic reticulum Ca(2+)-release channel by H2O2 and dithiothreitol. *American Journal of Physiology - Heart and Circulatory Physiology* **267**, H1010-H1016.

Bossuyt, J., Taylor, B. E., James-Kracke, M., and Hale, C. C. (2002). The cardiac sodium-calcium exchanger associates with caveolin-3. *Cellular And Molecular Physiology Of Sodium-Calcium Exchange* **976**, 197-204.

Bottcher, B., Wynne, S. A., and Crowther, R. A. (1997). Determination of the fold of the core protein of hepatitis B virus by electron cryomicroscopy. *Nature* **386**, 88.

Bucci, M., Gratton, J.-P., Rudic, R. D., Acevedo, L., Roviezzo, F., Cirino, G., and Sessa, W. C. (2000). In vivo delivery of the caveolin-1 scaffolding domain inhibits nitric oxide synthesis and reduces inflammation. *Nat Med* **6**, 1362.

Bujarski, J. J., Hardy, S. F., Miller, W. A., and Hall, T. C. (1982). Use of dodecyl-Î²-d-maltoside in the purification and stabilization of RNA polymerase from brome mosaic virus-infected barley. *Virology* **119**, 465.

Cagliani, R., Bresolin, N., Prelle, A., Gallanti, A., Fortunato, F., Sironi, M., Ciscato, P., Fagiolari, G., Bonato, S., Galbiati, S., Corti, S., Lamperti, C., Moggio, M., and Comi, G. P. (2003). A CAV3 microdeletion differentially affects skeletal muscle and myocardium. *Neurology* **61**, 1513-1519.

Cao, H., Courchesne, W. E., and Mastick, C. C. (2002). A Phosphotyrosine-dependent Protein Interaction Screen Reveals a Role for Phosphorylation of Caveolin-1 on Tyrosine 14. *Journal of Biological Chemistry* **277**, 8771-8774.

Carbone, I., Bruno, C., Sotgia, F., Bado, M., Broda, P., Masetti, E., Panella, A., Zara, F., Bricarelli, F. D., Cordone, G., Lisanti, M. P., and Minetti, C. (2000). Mutation in the CAV3 gene causes partial caveolin-3 deficiency and hyperCKemia. *Neurology* **54**, 1373-1376.

Carozzi, A. J., Ikonen, E., Lindsay, M. R., and Parton, R. G. (2000). Role of cholesterol in developing T-tubules: analogous mechanisms for T-tubule and caveolae biogenesis. *Traffic* **1**, 326-41.

Carrió, M. M., and Villaverde, A. (2001). Protein aggregation as bacterial inclusion bodies is reversible. *FEBS Letters* **489**, 29.

Cavalli, A., Eghbali, M., Minosyan, T. Y., Stefani, E., and Philipson, K. D. (2007). Localization of sarcolemmal proteins to lipid rafts in the myocardium. *Cell Calcium* **42**, 313-322.

Chang, W. J., Rothberg, K. G., Kamen, B. A., and Anderson, R. G. (1992). Lowering the cholesterol content of MA104 cells inhibits receptor-mediated transport of folate. *J Cell Biol* **118**, 63-9.

Chang, W. J., Ying, Y. S., Rothberg, K. G., Hooper, N. M., Turner, A. J., Gambliel, H. A., Degunzburg, J., Mumby, S. M., Gilman, A. G., and Anderson, R. G. W. (1994). Purification And Characterization Of Smooth-Muscle Cell Caveolae. *Journal Of Cell Biology* **126**, 127-138.

Chavis, P., Fagni, L., Lansman, J. B., and Bockaert, J. (1996). Functional coupling between ryanodine receptors and L-type calcium channels in neurons. *Nature* **382**, 719.

Cho, W. J., Chow, A. K., Schulz, R., and Daniel, E. E. (2010). Caveolin-1 exists and may function in cardiomyocytes. *Canadian Journal of Physiology and Pharmacology* **88**, 73.

Chu, A., Díaz-Muñoz, M., Hawkes, M. J., Brush, K., and Hamilton, S. L. (1990). Ryanodine as a probe for the functional state of the skeletal muscle sarcoplasmic reticulum calcium release channel. *Molecular Pharmacology* **37**, 735-741.

Chu, A., Dixon, M. C., Saito, A., Seiler, S., and Fleischer, S. (1988). Isolation of sarcoplasmic reticulum fractions referable to longitudinal tubules and junctional terminal cisternae from rabbit skeletal muscle. *Methods Enzymol* **157**, 36-46.

Chun, M. Y., Liyanage, U. K., Lisanti, M. P., and Lodish, H. F. (1994). Signal-Transduction Of A G-Protein-Coupled Receptor In Caveolae - Colocalization Of Endothelin And Its Receptor With Caveolin. *Proceedings Of The National Academy Of Sciences Of The United States Of America* **91**, 11728-11732.

Cohen, A. W., Hnasko, R., Schubert, W., and Lisanti, M. P. (2004). Role of caveolae and caveolins in health and disease. *Physiological Reviews* **84**, 1341-1379.

Cohen, A. W., Park, D. S., Woodman, S. E., Williams, T. M., Chandra, M., Shirani, J., De Souza, A. P., Kitsis, R. N., Russell, R. G., Weiss, L. M., Tang, B. Y., Jelicks, L. A., Factor, S. M., Shtutin, V., Tanowitz, H. B., and Lisanti, M. P. (2003). Caveolin-1 null mice develop cardiac hypertrophy with hyperactivation of p42/44 MAP kinase in cardiac fibroblasts. *American Journal Of Physiology-Cell Physiology* **284**, C457-C474.

Cole, C., Barber, J. D., and Barton, G. J. (2008). The Jpred 3 secondary structure prediction server. *Nucleic Acids Research* **36**, W197-W201.

Cong, P., Pricolo, V., Biancani, P., and Behar, J. (2010). Effects of cholesterol on CCK-1 receptors and caveolin-3 proteins recycling in human gallbladder muscle. *American Journal of Physiology - Gastrointestinal and Liver Physiology* **299**, G742-G750.

Conrad, P. A., Smart, E. J., Ying, Y. S., Anderson, R. G., and Bloom, G. S. (1995). Caveolin cycles between plasma membrane caveolae and the Golgi complex by microtubule-dependent and microtubule-independent steps. *The Journal of Cell Biology* **131**, 1421-1433.

Couchoux, H., Allard, B., Legrand, C., Jacquemond, V., and Berthier, C. (2007). Loss of caveolin-3 induced by the dystrophy-associated P104L mutation impairs L-type calcium channel function in mouse skeletal muscle cells. *Journal Of Physiology-London* **580**, 745-754.

Couet, J., Li, S. W., Okamoto, T., Ikezu, T., and Lisanti, M. P. (1997). Identification of peptide and protein ligands for the caveolin-scaffolding domain - Implications for the interaction of caveolin with caveolae-associated proteins. *Journal Of Biological Chemistry* **272**, 6525-6533.

Cronk, L. B., Ye, B., Kaku, T., Tester, D. J., Vatta, M., Makielski, J. C., and Ackerman, M. J. (2007). Novel mechanism for sudden infant death syndrome: persistent late sodium current secondary to mutations in caveolin-3. *Heart Rhythm* **4**, 161-6.

Cui, J., Rohr, L. R., Swanson, G., Speights, V. O., Maxwell, T., and Brothma, A. R. (2001). Hypermethylation of the caveolin-1 gene promoter in prostate cancer. *The Prostate* **46**, 249.

Daniel, E. E., Jury, J., and Wang, Y. F. (2001). nNOS in canine lower esophageal sphincter: colocalized with Cav-1 and Ca2+-handling proteins? *American Journal Of Physiology-Gastrointestinal And Liver Physiology* **281**, G1101-G1114.

Darby, P. J., Kwan, C. Y., and Daniel, E. E. (2000). Caveolae from canine airway smooth muscle contain the necessary components for a role in Ca(2+) handling. *Am J Physiol Lung Cell Mol Physiol* **279**, L1226-35.

Davies, L. M., Purves, G. I., Barrett-Jolley, R., and Dart, C. (2010). Interaction with caveolin-1 modulates vascular ATP-sensitive potassium (KATP) channel activity. *J Physiol* **588**, 3255-66.

de Castro, E., Sigrist, C., Gattiker, A., Bulliard, V., Langendijk-Genevaux, P., Gasteiger, E., Bairoch, A., and Hulo, N. (2006). ScanProsite: detection of PROSITE signature matches and ProRule-associated functional and structural residues in proteins. *Nucl. Acids Res.* **34**, W362.

de Paula, F., Vainzof, M., Bernardino, A. L. F., McNally, E., Kunkel, L. M., and Zatz, M. (2001). Mutations in the caveolin-3 gene: When are they pathogenic? *American Journal Of Medical Genetics* **99**, 303-307.

Decaffmeyer, M., Shulga, Y. V., Dicu, A. O., Thomas, A., Truant, R., Topham, M. K., Brasseur, R., and Epand, R. M. (2008). Determination of the Topology of the Hydrophobic Segment of Mammalian Diacylglycerol Kinase Epsilon in a Cell Membrane and Its Relationship to Predictions from Modeling. *Journal of Molecular Biology* **383**, 797.

Denizli, A., and Pişkin, E. (2001). Dye-ligand affinity systems. *Journal of Biochemical and Biophysical Methods* **49**, 391.

Deutscher, J. (2008). The mechanisms of carbon catabolite repression in bacteria. *Curr Opin Microbiol* **11**, 87-93.

deWeerd, W. F. C., and LeebLundberg, L. M. F. (1997). Bradykinin sequesters B2 bradykinin receptors and the receptor-coupled G alpha subunits G alpha(q) and G alpha(i) in caveolae in DDT1 MF-2 smooth muscle cells. *Journal Of Biological Chemistry* **272**, 17858-17866.

Dietzen, D. J., Hastings, W. R., and Lublin, D. M. (1995). Caveolin Is Palmitoylated On Multiple Cysteine Residues - Palmitoylation Is Not Necessary For Localization Of Caveolin To Caveolae. *Journal Of Biological Chemistry* **270**, 6838-6842.

Doerr, A. (2009). Membrane protein structures. *Nat Meth* **6**, 35.

Doyle, D. D., Goings, G., Upshaw-Earley, J., Ambler, S. K., Mondul, A., Palfrey, H. C., and Page, E. (2000). Dystrophin associates with caveolae of rat cardiac myocytes: relationship to dystroglycan. *Circ Res* **87**, 480-8.

Drab, M., Verkade, P., Elger, M., Kasper, M., Lohn, M., Lauterbach, B., Menne, J., Lindschau, C., Mende, F., Luft, F. C., Schedl, A., Haller, H., and Kurzchalia, T. V. (2001). Loss of caveolae, vascular dysfunction, and pulmonary defects in caveolin-1 gene-disrupted mice. *Science* **293**, 2449-2452.

Dupree, P., Parton, R. G., Raposo, G., Kurzchalia, T. V., and Simons, K. (1993). Caveolae And Sorting In The Trans-Golgi Network Of Epithelial-Cells. *Embo Journal* **12**, 1597-1605.

Dyson, H. J., and Wright, P. E. (1996). INSIGHTS INTO PROTEIN FOLDING FROM NMR. *Annual Review of Physical Chemistry* **47**, 369.

Edidin, M. (2001). Shrinking patches and slippery rafts: scales of domains in the plasma membrane. *Trends Cell Biol* **11**, 492-6.

Endo, M. (1977). Calcium release from the sarcoplasmic reticulum. *Physiological Reviews* **57**, 71-108.

Engelman, J. A., Chu, C., Lin, A., Jo, H., Ikezu, T., Okamoto, T., Kohtz, D. S., and Lisanti, M. P. (1998a). Caveolin-mediated regulation of signaling along the p42/44 MAP kinase cascade in vivo. A role for the caveolin-scaffolding domain. *FEBS Lett* **428**, 205-11.

Engelman, J. A., Zhang, X. L., and Lisanti, M. P. (1998b). Genes encoding human caveolin-1 and -2 are co-localized to the D7S522 locus (7q31.1), a known fragile site (FRA7G) that is frequently deleted in human cancers. *FEBS Letters* **436**, 403.

Engelman, J. A., Zhang, X. L., and Lisanti, M. P. (1999). Sequence and detailed organization of the human caveolin-1 and -2 genes located near the D7S522 locus (7q31.1): Methylation of a CpG island in the 5′ promoter region of the caveolin-1 gene in human breast cancer cell lines. *FEBS Letters* **448**, 221.

Epand, R. M., Sayer, B. G., and Epand, R. F. (2005). Caveolin scaffolding region and cholesterol-rich domains in membranes. *J Mol Biol* **345**, 339-50.

Epshtein, Y., Chopra, A. P., Rosenhouse-Dantsker, A., Kowalsky, G. B., Logothetis, D. E., and Levitan, I. (2009). Identification of a C-terminus domain critical for the sensitivity of Kir2.1 to cholesterol. *Proceedings of the National Academy of Sciences*.

Fantini, J., and Barrantes, F. J. (2009). Sphingolipid/cholesterol regulation of neurotransmitter receptor conformation and function. *Biochimica et Biophysica Acta (BBA) - Biomembranes* **1788**, 2345.

Fernandez, I., Ying, Y. S., Albanesi, J., and Anderson, R. G. W. (2002). Mechanism of caveolin filament assembly. *Proceedings Of The National Academy Of Sciences Of The United States Of America* **99**, 11193-11198.

Fernandez, J. M., and Hoeffler, J. P. (1999). Gene Expression Systems. Using nature for the art of expression.

Feron, O., Belhassen, L., Kobzik, L., Smith, T. W., Kelly, R. A., and Michel, T. (1996). Endothelial Nitric Oxide Synthase Targeting to Caveolae. *Journal of Biological Chemistry* **271**, 22810-22814.

Feron, O., Dessy, C., Opel, D. J., Arstall, M. A., Kelly, R. A., and Michel, T. (1998). Modulation of the endothelial nitric-oxide synthase caveolin interaction in cardiac myocytes - Implications for the autonomic regulation of heart rate. *Journal Of Biological Chemistry* **273**, 30249-30254.

Feron, O., Han, X., and Kelly, R. A. (1999). Muscarinic cholinergic signaling in cardiac myocytes: Dynamic targeting of M2AChR to sarcolemmal caveolae and eNOS activation. *Life Sciences* **64**, 471.

Fielding, C. J., Bist, A., and Fielding, P. E. (1997). Caveolin mRNA levels are up-regulated by free cholesterol and down-regulated by oxysterols in fibroblast monolayers. *Proceedings of the National Academy of Sciences* **94**, 3753-3758.

Fielding, C. J., and Fielding, P. E. (2001). Caveolae and intracellular trafficking of cholesterol. *Advanced Drug Delivery Reviews* **49**, 251.

Fielding, P. E., Chau, P., Liu, D., Spencer, T. A., and Fielding, C. J. (2004). Mechanism of Platelet-Derived Growth Factor-Dependent Caveolin-1 Phosphorylation: Relationship to Sterol Binding and the Role of Serine-80. *Biochemistry* **43**, 2578.

Fischer, D., Schroers, A., Blumcke, I., Urbach, H., Zerres, K., Mortier, W., Vorgerd, M., and Schroder, R. (2003). Consequences of a novel caveolin-3 mutation in a large German family. *Ann Neurol* **53**, 233-41.

Fiucci, G. R., D. Reich, R. Liscovitch, M. (2002). Caveolin-1 inhibits anchorage-independent growth, anoikis and invasiveness in MCF-7 human breast cancer cells. *Oncogene* **21**, 2365-2375.

Fra, A. M., Williamson, E., Simons, K., and Parton, R. G. (1995). De novo formation of caveolae in lymphocytes by expression of VIP21-caveolin. *Proc Natl Acad Sci U S A* **92**, 8655-9.

Frank, J., Goldfarb, W., Eisenberg, D., and Baker, T. S. (1978). Reconstruction of glutamine synthetase using computer averaging. *Ultramicroscopy* **3**, 283.

Frank, J., Radermacher, M., Penczek, P., Zhu, J., Li, Y., Ladjadj, M., and Leith, A. (1996). SPIDER and WEB: Processing and Visualization of Images in 3D Electron Microscopy and Related Fields. *Journal of Structural Biology* **116**, 190.

Frank, J., Shimkin, B., and Dowse, H. (1981). Spider - A modular software system for electron image processing. *Ultramicroscopy* **6**, 343.

Frank, P. G., and Lisanti, M. P. (2006). Defining lipid raft structure and function with proximity imaging. *American Journal Of Physiology-Heart And Circulatory Physiology* **290**, H2165-H2166.

Freeman, M. R., Yang, W., Vizio, D., Jasmin, J.-F., Frank, P. G., and Lisanti, M. P. (2012). Caveolin-1 and Prostate Cancer Progression

Caveolins and Caveolae. Vol. 729, pp. 95. Springer US.

Fujimoto, T. (1993). Calcium pump of the plasma membrane is localized in caveolae. *The Journal of Cell Biology* **120**, 1147-1157.

Fujimoto, T., Kogo, H., Nomura, R., and Une, T. (2000). Isoforms of caveolin-1 and caveolar structure. *Journal of Cell Science* **113**, 3509-3517.

Fujimoto, T., Nakade, S., Miyawaki, A., Mikoshiba, K., and Ogawa, K. (1992). Localization Of Inositol 1,4,5-Trisphosphate Receptor-Like Protein In Plasmalemmal-Caveolae. *Journal Of Cell Biology* **119**, 1507-1513.

Fujita, T., Otsu, K., Oshikawa, A., Hori, H., Kitamura, H., Ito, T., Umemura, S., Minamisawa, S., and Ishikawa, Y. (2006). Caveolin-3 inhibits growth signal in cardiac myoblasts in a Ca2+-dependent manner. *Journal Of Cellular And Molecular Medicine* **10**, 216-224.

Fulizio, L., Nascimbeni, A. C., Fanin, M., Piluso, G., Politano, L., Nigro, V., and Angelini, C. (2005). Molecular and muscle pathology in a series of caveolinopathy patients. *Hum Mutat* **25**, 82-9.

Galbiati, F., Engelman, J. A., Volonte, D., Zhang, X. L., Minetti, C., Li, M. M., Hou, H., Kneitz, B., Edelmann, W., and Lisanti, M. P. (2001a). Caveolin-3 null mice show a loss of caveolae, changes in the microdomain distribution of the dystrophin-glycoprotein complex, and T-tubule abnormalities. *Journal Of Biological Chemistry* **276**, 21425-21433.

Galbiati, F., Razani, B., and Lisanti, M. P. (2001b). Caveolae and caveolin-3 in muscular dystrophy. *Trends In Molecular Medicine* **7**, 435-441.

Galbiati, F., Volonte, D., Chu, J. B., Li, M., Fine, S. W., Fu, M. F., Bermudez, J., Pedemonte, M., Weidenheim, K. M., Pestell, R. G., Minetti, C., and Lisanti, M. P. (2000a). Transgenic overexpression of caveolin-3 in skeletal muscle fibers induces a Duchenne-like muscular dystrophy phenotype. *Proceedings Of The National Academy Of Sciences Of The United States Of America* **97**, 9689-9694.

Galbiati, F., Volonte, D., and Lisanti, M. P. (2001c). Caveolin-3 knock-out mice show a loss of caveolae, changes in the microdomain distribution of the dystrophin-glycoprotein complex, and T-tubule abnormalities. *Molecular Biology Of The Cell* **12**, 80A-81A.

Galbiati, F., Volonte, D., Minetti, C., Bregman, D. B., and Lisanti, M. P. (2000b). Limb-girdle muscular dystrophy (LGMD-1C) mutants of caveolin-3 undergo ubiquitination and proteasomal degradation. Treatment with proteasomal inhibitors blocks the dominant negative effect of LGMD-1C mutanta and rescues wild-type caveolin-3. *J Biol Chem* **275**, 37702-11.

Galbiati, F., Volonte, D., Minetti, C., Chu, J. B., and Lisanti, M. P. (1999). Phenotypic behavior of caveolin-3 mutations that cause autosomal dominant limb girdle muscular dystrophy (LGMD-1C). Retention of LGMD-1C caveolin-3 mutants within the golgi complex. *J Biol Chem* **274**, 25632-41.

Garcia-Cardena, G., Fan, R., Stern, D. F., Liu, J. W., and Sessa, W. C. (1996a). Endothelial nitric oxide synthase is regulated by tyrosine phosphorylation and interacts with caveolin-1. *Journal Of Biological Chemistry* **271**, 27237-27240.

Garcia-Cardena, G., Martasek, P., Masters, B. S. S., Skidd, P. M., Couet, J., Li, S., Lisanti, M. P., and Sessa, W. C. (1997). Dissecting the interaction between nitric oxide synthase (NOS) and caveolin. Functional significance of the NOS caveolin binding domain in vivo. *Journal of Biological Chemistry* **272**, 25437-25440.

Garcia-Cardena, G., Oh, P., Liu, J. W., Schnitzer, J. E., and Sessa, W. C. (1996b). Targeting of nitric oxide synthase to endothelial cell caveolae via palmitoylation: Implications for nitric oxide signaling. *Proceedings Of The National Academy Of Sciences Of The United States Of America* **93**, 6448-6453.

Garg, V., Jiao, J., and Hu, K. (2009a). Regulation of ATP-sensitive K+ channels by caveolin-enriched microdomains in cardiac myocytes. *Cardiovasc Res* **82**, 51-8.

Garg, V., Sun, W., and Hu, K. (2009b). Caveolin-3 negatively regulates recombinant cardiac K(ATP) channels. *Biochem Biophys Res Commun* **385**, 472-7.

Geertsma, E. R., Mahmood, N. A., Schuurman-Wolters, G. K., and Poolman, B. (2008). Membrane reconstitution of ABC transporters and assays of translocator function. *Nat Protoc* **3**, 256-66.

Gennis, R. B. (1989). Biomembranes:molecular structure and function. *Springer-Verlag*.
Georgiou, G., Valax, P., and Ronald, W. (1999). Isolating inclusion bodies from bacteria. *In* "Methods in Enzymology", Vol. Volume 309, pp. 48. Academic Press.
Gerbal, M., Fournier, P., Barry, P., Mariller, M., Odier, F., Devauchelle, G., and Duonor-Cerutti, M. (2000). Adaptation of an Insect Cell Line of Spodoptera frugiperda to Grow at 37°C: Characterization of an Endodiploid Clone. *In Vitro Cellular & Developmental Biology. Animal* **36**, 117.
Glenney, J. R. (1992). The Sequence Of Human Caveolin Reveals Identity With Vip21, A Component Of Transport Vesicles. *Febs Letters* **314**, 45-48.
Glenney, J. R., and Zokas, L. (1989). Novel Tyrosine Kinase Substrates From Rous-Sarcoma Virus-Transformed Cells Are Present In The Membrane Skeleton. *Journal Of Cell Biology* **108**, 2401-2408.
Goll, C. M., Pastore, A., and Nilges, M. (1998). The three-dimensional structure of a type I module from titin: a prototype of intracellular fibronectin type III domains. *Structure* **6**, 1291.
Gonzalez, E., Nagiel, A., Lin, A. J., Golan, D. E., and Michel, T. (2004). Small Interfering RNA-mediated Down-regulation of Caveolin-1 Differentially Modulates Signaling Pathways in Endothelial Cells. *Journal of Biological Chemistry* **279**, 40659-40669.
Graf, G. A., Connell, P. M., van der Westhuyzen, D. R., and Smart, E. J. (1999). The class B, type I scavenger receptor promotes the selective uptake of high density lipoprotein cholesterol ethers into caveolae. *Journal Of Biological Chemistry* **274**, 12043-12048.
Gratton, J. P., Bernatchez, P., and Sessa, W. C. (2004). Caveolae and caveolins in the cardiovascular system. *Circulation Research* **94**, 1408-1417.
Guo, W., and Campbell, K. P. (1995). Association of Triadin with the Ryanodine Receptor and Calsequestrin in the Lumen of the Sarcoplasmic Reticulum. *Journal of Biological Chemistry* **270**, 9027-9030.
Gustavsson, J., Parpal, S., Karlsson, M., Ramsing, C., Thorn, H., Borg, M., Lindroth, M., Peterson, K. H., Magnusson, K.-E., and Strålfors, P. (1999). Localization of the insulin receptor in caveolae of adipocyte plasma membrane. *The FASEB Journal* **13**, 1961-1971.
Györke, S., Stevens, S. C. W., and Terentyev, D. (2009). Cardiac calsequestrin: quest inside the SR. *The Journal of Physiology* **587**, 3091-3094.
Haasemann, M., Cartaud, J., Muller-Esterl, W., and Dunia, I. (1998). Agonist-induced redistribution of bradykinin B-2 receptor in caveolae. *Journal Of Cell Science* **111**, 917-928.
Hagiwara, Y., Nishina, Y., Yorifuji, H., and Kikuchi, T. (2002). Immunolocalization of caveolin-1 and caveolin-3 in monkey skeletal, cardiac and uterine smooth muscles. *Cell Struct Funct* **27**, 375-82.
Hakamata, Y., Nakai, J., Takeshima, H., and Imoto, K. (1992). Primary structure and distribution of a novel ryanodine receptor/calcium release channel from rabbit brain. *FEBS Letters* **312**, 229.
Hanahan, D. (1983). Studies on transformation of Escherichia coli with plasmids. *J Mol Biol* **166**, 557-80.
Hausenloy, D. J., Tsang, A., and Yellon, D. M. (2005). The Reperfusion Injury Salvage Kinase Pathway: A Common Target for Both Ischemic Preconditioning and Postconditioning. *Trends in Cardiovascular Medicine* **15**, 69.
Hausenloy, D. J., and Yellon, D. M. (2004). New directions for protecting the heart against ischaemia-reperfusion injury: targeting the Reperfusion Injury Salvage Kinase (RISK)-pathway. *Cardiovascular Research* **61**, 448-460.
Hayashi, T., Arimura, T., Ueda, K., Shibata, H., Hohda, S., Takahashi, M., Hori, H., Koga, Y., Oka, N., Imaizumi, T., Yasunami, M., and Kimura, A. (2004). Identification and functional analysis of a caveolin-3 mutation associated with familial

hypertrophic cardiomyopathy. *Biochemical And Biophysical Research Communications* **313**, 178-184.

Head, B. P., Patel, H. H., Roth, D. M., Lai, N. C., Niesman, I. R., Farquhar, M. G., and Insel, P. A. (2005). G-protein-coupled receptor signaling components localize in both sarcolemmal and intracellular caveolin-3-associated microdomains in adult cardiac myocytes. *Journal Of Biological Chemistry* **280**, 31036-31044.

Heibeck, T. H., Ding, S.-J., Opresko, L. K., Zhao, R., Schepmoes, A. A., Yang, F., Tolmachev, A. V., Monroe, M. E., Camp, D. G., Smith, R. D., Wiley, H. S., and Qian, W.-J. (2009). An Extensive Survey of Tyrosine Phosphorylation Revealing New Sites in Human Mammary Epithelial Cells. *Journal of Proteome Research* **8**, 3852.

Hellebust, H., Murby, M., Abrahmsen, L., Uhlen, M., and Enfors, S.-O. (1989). Different Approaches to Stabilize a Recombinant Fusion Protein. *Nat Biotech* **7**, 165.

Herrmann, R., Straub, V., Blank, M., Kutzick, C., Franke, N., Jacob, E. N., Lenard, H. G., Kroger, S., and Voit, T. (2000). Dissociation of the dystroglycan complex in caveolin-3-deficient limb girdle muscular dystrophy. *Human Molecular Genetics* **9**, 2335-2340.

Hill, M. M., Bastiani, M., Luetterforst, R., Kirkham, M., Kirkham, A., Nixon, S. J., Walser, P., Abankwa, D., Oorschot, V. M. J., Martin, S., Hancock, J. F., and Parton, R. G. (2008). PTRF-Cavin, a Conserved Cytoplasmic Protein Required for Caveola Formation and Function. *Cell* **132**, 113.

Ho, C.-C., Huang, P.-H., Huang, H.-Y., Chen, Y.-H., Yang, P.-C., and Hsu, S.-M. (2002). Up-Regulated Caveolin-1 Accentuates the Metastasis Capability of Lung Adenocarcinoma by Inducing Filopodia Formation. *The American Journal of Pathology* **161**, 1647.

Hopkins, A. L., Mason, J. S., and Overington, J. P. (2006). Can we rationally design promiscuous drugs? *Current Opinion in Structural Biology* **16**, 127.

Hopp, T. P., and Woods, K. R. (1981). Prediction of protein antigenic determinants from amino acid sequences. *Proceedings of the National Academy of Sciences* **78**, 3824-3828.

Horikawa, Y. T., Patel, H. H., Tsutsumi, Y. M., Jennings, M. M., Kidd, M. W., Hagiwara, Y., Ishikawa, Y., Insel, P. A., and Roth, D. M. (2008). Caveolin-3 expression and caveolae are required for isoflurane-induced cardiac protection from hypoxia and ischemia/reperfusion injury. *J Mol Cell Cardiol* **44**, 123-30.

Huang, C.-T., Peretti, S. W., and Bryers, J. D. (1994). Effects of inducer levels on a recombinant bacterial biofilm formation and gene expression. *Biotechnology Letters* **16**, 903.

Ikonen, E., and Parton, R. G. (2000). Caveolins and Cellular Cholesterol Balance. *Traffic* **1**, 212.

Jasmin, J.-F., Frank, P. G., Lisanti, M. P., Panneerselvam, M., Patel, H. H., and Roth, D. M. (2012). Caveolins and Heart Diseases. *In* "Caveolins and Caveolae", Vol. 729, pp. 145-156. Springer US.

Jiao, J., Garg, V., Yang, B., Elton, T. S., and Hu, K. (2008). Protein Kinase C-ε Induces Caveolin-Dependent Internalization of Vascular Adenosine 5′-Triphosphate–Sensitive K+ Channels. *Hypertension* **52**, 499-506.

Jones, D. T. (1999). Protein secondary structure prediction based on position-specific scoring matrices. *Journal of Molecular Biology* **292**, 195.

Jones, P. G., VanBogelen, R. A., and Neidhardt, F. C. (1987). Induction of proteins in response to low temperature in Escherichia coli. *J Bacteriol* **169**, 2092-5.

Joo, H. J., Oh, D. K., Kim, Y. S., Lee, K. B., and Kim, S. J. (2004). Increased expression of caveolin-1 and microvessel density correlates with metastasis and poor prognosis in clear cell renal cell carcinoma. *BJU International* **93**, 291.

Ju, H., Venema, V. J., Liang, H. Y., Harris, M. B., Zou, F., and Venema, R. C. (2000). Bradykinin activates the Janus-activated kinase/signal transducers and activators of transcription (JAK/STAT) pathway in vascular endothelial cells: localization of JAK/STAT signalling proteins in plasmalemmal caveolae. *Biochemical Journal* **351**, 257-264.

Ju, H., Zou, R., Venema, V. J., and Venema, R. C. (1997). Direct interaction of endothelial nitric-oxide synthase and caveolin-1 inhibits synthase activity. *Journal Of Biological Chemistry* **272**, 18522-18525.

Juretić, D., Zoranić, L., and Zucić, D. (2002). Basic Charge Clusters and Predictions of Membrane Protein Topology. *Journal of Chemical Information and Computer Sciences* **42**, 620.

Kamishima, T., Burdyga, T., Gallagher, J. A., and Quayle, J. M. (2007). Caveolin-1 and caveolin-3 regulate Ca2+ homeostasis of single smooth muscle cells from rat cerebral resistance arteries. *American Journal Of Physiology-Heart And Circulatory Physiology* **293**, H204-H214.

Kane, J. F. (1995). Effects of rare codon clusters on high-level expression of heterologous proteins in Escherichia coli. *Curr Opin Biotechnol* **6**, 494-500.

Kane, J. F., and Hartley, D. L. (1988). Formation of recombinant protein inclusion bodies in Escherichia coli. *Trends in Biotechnology* **6**, 95.

Kasahara, T., Hara, N., Bilim, V., Tomita, Y., Tsutsui, T., and Takahashi, K. (2002). Immunohistochemical Studies of Caveolin-3 in Germ Cell Tumors of the Testis. *Urologia Internationalis* **69**, 63.

Kato, K., Hida, Y., Miyamoto, M., Hashida, H., Shinohara, T., Itoh, T., Okushiba, S., Kondo, S., and Katoh, H. (2002). Overexpression of caveolin-1 in esophageal squamous cell carcinoma correlates with lymph node metastasis and pathologic stage. *Cancer* **94**, 929.

Kato, T., Kageshima, A., Suzuki, F., and Park, E. Y. (2008). Expression and purification of human (pro)renin receptor in insect cells using baculovirus expression system. *Protein Expr Purif* **58**, 242-8.

Kelly, S. M., Jess, T. J., and Price, N. C. (2005). How to study proteins by circular dichroism. *Biochimica et Biophysica Acta (BBA) - Proteins & Proteomics* **1751**, 119.

Kendrew, J. C., Bodo, G., Dintzis, H. M., Parrish, R. G., Wyckoff, H., and Phillips, D. C. (1958). A Three-Dimensional Model of the Myoglobin Molecule Obtained by X-Ray Analysis. *Nature* **181**, 662.

Kikuchi, T., Oka, N., Koga, A., Miyazaki, H., Ohmura, H., and Imaizumi, T. (2005). Behavior of Caveolae and Caveolin-3 During the Development of Myocyte Hypertrophy. *Journal of Cardiovascular Pharmacology* **45**, 204-210.

Kirkham, M., Nixon, S. J., Howes, M. T., Abi-Rached, L., Wakeham, D. E., Hanzal-Bayer, M., Ferguson, C., Hill, M. M., Fernandez-Rojo, M., Brown, D. A., Hancock, J. F., Brodsky, F. M., and Parton, R. G. (2008). Evolutionary analysis and molecular dissection of caveola biogenesis. *J Cell Sci* **121**, 2075-86.

Kodan, A., Shibata, H., Matsumoto, T., Terakado, K., Sakiyama, K., Matsuo, M., Ueda, K., and Kato, H. (2009). Improved expression and purification of human multidrug resistance protein MDR1 from baculovirus-infected insect cells. *Protein Expr Purif* **66**, 7-14.

Koga, A., Oka, N., Kikuchi, T., Miyazaki, H., Kato, S., and Imaizumi, T. (2003). Adenovirus-mediated overexpression of caveolin-3 inhibits rat cardiomyocyte hypertrophy. *Hypertension* **42**, 213-219.

Kogo, H., Ishiguro, K., Kuwaki, S., and Fujimoto, T. (2002). Identification of a splice variant of mouse caveolin-2 mRNA encoding an isoform lacking the C-terminal domain. *Archives of Biochemistry and Biophysics* **401**, 108.

Koopmann, T. T., Beekman, L., Alders, M., Meregalli, P. G., Mannens, M., Moorman, A. F. M., Wide, A. A. M., and Bezzina, C. R. (2007). Exclusion of multiple candidate genes and large genomic rearrangements in SMA in a Dutch Brugada syndrome cohort. *Heart Rhythm* **4**, 752-755.

Kubisch, C., Schoser, B. G., von During, M., Betz, R. C., Goebel, H. H., Zahn, S., Ehrbrecht, A., Aasly, J., Schroers, A., Popovic, N., Lochmuller, H., Schroder, J. M., Bruning, T., Malin, J. P., Fricke, B., Meinck, H. M., Torbergsen, T., Engels, H., Voss, B., and Vorgerd, M. (2003). Homozygous mutations in caveolin-3 cause a severe form of rippling muscle disease. *Ann Neurol* **53**, 512-20.

Kurzchalia, T. V., Dupree, P., Parton, R. G., Kellner, R., Virta, H., Lehnert, M., and Simons, K. (1992). VIP21, a 21-kD membrane protein is an integral component of trans-Golgi-network-derived transport vesicles. *The Journal of Cell Biology* **118**, 1003-1014.

Kurzchalia, T. V., and Parton, R. G. (1999). Membrane microdomains and caveolae. *Current Opinion in Cell Biology* **11**, 424.

Kyte, J., and Doolittle, R. F. (1982). A simple method for displaying the hydropathic character of a protein. *Journal of Molecular Biology* **157**, 105.

Laemmli, U. K. (1970). Cleavage of structural proteins during the assembly of the head of bacteriophage T4. *Nature* **227**, 680-5.

Lai, F. A., Misra, M., Xu, L., Smith, H. A., and Meissner, G. (1989). The ryanodine receptor-Ca2+ release channel complex of skeletal muscle sarcoplasmic reticulum. Evidence for a cooperatively coupled, negatively charged homotetramer. *Journal of Biological Chemistry* **264**, 16776-16785.

Lanner, J. T., Georgiou, D. K., Joshi, A. D., and Hamilton, S. L. (2010). Ryanodine receptors: structure, expression, molecular details, and function in calcium release. *Cold Spring Harb Perspect Biol* **2**, a003996.

Larkin, M. A., Blackshields, G., Brown, N. P., Chenna, R., McGettigan, P. A., McWilliam, H., Valentin, F., Wallace, I. M., Wilm, A., Lopez, R., Thompson, J. D., Gibson, T. J., and Higgins, D. G. (2007). Clustal W and clustal X version 2.0. *Bioinformatics* **23**, 2947-2948.

Lasley, R. D., Narayan, P., Uittenbogaard, A., and Smart, E. J. (2000). Activated Cardiac Adenosine A1 Receptors Translocate Out of Caveolae. *Journal of Biological Chemistry* **275**, 4417-4421.

Laver, D. R., Baynes, T. M., and Dulhunty, A. F. (1997). Magnesium inhibition of ryanodine-receptor calcium channels: evidence for two independent mechanisms. *J Membr Biol* **156**, 213-29.

Layland, J., Li, J.-M., and Shah, A. M. (2002). Role of cyclic GMP-dependent protein kinase in the contractile response to exogenous nitric oxide in rat cardiac myocytes. *The Journal of Physiology* **540**, 457-467.

Lee, H., Volonte, D., Galbiati, F., Iyengar, P., Lublin, D. M., Bregman, D. B., Wilson, M. T., Campos-Gonzalez Boumediene Bouzahzah, R., Pestell, R. G., Scherer, P. E., and Lisanti, M. P. (2000). Constitutive and Growth Factor-Regulated Phosphorylation of Caveolin-1 Occurs at the Same Site (Tyr-14) in Vivo: Identification of a c-Src/Cav-1/Grb7 Signaling Cassette. *Molecular Endocrinology* **14**, 1750-1775.

Lee, H., Woodman, S. E., Engelman, J. A., Volonte, D., Galbiati, F., Kaufman, H. L., Lublin, D. M., and Lisanti, M. P. (2001). Palmitoylation of Caveolin-1 at a Single Site (Cys-156) Controls Its Coupling to the c-Src Tyrosine Kinase. *Journal of Biological Chemistry* **276**, 35150-35158.

Lee, J., and Glover, K. J. (2012). The transmembrane domain of caveolin-1 exhibits a helix–break–helix structure. *Biochimica et Biophysica Acta (BBA) - Biomembranes* **1818**, 1158.

Li, C. L., Duan, W. J., Yang, F. Y., and Zhang, X. J. (2006). Caveolin-3-anchored microdomains at the rabbit sarcoplasmic reticulum membranes. *Biochemical And Biophysical Research Communications* **344**, 1135-1140.

Li, S., Couet, J., and Lisanti, M. P. (1996a). Src tyrosine kinases, Galpha subunits, and H-Ras share a common membrane-anchored scaffolding protein, caveolin. Caveolin binding negatively regulates the auto-activation of Src tyrosine kinases. *J Biol Chem* **271**, 29182-90.

Li, S., Okamoto, T., Chun, M., Sargiacomo, M., Casanova, J. E., Hansen, S. H., Nishimoto, I., and Lisanti, M. P. (1995). Evidence for a regulated interaction between heterotrimeric G proteins and caveolin. *J Biol Chem* **270**, 15693-701.

Li, S., Song, K. S., Koh, S. S., Kikuchi, A., and Lisanti, M. P. (1996b). Baculovirus-based expression of mammalian caveolin in Sf21 insect cells. A model system for the biochemical and morphological study of caveolae biogenesis. *J Biol Chem* **271**, 28647-54.

Li, S., Song, K. S., and Lisanti, M. P. (1996c). Expression and characterization of recombinant caveolin. Purification by polyhistidine tagging and cholesterol-dependent incorporation into defined lipid membranes. *J Biol Chem* **271**, 568-73.

Li, S. W., Seitz, R., and Lisanti, M. P. (1996d). Phosphorylation of caveolin by Src tyrosine kinases - The alpha-isoform of caveolin is selectively phosphorylated by v-Src in vivo. *Journal Of Biological Chemistry* **271**, 3863-3868.

Li, S. W., Song, K. S., and Lisanti, M. P. (1996e). Expression and characterization of recombinant caveolin - Purification by polyhistidine tagging and cholesterol-dependent incorporation into defined lipid membranes. *Journal Of Biological Chemistry* **271**, 568-573.

Lisanti, M. P., Scherer, P. E., Tang, Z., and Sargiacomo, M. (1994a). Caveolae, caveolin and caveolin-rich membrane domains: A signalling hypothesis. *Trends in Cell Biology* **4**, 231-235.

Lisanti, M. P., Scherer, P. E., Vidugiriene, J., Tang, Z. L., Hermanowskivosatka, A., Tu, Y. H., Cook, R. F., and Sargiacomo, M. (1994b). Characterization Of Caveolin-Rich Membrane Domains Isolated From An Endothelial-Rich Source - Implications For Human-Disease. *Journal Of Cell Biology* **126**, 111-126.

Liu, L., Brown, D., McKee, M., LeBrasseur, N. K., Yang, D., Albrecht, K. H., Ravid, K., and Pilch, P. F. (2008). Deletion of Cavin/PTRF Causes Global Loss of Caveolae, Dyslipidemia, and Glucose Intolerance. *Cell Metabolism* **8**, 310.

Liu, L., Mohammadi, K., Aynafshar, B., Wang, H., Li, D., Liu, J., Ivanov, A. V., Xie, Z., and Askari, A. (2003). Role of caveolae in signal-transducing function of cardiac Na+/K+-ATPase. *American Journal of Physiology - Cell Physiology* **284**, C1550-C1560.

Liu, L., and Pilch, P. F. (2008). A critical role of cavin (polymerase I and transcript release factor) in caveolae formation and organization. *J Biol Chem* **283**, 4314-22.

Liu, Z., Wang, R., Zhang, J., Chen, S. R. W., and Wagenknecht, T. (2005). Localization of a Disease-associated Mutation Site in the Three-dimensional Structure of the Cardiac Muscle Ryanodine Receptor. *Journal of Biological Chemistry* **280**, 37941-37947.

Liu, Z., Zhang, J., Li, P., Chen, S. R. W., and Wagenknecht, T. (2002). Three-dimensional Reconstruction of the Recombinant Type 2 Ryanodine Receptor and Localization of Its Divergent Region 1. *Journal of Biological Chemistry* **277**, 46712-46719.

Liu, Z., Zhang, J., Sharma, M. R., Li, P., Chen, S. R. W., and Wagenknecht, T. (2001). Three-dimensional reconstruction of the recombinant type 3 ryanodine receptor and localization of its amino terminus. *Proceedings of the National Academy of Sciences* **98**, 6104-6109.

Liu, Z., Zhang, J., Wang, R., Wayne Chen, S. R., and Wagenknecht, T. (2004). Location of Divergent Region 2 on the Three-dimensional Structure of Cardiac Muscle

Ryanodine Receptor/Calcium Release Channel. *Journal of Molecular Biology* **338**, 533.
Lobo, P. A., and Van Petegem, F. (2009). Crystal Structures of the N-Terminal Domains of Cardiac and Skeletal Muscle Ryanodine Receptors: Insights into Disease Mutations. *Structure* **17**, 1505.
Ludtke, S. J., Baldwin, P. R., and Chiu, W. (1999). EMAN: semiautomated software for high-resolution single-particle reconstructions. *J Struct Biol* **128**, 82-97.
Ludtke, S. J., Serysheva, I. I., Hamilton, S. L., and Chiu, W. (2005). The Pore Structure of the Closed RyR1 Channel. *Structure (London, England : 1993)* **13**, 1203.
Luetterforst, R., Stang, E., Zorzi, N., Carozzi, A., Way, M., and Parton, R. G. (1999). Molecular Characterization of Caveolin Association with the Golgi Complex: Identification of a Cis-Golgi Targeting Domain in the Caveolin Molecule. *The Journal of Cell Biology* **145**, 1443-1459.
Machleidt, T., Li, W. P., Liu, P. S., and Anderson, R. G. W. (2000). Multiple domains in caveolin-1 control its intracellular traffic. *Journal Of Cell Biology* **148**, 17-28.
Madrid, R. E., Kubisch, C., and Hays, A. P. (2005). Early-onset toe walking in rippling muscle disease due to a new caveolin-3 gene mutation. *Neurology* **65**, 1301-1303.
Marheineke, K., Grünewald, S., Christie, W., and Reiländer, H. (1998). Lipid composition of Spodoptera frugiperda (Sf9) and Trichoplusia ni (Tn) insect cells used for baculovirus infection. *FEBS Letters* **441**, 49.
Markandeya, Y. S., Fahey, J. M., Pluteanu, F., Cribbs, L. L., and Balijepalli, R. C. (2011). Caveolin-3 regulates the protein kinase A modulation of CaV3.2 ({alpha}1H) T-type Ca2+ channels. *J Biol Chem*.
Martens, J. R., Sakamoto, N., Sullivan, S. A., Grobaski, T. D., and Tamkun, M. M. (2001). Isoform-specific localization of voltage-gated K+ channels to distinct lipid raft populations - Targeting of Kv1.5 to 3 caveolae. *Journal Of Biological Chemistry* **276**, 8409-8414.
Matsuda, C., Hayashi, Y. K., Ogawa, M., Aoki, M., Murayama, K., Nishino, I., Nonaka, I., Arahata, K., and Brown, R. H., Jr. (2001). The sarcolemmal proteins dysferlin and caveolin-3 interact in skeletal muscle. *Hum Mol Genet* **10**, 1761-6.
Maximciuc, A. A., Putkey, J. A., Shamoo, Y., and MacKenzie, K. R. (2006). Complex of Calmodulin with a Ryanodine Receptor Target Reveals a Novel, Flexible Binding Mode. *Structure (London, England : 1993)* **14**, 1547.
McNally, E. M., de Sa Moreira, E., Duggan, D. J., Bonnemann, C. G., Lisanti, M. P., Lidov, H. G., Vainzof, M., Passos-Bueno, M. R., Hoffman, E. P., Zatz, M., and Kunkel, L. M. (1998). Caveolin-3 in muscular dystrophy. *Hum Mol Genet* **7**, 871-7.
Meissner, G. (1984). Adenine nucleotide stimulation of Ca2+-induced Ca2+ release in sarcoplasmic reticulum. *Journal of Biological Chemistry* **259**, 2365-74.
Meissner, G., Darling, E., and Eveleth, J. (1986). Kinetics of rapid Ca2+ release by sarcoplasmic reticulum. Effects of Ca2+, Mg2+, and adenine nucleotides. *Biochemistry* **25**, 236-244.
Meissner, G., Rios, E., Tripathy, A., and Pasek, D. A. (1997). Regulation of Skeletal Muscle Ca2+ Release Channel (Ryanodine Receptor) by Ca2+ and Monovalent Cations and Anions. *Journal of Biological Chemistry* **272**, 1628-1638.
Meng, X., Wang, G., Viero, C., Wang, Q., Mi, W., Su, X. D., Wagenknecht, T., Williams, A. J., Liu, Z., and Yin, C. C. (2009). CLIC2-RyR1 interaction and structural characterization by cryo-electron microscopy. *J Mol Biol* **387**, 320-34.
Mercier, I., Casimiro, M. C., Zhou, J., Wang, C., Plymire, C., Bryant, K. G., Daumer, K. M., Sotgia, F., Bonuccelli, G., Witkiewicz, A. K., Lin, J., Tran, T. H., Milliman, J., Frank, P. G., Jasmin, J.-F. o., Rui, H., Pestell, R. G., and Lisanti, M. P. (2009). Genetic Ablation of Caveolin-1 Drives Estrogen-Hypersensitivity and the Development of DCIS-Like Mammary Lesions. *The American Journal of Pathology* **174**, 1172.

Mercier, I., Lisanti, M. P., Jasmin, J.-F., Frank, P. G., and Lisanti, M. P. (2012). Caveolin-1 and Breast Cancer: A New Clinical Perspective
Caveolins and Caveolae. Vol. 729, pp. 83. Springer US.
Merlini, L., Carbone, I., Capanni, C., Sabatelli, P., Tortorelli, S., Sotgia, F., Lisanti, M. P., Bruno, C., and Minetti, C. (2002). Familial isolated hyperCKaemia associated with a new mutation in the caveolin-3 (CAV-3) gene. *J Neurol Neurosurg Psychiatry* **73**, 65-7.
Michel, J. B., Feron, O., Sase, K., Prabhakar, P., and Michel, T. (1997). Caveolin versus Calmodulin. *Journal of Biological Chemistry* **272**, 25907-25912.
Mineo, C., Gill, G. N., and Anderson, G. W. (1999). Regulated migration of epidermal growth factor receptor from caveolae. *Journal Of Biological Chemistry* **274**, 30636-30643.
Minetti, C., Bado, M., Broda, P., Sotgia, F., Bruno, C., Galbiati, F., Volonte, D., Lucania, G., Pavan, A., Bonilla, E., Lisanti, M. P., and Cordone, G. (2002). Impairment of caveolae formation and T-system disorganization in human muscular dystrophy with caveolin-3 deficiency. *American Journal Of Pathology* **160**, 265-270.
Minetti, C., Sotgia, F., Bruno, C., Scartezzini, P., Broda, P., Bado, M., Masetti, E., Mazzocco, M., Egeo, A., Donati, M. A., Volonte, D., Galbiati, F., Cordone, G., Bricarelli, F. D., Lisanti, M. P., and Zara, F. (1998). Mutations in the caveolin-3 gene cause autosomal dominant limb-girdle muscular dystrophy. *Nature Genetics* **18**, 365-368.
Minor, D. L. (2001). Potassium channels: life in the post-structural world. *Current Opinion in Structural Biology* **11**, 408.
Monier, S., Parton, R. G., Vogel, F., Behlke, J., Henske, A., and Kurzchalia, T. V. (1995). Vip21-Caveolin, A Membrane-Protein Constituent Of The Caveolar Coat, Oligomerizes In-Vivo And In-Vitro. *Molecular Biology Of The Cell* **6**, 911-927.
Monnier, N., Ferreiro, A., Marty, I., Labarre-Vila, A., Mezin, P., and Lunardi, J. (2003). A homozygous splicing mutation causing a depletion of skeletal muscle RYR1 is associated with multi-minicore disease congenital myopathy with ophthalmoplegia. *Hum Mol Genet* **12**, 1171-1178.
Moore, C. P., Rodney, G., Zhang, J. Z., Santacruz-Toloza, L., Strasburg, G., and Hamilton, S. L. (1999). Apocalmodulin and Ca2+ calmodulin bind to the same region on the skeletal muscle Ca2+ release channel. *Biochemistry* **38**, 8532-7.
Mora, R., Bonilha, V. L., Marmorstein, A., Scherer, P. E., Brown, D., Lisanti, M. P., and Rodriguez-Boulan, E. (1999). Caveolin-2 Localizes to the Golgi Complex but Redistributes to Plasma Membrane, Caveolae, and Rafts when Co-expressed with Caveolin-1. *Journal of Biological Chemistry* **274**, 25708-25717.
Muntoni, F., Cau, M., Ganau, A., Congiu, R., Arvedi, G., Mateddu, A., Marrosu, M. G., Cianchetti, C., Realdi, G., Cao, A., and et al. (1993). Brief report: deletion of the dystrophin muscle-promoter region associated with X-linked dilated cardiomyopathy. *N Engl J Med* **329**, 921-5.
Murata, M., Peranen, J., Schreiner, R., Wieland, F., Kurzchalia, T. V., and Simons, K. (1995). Vip21/Caveolin Is A Cholesterol-Binding Protein. *Proceedings Of The National Academy Of Sciences Of The United States Of America* **92**, 10339-10343.
Murphy, R. M., Mollica, J. P., and Lamb, G. D. (2009). Plasma membrane removal in rat skeletal muscle fibers reveals caveolin-3 hot-spots at the necks of transverse tubules. *Exp Cell Res* **315**, 1015-28.
Murry, C. E., Jennings, R. B., and Reimer, K. A. (1986). Preconditioning with ischemia: a delay of lethal cell injury in ischemic myocardium. *Circulation* **74**, 1124-1136.
Murthy, K. S., and Makhlouf, G. M. (2000). Heterologous desensitization mediated by G protein-specific binding to caveolin. *Journal Of Biological Chemistry* **275**, 30211-30219.

Nabi, I. R., and Le, P. U. (2003). Caveolae/raft-dependent endocytosis. *The Journal of Cell Biology* **161**, 673-677.

Nagai, K., Thogersen, H. C., and Luisi, B. F. (1988). Refolding and crystallographic studies of eukaryotic proteins produced in Escherichia coli. *Biochemical Society transactions* **16**, 108-10.

Needleman, D. H., and Hamilton, S. L. (1997). Factors influencing [3H]ryanodine binding to the skeletal muscle Ca2+ release channel. *Anal Biochem* **248**, 173-9.

Nystrom, F. H., Chen, H., Cong, L.-N., Li, Y., and Quon, M. J. (1999). Caveolin-1 Interacts with the Insulin Receptor and Can Differentially Modulate Insulin Signaling in Transfected Cos-7 Cells and Rat Adipose Cells. *Molecular Endocrinology* **13**, 2013-2024.

O'Connell, K. M., Martens, J. R., and Tamkun, M. M. (2004). Localization of ion channels to lipid Raft domains within the cardiovascular system. *Trends Cardiovasc Med* **14**, 37-42.

Oh, P., McIntosh, D. P., and Schnitzer, J. E. (1998). Dynamin at the neck of caveolae mediates their budding to form transport vesicles by GTP-driven fission from the plasma membrane of endothelium. *Journal Of Cell Biology* **141**, 101-114.

Ohman, E., Nilsson, A., Madeira, A., Sjogren, B., Andren, P. E., and Svenningsson, P. (2008). Use of Surface Plasmon Resonance Coupled with Mass Spectrometry Reveals an Interaction between the Voltage-Gated Sodium Channel Type X alpha-Subunit and Caveolin-1. *Journal Of Proteome Research* **7**, 5333-5338.

Ohsawa, Y., Toko, H., Katsura, M., Morimoto, K., Yamada, H., Ichikawa, Y., Murakami, T., Ohkuma, S., Komuro, I., and Sunada, Y. (2004). Overexpression of P104L mutant caveolin-3 in mice develops hypertrophic cardiomyopathy with enhanced contractility in association with increased endothelial nitric oxide synthase activity. *Human Molecular Genetics* **13**, 151-157.

Okamoto, T., Schlegel, A., Scherer, P. E., and Lisanti, M. P. (1998). Caveolins, a family of scaffolding proteins for organizing "preassembled signaling complexes" at the plasma membrane". *Journal Of Biological Chemistry* **273**, 5419-5422.

Olivari, C., Meanti, C., De Michelis, M. I., and Rasi-Caldogno, F. (1998). Fusicoccin binding to its plasma membrane receptor and the activation of the plasma membrane H(+)-ATPase. IV. Fusicoccin induces the association between the plasma membrane H(+)-ATPase and the fusicoccin receptor. *Plant Physiol* **116**, 529-37.

Orlandi, P. A., and Fishman, P. H. (1998). Filipin-dependent Inhibition of Cholera Toxin: Evidence for Toxin Internalization and Activation through Caveolae-like Domains. *The Journal of Cell Biology* **141**, 905-915.

Orlova, E. V., Serysheva, I. I., van Heel, M., Hamilton, S. L., and Chiu, W. (1996). Two structural configurations of the skeletal muscle calcium release channel. *Nature Structural Biology* **3**, 547-552.

Örtegren, U., Karlsson, M., Blazic, N., Blomqvist, M., Nystrom, F. H., Gustavsson, J., Fredman, P., and Strålfors, P. (2004). Lipids and glycosphingolipids in caveolae and surrounding plasma membrane of primary rat adipocytes. *European Journal of Biochemistry* **271**, 2028.

Ostrom, R. S., Gregorian, C., Drenan, R. M., Xiang, Y., Regan, J. W., and Insel, P. A. (2001). Receptor number and caveolar co-localization determine receptor coupling efficiency to adenylyl cyclase. *Journal Of Biological Chemistry* **276**, 42063-42069.

Otsu, K., Willard, H. F., Khanna, V. K., Zorzato, F., Green, N. M., and MacLennan, D. H. (1990). Molecular cloning of cDNA encoding the Ca2+ release channel (ryanodine receptor) of rabbit cardiac muscle sarcoplasmic reticulum. *Journal of Biological Chemistry* **265**, 13472-13483.

Overington, J. P., Al-Lazikani, B., and Hopkins, A. L. (2006). How many drug targets are there? *Nat Rev Drug Discov* **5**, 993.

Palade, G. E. (1953). Fine structure of blood capillaries. *J Appl Physiol*, 1424–1436.
Parat, M.-O., and Fox, P. L. (2001). Palmitoylation of Caveolin-1 in Endothelial Cells Is Post-translational but Irreversible. *Journal of Biological Chemistry* **276**, 15776-15782.
Park, D. S., Woodman, S. E., Schubert, W., Cohen, A. W., Frank, P. G., Chandra, M., Shirani, J., Razani, B., Tang, B. Y., Jelicks, L. A., Factor, S. M., Weiss, L. M., Tanowitz, H. B., and Lisanti, M. P. (2002). Caveolin-1/3 double-knockout mice are viable, but lack both muscle and non-muscle caveolae, and develop a severe cardiomyopathic phenotype. *American Journal Of Pathology* **160**, 2207-2217.
Parton, R. G., Hanzal-Bayer, M., and Hancock, J. F. (2006). Biogenesis of caveolae: a structural model for caveolin-induced domain formation. *Journal of Cell Science* **119**, 787-796.
Parton, R. G., and Simons, K. (2007). The multiple faces of caveolae. *Nature Reviews Molecular Cell Biology* **8**, 185-194.
Parton, R. G., Way, M., Zorzi, N., and Stang, E. (1997). Caveolin-3 associates with developing T-tubules during muscle differentiation. *Journal Of Cell Biology* **136**, 137-154.
Patel, H. H., Head, B. P., Petersen, H. N., Niesman, I. R., Huang, D., Gross, G. J., Insel, P. A., and Roth, D. M. (2006). Protection of adult rat cardiac myocytes from ischemic cell death: role of caveolar microdomains and delta opioid receptors. *American Journal of Physiology - Heart and Circulatory Physiology*.
Patel, H. H., Tsutsumi, Y. M., Head, B. P., Niesman, I. R., Jennings, M., Horikawa, Y., Huang, D., Moreno, A. L., Patel, P. M., Insel, P. A., and Roth, D. M. (2007). Mechanisms of cardiac protection from ischemia/reperfusion injury: a role for caveolae and caveolin-1. *The FASEB Journal* **21**, 1565-1574.
Pattanaik, P., Fromondi, L., Ng, K. P., He, J., and van den Akker, F. (2009). Expression, purification, and characterization of the intra-cellular domain of the ANP receptor. *Biochimie* **91**, 888-93.
Pelkmans, L., Bürli, T., Zerial, M., and Helenius, A. (2004). Caveolin-Stabilized Membrane Domains as Multifunctional Transport and Sorting Devices in Endocytic Membrane Traffic. *Cell* **118**, 767.
Pelkmans, L., Kartenbeck, J., and Helenius, A. (2001). Caveolar endocytosis of simian virus 40 reveals a new two-step vesicular-transport pathway to the ER. *Nat Cell Biol* **3**, 473.
Pelkmans, L., Püntener, D., and Helenius, A. (2002). Local actin polymerization and dynamin recruitment in SV40-induced internalization of caveolae. *Science* **296**, 535.
Penel, S., Morrison, R. G., Dobson, P. D., Mortishire-Smith, R. J., and Doig, A. J. (2003). Length preferences and periodicity in β-strands. Antiparallel edge β-sheets are more likely to finish in non-hydrogen bonded rings. *Protein Engineering* **16**, 957-961.
Perez, C. F., Mukherjee, S., and Allen, P. D. (2003). Amino Acids 1–1,680 of Ryanodine Receptor Type 1 Hold Critical Determinants of Skeletal Type for Excitation-Contraction Coupling: ROLE OF DIVERGENCE DOMAIN D2. *Journal of Biological Chemistry* **278**, 39644-39652.
Pettersen, E. F., Goddard, T. D., Huang, C. C., Couch, G. S., Greenblatt, D. M., Meng, E. C., and Ferrin, T. E. (2004). UCSF Chimera—A visualization system for exploratory research and analysis. *Journal of Computational Chemistry* **25**, 1605.
Pol, A., Martin, S., FernÃ¡ndez, M. A., Ingelmo-Torres, M., Ferguson, C., Enrich, C., and Parton, R. G. (2005). Cholesterol and Fatty Acids Regulate Dynamic Caveolin Trafficking through the Golgi Complex and between the Cell Surface and Lipid Bodies. *Molecular Biology of the Cell* **16**, 2091-2105.

Porter Moore, C., Zhang, J. Z., and Hamilton, S. L. (1999). A role for cysteine 3635 of RYR1 in redox modulation and calmodulin binding. *J Biol Chem* **274**, 36831-4.

Pralle, A., Keller, P., Florin, E. L., Simons, K., and Horber, J. K. (2000). Sphingolipid-cholesterol rafts diffuse as small entities in the plasma membrane of mammalian cells. *J Cell Biol* **148**, 997-1008.

Priori, S. G., Napolitano, C., Tiso, N., Memmi, M., Vignati, G., Bloise, R., Sorrentino, V., and Danieli, G. A. (2001). Mutations in the Cardiac Ryanodine Receptor Gene (hRyR2) Underlie Catecholaminergic Polymorphic Ventricular Tachycardia. *Circulation* **103**, 196-200.

Pryor, W. A., and Squadrito, G. L. (1995). The chemistry of peroxynitrite: a product from the reaction of nitric oxide with superoxide. *American Journal of Physiology - Lung Cellular and Molecular Physiology* **268**, L699-L722.

Quane, K. A., Healy, J. M. S., Keating, K. E., Manning, B. M., Couch, F. J., Palmucci, L. M., Doriguzzi, C., Fagerlund, T. H., Berg, K., Ording, H., Bendixen, D., Mortier, W., Linz, U., Muller, C. R., and McCarthy, T. V. (1993). Mutations in the ryanodine receptor gene in central core disease and malignant hyperthermia. *Nat Genet* **5**, 51-55.

Radel, C., and Rizzo, V. (2005). Integrin mechanotransduction stimulates caveolin-1 phosphorylation and recruitment of Csk to mediate actin reorganization. *American Journal of Physiology - Heart and Circulatory Physiology* **288**, H936-H945.

Radermacher, M. (1988). Three-dimensional reconstruction of single particles from random and nonrandom tilt series. *Journal of electron microscopy technique* **9**, 359-94.

Radermacher, M., Rao, V., Grassucci, R., Frank, J., Timerman, A. P., Fleischer, S., and Wagenknecht, T. (1994). Cryo-electron microscopy and three-dimensional reconstruction of the calcium release channel/ryanodine receptor from skeletal muscle. *The Journal of Cell Biology* **127**, 411-423.

Radermacher, M., Wagenknecht, T., Grassucci, R., Frank, J., Inui, M., Chadwick, C., and Fleischer, S. (1992). Cryo-EM of the native structure of the calcium release channel/ryanodine receptor from sarcoplasmic reticulum. *Biophysical journal* **61**, 936.

Ralston, E., and Ploug, T. (1999). Caveolin-3 is associated with the T-tubules of mature skeletal muscle fibers. *Experimental Cell Research* **246**, 510-515.

Ratajczak, P., Oliviero, P., Marotte, F., Kolar, F., Ostadal, B., and Samuel, J. L. (2005). Expression and localization of caveolins during postnatal development in rat heart: implication of thyroid hormone. *J Appl Physiol* **99**, 244-51.

Razani, B., Engelman, J. A., Wang, X. B., Schubert, W., Zhang, X. L., Marks, C. B., Macaluso, F., Russell, R. G., Li, M. M., Pestell, R. G., Di Vizio, D., Hou, H., Kneitz, B., Lagaud, G., Christ, G. J., Edelmann, W., and Lisanti, M. P. (2001). Caveolin-1 null mice are viable but show evidence of hyperproliferative and vascular abnormalities. *Journal Of Biological Chemistry* **276**, 38121-38138.

Razani, B., Rubin, C. S., and Lisanti, M. P. (1999). Regulation of cAMP-mediated Signal Transduction via Interaction of Caveolins with the Catalytic Subunit of Protein Kinase A. *Journal of Biological Chemistry* **274**, 26353-26360.

Razani, B., Wang, X. B., Engelman, J. A., Battista, M., Lagaud, G., Zhang, X. L., Kneitz, B., Hou, H., Christ, G. J., Edelmann, W., and Lisanti, M. P. (2002a). Caveolin-2-deficient mice show evidence of severe pulmonary dysfunction without disruption of caveolae. *Molecular And Cellular Biology* **22**, 2329-2344.

Razani, B., Woodman, S. E., and Lisanti, M. P. (2002b). Caveolae: From cell biology to animal physiology. *Pharmacological Reviews* **54**, 431-467.

Ren, X., Ostermeyer, A. G., Ramcharan, L. T., Zeng, Y., Lublin, D. M., and Brown, D. A. (2004). Conformational Defects Slow Golgi Exit, Block Oligomerization, and

Reduce Raft Affinity of Caveolin-1 Mutant Proteins. *Molecular Biology of the Cell* **15**, 4556-4567.
Richards, A. A., Stang, E., Pepperkok, R., and Parton, R. G. (2002). Inhibitors of COP-mediated transport and cholera toxin action inhibit simian virus 40 infection. *Molecular Biology of the Cell* **13**, 1750.
Rietveld, A., Neutz, S., Simons, K., and Eaton, S. (1999). Association of Sterol- and Glycosylphosphatidylinositol-linked Proteins with Drosophila Raft Lipid Microdomains. *J. Biol. Chem.* **274**, 12049-12054.
Rigaud, J. L., Levy, D., Mosser, G., and Lambert, O. (1998). Detergent removal by non-polar polystyrene beads - Applications to membrane protein reconstitution and two-dimensional crystallization. *European Biophysics Journal With Biophysics Letters* **27**, 305-319.
Rinas, U., and Bailey, J. E. (1992). Protein compositional analysis of inclusion bodies produced in recombinant Escherichia coli. *Applied Microbiology and Biotechnology* **37**, 609.
Rios, E., and Brum, G. (1987). Involvement of dihydropyridine receptors in excitation-contraction coupling in skeletal muscle. *Nature* **325**, 717.
Robenek, H., Weissen-Plenz, G., and Severs, N. J. (2008). Freeze-fracture replica immunolabelling reveals caveolin-1 in the human cardiomyocyte plasma membrane. *Journal of Cellular and Molecular Medicine* **12**, 2519.
Rodney, G. G., Williams, B. Y., Strasburg, G. M., Beckingham, K., and Hamilton, S. L. (2000). Regulation of RYR1 Activity by Ca2+ and Calmodulin. *Biochemistry* **39**, 7807-7812.
Romanos, M. A., Scorer, C. A., and Clare, J. J. (1992). Foreign gene expression in yeast: a review. *Yeast* **8**, 423.
Rothberg, K. G., Heuser, J. E., Donzell, W. C., Ying, Y. S., Glenney, J. R., and Anderson, R. G. W. (1992). Caveolin, A Protein-Component Of Caveolae Membrane Coats. *Cell* **68**, 673-682.
Rybin, V. O., Grabham, P. W., Elouardighi, H., and Steinberg, S. F. (2003). Caveolae-associated proteins in cardiomyocytes: caveolin-2 expression and interactions with caveolin-3. *Am J Physiol Heart Circ Physiol* **285**, H325-32.
Rybin, V. O., Xu, X. H., Lisanti, M. P., and Steinberg, S. F. (2000). Differential targeting of beta-adrenergic receptor subtypes and adenylyl cyclase to cardiomyocyte caveolae - A mechanism to functionally regulate the cAMP signaling pathway. *Journal Of Biological Chemistry* **275**, 41447-41457.
Sabourin, T., Bastien, L., Bachvarov, D. R., and Marceau, F. (2002). Agonist-induced translocation of the kinin B-1 receptor to caveolae-related rafts. *Molecular Pharmacology* **61**, 546-553.
Sachdev, D., and Chirgwin, J. M. (1998). Order of Fusions between Bacterial and Mammalian Proteins Can Determine Solubility inEscherichia coli. *Biochemical and Biophysical Research Communications* **244**, 933.
Samsó, M., Feng, W., Pessah, I. N., and Allen, P. D. (2009). Coordinated Movement of Cytoplasmic and Transmembrane Domains of RyR1 upon Gating. *PLoS Biol* **7**, e1000085.
Samsó , M., and Wagenknecht, T. (2002). Apocalmodulin and Ca2+-Calmodulin Bind to Neighboring Locations on the Ryanodine Receptor. *Journal of Biological Chemistry* **277**, 1349-1353.
Samsó, M., and Wagenknecht, T. (2002). Apocalmodulin and Ca2+-Calmodulin Bind to Neighboring Locations on the Ryanodine Receptor. *Journal of Biological Chemistry* **277**, 1349-1353.
Samsó, M., Wagenknecht, T., and Allen, P. D. (2005). Internal structure and visualization of transmembrane domains of the RyR1 calcium release channel by cryo-EM. *Nat Struct Mol Biol* **12**, 539-544.

Sargiacomo, M., Scherer, P. E., Tang, Z. L., Kubler, E., Song, K. S., Sanders, M. C., and Lisanti, M. P. (1995). Oligomeric Structure Of Caveolin - Implications For Caveolae Membrane Organization. *Proceedings Of The National Academy Of Sciences Of The United States Of America* **92**, 9407-9411.

Sargiacomo, M., Sudol, M., Tang, Z., and Lisanti, M. P. (1993a). Signal transducing molecules and glycosyl-phosphatidylinositol-linked proteins form a caveolin-rich insoluble complex in MDCK cells. *The Journal of Cell Biology* **122**, 789-807.

Sargiacomo, M., Sudol, M., Tang, Z. L., and Lisanti, M. P. (1993b). Signal-Transducing Molecules And Glycosyl-Phosphatidylinositol-Linked Proteins Form A Caveolin-Rich Insoluble Complex In Mdck Cells. *Journal Of Cell Biology* **122**, 789-807.

Sato, I., Wu, S., Ibarra, M. C. A., Hayashi, Y. K., Fujita, H., Tojo, M., Oh, S. J., Nonaka, I., Noguchi, S., and Nishino, I. (2008). Congenital neuromuscular disease with uniform type 1 fiber and RYR1 mutation. *Neurology* **70**, 114-122.

Schaechter, M., Maaloe, O., and Kjeldgaard, N. O. (1958). Dependency on medium and temperature of cell size and chemical composition during balanced grown of Salmonella typhimurium. *J Gen Microbiol* **19**, 592-606.

Scheiffele, P., Verkade, P., Fra, A. M., Virta, H., Simons, K., and Ikonen, E. (1998). Caveolin-1 and -2 in the Exocytic Pathway of MDCK Cells. *The Journal of Cell Biology* **140**, 795-806.

Schein, C. H., and Noteborn, M. H. M. (1988). Formation of Soluble Recombinant Proteins in Escherichia Coli is Favored by Lower Growth Temperature. *Nat Biotech* **6**, 291.

Scherer, P. E., Lewis, R. Y., Volonté, D., Engelman, J. A., Galbiati, F., Couet, J., Kohtz, D. S., van Donselaar, E., Peters, P., and Lisanti, M. P. (1997). Cell-type and Tissue-specific Expression of Caveolin-2. *Journal of Biological Chemistry* **272**, 29337-29346.

Scherer, P. E., Lisanti, M. P., Baldini, G., Sargiacomo, M., Mastick, C. C., and Lodish, H. F. (1994). Induction of caveolin during adipogenesis and association of GLUT4 with caveolin-rich vesicles. *The Journal of Cell Biology* **127**, 1233-1243.

Scherer, P. E., Okamoto, T., Chun, M. Y., Nishimoto, I., Lodish, H. F., and Lisanti, M. P. (1996). Identification, sequence, and expression of caveolin-2 defines a caveolin gene family. *Proceedings Of The National Academy Of Sciences Of The United States Of America* **93**, 131-135.

Scherer, P. E., Tang, Z. L., Chun, M. Y., Sargiacomo, M., Lodish, H. F., and Lisanti, M. P. (1995). Caveolin Isoforms Differ In Their N-Terminal Protein-Sequence And Subcellular-Distribution - Identification And Epitope Mapping Of An Isoform-Specific Monoclonal-Antibody Probe. *Journal Of Biological Chemistry* **270**, 16395-16401.

Schlegel, A., and Lisanti, M. P. (2000). A molecular dissection of caveolin-1 membrane attachment and oligomerization - Two separate regions of the caveolin-1 C-terminal domain mediate membrane binding and oligomer/oligomer interactions in vivo. *Journal Of Biological Chemistry* **275**, 21605-21617.

Schlegel, A., Schwab, R. B., Scherer, P. E., and Lisanti, M. P. (1999). A role for the caveolin scaffolding domain in mediating the membrane attachment of caveolin-1 - The caveolin scaffolding domain is both necessary and sufficient for membrane binding in vitro. *Journal Of Biological Chemistry* **274**, 22660-22667.

Schlegel, A., Volonte, D., Engelman, J. A., Galbiati, F., Mehta, P., Zhang, X.-L., Scherer, P. E., and Lisanti, M. P. (1998). Crowded Little Caves: Structure and Function of Caveolae. *Cellular Signalling* **10**, 457.

Schnitzer, J. E. (2001). Caveolae: from basic trafficking mechanisms to targeting transcytosis for tissue-specific drug and gene delivery in vivo. *Advanced Drug Delivery Reviews* **49**, 265-280.

Scholtz, J. M., Qian, H., York, E. J., Stewart, J. M., and Baldwin, R. L. (1991). Parameters of helix-coil transition theory for alanine-based peptides of varying chain lengths in water. *Biopolymers* **31**, 1463-70.

Schroeder, F., Atshaves, B. P., Gallegos, A. M., McIntosh, A. L., Liu, J. C. S., Kier, A. B., Huang, H., Ball, J. M., and Philippe, G. F. a. M. P. L. (2005). Chapter 1 Lipid Rafts and Caveolae Organization. *In* "Advances in Molecular and Cell Biology", Vol. Volume 36, pp. 1. Elsevier.

Schwencke, C., Okumura, S., Yamamoto, M., Geng, Y. J., and Ishikawa, Y. (1999). Colocalization of beta-adrenergic receptors and caveolin within the plasma membrane. *Journal Of Cellular Biochemistry* **75**, 64-72.

Scriven, D. R. L., Klimek, A., Asghari, P., Bellve, K., and Moore, E. D. W. (2005). Caveolin-3 Is Adjacent to a Group of Extradyadic Ryanodine Receptors. *Biophysical Journal* **89**, 1893.

Serysheva, I. I., Hamilton, S. L., Chiu, W., and Ludtke, S. J. (2005). Structure of Ca2+ Release Channel at 14 Å Resolution. *J Mol Biol* **345**, 427–431.

Serysheva, I. I., Ludtke, S. J., Baker, M. L., Cong, Y., Topf, M., Eramian, D., Sali, A., Hamilton, S. L., and Chiu, W. (2008). Subnanometer-resolution electron cryomicroscopy-based domain models for the cytoplasmic region of skeletal muscle RyR channel. *Proceedings of the National Academy of Sciences* **105**, 9610-9615.

Serysheva, I. I., Orlova, E. V., Chiu, W., Sherman, M. B., Hamilton, S. L., and Heel, M. v. (1995). Electron cryomicroscopy and angular reconstitution used to visualize the skeletal muscle calcium release channel. *Nat Struct Mol Biol* **2**, 18.

Serysheva, I. I., Schatz, M., van Heel, M., Chiu, W., and Hamilton, S. L. (1999). Structure of the skeletal muscle calcium release channel activated with Ca2+ and AMP-PCP. *Biophys J* **77**, 1936-44.

Sharma, M. R., Jeyakumar, L. H., Fleischer, S., and Wagenknecht, T. (2000). Three-dimensional Structure of Ryanodine Receptor Isoform Three in Two Conformational States as Visualized by Cryo-electron Microscopy. *Journal of Biological Chemistry* **275**, 9485-9491.

Sharma, M. R., Jeyakumar, L. H., Fleischer, S., and Wagenknecht, T. (2006). Three-dimensional visualization of FKBP12.6 binding to an open conformation of cardiac ryanodine receptor. *Biophys J* **90**, 164-72.

Sharma, M. R., Penczek, P., Grassucci, R., Xin, H.-B., Fleischer, S., and Wagenknecht, T. (1998). Cryoelectron Microscopy and Image Analysis of the Cardiac Ryanodine Receptor. *Journal of Biological Chemistry* **273**, 18429-18434.

Shaul, P. W., and Anderson, R. G. W. (1998). Role of plasmalemmal caveolae in signal transduction. *American Journal of Physiology - Lung Cellular and Molecular Physiology* **275**, L843-L851.

Shaul, P. W., Smart, E. J., Robinson, L. J., Yuhanna, Z. V. G. S., Ying, Y., Anderson, R. G. W., and Michel, T. (1996). Acylation targets endothelial nitric-oxide synthase to plasmalemmal caveolae. *Journal of Biological Chemistry* **271**, 6518-6522.

Sheets, E. D., Lee, G. M., Simson, R., and Jacobson, K. (1997). Transient confinement of a glycosylphosphatidylinositol-anchored protein in the plasma membrane. *Biochemistry* **36**, 12449-58.

Sheridan, D. C., Takekura, H., Franzini-Armstrong, C., Beam, K. G., Allen, P. D., and Perez, C. F. (2006). Bidirectional signaling between calcium channels of skeletal muscle requires multiple direct and indirect interactions. *Proceedings of the National Academy of Sciences* **103**, 19760-19765.

Simionescu, N. (1983). Cellular aspects of transcapillary exchange. *Physiol Rev* **63**, 1536-79.

Simons, K., and Ikonen, E. (1997). Functional rafts in cell membranes. *Nature* **387**, 569.

Simons, K., and Toomre, D. (2000). Lipid rafts and signal transduction. *Nature Reviews Molecular Cell Biology* **1**, 31-39.

Singer, S. J., and Nicolson, G. L. (1972). Fluid Mosaic Model Of Structure Of Cell-Membranes. *Science* **175**, 720-&.

Smart, E. J., Graf, G. A., McNiven, M. A., Sessa, W. C., Engelman, J. A., Scherer, P. E., Okamoto, T., and Lisanti, M. P. (1999). Caveolins, liquid-ordered domains, and signal transduction. *Molecular And Cellular Biology* **19**, 7289-7304.

Smart, E. J., Ying, Y.-s., Donzell, W. C., and Anderson, R. G. W. (1996). A Role for Caveolin in Transport of Cholesterol from Endoplasmic Reticulum to Plasma Membrane. *Journal of Biological Chemistry* **271**, 29427-29435.

Smart, E. J., Ying, Y. S., Conrad, P. A., and Anderson, R. G. W. (1994). Caveolin Moves From Caveolae To The Golgi-Apparatus In Response To Cholesterol Oxidation. *Journal Of Cell Biology* **127**, 1185-1197.

Smyth, M. S., and Martin, J. H. J. (2000). x Ray crystallography. *Molecular Pathology* **53**, 8-14.

Smythe, G. M., Eby, J. C., Disatnik, M. H., and Rando, T. A. (2003). A caveolin-3 mutant that causes limb girdle muscular dystrophy type 1C disrupts Src localization and activity and induces apoptosis in skeletal myotubes. *Journal Of Cell Science* **116**, 4739-4749.

Sommer, S., and Fuqua, S. A. W. (2001). Estrogen receptor and breast cancer. *Seminars in Cancer Biology* **11**, 339.

Song, K. S., Li, S., Okamoto, T., Quilliam, L. A., Sargiacomo, M., and Lisanti, M. P. (1996a). Co-purification and direct interaction of Ras with caveolin, an integral membrane protein of caveolae microdomains. Detergent-free purification of caveolae microdomains. *J Biol Chem* **271**, 9690-7.

Song, K. S., Scherer, P. E., Tang, Z. L., Okamoto, T., Li, S. W., Chafel, M., Chu, C., Kohtz, D. S., and Lisanti, M. P. (1996b). Expression of caveolin-3 in skeletal, cardiac, and smooth muscle cells - Caveolin-3 is a component of the sarcolemma and co-fractionates with dystrophin and dystrophin-associated glycoproteins. *Journal Of Biological Chemistry* **271**, 15160-15165.

Song, K. S., Tang, Z. L., Li, S. W., and Lisanti, M. P. (1997). Mutational analysis of the properties of caveolin-1 - A novel role for the C-terminal domain in mediating homo-typic caveolin-caveolin interactions. *Journal Of Biological Chemistry* **272**, 4398-4403.

Sotgia, F., Casimiro, M. C., Bonuccelli, G., Liu, M., Whitaker-Menezes, D., Er, O., Daumer, K. M., Mercier, I., Witkiewicz, A. K., Minetti, C., Capozza, F., Gormley, M., Quong, A. A., Rui, H., Frank, P. G., Milliman, J. N., Knudsen, E. S., Zhou, J., Wang, C., Pestell, R. G., and Lisanti, M. P. (2009). Loss of Caveolin-3 Induces a Lactogenic Microenvironment that Is Protective Against Mammary Tumor Formation. *The American Journal of Pathology* **174**, 613.

Sotgia, F., Lee, J. K., Das, K., Bedford, M., Petrucci, T. C., Macioce, P., Sargiacomo, M., Bricarelli, F. D., Minetti, C., Sudol, M., and Lisanti, M. P. (2000). Caveolin-3 directly interacts with the C-terminal tail of beta-dystroglycan - Identification of a central WW-like domain within caveolin family members. *Journal Of Biological Chemistry* **275**, 38048-38058.

Sotgia, F., Williams, T. M., Schubert, W., Medina, F., Minetti, C., Pestell, R. G., and Lisanti, M. P. (2006). Caveolin-1 Deficiency (-/-) Conveys Premalignant Alterations in Mammary Epithelia, with Abnormal Lumen Formation, Growth Factor Independence, and Cell Invasiveness. *The American Journal of Pathology* **168**, 292.

Splawski, I., Timothy, K. W., Sharpe, L. M., Decher, N., Kumar, P., Bloise, R., Napolitano, C., Schwartz, P. J., Joseph, R. M., Condouris, K., Tager-Flusberg, H., Priori, S. G., Sanguinetti, M. C., and Keating, M. T. (2004). Ca(v)1.2 calcium

channel dysfunction causes a multisystem disorder including arrhythmia and autism. *Cell* **119**, 19-31.
Sreerama, N., Venyaminov, S. Y. U., and Woody, R. W. (1999). Estimation of the number of α-helical and β-strand segments in proteins using circular dichroism spectroscopy. *Protein Science* **8**, 370.
Sreerama, N., and Woody, R. W. (1993). A self-consistent method for the analysis of protein secondary structure from circular dichroism. *Anal Biochem* **209**, 32-44.
Sreerama, N., Woody, R. W., and Ludwig Brand and Michael, L. J. (2004). Computation and Analysis of Protein Circular Dichroism Spectra. *In* "Methods in Enzymology", Vol. Volume 383, pp. 318. Academic Press.
Stagg, S. M., Lander, G. C., Pulokas, J., Fellmann, D., Cheng, A., Quispe, J. D., Mallick, S. P., Avila, R. M., Carragher, B., and Potter, C. S. (2006). Automated cryoEM data acquisition and analysis of 284 742 particles of GroEL. *Journal of Structural Biology* **155**, 470.
Stewart, R., Zissimopoulos, S., and Lai, F. A. (2003). Oligomerization of the cardiac ryanodine receptor C-terminal tail. *Biochem. J.* **376**, 795-799.
Stoyanovsky, D., Murphy, T., Anno, P. R., Kim, Y. M., and Salama, G. (1997). Nitric oxide activates skeletal and cardiac ryanodine receptors. *Cell Calcium* **21**, 19-29.
Sun, J., Xin, C., Eu, J. P., Stamler, J. S., and Meissner, G. (2001). Cysteine-3635 is responsible for skeletal muscle ryanodine receptor modulation by NO. *Proceedings of the National Academy of Sciences* **98**, 11158-11162.
Sun, Q. Y., Ding, L. W., He, L. L., Sun, Y. B., Shao, J. L., Luo, M., and Xu, Z. F. (2009). Culture of Escherichia coli in SOC medium improves the cloning efficiency of toxic protein genes. *Anal Biochem* **394**, 144-6.
Sunada, Y., Ohi, H., Hase, A., Ohi, H., Hosono, T., Arata, S., Higuchi, S., Matsumura, K., and Shimizu, T. (2001). Transgenic mice expressing mutant caveolin-3 show severe myopathy associated with increased nNOS activity. *Human Molecular Genetics* **10**, 173-178.
Tagawa, A., Mezzacasa, A., Hayer, A., Longatti, A., Pelkmans, L., and Helenius, A. (2005). Assembly and trafficking of caveolar domains in the cell. *The Journal of Cell Biology* **170**, 769-779.
Takeshima, H., Nishimura, S., Matsumoto, T., Ishida, H., Kangawa, K., Minamino, N., Matsuo, H., Ueda, M., Hanaoka, M., Hirose, T., and Numa, S. (1989). Primary structure and expression from complementary DNA of skeletal muscle ryanodine receptor. *Nature* **339**, 439-445.
Tang, Z. L., Scherer, P. E., Okamoto, T., Song, K., Chu, C., Kohtz, D. S., Nishimoto, I., Lodish, H. F., and Lisanti, M. P. (1996). Molecular cloning of caveolin-3, a novel member of the caveolin gene family expressed predominantly in muscle. *Journal Of Biological Chemistry* **271**, 2255-2261.
Tateyama, M., Aoki, M., Nishino, I., Hayashi, Y. K., Sekiguchi, S., Shiga, Y., Takahashi, T., Onodera, Y., Haginoya, K., Kobayashi, K., Iinuma, K., Nonaka, I., Arahata, K., and Itoyoma, Y. (2002). Mutation in the caveolin-3 gene causes a peculiar form of distal myopathy. *Neurology* **58**, 323-325.
Terstappen, G. C., and Reggiani, A. (2001). In silico research in drug discovery. *Trends in Pharmacological Sciences* **22**, 23.
Thiele, C., Hannah, M. J., Fahrenholz, F., and Huttner, W. B. (2000). Cholesterol binds to synaptophysin and is required for biogenesis of synaptic vesicles. *Nature Cell Biology* **2**, 42-49.
Thuman-Commike, P. A. (2001). Single particle macromolecular structure determination via electron microscopy. *FEBS Letters* **505**, 199.
Tiso, N., Stephan, D. A., Nava, A., Bagattin, A., Devaney, J. M., Stanchi, F., Larderet, G., Brahmbhatt, B., Brown, K., Bauce, B., Muriago, M., Basso, C., Thiene, G., Danieli, G. A., and Rampazzo, A. (2001). Identification of mutations in the cardiac

ryanodine receptor gene in families affected with arrhythmogenic right ventricular cardiomyopathy type 2 (ARVD2). *Human Molecular Genetics* **10**, 189-194.
Tsai, B., Gilbert, J. M., Stehle, T., Lencer, W., Benjamin, T. L., and Rapoport, T. A. (2003). Gangliosides are receptors for murine polyoma virus and SV40. *EMBO J* **22**, 4346.
Tsutsumi, Y. M., Horikawa, Y. T., Jennings, M. M., Kidd, M. W., Niesman, I. R., Yokoyama, U., Head, B. P., Hagiwara, Y., Ishikawa, Y., Miyanohara, A., Patel, P. M., Insel, P. A., Patel, H. H., and Roth, D. M. (2008). Cardiac-specific overexpression of caveolin-3 induces endogenous cardiac protection by mimicking ischemic preconditioning. *Circulation* **118**, 1979-88.
Tunwell, R. E., Wickenden, C., Bertrand, B. M., Shevchenko, V. I., Walsh, M. B., Allen, P. D., and Lai, A. F. (1996). The human cardiac muscle ryanodine receptor-calcium release channel: identification, primary structure and topological analysis. *Biochem J* **318**, 477-487.
Ueda, H., Kawagishi, K., Terasawa, F., Nakamura, A., and Moriizumi, T. (2004). Caveolin-3 at the T-tubule colocalizes with alpha-actinin in the adult murine cardiac muscle. *Acta Histochemica Et Cytochemica* **37**, 373-378.
Uittenbogaard, A., Shaul, P. W., Yuhanna, I. S., Blair, A., and Smart, E. J. (2000). High density lipoprotein prevents oxidized low density lipoprotein-induced inhibition of endothelial nitric-oxide synthase localization and activation in caveolae. *Journal Of Biological Chemistry* **275**, 11278-11283.
Uittenbogaard, A., and Smart, E. J. (2000). Palmitoylation of Caveolin-1 Is Required for Cholesterol Binding, Chaperone Complex Formation, and Rapid Transport of Cholesterol to Caveolae. *Journal of Biological Chemistry* **275**, 25595-25599.
Uittenbogaard, A., Ying, Y. S., and Smart, E. J. (1998). Characterization of a cytosolic heat-shock protein caveolin chaperone complex - Involvement in cholesterol trafficking. *Journal Of Biological Chemistry* **273**, 6525-6532.
Ullrich, N. D., Fischer, D., Kornblum, C., Walter, M. C., Niggli, E., Zorzato, F., and Treves, S. (2011). Alterations of excitation–contraction coupling and excitation coupled Ca2+ entry in human myotubes carrying CAV3 mutations linked to rippling muscle. *Human Mutation* **32**, 309.
Van Heel, M. (1987). Angular reconstitution: A posteriori assignment of projection directions for 3D reconstruction. *Ultramicroscopy* **21**, 111.
van Heel, M., Harauz, G., Orlova, E. V., Schmidt, R., and Schatz, M. (1996). A New Generation of the IMAGIC Image Processing System. *Journal of Structural Biology* **116**, 17.
Vassilopoulos, S. p., Oddoux, S., Groh, S. v., Cacheux, M., Fauré, J., Brocard, J., Campbell, K. P., and Marty, I. (2010). Caveolin 3 Is Associated with the Calcium Release Complex and Is Modified via in Vivo Triadin Modification. *Biochemistry* **49**, 6130.
Vatta, M., Ackerman, M. J., Ye, B., Makielski, J. C., Ughanze, E. E., Taylor, E. W., Tester, D. J., Balijepalli, R. C., Foell, J. D., Li, Z. H., Kamp, T. J., and Towbin, J. A. (2006). Mutant caveolin-3 induces persistent late sodium current and is associated with long-QT syndrome. *Circulation* **114**, 2104-2112.
Voeltz, G. K., Prinz, W. A., Shibata, Y., Rist, J. M., and Rapoport, T. A. (2006). A Class of Membrane Proteins Shaping the Tubular Endoplasmic Reticulum. *Cell* **124**, 573.
Volonte, D., McTiernan, C. F., Drab, M., Kasper, M., and Galbiati, F. (2008). Caveolin-1 and caveolin-3 form heterooligomeric complexes in atrial cardiac myocytes that are required for doxorubicin-induced apoptosis. *American Journal Of Physiology-Heart And Circulatory Physiology* **294**, H392-H401.
Vorgerd, M., Ricker, K., Ziemssen, F., Kress, W., Goebel, H. H., Nix, W. A., Kubisch, C., Schoser, B. G. H., and Mortier, W. (2001). A sporadic case of rippling muscle disease caused by a de novo caveolin-3 mutation. *Neurology* **57**, 2273-2277.

Wagenknecht, T., Radermacher, M., Grassucci, R., Berkowitz, J., Xin, H.-B., and Fleischer, S. (1997). Locations of Calmodulin and FK506-binding Protein on the Three-dimensional Architecture of the Skeletal Muscle Ryanodine Receptor. *Journal of Biological Chemistry* **272**, 32463-32471.

Walsh, C. P., Davies, A., Butcher, A. J., Dolphin, A. C., and Kitmitto, A. (2009a). Three-dimensional Structure of CaV3.1. *Journal of Biological Chemistry* **284**, 22310-22321.

Walsh, C. P., Davies, A., Butcher, A. J., Dolphin, A. C., and Kitmitto, A. (2009b). Three-dimensional structure of CaV3.1: comparison with the cardiac L-type voltage-gated calcium channel monomer architecture. *J Biol Chem* **284**, 22310-21.

Waugh, D. S. (2005). Making the most of affinity tags. *Trends in Biotechnology* **23**, 316.

Way, M., and Parton, R. G. (1996). M-caveolin, a muscle-specific caveolin-related protein. *FEBS Lett* **378**, 108-12.

Wehrens, X. H., Lehnart, S. E., Reiken, S. R., and Marks, A. R. (2004). Ca2+/calmodulin-dependent protein kinase II phosphorylation regulates the cardiac ryanodine receptor. *Circ Res* **94**, e61-70.

Wei, L., Hanna, A. D., Beard, N. A., and Dulhunty, A. F. (2009). Unique isoform-specific properties of calsequestrin in the heart and skeletal muscle. *Cell Calcium* **45**, 474-484.

Weiss, N., Keller, C., Hoffmann, U., and Loscalzo, J. (2002). Endothelial dysfunction and atherothrombosis in mild hyperhomocysteinemia. *Vascular Medicine* **7**, 227-239.

West, D. J., Smith, E. C., and Williams, A. J. (2002). A novel and rapid approach to isolating functional ryanodine receptors. *Biochem Biophys Res Commun* **294**, 402-7.

Whitmore, L., and Wallace, B. A. (2004). DICHROWEB, an online server for protein secondary structure analyses from circular dichroism spectroscopic data. *Nucleic Acids Res* **32**, W668-73.

Whitmore, L., and Wallace, B. A. (2008). Protein secondary structure analyses from circular dichroism spectroscopy: methods and reference databases. *Biopolymers* **89**, 392-400.

Williams, T. M., Hassan, G. S., Li, J. W., Cohen, A. W., Medina, F., Frank, P. G., Pestell, R. G., Di Vizio, D., Loda, M., and Lisanti, M. P. (2005). Caveolin-1 promotes tumor progression in an autochthonous mouse model of prostate cancer - Genetic ablation of Cav-1 delays advanced prostate tumor development in tramp mice. *Journal Of Biological Chemistry* **280**, 25134-25145.

Williams, T. M., Medina, F., Badano, I., Hazan, R. B., Hutchinson, J., Muller, W. J., Chopra, N. G., Scherer, P. E., Pestell, R. G., and Lisanti, M. P. (2004). Caveolin-1 gene disruption promotes mammary tumorigenesis and dramatically enhances lung metastasis in vivo - Role of Cav-1 in cell invasiveness and matrix metalloproteinase (MMP-2/9) secretion. *Journal Of Biological Chemistry* **279**, 51630-51646.

Winther, A.-M. L., Liu, H., Sonntag, Y., Olesen, C., le Maire, M., Soehoel, H., Olsen, C.-E., Christensen, S. B., Nissen, P., and Møller, J. V. (2010). Critical Roles of Hydrophobicity and Orientation of Side Chains for Inactivation of Sarcoplasmic Reticulum Ca2+-ATPase with Thapsigargin and Thapsigargin Analogs. *Journal of Biological Chemistry* **285**, 28883-28892.

Wlodawer, A., Minor, W., Dauter, Z., and Jaskolski, M. (2008). Protein crystallography for non-crystallographers, or how to get the best (but not more) from published macromolecular structures. *FEBS Journal* **275**, 1.

Woodman, S. E., Park, D. S., Cohen, A. W., Cheung, M. W. C., Chandra, M., Shirani, J., Tang, B. Y., Jelicks, L. A., Kitsis, R. N., Christ, G. J., Factor, S. M., Tanowitz, H. B., and Lisanti, M. P. (2002). Caveolin-3 knock-out mice develop a progressive cardiomyopathy and show hyperactivation of the p42/44 MAPK cascade. *Journal Of Biological Chemistry* **277**, 38988-38997.

Wu, B., Chien, E. Y. T., Mol, C. D., Fenalti, G., Liu, W., Katritch, V., Abagyan, R., Brooun, A., Wells, P., Bi, F. C., Hamel, D. J., Kuhn, P., Handel, T. M., Cherezov, V., and Stevens, R. C. (2010). Structures of the CXCR4 Chemokine GPCR with Small-Molecule and Cyclic Peptide Antagonists. *Science* **330**, 1066-1071.

Wu, P., Wang, X., Li, F., Qi, B., Zhu, H., Liu, S., Cui, Y., and Chen, J. (2008). Growth suppression of MCF-7 cancer cell-derived xenografts in nude mice by caveolin-1. *Biochemical and Biophysical Research Communications* **376**, 215.

Wüthrich, K. (1990). Protein structure determination in solution by NMR spectroscopy. *Journal of Biological Chemistry* **265**, 22059-62.

Xiang, Y., Rybin, V. O., Steinberg, S. F., and Kobilka, B. (2002). Caveolar localization dictates physiologic signaling of beta(2)-adrenoceptors in neonatal cardiac myocytes. *Journal Of Biological Chemistry* **277**, 34280-34286.

Xiao, B., Zhong, G., Obayashi, M., Yang, D., Chen, K., Walsh, M. P., Shimoni, Y., Cheng, H., Ter Keurs, H., and Chen, S. R. W. (2006). Ser-2030, but not Ser-2808, is the major phosphorylation site in cardiac ryanodine receptors responding to protein kinase A activation upon beta-adrenergic stimulation in normal and failing hearts. *Biochem J* **396**, 7–16.

Xu, M., Ogawa, T., Pakrasi, H. B., and Mi, H. (2008). Identification and Localization of the CupB Protein Involved in Constitutive CO2 Uptake in the Cyanobacterium, Synechocystis sp. Strain PCC 6803. *Plant and Cell Physiology* **49**, 994-997.

Yagi, T., Hon-Nami, K., and Ohnishi, T. (1988). Purification and characterization of two types of NADH-quinone reductase from Thermus thermophilus HB-8. *Biochemistry* **27**, 2008.

Yamada, E. (1955). THE FINE STRUCTURE OF THE GALL BLADDER EPITHELIUM OF THE MOUSE. *The Journal of Biophysical and Biochemical Cytology* **1**, 445-458.

Yamamoto, M., Toya, Y., Schwencke, C., Lisanti, M. P., Myers, M. G., and Ishikawa, Y. (1998). Caveolin Is an Activator of Insulin Receptor Signaling. *Journal of Biological Chemistry* **273**, 26962-26968.

Yarbrough, T. L., Lu, T., Lee, H. C., and Shibata, E. F. (2002). Localization of cardiac sodium channels in caveolin-rich membrane domains - Regulation of sodium current amplitude. *Circulation Research* **90**, 443-449.

Ye, B., Balijepalli, R. C., Foell, J. D., Kroboth, S., Ye, Q., Luo, Y. H., and Shi, N. Q. (2008). Caveolin-3 Associates with and Affects the Function of Hyperpolarization-Activated Cyclic Nucleotide-Gated Channel 4. *Biochemistry* **47**, 12312-12318.

Yourassowsky, E., Van der Linden, M. P., Lismont, M. J., Crokaert, F., and Glupczynski, Y. (1985). Effect on growth curve patterns of brief exposure of bacteria to different concentrations of beta-lactam antibiotics. *J Antimicrob Chemother* **15 Suppl A**, 27-36.

Zaidi, M., Shankar, V. S., Towhidul Alam, A. S. M., Moonga, B. S., Pazianas, M., and Huang, C. L. H. (1992). Evidence that a ryanodine receptor triggers signal transduction in the osteoclast. *Biochemical and Biophysical Research Communications* **188**, 1332.

Zhang, W., Razani, B., Altschuler, Y., Bouzahzah, B., Mostov, K. E., Pestell, R. G., and Lisanti, M. P. (2000). Caveolin-1 Inhibits Epidermal Growth Factor-stimulated Lamellipod Extension and Cell Migration in Metastatic Mammary Adenocarcinoma Cells (MTLn3). *Journal of Biological Chemistry* **275**, 20717-20725.

Zhang, X., Shen, P., Coleman, M., Zou, W. E. I., Loggie, B. W., Smith, L. M., and Wang, Z. (2005). Caveolin-1 Down-regulation Activates Estrogen Receptor Alpha Expression and Leads to 17β-estradiol-stimulated Mammary Tumorigenesis. *Anticancer Research* **25**, 369-375.

Zhang, Y., Chen, H. S., Khanna, V. K., De Leon, S., Phillips, M. S., Schappert, K., Britt, B. A., Browell, A. K., and MacLennan, D. H. (1993). A mutation in the human ryanodine receptor gene associated with central core disease. *Nature Genetics* **5**, 46-50.

Zhao, M., Li, P., Li, X., Zhang, L., Winkfein, R. J., and Chen, S. R. W. (1999). Molecular Identification of the Ryanodine Receptor Pore-forming Segment. *Journal of Biological Chemistry* **274**, 25971-25974.

Zhao, Y. Y., Liu, Y., Stan, R. V., Fan, L., Gu, Y. S., Dalton, N., Chu, P. H., Peterson, K., Ross, J., and Chien, K. R. (2002). Defects in caveolin-1 cause dilated cardiomyopathy and pulmonary hypertension in knockout mice. *Proceedings Of The National Academy Of Sciences Of The United States Of America* **99**, 11375-11380.

Zorzato, F., Fujii, J., Otsu, K., Phillips, M., Green, N. M., Lai, F. A., Meissner, G., and MacLennan, D. H. (1990). Molecular cloning of cDNA encoding human and rabbit forms of the Ca2+ release channel (ryanodine receptor) of skeletal muscle sarcoplasmic reticulum. *J Biol Chem* **265**, 2244-56.

Zundel, W., Swiersz, L. M., and Giaccia, A. (2000). Caveolin 1-Mediated Regulation of Receptor Tyrosine Kinase-Associated Phosphatidylinositol 3-Kinase Activity by Ceramide. *Molecular and Cellular Biology* **20**, 1507-1514.